JYU DISSERTATIONS 613

Anni Taponen

Radical-Ion Salts based on Thiazyls and Tetracyanoquinodimethane

Hysteretic Magnetic Bistability in a Multicomponent System

UNIVERSITY OF JYVÄSKYLÄ
FACULTY OF MATHEMATICS
AND SCIENCE

JYU DISSERTATIONS 613

Anni Taponen

Radical-Ion Salts based on Thiazyls and Tetracyanoquinodimethane

Hysteretic Magnetic Bistability in a Multicomponent System

Esitetään Jyväskylän yliopiston matemaattis-luonnontieteellisen tiedekunnan suostumuksella
julkisesti tarkastettavaksi yliopiston Ylistönrinteen salissa Kem4
maaliskuun 24. päivänä 2023 kello 12.

Academic dissertation to be publicly discussed, by permission of
the Faculty of Mathematics and Science of the University of Jyväskylä,
in Ylistönrinne, auditorium Kem4, on March 24, 2023 at 12 o'clock noon.

JYVÄSKYLÄN YLIOPISTO
UNIVERSITY OF JYVÄSKYLÄ

JYVÄSKYLÄ 2023

Editors
Heikki M. Tuononen
Department of Chemistry, University of Jyväskylä
Ville Korkiakangas
Open Science Centre, University of Jyväskylä

ISBN 978-951-39-9507-2 (PDF)
URN:ISBN:978-951-39-9507-2
ISSN 2489-9003

Permanent link to this publication: http://urn.fi/URN:ISBN:978-951-39-9507-2

ABSTRACT

Taponen, Anni
Radical-Ion Salts based on Thiazyls and Tetracyanoquinodimethane: Hysteretic Magnetic Bistability in a Multicomponent System
Jyväskylä: University of Jyväskylä, 2023, 66 p.
(JYU Dissertations
ISSN 2489-9003; 613)
ISBN 978-951-39-9507-2 (PDF)

Organic radicals are subvalent molecules with one or more unpaired electrons. Typically, such species are reactive intermediates that are short-lived unless they are stabilized by steric protection, electronic delocalization, or a combination of both. Organothiazyls and their heavier selenazyl analogues are a broad class of stable radicals containing NS or NSe units combined with carbon. In recent decades, they have become important building blocks for synthesizing advanced materials with fascinating and useful solid-state properties, such as conductivity, magnetism, and bistability. The first part of this thesis introduces some common stable radicals and the factors affecting their stability and discusses their use in making organic ferro- and ferrimagnetic materials and magnetically bistable systems exhibiting a hysteretic memory effect. The focus is on thiazyl and selenazyl radicals 1,2,3,5-dithia- (DTDAs) and 1,2,3,5-diselenadiazolyls (DSDAs) as well as the radical-anion formed from the quintessential electron acceptor 7,7´,8,8´-tetracyanoquinodimethane (TCNQ). The second part of the thesis summarizes the research published in the four original journal articles associated with this work. It details the synthesis and characterization of new pyridyl-substituted DTDA and DSDA radicals and their *N*-alkylation to the corresponding radical-cations. The cations were subsequently combined with the radical-anion of TCNQ to generate radical-ion salts, leading to the realization of room-temperature hysteretic magnetic bistability owing to the reversible association of monomeric TCNQ radicals to weakly C–C σ-bonded dimers. Consequently, a systematic study of substituent, solvent, and atom-to-atom replacement effects on the solid-state structure and properties of the synthesized salt was carried out, providing insight into designing a new type of multicomponent functional molecular materials.

Keywords: stable radicals, dithiadiazolyl, diselenadiazolyl, tetracyanoquinodimethane, solid-state structures, solvates, hysteresis, magnetic properties, magnetic bistability, multicomponent materials

TIIVISTELMÄ (ABSTRACT IN FINNISH)

Taponen, Anni
Tiatsyyli- ja tetrasyanokinodimetaaniradikaali-ionien muodostamat suolat: magneettinen bistabiilisuus monikomponettisessa yhdisteessä
Jyväskylä: Jyväskylän yliopisto, 2023, 66 s.
(JYU Dissertations
ISSN 2489-9003; 613)
ISBN 978-951-39-9507-2 (PDF)

Orgaaniset radikaalit ovat molekyylejä, joissa on joko yksi tai useampi pariton elektroni. Tällaiset yhdisteet esiintyvät tyypillisesti kemiallisten reaktioiden välituotteina, ellei niitä stabiloida joko steerisen suojauksen, elektronisen delokalisaation tai näiden molempien avulla. Organotiatsyyli- ja -selenatsyyliradikaalien perusrakenne koostuu NS ja NSe yksiköistä sekä hiiliatomeista. Viime vuosikymmenten aikana niitä on käytetty materiaalikemian sovelluksissa sähköä johtavien, magneettisten ja bistabiilisten molekulaaristen materiaalien rakennusosina. Tämän väitöskirjan ensimmäinen osa käsittelee tunnetuimpia pysyviä orgaanisia radikaaleja, niiden pysyvyyteen vaikuttavia tekijöitä sekä kyseisiä radikaaleja rakenneosina hyödyntäviä ferro- ja ferrimagneettisia sekä hystereettisiä magneettisesti bistabiileja materiaaleja. Pääpaino käsittelyssä on tiatsyyli- ja selenatsyyliradikaaleilla 1,2,3,5-ditia- (DTDA) ja 1,2,3,5-diselenadiatsolyyleillä (DSDA) sekä 7,7´,8,8´-tetrasyanokinodimetaanin (TCNQ) muodostamalla anioniradikaalilla. Väitöskirjan toinen osa puolestaan keskittyy työn taustalla olevassa neljässä osajulkaisussa raportoituun tutkimukseen, jossa valmistettiin ja karakterisoitiin joukko uusia pyridyylisubstituoituja DTDA- ja DSDA-radikaaleja sekä niiden *N*-alkyloituja kationianalogeja. Valmistetut radikaalikationit yhdistettiin tämän jälkeen TCNQ:n anioniradikaalin kanssa, jolloin muodostui radikaaleista koostuvia suoloja. Yhdellä valmistetuista suoloista havaittiin kiinteässä tilassa reversiibeli magneettinen bistabiilisuus ja siihen liittyvä hystereesi-ilmiö, jossa monomeeriset TCNQ-radikaalit muodostavat lämpötilan muuttuessa C–C-sidoksellisia σ-dimeerejä. Tämän havainnon innoittamana substituentin, liuottimen ja kalkogeeniatomin vaikutus valmistettujen suolojen kiinteän tilan rakenteisiin ja ominaisuuksiin kartoitettiin laaja-alaisesti. Kokonaisuutena työn tulokset antavat arvokasta lisäinfoa monikomponenttisten funktionaalisten molekulaaristen materiaalien suunnitteluun ja valmistamiseen.

Avainsanat: pysyvät radikaalit, ditiadiatsolyylit, diselenadiatsolyylit, tetrasyanokinodimetaani, kiinteän tilan rakenteet, solvaatit, hystereesi, magneettiset ominaisuudet, magneettinen bistabiilisuus, multikomponenttiset materiaalit

Author

Anni Taponen
Department of Chemistry
University of Jyväskylä
anni.taponen@jyu.fi

Supervisors

Professor Heikki M. Tuononen
Department of Chemistry
University of Jyväskylä

Academy Research Fellow Aaron Mailman
Department of Chemistry
University of Jyväskylä

Reviewers

Professor Emeritus Risto Laitinen
Department of Chemistry
University of Oulu

Associate Professor Louise N. Dawe
Department of Chemistry and Biochemistry
Wilfrid Laurier University

Opponent

Professor Delia Haynes
Department of Chemistry and Polymer Science
Stellenbosch University

FOREWORD

The research presented in this thesis has been carried out at the University of Jyväskylä during two periods, from June 2017 to December 2020 and from January 2022 to December 2022, which also included a research visit to the University of Ottawa, Canada, from January 2019 to July 2019.

First, I would like to thank my supervisor Professor Heikki M. Tuononen for giving me the opportunity to conduct research at the Main Group Chemistry Research Group and as a result, complete this Ph.D. dissertation. I cannot communicate in words how much his support has meant to me. Second, I want to express my deepest gratitude to Academy Research Fellow Dr. Aaron Mailman for his hands-on supervision in the lab throughout my graduate studies. His endless enthusiasm towards chemistry acts as inspiration for everyone who has a chance to work with him. Third, I would like to thank Assistant Professor Jaclyn Brusso for giving me both research challenge and support during my stay at the University of Ottawa. Professor Risto Laitinen and Associate Professor Louise N. Dawe, the two reviewers of this thesis, are sincerely thanked for their time and helpful comments.

During the past five years, I have learnt a great deal not just about chemistry but also about myself. Some days I came home and simply wanted to give up, but the very next morning I decided to try again and see what comes up next. In this context, I want to present my thanks to Nathan Yutronkie. Our discussions about chemistry were invaluable and he made my short visit to the University of Ottawa so much fun. I also wish to acknowledge all the other co-workers that I have had a chance to work with. All of you have taught me many things and even though chemistry did not always go as planned, you made the last five years fly by way too fast.

I want to thank my family, my mom and dad, who have always been there for me and trusted that I do well whatever I decide to pursue in life. My sisters Eeva and Elina, your support has meant a great deal during my studies. I also wish to thank everyone who participated in helping to take care of Kaarlo and Urho during the last year. Without you, this book would not have seen the day of light. Last, I want to thank Mikko for bearing with me and always cheering me up when work was causing stress.

Jyväskylä 17.12.2022
Anni Taponen

LIST OF INCLUDED PUBLICATIONS

(I) Taponen, A. I.; Wong, J. W. L.; Lekin, K.; Assoud, A.; Robertson, C. M.; Lahtinen, M.; Clérac, R.; Tuononen, H. M.; Mailman, A.; Oakley, R. T. Non-Innocent Base Properties of 3- and 4-Pyridyl-Dithia- and Diselenadiazolyl Radicals: The Effect of *N*-Methylation. *Inorganic Chemistry* **2018**, *57* (21), 13901–13911.

(II) Taponen, A. I.; Ayadi, A.; Lahtinen, M. K.; Oyarzabal, I.; Bonhommeau, S.; Rouzières, M.; Mathonière, C.; Tuononen, H. M.; Clérac, R.; Mailman, A. Room-Temperature Magnetic Bistability in a Salt of Organic Radical Ions. *Journal of the American Chemical Society* **2021**, *143* (39), 15912–15917.

(III) Taponen, A. I.; Ayadi, A.; Svahn, N.; Lahtinen, M. K.; Rouzières, M.; Clérac, R.; Tuononen, H. M.; Mailman, A. Role of Alkyl Substituent and Solvent on the Structural, Thermal, and Magnetic Properties of Binary Radical Salts of 1,2,3,5-Dithia- or Diselenadiazolyl Cations and the TCNQ Anion. *Crystal Growth &Design* **2022**, *22* (12) 7110–7122.

(IV) Naik, A.; Taponen, A. I.; Horváth, D.; Ayadi, A.; Svahn, N.; Lahtinen, M. K.; Rouzières, M.; Clérac, R..; Tuononen, H. M.; Mailman, A. Role of Solvent and Counterion on the Formation of Simple, Mixed and Complex Cyanocarbon Salts of 1,2,3,5-Dithiadiazolyl Radical Cation and Thermally Induced Structural Transformations of Their Solvates. *Manuscript in preparation.*

Author's contribution

The author has carried out most of the syntheses and spectroscopic characterizations reported in Papers **II** and **III**, along with those of dithiadiazolyl radicals and mixed and "complex" salts reported in Papers **I** and **IV**. The author also carried out crystallizations of many of the synthetized compounds and participated in the analysis of the collected structural and thermal data throughout the work. In the case of Papers **I** and **II**, the author helped to compile the synthetic and spectroscopic data reported in the publications and in the associated supporting information, and contributed to the revision process in writing. In the case of Papers **III** and **IV**, the author served as the sole and second principal writer of the initial draft and the associated supporting information, respectively, and contributed significantly to the revision process in writing.

FIGURES AND TABLES

CONTENTS

1 INTRODUCTION

Metals have been central in shaping our modern lifestyle. Earth abundant metals, such as iron and copper, are abundant and omnipresent, and humankind has used them since prehistoric times. Over the past decades, using less common metals, such as rare-earth elements, has significantly increased due to the widespread adoption of many high-tech innovations.[1] For example, the single largest and most important end use for rare-earth elements is in manufacturing permanent magnets that are used virtually everywhere from consumer electronics, such as cell phones and tablets, to technologies advancing the green transition, such as electric motors and wind turbines.[2]

Despite their name, rare-earth elements are abundant in the Earth's crust but heavily dispersed.[1] Thus, many are considered critical as they are vital to our modern technologies, but economically exploitable deposits are few and far between, with access to them depending on geopolitical factors.[3] Consequently, strategies to reduce our dependence on primary mineral resources of rare-earth elements have been devised, including usage optimization, recycling, and substitution.

While usage optimization is the simplest strategy and works perfectly in many contexts, it is of limited use when strong small-scale permanent magnets are considered. Rare-earth elements have high magnetic anisotropies and moments, which are difficult to achieve with other metals.[2,4] Conversely, extracting and recycling rare-earth elements from scrap electronics is a more viable and underused route. However, such processes must be economical, scalable, and environmentally friendly to be widely adopted.[5]

The third strategy listed above—material substitution—is the most difficult of the three and presents a major research challenge. Concerning magnetic materials, molecule-based magnets combining the inherent characteristics of molecular and primarily organic compounds to achieve bulk-scale magnetic properties have been of interest since the early 1960s.[6] Although molecule-based magnets are unlikely to completely replace rare-earth elements on permanent magnets any time soon, they hold the potential for many next-generation technological applications as they offer significant benefits over their mostly

metal-based counterparts. Compared to pure metals, metal alloys, and metal oxides, molecular materials are lightweight, soluble to common laboratory solvents, (post)synthetically modifiable, chemically processable, and tunable to be multi-functional.

The key components necessary to achieve a molecule-based magnetic material are spin carriers.[6] In purely organic species, molecular radicals are the sole spin-bearing units, whereas in hybrid metal–organic systems, organic molecules and metal atoms can hold unpaired electrons. These design principles introduce significant drawbacks to organic radical-based magnetic materials as free radicals are often unstable, typically possess only one or two unpaired electrons, and propagate magnetic interactions primarily through weak intermolecular exchange interactions. Collectively, these lead to air- and moisture-sensitivity of many materials using organic radicals as building blocks along with low magnetic moments and magnetic ordering temperatures.

It is clear from the above that the design and synthesis of organic materials with bulk magnetic properties for practical applications is not straightforward. However, one must remember that most things in science are complex and multi-faceted, and the field of molecule-based magnetic materials has matured dramatically since its inception. In 1991, the synthesis and characterization of the β-phase of *para*-nitrophenyl nitronyl nitroxide showed that bulk ferromagnetism can be achieved with an organic, metal-free, species. However, this was realized only at extremely low temperatures.[7] During the last 30 years, progress has been rapid. For example, the recent report on structurally well-defined 1,3,5-triazine-linked porous organic radical frameworks shows that spontaneous room-temperature magnetization with characteristics typical to ferromagnets is possible in an entirely organic setting.[8] The magnetization of the synthetized polymeric material, or "plastic magnet", is yet low. However, as the history of the field allows one to expect, further improvements will be realized in the coming years.

1.1 Aim of the work

The work reported in this thesis revolves around thiazyl radicals: 1,2,3,5-dithiadiazolyls (DTDAs) and their heavier selenium congeners, 1,2,3,5-diselenadiazolyls (DSDAs). Organothiazyl radicals, that is, radicals containing NS unit(s) combined with carbon, have been widely used as building blocks in the field of molecule-based magnetic and other advanced materials.[9] For example, members from this class of free radicals show the highest magnetic ordering temperatures for purely organic molecular systems. Furthermore, many thiazyl radicals display hysteresis and magnetic bistability between a diamagnetic and a paramagnetic state that can even be controlled with external stimuli.

Paper **I** focused on the synthesis of 3- and 4-pyridyl-substituted 1,2,3,5-dithiadiazolylium cations and their selenium analogues in which the pyridyl

nitrogen can function as a base. The cations were reduced to the corresponding neutral DTDA and DSDA radicals, and the basicity of their pyridyl nitrogen was taken use of by alkylation, leading to the synthesis of 4-(*N*-methylpyridinium-3-yl)- and 4-(*N*-methylpyridinium-4-yl)-1,2,3,5-dithiadiazolyl radical-cations as their triflate (trifluoromethanesulfonate) salts, [MepyDTDA][OTf], along with the heavier DSDA analogues.

In Paper **II**, the emphasis was on generating a mixed radical-ion salt coupling the cation $[3\text{-MepyDTDA}]^{+\bullet}$ with the radical-anion obtained from 7,7′,8,8′-tetracyanoquinodimethane (TCNQ). Although much of the motivation behind this study came from the propensity of thiazyl radicals to exhibit ferromagnetic ordering and various charge transfer salts incorporating thiazyl radicals and TCNQ, it was soon realized that the room-temperature hysteretic magnetic bistability observed for [3-MepyDTDA][TCNQ] is a far more interesting phenomenon as it originates from structural changes associated with the TCNQ radical-anions rather than those involving the thiazyl radical-cations.

Papers **III** and **IV** continued the investigations initiated by the characterization of the salt [3-MepyDTDA][TCNQ] and involved the preparation of a series of substituted derivatives of cations $[3\text{-RpyDTDA}]^{+\bullet}$ (R = Me, Et, Pr, or Bu) along with their selenium analogues and their subsequent use in the generation of binary radical-ion salts with TCNQ. In addition to the effects related to the length of the *N*-alkyl substituent, the impact of the crystallization solvent and the counterion to the solid-state structures and magnetic properties of the synthetized salts was thoroughly investigated.

The structure of the thesis is as follows: First, stable organic radicals are briefly described, focusing on historical aspects, factors affecting radical stability, and classes of organic radicals that are most relevant to the topic of the performed research work. Next, the fundamentals of magnetically ordered molecule-based materials are outlined with an emphasis on thiazyl radicals and phenomena such as bulk ferromagnetism, exchange coupling pathways, and magnetic bistability. Last, a summary of the original research and results reported in Papers **I–IV** is presented along with concluding remarks.

2 ORGANIC RADICALS

This chapter focusses on various types of organic radicals and the factors affecting their stability. The idea is not to exhaustively describe all existing classes of radicals but highlight some of the key discoveries in the field over its century of history and introduce the species most relevant to the research reported in Papers **I–IV**. The latter includes thiazyl and selenazyl radicals 1,2,3,5-dithidiazolyls (DTDAs) and 1,2,3,5-diselenadiazolyls (DSDAs), respectively, and the anion radical formed from the quintessential electron acceptor 7,7´,8,8´-tetracyanoquinodimethane (TCNQ). For a more detailed account on the topic, the book *Stable Radicals: Fundamentals and Applied Aspects of Odd-Electron Compounds* is highly recommended and used as the leading reference for most of the following discussions.[10]

2.1 Historical background

At the beginning of the 19th century, knowledge of the structure of organic molecules was advancing rapidly, but targeted synthetic methods were still in their infancy. A chemist named Moses Gomberg had recently succeeded in synthesizing tetraphenylmethane (**1**).[11]. Motivated by the success, he started preparing a closely related system, hexaphenylethane (**2**). Surprisingly, the compound he synthesized did not behave like a saturated hydrocarbon as it readily reacted with air. Gomberg rightly deduced that instead of hexaphenylethane, he had synthesized the triphenylmethyl radical (**3**) that can easily react with air and oxidize to the peroxide (**4**).[12]

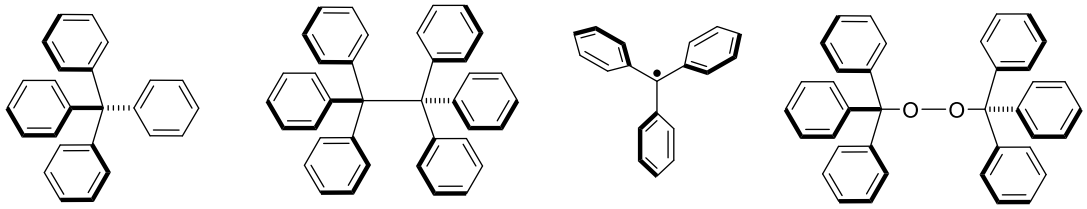

1 2 3 4

Unsurprisingly, tremendous skepticism surrounded Gomberg´s discovery as the structure proposed for **3** defied the fundamental tenet in organic chemistry: carbon is a tetravalent atom and always forms four bonds. The subvalent nature of the central carbon atom in **3** continued to cause suspicion among chemists until another related radical, tris(4-biphenyl)methyl (**5**), was discovered by Wilhelm Schlenk and co-workers in 1910.[13] However, some uncertainty of the exact structure of **3** remained as its isolation by desolvation afforded a solid molecular weight twice that calculated for **3**. Again, Gomberg correctly predicted that in an oxygen-free environment, the radical **3** associates with itself and forms a dimer in the solid state.[12] Without the now commonplace structural characterization techniques, such as single crystal X-ray diffraction, the exact molecular structure of the dimer remained a mystery for almost 70 years until it was finally shown to be the asymmetric quinoid σ-bonded species (**6**).[14]

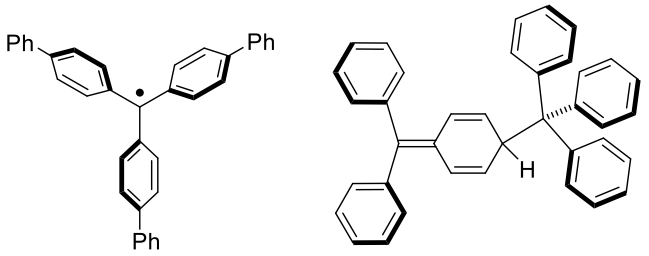

5 6

2.2 Stability of organic radicals

As the chemistry of Gomberg's radical **3** demonstrates,[12] radical species can be reactive and undergo oxidation or dimerization. Other types of reactivity common to radicals are hydrogen abstraction, reduction, or disproportionation.[10] However, under the right conditions, radicals can be stable enough to be detected (persistent) or even isolated (stable). According to these definitions, Gomberg's radical is persistent as it can be detected in an oxygen-free solution, while all attempts at its isolation lead to the formation of the σ-bonded dimer **6**. Adding steric bulk to **3** by chlorination gives the polychlorotriphenylmethyl radical (**7**) that is isolable and stable towards oxygen and σ-dimerization due to the additional kinetic (steric) stabilization that the halogen atoms provide.[15]

In addition to steric protection, organic radicals can be stabilized by delocalizing their spin density over a π-manifold. An illustrative example is the phenalenyl radical (**8**), in which the unpaired electron, while typically drawn localized on the central carbon atom, becomes equally distributed over the six carbon atoms at the α-positions.[16] This not only contributes to thermodynamic stabilization through resonance but also affects further reactivity, such as σ-dimerization, by making C–C bond formation energetically less favorable. Nevertheless, under an inert atmosphere, the phenalenyl radical **8** is only persistent and exists in equilibrium with its σ-dimer in solution. However, further fine-tuning of the steric bulk at the three β-positions, such as by introducing *tert*-butyl substituents (**9**), is all that is required to prevent σ-dimerization *via* α-carbon atoms, making the 2,5,8-tri-*tert*-butyl-phenalenyl radical **9** stable and isolable.[17]

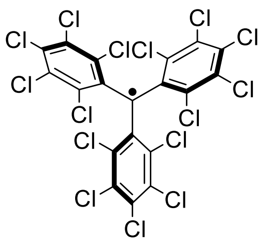

7

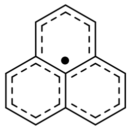

8

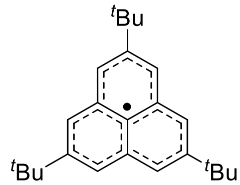

9

In the solid state, many isolable organic radicals, such as **9**, form weakly bound π-dimers in which the unpaired electrons couple antiferromagnetically, which can be expected for p-block radicals with their unpaired electron(s) residing in planar frameworks. This kind of π-type intermolecular interaction between open-shell organic species has been dubbed pancake bonding.[18] It differs greatly from dispersion-type π-stacking of closed-shell molecules by having a covalent-like component arising from the overlap of the singly occupied molecular orbitals (SOMOs) of adjacent radicals, giving rise to a singlet ground state with a varying amount of diradical character. Thus, although closed-shell molecular systems typically show no orientational preference for weak π–π interactions, the cofacial (face-to-face) orientation dominates in the case of *p*-block open-shell species and the intermolecular distances between the nearest radicals in their solid-state structures are often significantly shorter than the sum of the van der Waals radii of the respective elements.

In the examples discussed above, the kinetic and thermodynamic stabilization of radicals occurs independently. However, the two effects can be combined and achieved simultaneously. This can be realized, for example, using electron-donating and/or electron-withdrawing substituents near the unpaired electron that simultaneously introduce steric bulk and tune the electron distribution through conjugative and inductive effects. The synergistic influence of electron-donating and electron-withdrawing substituents is called the captodative effect.[19]

2.3 Heteroatom-based organic radicals

An efficient way to stabilize organic radicals is to introduce heteroatoms, especially N, O, and S, on the spin-bearing position(s) because the corresponding N–N, O–O, and S–S σ-bonds are all significantly weaker than a C–C bond, translating to a reduced tendency of the radicals to form σ-dimers. Based on similar arguments, the stability of heteroatom-based radicals towards molecular oxygen is often better than that of carbon-centered radicals. However, the atom E's identity does not significantly affect the E–H bond energy. Thus, heteroatom-based radicals are prone to hydrogen abstraction unless other means are used to stabilize them.

Phenoxyls are among the simplest oxygen-based radicals. The resonance structures drawn for the parent phenoxyl radical (**10**) suggest a significant amount of spin density at the *ortho*- and *para*-positions. In agreement with this notion, phenoxyls without substituents at these locations typically have limited stability. A particularly noteworthy and stable member of this group of radicals is galvinoxyl (**11**) that is one of the few commercially available organic compounds with unpaired electrons.[20] It is often used as a radical scavenger or a probe to study the mechanisms of radical reactions.[21]

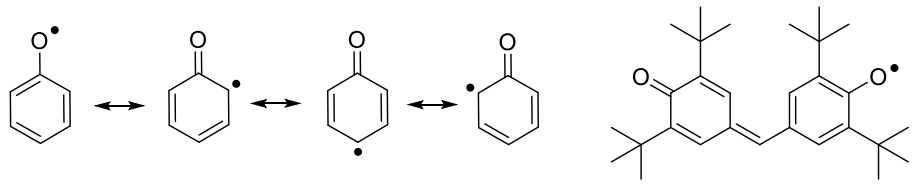

10 **11**

Hydrazyl radicals (**12**) have nitrogen as the primary spin-bearing atom. Most simple hydrazyls are persistent with limited stability, the most notable exception being *N*,*N*-diphenyl-*N*′-picrylhydrazyl (DPPH, **13**) that is stable and commercially available[22] and used as an EPR standard, a radical scavenger, and an indicator.[23] Removing only one of the three electron-withdrawing nitro groups in **13** is enough to disturb the balance and make the resulting radical persistent.

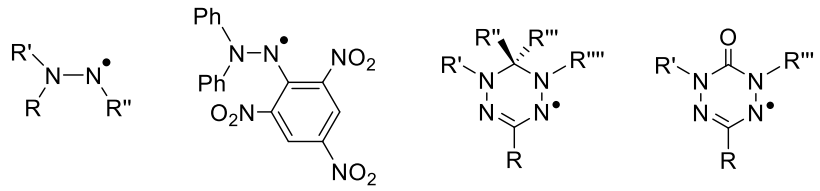

12 **13** **14** **15**

Verdazyls (**14**) and oxo-verdazyls (**15**) are radicals that effectively contain two hydrazyl subunits incorporated into a conjugated π-framework offering significant resonance stabilization.[24,25] These radicals have been extensively

explored because of their excellent stability. Most verdazyls are isolable and can be handled and stored indefinitely without decomposition, allowing their use as spin-bearing ligands in coordination chemistry, the denticity of the ligand depending on its substituents and the coordination sphere of the metal.[26]

The combination of nitrogen and oxygen has given rise to numerous nitroxide (aminoxyl) radicals with one or many NO functionalities. The nitroxide group (**16**) can be described with two resonance forms in which the unpaired electron is on the nitrogen or the oxygen atom, the latter having a slight preference over the former. Many substituted nitroxides are stable and do not react with oxygen or water or undergo other reactions typical to radicals, such as dimerization. One of the most well-known members of this group of radicals is (2,2,6,6-tetramethylpiperidin-1-yl)oxyl (**17**), or TEMPO,[27] in which the four methyl groups sterically protect the unpaired electron. TEMPO is commercially available and has applications in many areas, including spin labeling, spin trapping, and catalysis.[28] Nitronyl nitroxides (**18**) are another class of well-known nitroxide radicals with *para*-nitrophenyl nitronyl nitroxide being the most famous example.[7] As mentioned in the introduction, it was the first organic radical to display bulk ferromagnetism, albeit only at temperatures below 0.65 K.

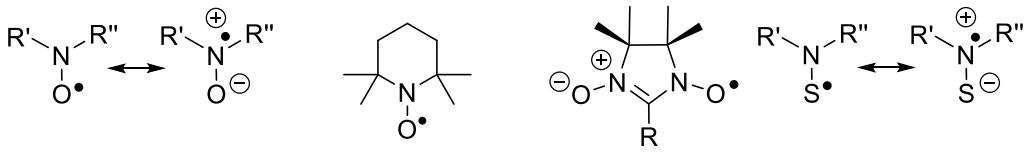

16 **17** **18** **19**

One could think substituting oxygen with sulfur in nitroxides to generate the corresponding thionitroxides (**19**) is simple. However, the electronegativity of sulfur is much less than that of oxygen, completely reversing the charge polarization in the NS functionality compared to the NO, and affecting the stability of thionitroxides.[29] Thus, thionitroxides have their unpaired electron mostly localized on the sulfur atom and are prone to form σ-dimers. However, the S–S bond energy is rather low, and the dimers readily dissociate to monomers in solution, especially at elevated temperatures.

Although thionitroxides are not the most stable organic heteroatom radicals, the thiazyl unit (NS) is common in radical chemistry. Eugène-Anatole Demarçay prepared the first thiazyl-based radical (**20**) as early as 1880,[30] but its structural determination by X-ray crystallography was reported almost a century later in 1974.[31] Despite the great interest the metallic and superconducting properties of poly(thiazyl), $(SN)_x$,[32] aroused, many binary sulfur-nitrogen compounds are sensitive to heat, friction, and shock and decompose violently to S_8 and N_2, which are thermodynamically much more stable species. Demarçay acquired firsthand experience of the sensitivity of these compounds, losing his eye in one of the accidents. Consequently, organothiazyl radicals in which the NS unit(s) is(are) combined with carbon have been put to the fore due to their greater stability and synthetic accessibility.[9]

Many different classes of organothiazyl radicals exists of which cyclic 1,2,3,5- (**21**) and 1,3,2,4-dithiadiazolyls (DTDAs) (**22**) and 1,2,3- (**23**) and 1,3,2-dithiazolyls (**24**) (DTAs) are among the most common.[9] Despite the apparent similarities in their structures, the properties of DTDA and DTA radicals, such as their EPR hyperfine coupling constants, redox potentials, and π-dimerization enthalpies are, in fact, vastly different and depend on the exact isomer in question through the morphologies of their SOMOs. Furthermore, while both isomers of DTAs are stable, 1,3,2,4-DTDAs undergo thermal and photochemical rearrangement to the corresponding 1,2,3,5 isomers. Perhaps the most notable member of organothiazyl radicals is *para*-cyano-tetrafluorophenyl-dithiadiazolyl, whose β-polymorph exhibits a spontaneous magnetic moment below 35.5 K, the highest magnetic ordering temperature known for any neutral organic radical.[33]

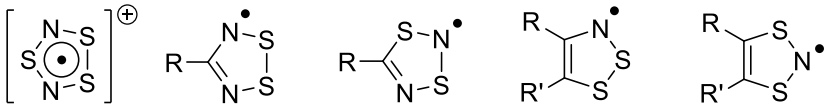

20 **21** **22** **23** **24**

2.3.1 1,2,3,5-Dithiadiazolyls (DTDAs)

The first 1,2,3,5-dithiadiazolium cation was reported in 1977 as its chloride salt,[34] while its reduction to the corresponding radical was achieved shortly after in 1982.[35] The early synthetic route to 1,2,3,5-dithiadiazolium cations employed a reaction between thiazyl chloride (N≡S–Cl), obtained by heating trithiazyl trichloride ($(SNCl)_3$) and a suitable nitrile (R–C≡N) to form the respective 1,2,3,5-dithiadiazolium chloride in low to moderate yields (Figure 1a).[34] Another synthetic route (Figure 1b) uses the reaction between sulfur dichloride (SCl_2) and an amidine ($RC(NH)NH_2$) or an amidinium chloride ($[RC(NH_2)NH_2]Cl$).[36] The yield of this reaction can be improved using a persilylated amidine (Figure 1c).[37] The last route is the preferred method for synthesizing many 1,2,3,5-dithiadiazolium chlorides (**25**), which can then be reduced directly to the corresponding neutral radicals.

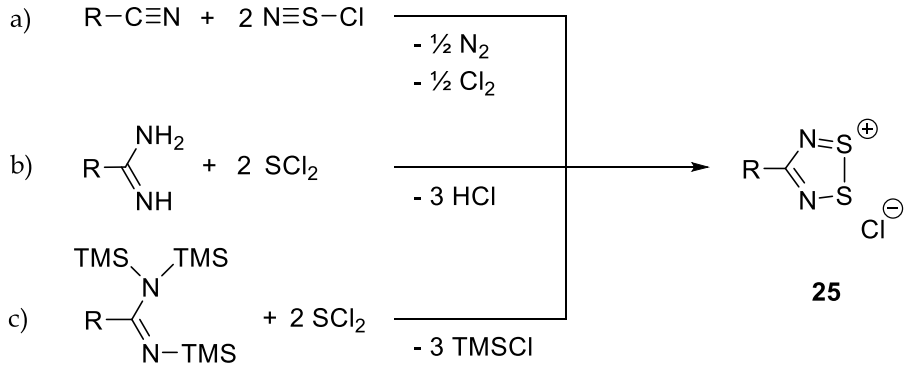

Figure 1. Synthetic routes to 1,2,3,5-dithiadiazolium cations as their chloride salts (**25**).

The SOMO of 1,2,3,5-dithiadiazolyl radicals (Figure 2) is a π*-orbital and, therefore, antibonding regarding S–N and S–S bonds. It is also characterized by a node at the carbon atom. Consequently, the key electronic properties of 1,2,3,5-dithiadiazolyls, such as their EPR hyperfine coupling constants and oxidation/reduction potentials, vary relatively little regarding the identity of the substituent R unless strongly electron withdrawing or donating groups are used. Nevertheless, the electronic and steric properties of the substituent R are significant in determining the association of the 1,2,3,5-dithiadiazolyl radicals in the solution and the solid state.

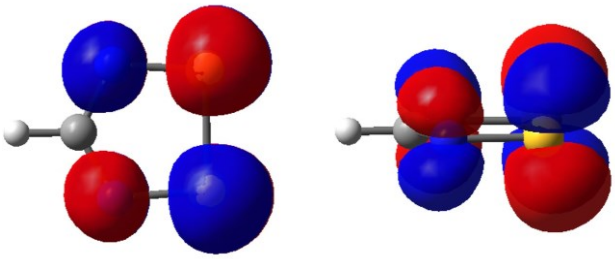

Figure 2. The SOMO of a parent DTDA radical visualized from two orientations.

Although 1,2,3,5-dithiadiazolyls avoid σ-dimerization, they typically form π-dimers in the solid state. Several dimerization modes have been structurally characterized (Figure 3) that all involve the SOMO···SOMO overlap of adjacent radicals.[38] The *cis*-cofacial mode (Figure 3a) with superimposed DTDA radicals is the most common and is frequently observed for molecules with small, structurally simple, or planar substituents R (for example, **26**[39] and **27**[40]). There are two *trans*-type dimerization modes in which the substituents R point to the opposite directions: *trans*-cofacial (Figure 3b) in which the DTDA rings are superimposed and *trans*-antarafacial (Figure 3c) in which the DTDA radicals interact solely through the sulfur atoms. These dimerization modes are often observed for radicals with sterically bulkier substituents R (for example, *trans*-cofacial for **28**[41] and **29**,[42] and *trans*-antarafacial for **30**[43] and **31**[44]). The fourth dimerization mode is a variation of the *cis*-cofacial structure with the two DTDA rings rotated by approximately 90° with respect to each other (Figure 3d). Such a twisted-cofacial structure is commonly observed with small, structurally simple substituents R (for example, **32**[45] and **33**)[46] that, nevertheless, prohibit *cis*-cofacial dimers from forming. The fifth dimerization mode differs markedly from all others as it involves DTDA radicals not parallel but orthogonal to one another (Figure 3e). Thus far, these edge-to-face dimers have been observed in only one instance (**34**) and even in that case, the second crystallographically independent dimer in the structure associates in *cis*-cofacial manner.[47]

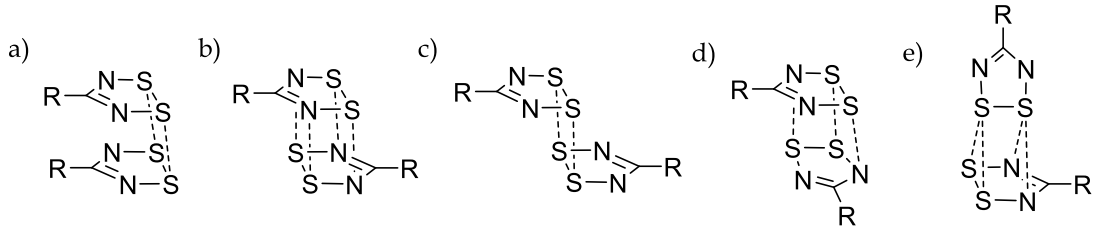

Figure 3. Different dimerization modes of DTDA radicals: a) *cis*-cofacial, b) *trans*-cofacial, c) *trans*-antarafacial, d) twisted-cofacial, and e) orthogonal.

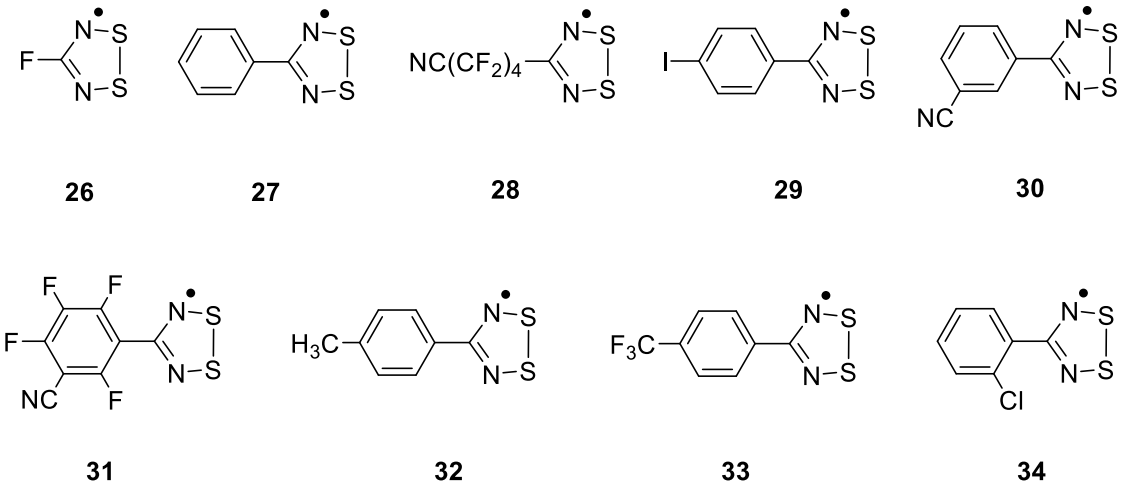

For a few simple derivatives of **21**, the dimerization has been studied using variable temperature EPR spectroscopy.[48–50] The determined dimerization enthalpy is largely independent of the R group and at around −35 kJ mol^{-1}, comparable to a strong hydrogen bond. Thus, it is easy to understand that monomeric DTDA radicals are preferred in solutions at elevated temperatures, whereas most DTDAs tend to dimerize in the solid state. Although the steric bulk of the substituent R often determines whether the radicals form *cis* or *trans* dimers, no simple correlation exists between the identity of the substituent R and the observed dimerization mode. This is further emphasized by the fact that some of the structurally simplest DTDA radicals (for example, **35**) exhibit polymorphism and readily form solids that exist in two or more crystalline forms with different association modes observed in different phases.[39,51,52] Moreover, for some DTDA derivatives (for example, **34**),[47] more than one association mode can be observed in a single solid-state structure, illustrating the fine energetic balance among different types of dimers. Nevertheless, when using substituents with a large enough steric bulk to induce a twist between the heterocyclic ring and the aryl substituent R (for example, **36**)[53] or employing aryl substituents R that can form strong and directional noncovalent interactions, such as halogen bonds, (for example, **37**),[54] π-dimerization of DTDA radicals can be prevented in the solid state. Using crystal engineering strategies in controlling the solid-state association of DTDA radicals has been thoroughly examined and reviewed.[38]

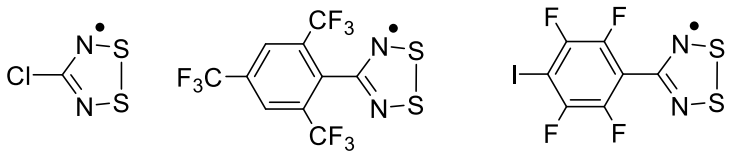

35 **36** **37**

2.3.2 1,2,3,5-Diselenadiazolyls (DSDAs)

The selenium analogues of DTDA radicals, the 1,2,3,5-diselenadiazolyls (DSDAs), have received less attention than their lighter congeners, with the first example reported in 1989.[55] The most common synthetic route to the DSDA ring proceeds *via* cyclocondensation between a persilylated amidine and *in situ* prepared $SeCl_2$ to produce 1,2,3,5-diselenadiazolium chloride, which can then be reduced to the corresponding DSDA radical (analogous to the route c) in Figure 1).

The properties of DSDA radicals are largely like those of DTDAs and need not be repeated herein. However, the increased spin density at selenium in DSDAs, compared to sulfur in DTDAs, leads to a stronger interaction between adjacent DSDA radicals and, therefore, to π-dimers that dissociate less easily to monomers.[56] Consequently, although structurally characterized examples of DSDA radicals with various dimerization modes exist, the *cis*-cofacial structure is by far the most common, with only a few isolated examples of other modes shown in Figure 3. Furthermore, only one instance exists of a DSDA radical that does not form π-dimers in the solid state.[57] Also, the orthogonal edge-to-face dimerization mode differs slightly between DSDA and DTDA radicals as the Se–Se "edge" is not parallel but perpendicular to the Se–Se bond in the "face" (Figure 3e).[56,58] Interestingly, the two structurally characterized examples of orthogonal DSDA dimers do not readily dissociate into monomers at higher temperatures, contrasting the behavior observed for the related DTDA system.[47] This supports the above notion of stronger radical···radical interactions between DSDAs compared to DTDAs. The structural properties of a series of DSDA radicals with perfluoroaryl substituents have recently been determined, compared to, and contrasted with the corresponding DTDAs.[56]

2.3.3 7,7′,8,8′-Tetracyanoquinodimethane (TCNQ)

The quintessential electron acceptor 7,7′,8,8′-tetracyanoquinodimethane (**38**), commonly abbreviated TCNQ, was first synthesized in 1962.[59] It was soon realized that **38** could readily accept an electron to afford a radical-anion (**39**) that is stable towards aerial oxidation but susceptible to hydrolysis.[60,61] The radical **39** can accept one more electron to form a closed-shell dianion (**40**) that readily oxidizes upon exposure to air.

TCNQ can act as a versatile non-chelating polydentate ligand towards metals.[62] Collectively, the three different charge states, the ability to coordinate in σ- (through nitrogen atoms) or π-fashion (through carbon atoms), and the propensity of forming π-stacks give rise to a plethora of oligonuclear metal

complexes and coordination polymers involving TCNQ. More relevant to the topic of this thesis are, however, various charge transfer complexes in which TCNQ acts as an electron acceptor.[63] Arguably, the best-known of such compounds is the one with tetrathiafulvalene (TTF, **41**) as the electron donor.[64]

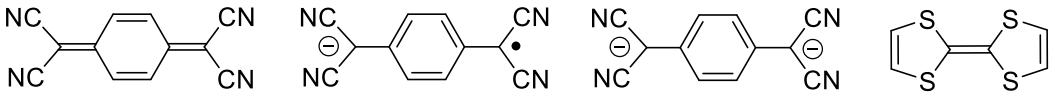

38 **39** **40** **41**

The solid-state structure of the charge transfer complex TTF–TCNQ consists of separate parallel 1-D π-stacks of TTF and TCNQ units (Figure 4).[65] As there is an incomplete electron transfer from all donors to acceptors, partially filled conduction bands arise, and the compound displays metal-like electrical conductivity. Thus, TTF–TCNQ was the first-ever reported "organic metal". However, at sufficiently low temperatures, the segregated and equidistant columnar stacks undergo independent Peierls transitions (at 38 and 54 K for TTF and TCNQ stacks, respectively), and the compound becomes an insulator.[66]

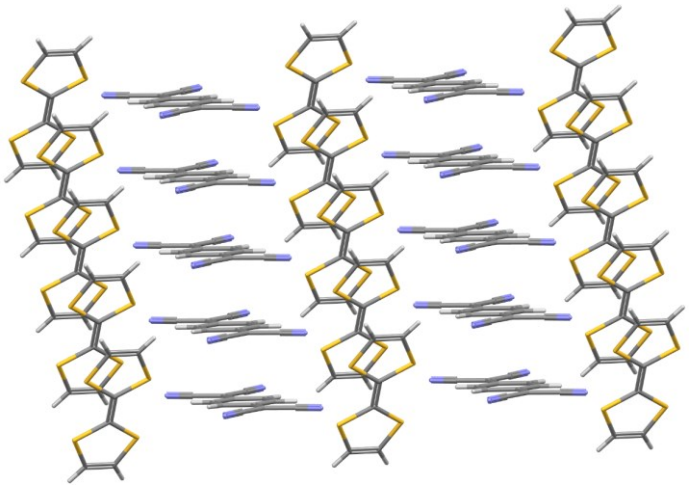

Figure 4. Illustration of the solid-state structure of TTF–TCNQ, consisting of separate parallel 1-D π-stacks of TTF and TCNQ.

Thiazyl radicals have also been explored as electron donors in charge transfer complexes with TCNQ. The first of such species was with a benzo-1,3,2-dithiazolyl radical (**42**).[67] The structure of this compound was eventually found to be analogous to TTF–TCNQ, albeit with a vastly different conductivity.[68] Several charge transfer complexes based on the DTDA framework have also been reported, but none contains TCNQ as the anionic component. Of these, the iodine complexes of 1,2,3,5-dithiadiazolyl-based diradicals are the most numerous, with several systems displaying interesting conductive properties.[69] The only example of a conductive charge transfer complex incorporating a DTDA monoradical is that of the parent species of **21** (R = H) with iodine.[70]

Evenly spaced π-stacks of TCNQ radical-anions **39** do not readily form in the solid state. Instead, radicals **39** typically associate to form antiferromagnetically coupled eclipsed- or non-eclipsed-cofacial π-dimers $(TCNQ)_2^{2-}$ (Figures 5a and 5b, respectively). A comprehensive study on the potential energy landscape of **39** has shown that the former geometry involves a transversal offset of around 1.0 Å, while a longitudinal offset of approximately 2.1 Å characterizes the latter.[71] In addition to association *via* π-stacking, TCNQ radical-anions **39** are known to form C–C bonded σ-dimers in the solid state (Figure 5c). While there are several examples of metal salts of TCNQ with this structural unit, only two solid-state structures of organic charge transfer complexes of TCNQ are known to contain σ-dimers of the anion radical.[72,73]

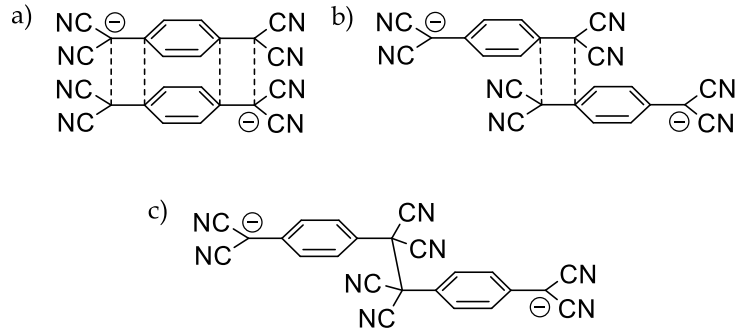

Figure 5. Different dimerization modes of TCNQ radical-anions: a) eclipsed-cofacial, b) non-eclipsed-cofacial, and c) σ-dimer.

Charge transfer complexes of TCNQ can be further classified based on the charge state(s) of the TCNQ units, as detailed in a detailed account on crystal structures containing TCNQ in various guises.[74] In "simple" salts, the charge state of TCNQ is 0 or −1, or two monoanions form a dianionic dimer $(TCNQ)_2^{2-}$, as described above. In "complex" salts, the charge states of different TCNQ units are less well-defined and can form, for example, monoanionic π-dimers $(TCNQ)_2^{\bullet-}$ (formally a heterodimer between a neutral TCNQ and a TCNQ radical-anion), dianionic π-trimers $(TCNQ)_3^{2-}$ (formally a trimer of a neutral TCNQ and two TCNQ radical-anions), or other less symmetrical and more complex combinations. In many cases, the charge state of different TCNQ units in "complex" salts can be deduced from high-quality structural data, IR and Raman spectra, and theoretical calculations.

The factors determining the association mode and charge state of TCNQ units in their "simple" and "complex" salts are necessarily complicated. The available structural data is far from being systematic in this respect, and very few generalizations of the effect of the cation have, for example, been made.[74] An illustrative example of how small substituent-based changes in the cation can significantly affect the solid-state structure and, therefore, the properties of TCNQ charge transfer complexes is offered by compounds incorporating *N*-alkylated phenazinium (PHN) cations. The methyl derivative (**43**) yields two different structures with TCNQ: one that is analogous to TTF–TCNQ,[75] although

with significantly reduced conductivity, and another that is a "complex" salt with a formula [Me-PHN]$_2$[(TCNQ)$_3$].[76] Lengthening the *N*-alkyl chain in the PHN ion by a single carbon atom (**44**) leads to the "simple" salt [Et-PHN][TCNQ] in which the TCNQ units form C–C bonded σ-dimers,[72] whereas the propyl derivative (**45**) forms a "complex" salt with TCNQ with a formula [Pr-PHN]$_2$[(TCNQ)$_3$].[77] Finally, the derivative with the longest butyl chain (**46**) gives the "simple salt" [Bu-PHN][TCNQ] in which the TCNQ units associate to non-eclipsed-cofacial π-dimers.[78]

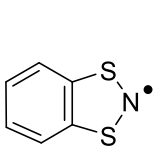

42

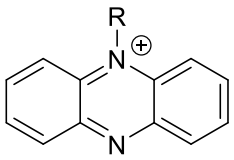

43 R = Me **45** R = Pr
44 R = Et **46** R = Bu

3 MATERIALS BASED ON MAGNETIC PROPERTIES OF ORGANIC RADICALS

This chapter focuses on magnetic materials built from organic radicals with a focus on systems based on thiazyls. First, an overview of organic ferro- and ferrimagnets is given to highlight early achievements and some of the latest developments in the field. Next, the connection between magnetic exchange interactions and ferromagnetic ordering is discussed to illustrate the challenges in achieving bulk ferromagnetism solely with organic radicals. Last, the magnetic bistability phenomena is briefly described in the context of organic radicals.

3.1 Organic ferro- and ferrimagnets

Unpaired electrons and their spins are essential for any magnetic material as their exchange interactions determine the magnetic properties of the material.[6] In the solid state, materials composed of organic radicals with no interactions between their spins (magnetic moments) are paramagnetic, meaning their spins are isolated and thermally randomized (Figure 6a). When the temperature is lowered, the interaction energy between the spins can become greater than the thermal energy responsible for their randomization, allowing magnetic ordering to occur, leading to ferromagnetic materials with perfectly aligned spins (Figure 6b) or antiferromagnetic materials with perfectly opposed spins (Figure 6c). The temperature at which the ordering occurs is called the Curie (T_C) or Néel (T_N) temperature for ferromagnetic and antiferromagnetic materials, respectively.

In some antiferromagnetically ordered materials, competing isotropic and antisymmetric exchange effects can lead to spin canting, that is, to a situation in which the spins are not perfectly opposed but slightly tilted, giving rise to a net magnetic moment (Figure 6d). Such materials are called canted antiferromagnets or weak ferromagnets. Furthermore, if an antiferromagnetically ordered material has two different spin sites, a net magnetic moment arises in instances where complete cancellation cannot occur. These kinds of materials are called

ferrimagnetic (Figure 6e). Although the diamagnetism arising from the orbital motions of electrons appears in all materials, its implications are negligible compared to the effects arising from the spins of the unpaired electrons.

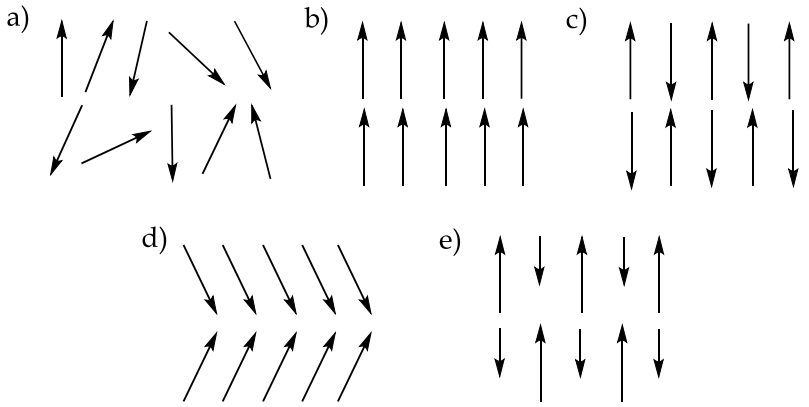

Figure 6. Schematic 2-D representations of the alignment of individual spins (magnetic moments) in a) paramagnetic, b) ferromagnetic, c) antiferromagnetic, d) canted antiferromagnetic, and e) ferrimagnetic material.

All materials exhibit some type of magnetism, and magnetic materials can be classified according to their bulk magnetic susceptibility (χ), which is a measure of how easy it is to align the electron spins with an external magnetic field. The induced magnetic moment is proportional to the applied field, with χ being the proportionality constant, that is, the ratio of magnetization (M) to the intensity of the field (H). The variation of magnetic susceptibility with temperature is described in Figure 7 for paramagnetic, ferromagnetic, and antiferromagnetic materials. As paramagnetic materials are cooled, more spins become aligned as thermal motion is reduced, and the magnetic susceptibility

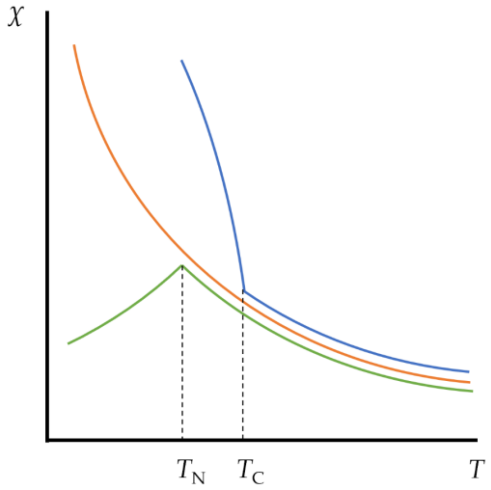

Figure 7. Illustration of the temperature (T) dependence of magnetic susceptibility (χ) of a) paramagnetic (orange), b) ferromagnetic (blue), and c) antiferromagnetic (green) materials. The two discontinuity points denote the locations of Curie (T_C) and Néel (T_N) temperatures.

increases. If the material remains paramagnetic upon lowering the temperature, the magnetic susceptibility continues to increase steadily (Figure 7, orange curve). However, as discussed above, if the interaction energy between the spins overcomes randomization arising from the available thermal energy, the magnetic susceptibility can either increase (Figure 7, blue curve) or decrease rapidly (Figure 7, green curve) depending on if the spins couple to a perfectly aligned or opposing orientation, respectively. The discontinuity points in the blue and green curves in Figure 7 occur at the temperatures at which the ordering occurs.

In 1928, Heisenberg argued that metal atoms with a principal quantum number higher than 3, that is, elements with d- or f-orbital sets, were required to achieve sufficiently strong exchange interactions so that bulk ferromagnetic ordering could arise.[79] However, Heisenberg's analysis focused entirely on atomic lattices built from metals and noted that principal quantum number 2 might suffice. Nevertheless, the possibility of ferromagnetism with organic molecules having their spins at p-type orbitals was not significantly researched before the early 1960s. At that time, it was suggested that certain free radicals become ferromagnetic at sufficiently low temperatures, as the reported magnetic data seemed to indicate.[80] Some of these claims were later found to be based on impure samples, but the question of achieving ferromagnetic ordering and bulk ferromagnetism using only organic radicals was nevertheless considered.[81]

Strong ferromagnetic coupling of organic radicals was first observed for galvinoxyl (**11**) in 1967, but the compound does not order ferromagnetically at cryogenic temperatures.[82] Consequently, it took another 20 years of research before the first ferromagnetically ordered organic radical, the β-phase of *para*-nitrophenyl nitronyl nitroxide (**47**), was characterized in the bulk phase in 1991.[7] Later that year, the α-phase of the charge transfer salt between tetrakis(dimethylamino)ethylene (TDAE) and fullerene, formally [TDAE][C_{60}] (**48**), was shown to be a canted antiferromagnet at temperatures below 16.1 K.[83] The first and only reported example of an organic ferrimagnet is the mixed nitronyl nitroxide/nitroxide triradical (**49**) that displays a bulk magnetic order below 0.3 K.[84]

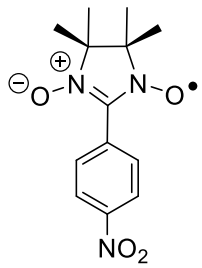

47

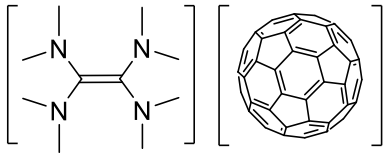

48

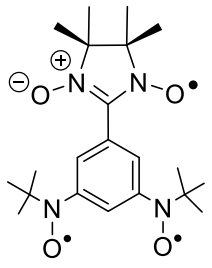

49

More aligned with the research topic presented herein are ferromagnetically ordered thiazyl radicals, of which there are many examples. The first one to be reported was the β-phase of *para*-cyano-tetrafluorophenyl-

dithiadiazolyl (**50**),[33] published in 1996, that is a canted antiferromagnet at temperatures below 35.5 K. The ordering temperature can be increased to 65.4 K by increasing the external pressure to 16 kbar, albeit with a suppressed magnetic moment.[85] Despite intense investigations over the past 25 years, compound **50** remains the record holder even today, meaning it has the highest magnetic ordering temperature for any organic radical known.

The first thiazyl radical to display true ferromagnetic ordering was *para*-nitro-tetrafluorophenyl-dithiadiazolyl (**51**) described in 2003.[86] Along with the diradical *N*,*N*'-dioxy-1,3,5,7-tetramethyl-2,6-diazaadamantane (**52**),[87] it represented a rare example of a neutral organic radical with a ferromagnetic ordering temperature above 1 K. In this context, the tetrachlorogallate salt of a cationic benzo-bridged bis(1,3,2-dithiazolyl) radical (**53**) had been reported a year before with an ordering temperature of 6.7 K and transition to a ferromagnetic state driven by the solvent evaporation at reduced pressure.[88] The related hybrid system between **53** and tetrachloroferrate is ferrimagnetic below 44.0 K.[89]

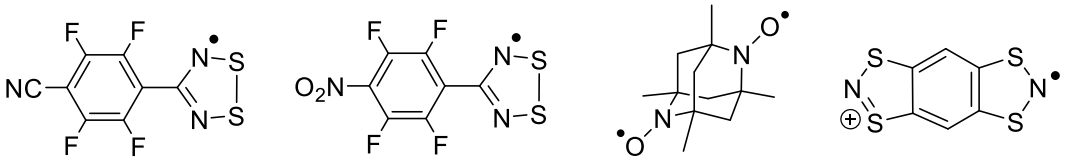

50 **51** **52** **53**

The family of radicals based on a semiquinone-bridged bis(1,2,3-dithiazole) structure (**54**) contains several examples of systems that are canted antiferromagnets at cryogenic temperatures with ordering temperatures up to 35.0 K, meaning very close to the value reported for **50**.[90–93] The related pyridine-bridged frameworks incorporating two or four selenium atoms (**55–58**) are even more spectacular as many of them are bulk ferromagnets with ordering temperatures as high as 17.0 K. [94–97] It is safe to say the bis(1,2,3-dithiazole) radical family is one of the most exciting among all organic radicals regarding magnetic properties.

Although less aligned with the topic of this thesis, two of the early landmarks from the field of molecule-based magnetic materials incorporating organic radicals and metal atoms should be mentioned. The charge transfer salt between decamethylferrocene and tetracyanoethylene (TCNE), $[Fe(C_5Me_5)_2][TCNE]$ (**59**),[98] was the first metal-organic molecular magnet with a ferromagnetic ordering temperature of 4.8 K. Its characterization was reported in 1987, preceding the synthesis of the first ferromagnetically ordered purely organic species by only a few years. Progress with molecule-based magnetic materials employing metals and radicals has also been faster than their purely organic counterparts. In 1991, a material with an approximate composition $V(TCNE)_2 \cdot ½\ CH_2Cl_2$ (**60**) was found to be a room-temperature ferrimagnet with an ordering temperature above 400 K,[99] setting the bar high for all further developments in the field of molecule-based magnetic materials.

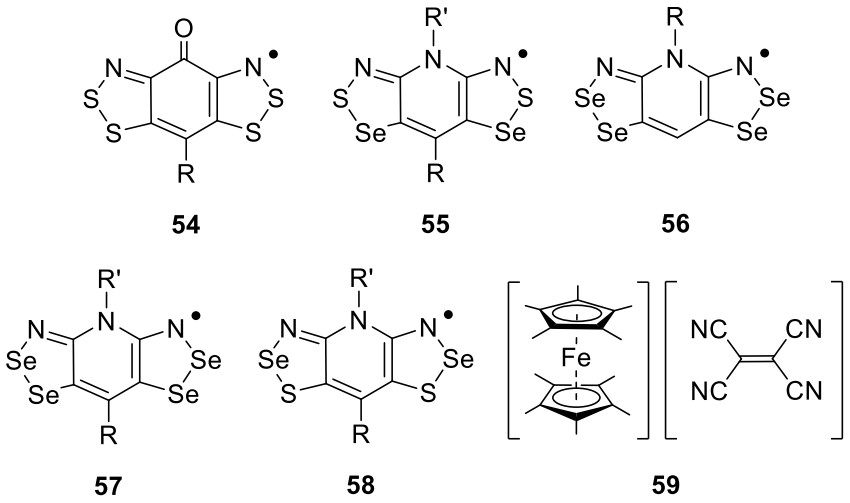

54 **55** **56**

57 **58** **59**

3.2 Magnetic exchange interactions and ferromagnetic ordering

As the previous chapter described, several stable radical frameworks have been reported since the synthesis of Gomberg's triphenylmethyl in 1900. However, using these building blocks to form crystalline solids that display long-range magnetic ordering of spins remains a formidable challenge, as exemplified by the limited number of organic radicals that are bulk ferromagnets at low temperatures.

In systems comprised solely of molecular radicals, ferromagnetic coupling of spins generally requires the SOMOs of the interacting radicals to have large amplitudes in the same spatial region (to ensure sufficient exchange interaction between spins) but remain orthogonal to each other (to prevent spin pairing).[100] Thus, the direct exchange dominates all other effects, and the ferromagnetic ordering of spins is typically achieved when the supramolecular arrangement of radicals leads to an appropriate exchange between their unpaired electrons and these interactions are propagated throughout the crystal lattice *via* intermolecular contacts.[101] Such situations of accidental orthogonality are difficult to achieve by design, let alone control, as even minor modifications to steric and electronic properties of radicals often lead to their dimerization or complete isolation, which are detrimental to the propagation of ferromagnetic coupling.

An analysis of the solid-state crystal structures of some known organic ferromagnetic materials clearly illustrates the challenge these systems pose to crystal engineering. For example, *para*-nitrophenyl nitronyl nitroxide **47** exists in four different polymorphic forms, α, β, δ, and γ, of which only one, the β-form, becomes a bulk ferromagnet at extremely low temperatures.[102] The ferromagnetic polymorph is the most stable of the four, and it is rather striking that its solid-state structure shows no strong electrostatic interactions, namely hydrogen bonds, between the radicals although most of the spin density is on the nitronyl nitroxide moiety and the terminal nitro group.[7] Theoretical analyses have revealed that two of the three dominant exchange pathways are

ferromagnetic in this system and involve very weak interactions linking the molecules within the crystallographic *ac*-plane and between adjacent *ac*-planes, generating a 3-D network required for the bulk magnetic behavior to arise.[102]

Unlike the more complex solid-state energy landscape of **47**, *para*-cyano-tetrafluorophenyl-dithiadiazolyl **50** forms only two polymorphs, α- and β,[33,103] of which each can be made by careful control of the exact sublimation conditions. Both phases are composed of parallel linear 1-D chains in which the radicals connect in head-to-tail fashion *via* $CN^{\delta-}\cdots S^{\delta+}$ interactions that can be characterized as chalcogen bonds (Figure 8). The most obvious structural difference between the phases is the relative orientation of the 2-D sheets formed from the 1-D chains. In the β-phase, the sheets pack on one another in a parallel fashion,[33] whereas their relative orientation is anti-parallel in the α-phase.[103] Thus, different 3-D networks are formed, and only the one observed in the structure of the β-polymorph leads to the long-range ordering of spins at low temperatures. The ordering in **50** is antiferromagnetic, but the alignment of spins in the structure is canted, creating a net magnetic moment. Detailed investigations of the crystal structure of the β-phase have shown that systematic twisting of the heterocyclic ring occurs at elevated pressures along with the shortening of intermolecular $S^{\delta+}\cdots N^{\delta-}$ contacts between atoms from the DTDA rings at adjacent planes.[85] These interactions are crucial for propagating the exchange interaction in the β-phase of **50** and in the case of para-nitro-tetrafluorophenyl-dithiadiazolyl **51**, which orders ferromagnetically.[86] Weak intermolecular $S^{\delta+}\cdots N^{\delta-}$ interactions are a recurring theme in the solid-state structures of DTDAs, and their importance as a structure-directing feature has been carefully analyzed.[104]

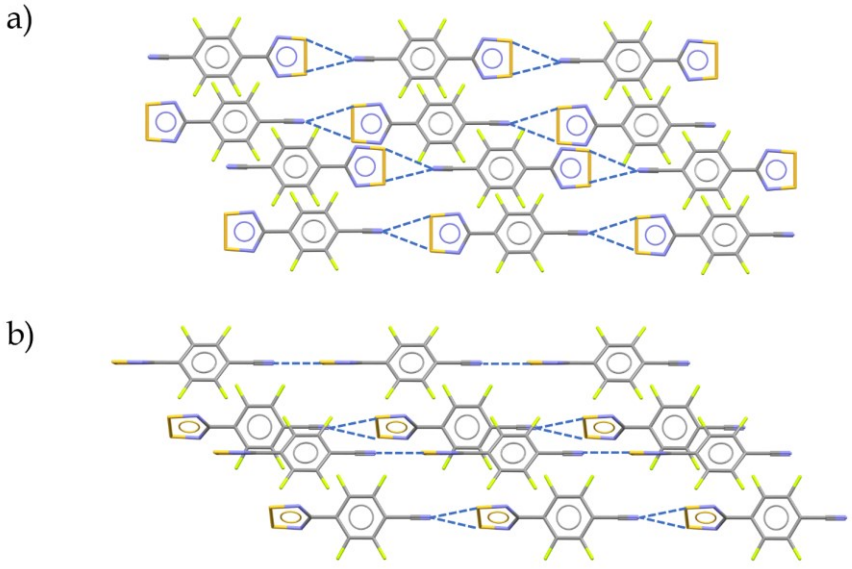

Figure 8. Illustration of the solid-state structures of a) α- and b) β-polymorphs of *para*-cyano-tetrafluorophenyl-dithiadiazolyl **50** showing the anti-parallel and parallel orientation of the 2-D sheets, respectively. Intermolecular $CN^{\delta-}\cdots S^{\delta+}$ interactions have been highlighted with blue dashed lines.

Based on the two examples described above, achieving (ferro)magnetic ordering with systems comprised of molecular, effectively 0-dimensional, subunits requires complete fulfillment of the "Goldilocks' principle": all factors that play a role in achieving the desired structure and, thereby, the properties must be "just right". Naturally, this feat is complicated, and radicals **50** and **51** remain the only DTDAs showing long-range magnetic ordering despite the numerous derivatives synthetized over the years. Furthermore, even the simplest structural modifications can sometimes have unexpected consequences, as the heavier DSDA congeners demonstrate. Although an atom-to-atom replacement of sulfur with selenium could be expected to lead to favorable changes in magnetic properties owing to the increased size of the heteroatom along with the enhancement of spin-orbit effects,[105] the relatively high tendency of DSDAs to dimerize has thus far prevented the observation of monomeric radicals in the solid state in all but one instance.[57]

The large amount of experimental and computational data available on the various bis(1,2,3-dithiazole) radicals and their heavier selenium-containing variants **54–58** have provided insight into the relationship between structure (slippage of π-stacked planes) and properties (nature of magnetic exchange interaction).[90–97] While these analyses allow identifying the relative orientations of the radicals leading to enhanced ferromagnetic coupling, the realization of the corresponding structural modifications in practice using crystal engineering is virtually impossible as no possibilities exist to modify solid-state structures with such fine precision. A conceptually different approach to attain ferromagnetic coupling and long-range ordering with organic radicals is to use strict orthogonality,[101] originally discussed in the context of transition metal ions, although this approach comes with its difficulties.

Strict orthogonality can be achieved with organic radicals if their interacting SOMOs have morphologies that differ from one another by having different symmetry properties, which can ensure orthogonality when the radicals arrange in the solid state to form stacks.[106] Thus, more than one type of functional building block must be present in the crystal lattice requiring cocrystals of neutral radicals. Herein lies the difficulty with this approach as the cocrystallization of pre-selected radicals is neither straightforward nor does it ensure the desired stacking and SOMO···SOMO interactions occur as the resulting ferromagnetic coupling typically gives no energetic gain over other alternative association modes. Hence, while the cocrystallization of different radicals can significantly help achieve ferromagnetic coupling, crystal engineering strategies are nevertheless required to direct the arrangement of the radicals in the solid state.

Cocrystallization has been heavily exploited in pharmaceutical research to alter the physicochemical properties of drugs, such as their bioavailability, solubility, mechanical or thermal durability, and, consequently, better shelf life.[107] The first examples of cocrystals of organic radicals date back to the early 1990s and employed nitronyl niroxides.[108,109] While many other examples of cocrystallized neural organic radicals have since been reported, the investigated systems use building blocks with qualitatively similar SOMOs, and practical

exploitation of the strict orthogonality condition has yet to occur. Regarding thiazyl radicals, the solid-state structures of cocrystals of the phenyl-substituted DTDA radical **27** and its perfluorinated analogue (**61**) or the related pyridyl species (**62**) have been reported.[110,111] The crystals were obtained by using co-sublimation and solution methods and in both cases the radicals were found to form mixed *cis*-cofacial dimers in the solid state. In another two recent cocrystallization studies, several DTDA radicals with perhalogenated phenyl substituents were cocrystallized with TEMPO **17**.[112,113] The solid-state structures of these species contain *cis*-cofacial dimers of DTDAs that form strong $S^{\delta+}\cdots O^{\delta-}$ interactions with TEMPO. These studies also report the first cocrystal between DTDA and DTA radicals. The motivation behind these investigations was not to achieve systems with strict orthogonality of SOMOs but the possibility of obtaining long-range antiferromagnetic exchange between unpaired electrons with highly dissimilar *g*-factors and, consequently, ferrimagnetism.

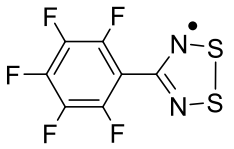

61

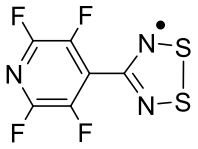

62

3.3 Organic radicals and magnetic bistability

Molecular bistability, the property of a molecular system to evolve from one stable electronic state to another in a reversible fashion within applying a certain perturbation, has raised considerable interest over the years.[114] Perhaps the most famous manifestation of bistability, known since the early 1930s, is the spin-crossover phenomenon that typically occurs in first row transition metal complexes with an octahedral metal ion in d^4 to d^7 configuration.[115] The spin-state of these compounds can be reversibly changed *via* external stimuli, such as temperature, pressure, or light, inducing changes to structural, magnetic, and/or optical properties of the system. If the spin-crossover phenomenon is accompanied by hysteresis, a lag in the (magnetic) response of the compound to the perturbation, the two possible spin states can exist under the same external conditions, with the exact state in question depending on how the system was perturbed. Thus, hysteretic systems possess intrinsic "memory". Provided that the hysteresis loop, known as the bistability window, is wide enough and centered around room temperature, the memory effect allows spin-crossover materials to find use in practical applications in molecular spintronics, for example, as switches or information storage devices.[116]

In addition to spin-crossover systems, magnetic bistability and hysteresis can be observed for other systems, such as organic radicals. In the case of radicals, magnetic bistability typically involves the coexistence of two solid-state

structures over a certain temperature range: a paramagnetic (high-temperature) state (S = ½) consisting of essentially non-interacting, monomeric radicals and a diamagnetic (low-temperature) state (S = 0) formed by radical dimers.[117]. Recently, hysteretic magnetic bistability was observed in a discrete organic radical with two different singlet states (**63**).[118]

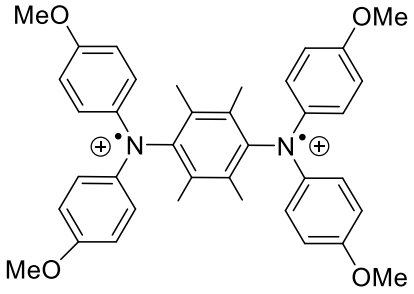

63

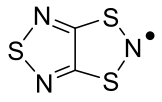

64

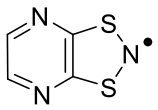

65

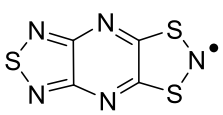

66

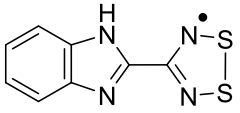

67

Hysteretic magnetic bistability has been observed for several types of organic radicals including phenalenyl-,[119] nitroxyl-,[120] and thiazyl-based frameworks, of which different thiazyls have the greatest number of characterized examples (for example, **64–66**).[121–123] This is largely due to the negligible π-dimerization enthalpies of DTA radicals that allow easy conversion between monomeric and dimeric states, although bistability in these systems can involve S–S or N–N σ-bond formation.[124,125] A prototypical thiazyl radical showing bistability is 1,3,5-trithia-2,4,6-triazapentalenyl (TTTA) **64** that has a large hysteresis loop from $T_{c\downarrow}$ = 230 to $T_{c\uparrow}$ = 305 K (ΔT_c = 75 K) (Figure 9).[121] Furthermore, spin state changes in **64** can be induced by light, and the position of the hysteresis loop on the temperature scale can be adjusted by changing the external pressure.[126,127]

Magnetic bistability is a much less frequent phenomenon for DTDAs than DTAs. Currently, 4-(2′-benzimidazolyl)-1,2,3,5-dithiadiazolyl (**67**) is the only example of a DTDA radical showing bistability and hysteresis in the solid state,[128] although related solid-to-liquid transitions have been reported for other derivatives.[41,49,129–131] In **67**, the low-temperature diamagnetic phase consists of *trans*-cofacial π-dimers of DTDA radicals, whereas the paramagnetic high-temperature phase contains effectively monomeric radicals, which, however, remain associated with each other *via* hydrogen bonds and other weak interactions (Figure 10). Thus, a cooperative network of intermolecular interactions linking the radicals allows the observed first-order phase transition to occur, resulting in the two states with a rather narrow hysteresis loop (ΔT_c = 7 K) with a midpoint at 270 K, that is, close to room temperature.

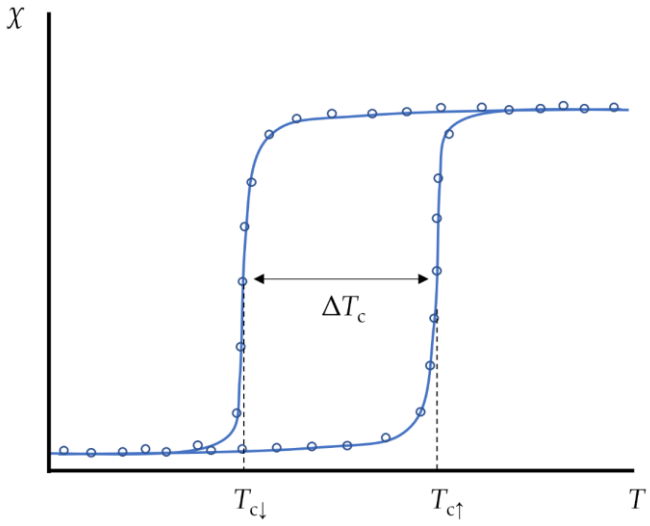

Figure 9. Illustration of the temperature (T) dependence of magnetic susceptibility (χ) for a magnetically bistable organic radical showing a hysteresis loop. The critical points of the two curves (T_c) define the width of the loop (ΔT_c) in the temperature scale.

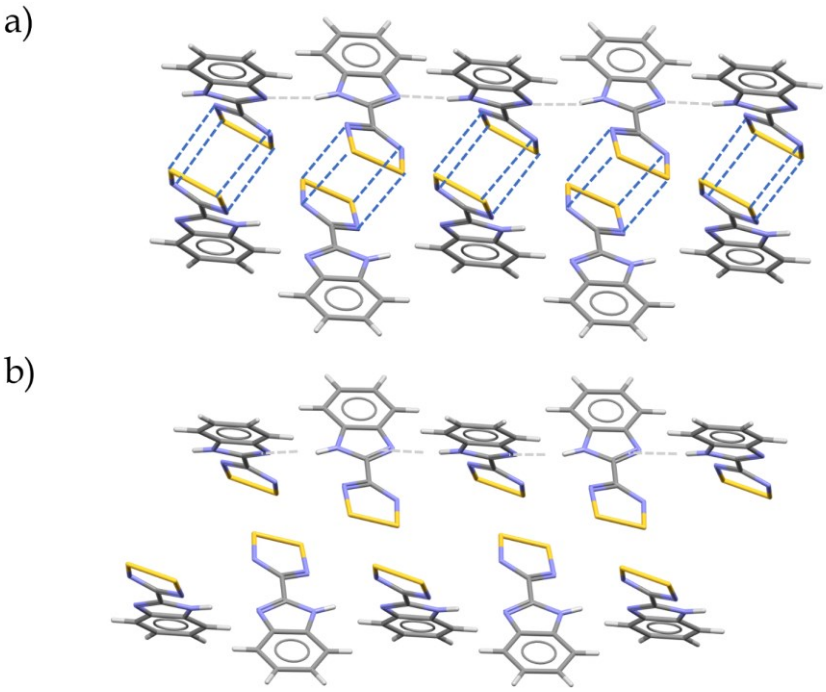

Figure 10. Illustration of the solid-state structure of the DTDA radical **67** at a) 100 K and b) 300 K. Intermolecular hydrogen bonds and π-type interactions in the *trans*-cofacial DTDA dimers have been highlighted with gray and blue dashed lines, respectively.

4 RESULTS AND DISCUSSION

The birth of the research project leading to the present thesis was in the realization that there is a dearth of information on 3- and 4-pyridyl substituted DTDA and DSDA radicals, although the corresponding 2-pyridyl derivatives are well-known and used as chelating ligands. Consequently, a synthetic venture towards these radicals was initiated to take further advantage of the target frameworks in achieving *N*-alkylpyridinium-substituted DTDA and DSDA radical-cations through alkylation. This could be accomplished with only minor modifications to the well-established synthetic protocol for DTDA and DSDA radicals.

Once the desired radicals were at hand, they could be used as building blocks for synthesizing systems with potentially interesting properties. As the previous chapters discussed, many attractive paths could have been followed, but the chosen journey began with combining the radical-cations with the TCNQ radical-anion. There were many reasons behind this choice. First, DTDAs and TCNQ have been used as components in charge transfer complexes but never simultaneously. Second, the cyano groups of TCNQ and the Ch–Ch (Ch = S, Se) unit of the DTDA/DSDA ring form highly directional $Ch^{\delta+}\cdots N^{\delta-}$ interactions that could lock the ions into ribbons and other well-defined 2-D and 3-D structures in the solid state. Third, the potential energy landscapes of DTDAs/DSDAs and TCNQ are complex and can influence one another so that monomeric radicals, their σ- or π-dimers, or even infinite stacks can be realized in the solid state, offering the means to achieve functionality through structural changes.

The chosen investigations led to the characterization of a twofold single-crystal-to-single-crystal transformation involving monomeric TCNQ radical-anions, their σ- and π-dimers, and the associated room-temperature hysteretic magnetic bistability in a two-component system. Consequently, a broader study probing different factors affecting the structure and properties of the synthetized salt was conducted to obtain insight into a new type of multicomponent functional molecular material. In the following, a summary of the most important results published in Papers **I–IV** is presented.

4.1 Neutral pyridyl-substituted DTDA and DSDA radicals

The synthetic sequence to neutral pyridyl-substituted DTDA radicals 3-pyDTDA (**68**) and 4-pyDTDA (**69**) followed the pathway described in Figure 1c. Specifically, a reaction between 3- or 4-cyanopyridine and lithium bis(trimethylsilyl)amide ($LiN(TMS)_2{\cdot}Et_2O$) in THF gave a lithiated amidinate intermediate that could be reacted with TMSCl to afford the corresponding persilylated amidine (Figure 11, step i). In the next step, the persilylated amidine was reacted with S_2Cl_2, giving the moisture-sensitive double salts $[HpyDTDA][Cl]_2$ due to the combination of a basic nitrogen atom in the pyridyl substituent with excess S_2Cl_2 (Figure 11, step ii). The double salts were then reduced with triphenylantimony ($SbPh_3$) to give [HpyDTDA]Cl in MeCN (Figure 11, step iii), from which the desired neutral radicals could be liberated by treatment with triethylamine (Et_3N) (Figure 11, step iv). As a last step, the radicals **68** and **69** were purified by fractional sublimation.

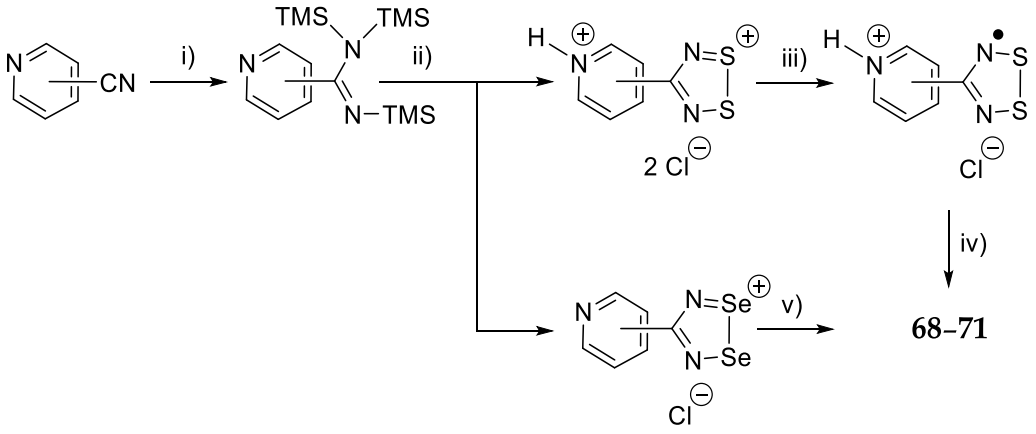

Figure 11. Synthetic routes to 3- or 4-pyridyl-substituted DTDAs (**68** and **69**) and DSDAs (**70** and **71**). Reagents used: i) $LiN(TMS)_2{\cdot}Et_2O$ and TMSCl; ii) excess S_2Cl_2 or a quantitative amount of $SeCl_2$; iii) $SbPh_3$/[$BzEt_3N$]Cl; iv) Et_3N; v) $SbPh_3$.

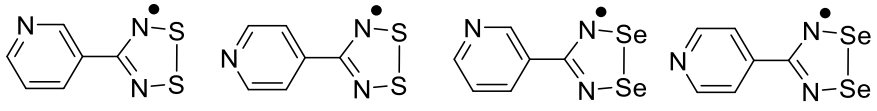

68 **69** **70** **71**

The syntheses of the DSDA radicals **70** and **71** were more straightforward than their sulfur analogues as using stoichiometric amounts of *in situ* formed $SeCl_2$ (comproportionation of Se and $SeCl_4$) completely avoided the formation of adventitious HCl and, thereby, the double salts (Figure 11, step ii). Subsequent reduction of the chloride salts thus formed with $SbPh_3$ (Figure 11, step v) led to the selenium-containing radicals **70** and **71** that were purified by fractional sublimation.

Single crystals suitable for X-ray diffraction studies could be grown from radicals **68**, **70**, and **71**. Conversely, compound **69** formed powdery nodules, but its powder X-ray diffraction pattern could be indexed, and the data modeled, giving a plausible solution similar to the structure of **71**. In all four cases, the radicals form *cis*-cofacial π-dimers in the solid state, further organizing to layers of head-to-tail 1-D ribbons through intermolecular $S^{\delta+}\cdots N^{\delta-}$ interactions. Depending on the identity of the pyridyl substituent, the ribbons are linear (**69** and **71**) or zigzag-shaped (**68** and **70**), which also affect how they stack on each other in layers (head-over-tail in **69** and **71** and head-over-head in **68** and **70**). Full details of the synthesis and characterization of **68–71** are provided in Paper **I**.

4.2 Triflate salts of *N*-alkylpyridinium-substituted DTDA and DSDA radical-cations

The synthetic sequence leading to neutral radicals **68–71** (Figure 11) was modified to obtain their cationic *N*-alkylated analogues as their triflate salts (**72–79**). This took place by treating the persilylated amidines with an alkyl triflate (ROTf; R = Me, Et, Pr, or Bu) before cyclocondensation with S_2Cl_2 or $SeCl_2$ (Figure 12, steps i and ii). The cyclocondensation yielded double chloride salts of the desired dications, which were converted to more soluble triflates by metathesis (Figure 12, step iii). Finally, a reduction with potassium iodide (KI) or tetrabutylammonium iodide ([NBu_4]I) gave iodide salts of the target radical-cations (Figure 12, step iv), which were, again, converted to corresponding triflates by metathesis (Figure 12, step v). The compounds **72–79** were purified by repeated recrystallizations from suitable solvents.

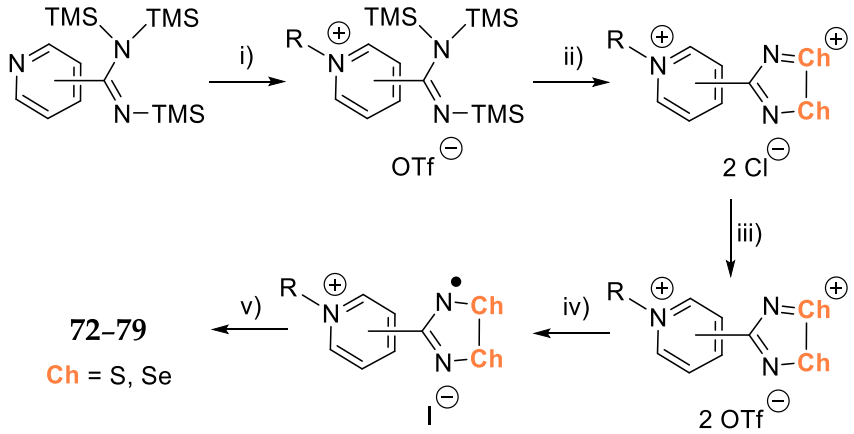

Figure 12. General synthetic sequence leading to the salts **72–79**. Reagents used: i) ROTf (R = Me, Et, Pr, or Bu); ii) excess S_2Cl_2 or quantitative amount of $SeCl_2$; iii) TMSOTf; iv) KI/[NBu_4]I; v) Ag[OTf].

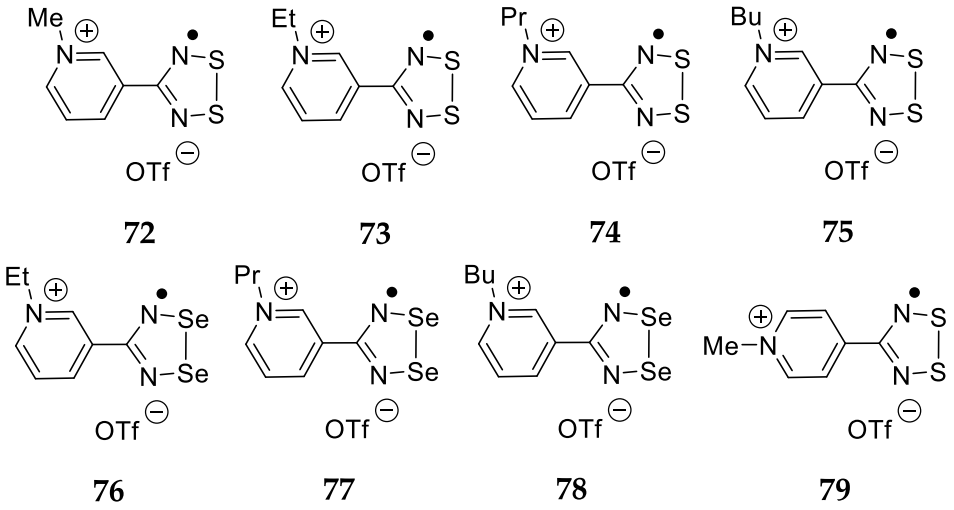

Single crystals suitable for X-ray diffraction studies could be grown from all salts **72–79**, showing strong ion-paring and *trans*-cofacial association mode between the radicals in all but one case, **75**, which displays rare twisted-cofacial π-dimers (Figure 13). Irrespective of the dimerization mode, the π-dimers pack in the solid state to head-over-tail stacks. Interestingly, a second polymorph of **72** could also be obtained, which shows DTDA dimers in twisted-cofacial and *trans*-cofacial geometries. Full details of the synthesis and characterization of **72–79** are provided in Papers **I–IV**.

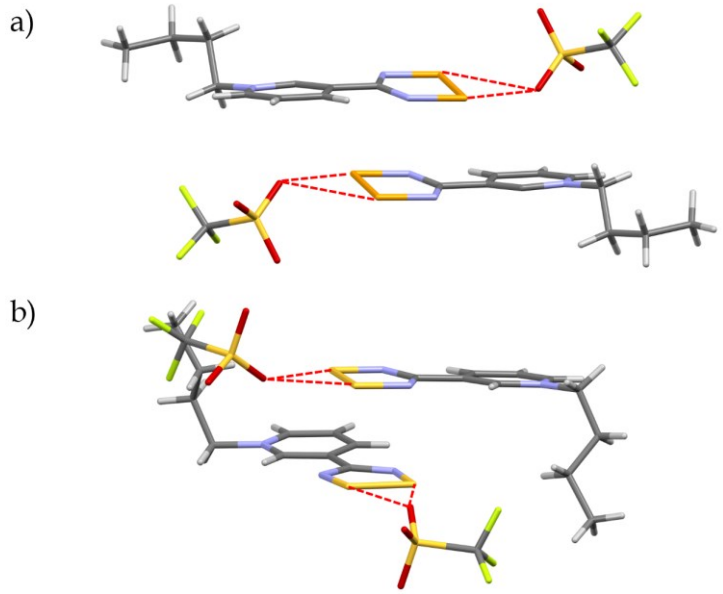

Figure 13. Illustrations of a) *trans*-cofacial and b) twisted-cofacial dimers of DTDA and DSDA radical-cations in **78** and **75**, respectively. Intermolecular $S^{\delta+}\cdots O^{\delta-}$ and $Se^{\delta+}\cdots O^{\delta-}$ interactions have been highlighted with red dashed lines.

4.3 "Simple" TCNQ salts of *N*-alkylpyridinium-substituted DTDA and DSDA radical-cations

4.3.1 Magnetic bistability in [3-Mepy-DTDA][OTf]

The *N*-methylated derivative [3-Mepy-DTDA][OTf] **72** was reported early on in Paper **I** and was among the first salts subjected to a double-displacement reaction with [K(18c6)][TCNQ] (**80**). Crystallizing the product from acetonitrile (MeCN) or propionitrile (EtCN) with slow diffusion afforded the solvates [3-Mepy-DTDA][TCNQ] · MeCN (**81 · MeCN**) and [3-Mepy-DTDA][TCNQ] · EtCN (**81 · EtCN**) as analytically pure solids. Single crystal X-ray structural studies showed that the solvates are isostructural (triclinic $P\bar{1}$) and contain *trans*-cofacial dimers of the DTDA radical-cation and eclipsed-cofacial π-dimers of the TCNQ radical-anion (Figure 14a). The cations are linked to solvent molecules *via* $CN^{\delta-}\cdots S^{\delta+}$ interactions, and the ions generate repeating π-stacked $A^{+}–A^{+}\cdots B^{-}–B^{-}$ motifs with hydrogen bonding between the out-of-register neighboring stacks.

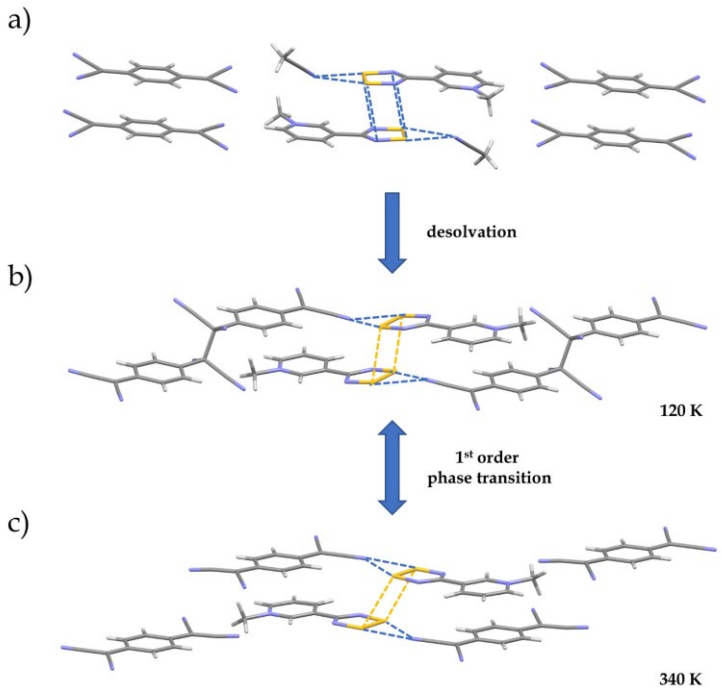

Figure 14. Illustrations of solid-state structures of a) **81 · MeCN** and b) low- and c) high-temperature phases of **81**. Intermolecular $S^{\delta+}\cdots N^{\delta-}$ and $S^{\delta+}\cdots S^{\delta+}$ interactions have been highlighted with blue and orange dashed lines, respectively.

Thermogravimetric analyses conducted for crystalline samples of the solvates **81 · MeCN** and **81 · EtCN** indicated that a loss of lattice solvent occurs at 396 and 365 K, respectively. Subsequent magnetic susceptibility measurements showed a sudden increase in the χT product around the same temperatures, indicating the formation of a paramagnetic phase. Remarkably, the χT product

did not follow the same track upon cooling, and an abrupt decrease was recorded below 270 and 290 K for MeCN and EtCN solvate, respectively (Figure 15). Successive heating and cooling cycles revealed a reversible hysteretic response of the magnetic susceptibility near room temperature, consistent with a first-order phase transition in **81 · MeCN** and **81 · EtCN**.

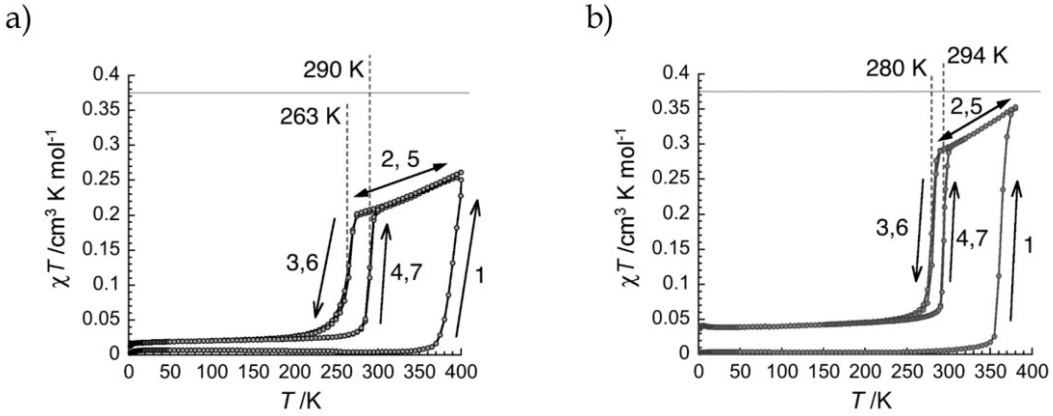

Figure 15. Temperature dependence of the χT product of neat samples of a) **81 · MeCN** and b) **81 · EtCN**. Steps: 1) desolvation upon heating, 2) and 3) cooling, 4) and 5) heating, and 6) and 7) additional cooling/heating. The gray line indicates the expected χT value for an S = ½ and g = 2 Curie paramagnet.

Heating of a crystalline sample of **81 · EtCN** *in vacuo* over 48 h resulted in complete loss of lattice solvent and formation of [3-Mepy-DTDA][TCNQ] (**81**), as evidenced by X-ray crystallography (monoclinic $P2_1/n$). Further crystallographic studies confirmed the existence of two phases: a low-temperature diamagnetic phase and a high-temperature paramagnetic phase. The structure of the low-temperature phase of **81** contains *trans*-antarafacial dimers of DTDA radical-cations (S···S´ distance of 3.184 (1) Å) and σ-dimers of TCNQ radical-anions (C–C bond of 1.656 (8) Å). The ions form zigzag-shaped chains *via* intermolecular $CN^{\delta-}\cdots S^{\delta+}$ interactions (2.841(4) and 2.879(4) Å) and adopt a chevron motif (Figure 14b). The high-temperature phase of **81** shows the layered zigzag chains and the chevron packing are largely maintained (Figure 14c), but the S···S contacts (3.2626(7) Å) in *trans*-antarafacial dimers of DTDA radical-cations have elongated significantly, leading to simultaneous slipping of the TCNQ radical-anions and, consequently, to the breakup of the C–C bond, in agreement with the observed paramagnetism.

Powder X-ray diffraction data collected for the solvates **81 · MeCN** and **81 · EtCN** at various temperatures showed that the bulk phases are equivalent to the corresponding single-crystal structures and can be desolvated to **81** by heating, although traces of solvated material remain present. The magnetothermal behavior of non-solvated **81** was consistent with the measurements performed on the solvates after the initial heating cycle, showing that it exhibits reversible hysteretic magnetic bistability at room temperature. The enthalpy of change associated with this process was estimated to be approximately 7 kJ mol^{-1} using differential scanning calorimetry. Full details of the synthesis and

characterization of the solvates **81 · MeCN** and **81 · EtCN** and the non-solvate **81** are provided in Paper **II**.

4.3.2 Syntheses and solid-state structures

The twofold single-crystal-to-single-crystal transformation observed for the solvates **81 · MeCN** and **81 · EtCN**, and the room-temperature magnetic bistability exhibited by the non-solvate **81** provided the impetus for a thorough investigation on the influence of the *N*-alkyl substituent R and the crystallization solvent to the solid-state structures and magnetic properties of the salts with a formula [3-RpyDTDA][TCNQ] · n Solv (**82–84**; R = Et, Pr, or Bu; Solv = MeCN or EtCN; n = 0, 0.5, or 1). The effect of the identity of the chalcogen atom was probed by preparing the selenium analogues [3-RpyDSDA][TCNQ] · n MeCN (**85–87**; R = Et, Pr, or Bu; n = 0 or 1), although the low solubility of the DSDA radical-cations to EtCN limited the scope of experiments.

Slow diffusion of [K(18c6)][TCNQ] into **73–75** or **76–78** resulted in the crystallization of TCNQ salts of the target DTDA and DSDA radicals, respectively, as analytically pure solvate or non-solvate solids as illustrated in Figure 16. All solvates were found to be isostructural with **81 · MeCN** and **81 · EtCN** (Figure 14a) except for [3-Bupy-DTDA][TCNQ] · 0.5 MeCN (**84 · 0.5 MeCN**), which differs from all others by having an asymmetric unit with a cation:anion:solvent ratio of 2:2:1. Consequently, the solvent molecules present in the crystal lattice of **84 · 0.5 MeCN** are not interacting with the DTDA ring *via* intermolecular $CN^{\delta-}\cdots S^{\delta+}$ interactions but are disordered and embedded between the *N*-butyl chains with which they form weak C–H···N hydrogen bonds. A plausible explanation for the observed change in structure is the steric bulk and flexibility of the butyl chain, also visible in the increased structural disorder, which leads to a different cation:anion:solvent ratio and altogether different packing of the molecular constituents in the solid state.

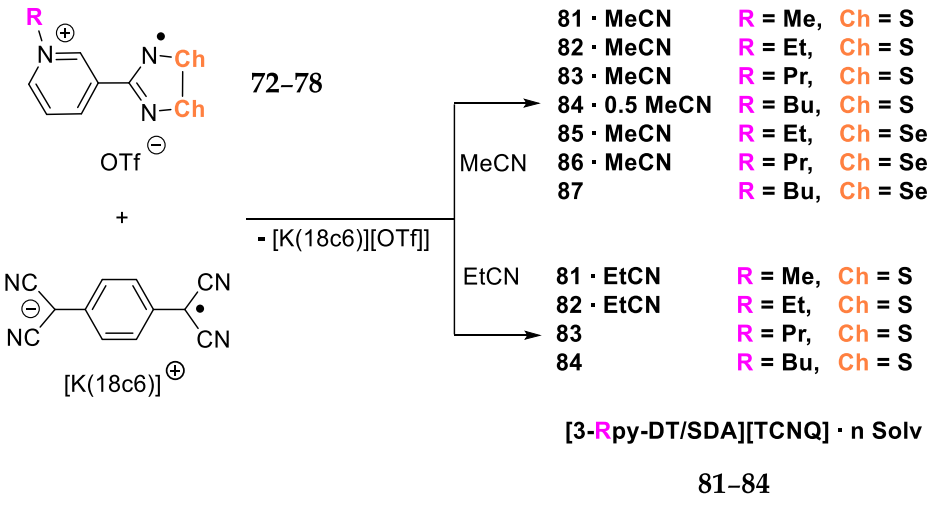

Figure 16. Radical-ion salts **81–87** obtained from double-displacement reaction of **72–78** with [K(18c6)[TCNQ] in MeCN or EtCN.

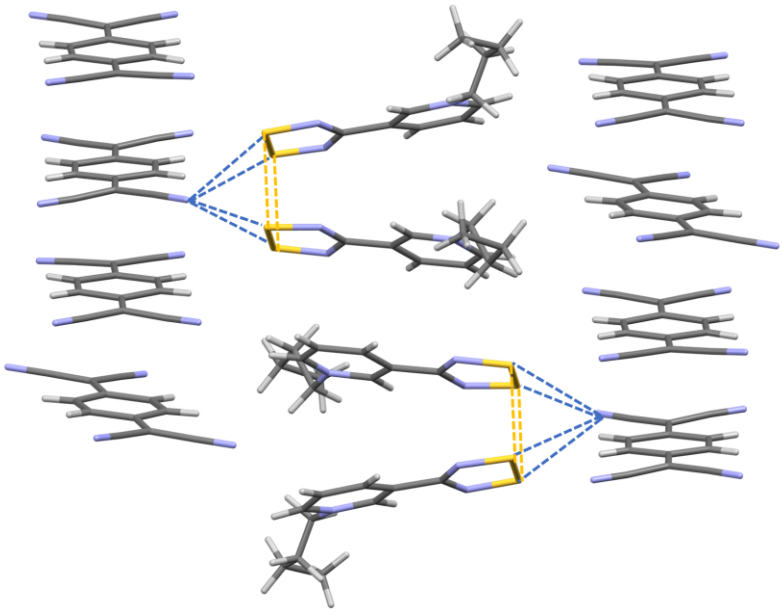

Figure 17. Illustration of the solid-state structure of **84 · 0.5 MeCN** with disordered solvent molecules hidden. Key intermolecular $S^{\delta+}\cdots N^{\delta-}$ and $S^{\delta+}\cdots S^{\delta+}$ interactions have been highlighted with blue and orange dashed lines, respectively.

The crystal structure of **84 · 0.5 MeCN** (triclinic $P\bar{1}$, Figure 17) shows that the DTDA radical-cations are arranged to *cis*-cofacial dimers forming A^+–$A^+\cdots A^+$–A^+ stacks with head-over-tail orientation of the dimeric subunits. The intradimer S···S distances are almost identical (2.984(7) and 2.946(8) Å) and within typical range. The cations are significantly wedged from coplanarity (tilt angle of 12°), presumably owing to the steric demand of the butyl substituents. The TCNQ radical-anions form π-dimers with non-eclipsed-cofacial geometry that generate almost evenly spaced staircase-like B^-–$B^-\cdots B^-$–B^- stacks. The neighboring radicals are not perfectly aligned along the stacking direction, but every fourth radical is rotated perpendicular to the stack, owing to the alignment of one of the nitrile groups in the space between two *N*-butylpyridinium substituents. Similar columnar structures, though rare, have been encountered in crown ether complexes of alkali metal salts of TCNQ.[132]

The performed double displacement reactions led to three non-solvate structures **83**, **84**, and **87** (Figure 16). These results agreed with the expectation that the tendency to obtain non-solvates increases with the length of the *N*-alkyl substituents and the size of the crystallization solvent. Although not explicitly highlighted in Figure 16, small amounts of non-solvated **84** crystallized together with **84 · 0.5 MeCN**. The crystals could be separated by hand and their structures determined using single crystal X-ray diffraction. This suggests only a minor energetic preference for the formation of the solvate over the corresponding non-solvate under the employed crystallization conditions.

The crystal structure of the non-solvated *N*-propyl derivative **83** (triclinic $P\bar{1}$) shows *trans*-cofacial DTDA dimers, which organize to A^+–$A^+\cdots A^+$–A^+ stacks with head-over-tail orientation of the dimeric subunits (Figure 18). The TCNQ

radical-anions have formed non-eclipsed-cofacial dimers that generate staircase-like B^{-}–B^{-}···B^{-}–B^{-} stacking motifs. The different stacks are connected *via* intermolecular $CN^{\delta-}$···$S^{\delta+}$ interactions (2.948(2) and 3.025(2) Å) and weak C–H···N hydrogen bonds.

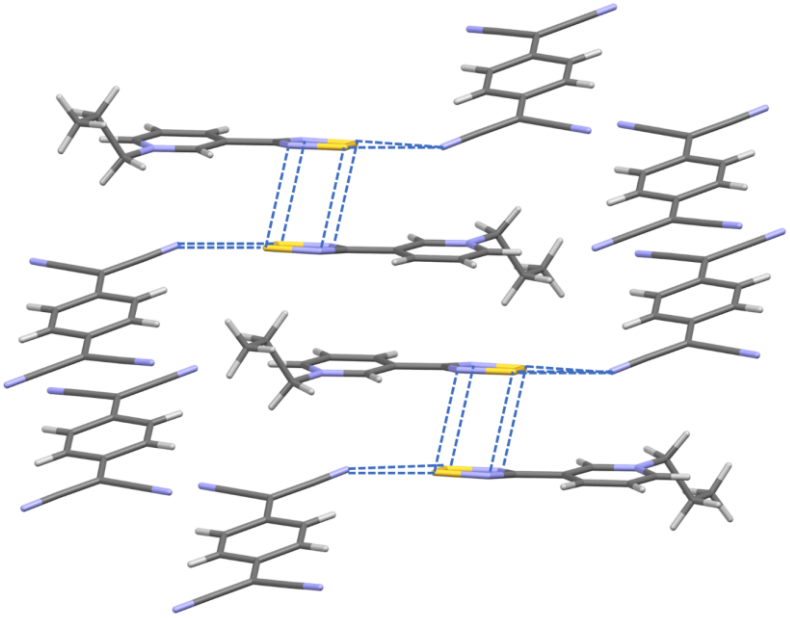

Figure 18. Illustration of the solid-state structure of **83**. Intermolecular $S^{\delta+}$···$N^{\delta-}$ interactions have been highlighted with blue dashed lines.

The crystal structures of the two non-solvated *N*-butyl derivatives **84** and **87** differ from **83** but are mutually isostructural (triclinic $P\bar{1}$) and contain a single cation:anion pair in the asymmetric unit. The radical-cations are in a rare *trans*-antarafacial arrangement and form A^{+}–A^{+}···A^{+}–A^{+} stacks with head-over-tail orientation of the dimeric subunits (Figure 19). The intradimer S···S and Se···Se distances are 3.172(2) and 3.241(1) Å, respectively, and are comparable to the limited data in the literature. The TCNQ dimers adopt non-eclipsed-cofacial geometry in **84** and **87** and generate staircase-like B^{-}–B^{-}···B^{-}–B^{-} stacking motifs that connect to the cations *via* intermolecular $CN^{\delta-}$···$S^{\delta+}$ (2.869(3)Å and 2.962(3) Å) and $CN^{\delta-}$···$Se^{\delta+}$ (2.937(5) and 3.017(6) Å) interactions and weak C–H···N hydrogen bonds.

The non-solvated structures **83**, **84**, and **87** have three important features in common. First, the cations and anions are connected *via* $CN^{\delta-}$···$Ch^{\delta+}$ (Ch = S, Se) interactions. Second, in all three instances, the TCNQ dimers adopt non-eclipsed-cofacial geometry, while the dimerization mode of the cation changes with the size of the *N*-alkyl substituent. Third, all structures display strongly antiferromagnetically coupled DTDA/DSDA and TCNQ radicals and differ from the non-solvated structure of **81**. This suggests limited possibilities for observing temperature-related changes in structure and magnetic properties of **83**, **84**, and **87** akin to **81**. Full details of the syntheses and structures of the various solvates and non-solvates of salts **82–87** are provided in Paper **III**.

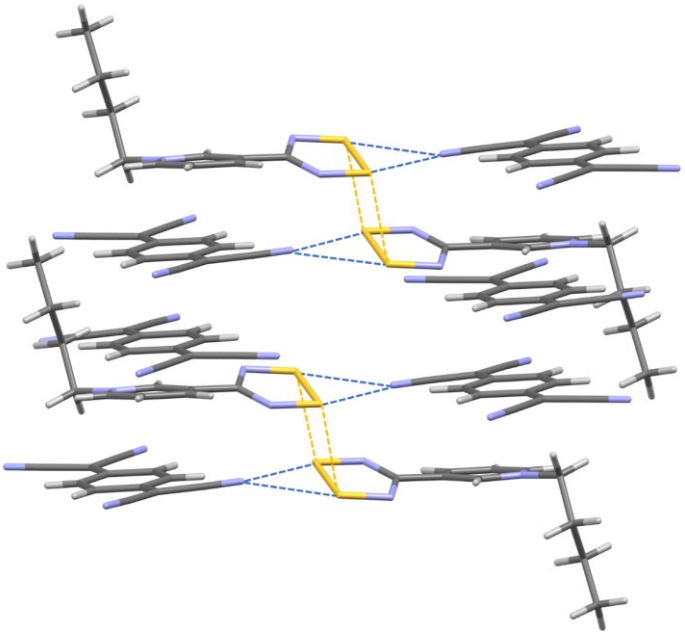

Figure 19. Illustration of the solid-state structure of **84** (isostructural with **87**). Intermolecular $S^{\delta+}\cdots N^{\delta-}$ and $S^{\delta+}\cdots S^{\delta+}$ interactions have been highlighted with blue and orange dashed lines, respectively.

4.3.3 Thermal and magnetic properties

The thermal behavior of the various solvates and non-solvates of salts **82–87** was investigated by thermogravimetric analyses to determine their desolvation and decomposition temperatures. This was necessary to determine that the single crystals of the examined solvates represent the bulk material, which was confirmed by comparing the stoichiometries determined from gravimetric analyses to those inferred from the unit cell data. For non-solvates, thermogravimetric analyses were run to verify that the samples were completely desolvated. Thermogravimetric analyses also determined the range between desolvation and decomposition for each solvate and whether the solvent removal occurs rapidly or is more gradual (Figure 20).

Compounds **82 · MeCN** and **82 · EtCN** with *N*-ethyl substituents were of interest regarding thermal desolvation as non-solvated structures could be obtained for other DTDA derivatives simply by using EtCN as the crystallization solvent (Figure 16). Furthermore, **82 · MeCN** and **82 · EtCN** are isostructural with the corresponding *N*-methyl derivatives, and loss of lattice solvent could give rise to a solid-state arrangement like that in **81** and to new magnetically bistable systems. However, despite several attempts, thermal desolvation of **82 · MeCN** and **82 · EtCN** was always met with failure, most likely due to the narrow region of stability between their desolvation and decomposition temperatures, as seen in the data from thermogravimetric analyses (Figure 20). Consequently, no attempts were made to achieve single-crystal-to-single-crystal transformations in these two cases.

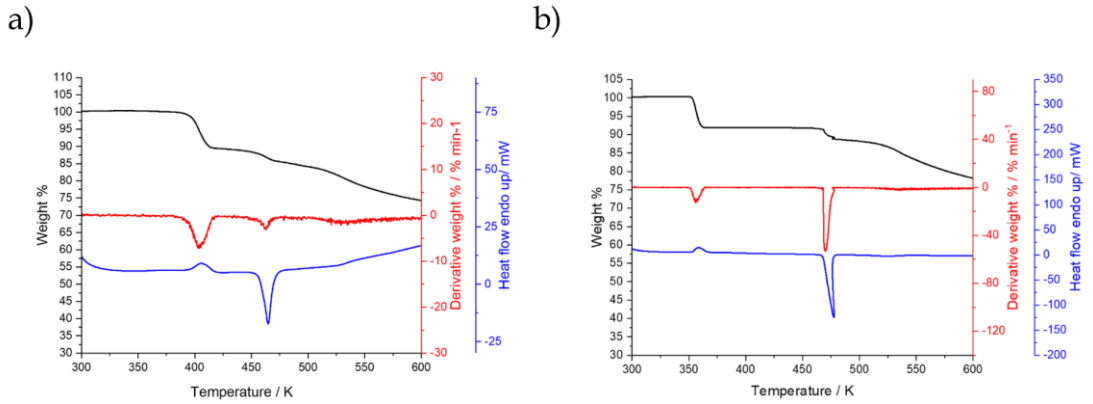

Figure 20. Thermogravimetric weight loss curve (black line) of a) **82 · EtCN** and b) **83 · MeCN** at temperature range 300–600 K. Gradual decomposition after solvent loss (400 K) is observed for **82 · EtCN**, whereas a wide plateau between desolvation (360 K) and decomposition (450 K) is seen for **83 · MeCN**. The derivative and heat flow curves are shown in red and blue, respectively.

During the performed investigations, no attempts were made to examine the possibility of a single-crystal-to-single-crystal transformation in the DSDA derivatives **85 · MeCN** and **86 · MeCN**, although they showed the most robust thermal behavior. These compounds contain aniferromagnetically coupled *trans*-cofacial DSDA dimers that are typically more strongly bound than the corresponding DTDA derivatives, which can prevent the desired structural changes from occurring upon desolvation. Hence, the focus shifted to compounds **83 · MeCN** and **84 · 0.5 MeCN**, which were found to undergo thermally induced desolvation. The poor crystalline quality of all samples of **84 · 0.5 MeCN** did not allow a single-crystal-to-single-crystal transformation to be observed, but it could be performed for **83 · MeCN**, which showed robust thermal behavior (Figure 20) and retained crystallinity during *in situ* desolvation by heating on the goniometer head. The high-temperature crystal structure of **83** obtained *via* this route was found to be identical to the low-temperature structure of the same non-solvate obtained from EtCN. This indicated that desolvation alone is not driving the structural changes seen in the case of **81**, but the perfectly sized *N*-methyl substituent facilitates these changes.

The bulk magnetic properties of the solvates **82 · MeCN**, **82 · EtCN**, **83 · MeCN**, and **84 · 0.5 MeCN**, and the non-solvates **84** and **87** were investigated with variable-temperature magnetic susceptibility measurements. The solvates **82 · MeCN** and **82 · EtCN** showed only a slight increase in the χT product above 350 K, consistent with the gradual loss of lattice solvent upon heating, and the magnetic properties remained quantitatively unchanged upon successive cooling and heating cycles. The solvates **83 · MeCN** and **84 · 0.5 MeCN**, however, showed a steady increase in the χT product to the limit of the experiments (400 K) during the first heating cycle, with subsequent cooling and heating cycles deviating from the initial track in both cases (Figure 21a). Regarding **84 · 0.5 MeCN**, a small amount (~10 %) of spin-defect impurities in the crystal lattice could explain the observed behavior. However, concerning **83 · MeCN**, the χT *vs.* T plot after a

solvent loss could be explained with a thermally populated magnetic state above 250 K that arises from the weakly interacting non-eclipsed-cofacial dimers of TCNQ radical-anions as results from density functional theory calculations indicated.

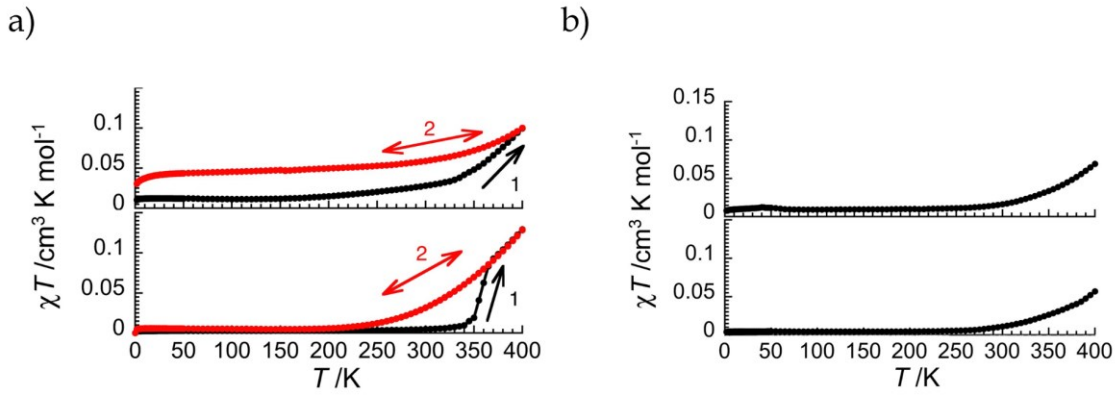

Figure 21. Temperature dependence of the χT product of neat samples of a) **83 · MeCN** (bottom) and **84 · 0.5 MeCN** (top), and b) **84** (bottom) and **87** (top). Steps: 1) desolvation upon heating and 2) additional cooling and heating.

Magnetic susceptibility measurements of the non-solvates **84** and **87** gave similar results as obtained for **83 · MeCN** after solvent loss (Figure 21b), indicating the presence of thermally accessible magnetic states above 250 K. Results from density functional theory calculations suggest that these states originate from the weakly interacting non-eclipsed-cofacial dimers of TCNQ radical-anions that have smaller singlet–triplet gaps than dimers of DTDA or DSDA radical-cations. Full details of thermogravimetric analyses, magnetic susceptibility measurements, and density functional theory calculations performed for the various solvates and non-solvates of the salts **82–87** are provided in Paper **III**.

4.4 Mixed and "complex" TCNQ salts of *N*-alkylpyridinium-substituted DTDA and DSDA radical-cations

Until now, the only route to [3-Mepy-DTDA][TCNQ] **81** involves post-synthetic modifications, that is, desolvation of the solvates **81 · MeCN** or **81 · EtCN**, which is not only tedious but leads to products of poor crystalline quality. Thus, the double displacement reaction between **72** and [K(18c6)][TCNQ] was performed in butyronitrile (PrCN) and isobutyronitrile (^{i}PrCN) with slightly longer chain lengths in an attempt to crystallize solvent-free **81** directly. However, this led to unexpected redox processes and crystallization of the product [3-Mepy-DTDA]$_2$[OTf][TCNQ] · 0.5 TCNQ (**88**), which contains two different anions and a neutral molecule of TCNQ in the crystal lattice.

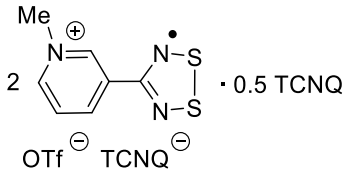

88

The crystal structure of **88** (monoclinic I_2/m) contains DTDA radical-cations arranged as *cis*-cofacial dimers that organize to A^+–A^+···A^+–A^+ stacks with head-over-tail orientation of the dimeric subunits. (Figure 22) The intradimer S···S distances (2.947(1) and 3.143(1) Å) are similar to *cis*-cofacial dimers obtained for other similar systems and the two cations are significantly wedged from coplanarity (tilt angle of 13°), presumably owing to the steric demand of the neutral TCNQ molecule in the crystal lattice. The cations show strong ion-pairing with the triflate anions *via* intermolecular $S^{\delta+}$···$O^{\delta-}$ interactions (2.815(2) and 2.967(2) Å) and only a network of weak C–H···N and C–H···O hydrogen bonds connects the DTDA radical-cations and triflate anions to the eclipsed-cofacial dimers of TCNQ radical-anions.

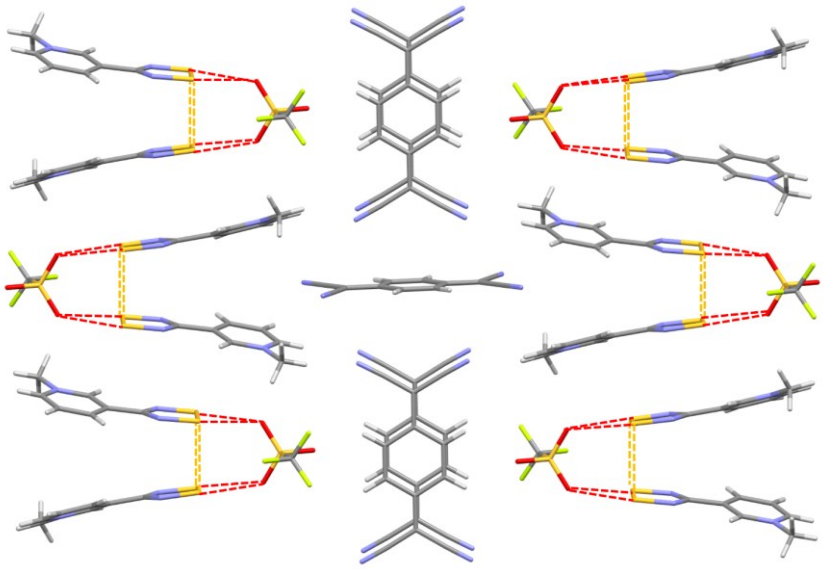

Figure 22. Illustration of the solid-state structure of **88**. Intermolecular $S^{\delta+}$···$O^{\delta-}$ and $S^{\delta+}$···$S^{\delta+}$ interactions have been highlighted with red and orange dashed lines, respectively.

The different charge states of TCNQ in **88** can be inferred from the metrical parameters determined by X-ray crystallography. The TCNQ molecules residing in the cavities are charge neutral, as seen from their C–C bond distance that alternate from short to long and long to short (*cf.* **38**). In contrast, the two TCNQ units in the eclipsed-cofacial dimers show more uniform C–C bond lengths and are anionic (*cf.* **39**). Similar conclusions can be drawn from the IR data of **88** showing C–H and C≡N stretches that are characteristic to neutral TCNQ (3050

and 2220 cm^{-1}) and C≡N stretches that can be assigned to the TCNQ radical-anion (2170 and 2152 cm^{-1}).[133]

As a last investigation, a double displacement reaction was performed between **72** and the "complex" salt $[K(18c6)]_2[(TCNQ)_3] \cdot 2$ TCNQ in ^{i}PrCN, leading to the characterization of the product $[3\text{-Mepy-DTDA}]_2[(TCNQ)_3]$ (**89**) containing dianionic cofacial π-trimers of TCNQ. Single crystal X-ray diffractometry was used to determine the structure of **89** (triclinic $P\bar{1}$, Figure 23). Interestingly, the DTDA radical-cations in **89** do not form π-dimers but interact laterally *via* intermolecular $S^{\delta+}\cdots N^{\delta-}$ interactions (3.286(2) Å). The individual TCNQ units are structurally indistinguishable in the trimer, showing that the anionic charge is delocalized. The trimers are further arranged into 1-D stacks with almost equidistant spacing between layers. The cations and anions interact primarily *via* intermolecular $S^{\delta+}\cdots N^{\delta-}$ interactions (2.825(3) and 3.166(3) Å) that only involve the central TCNQ unit in the trimer.

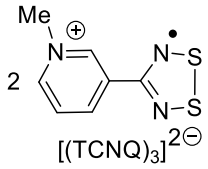

89

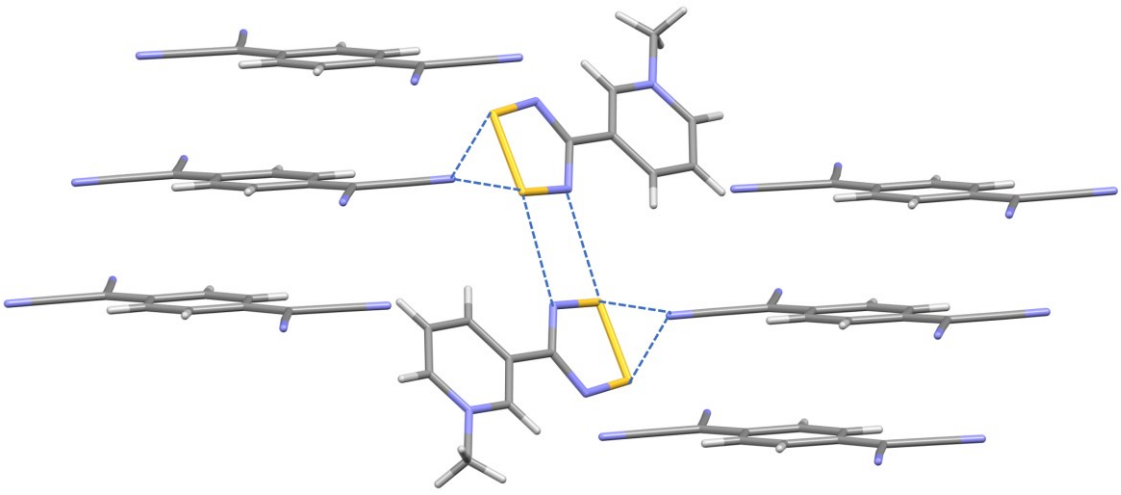

Figure 23. Illustration of the solid-state structure of **89**. Intermolecular $S^{\delta+}\cdots N^{\delta-}$ interactions have been highlighted with blue dashed lines.

Compound **88** was not subjected to detailed magnetic measurements as it contains strongly antiferromagnetically coupled DTDA and TCNQ dimers and is expected to be diamagnetic throughout the experimental temperature range. However, compound **89** was of interest as it is a "complex" salt of TCNQ that contains essentially monomeric DTDA radicals. Consequently, it was found to be a paramagnetic solid with a χT product of about 0.8 cm^3 K mol^{-1} at 100 K (Figure 24), which is close to the expected value for a system of two S = ½ and g = 2 spins (0.750 cm^3 K mol^{-1}). The increase in the χT product above 200 K is consistent with

thermally populated magnetic states associated with the weakly interacting $(TCNQ)_3^{2-}$ trimer subunits. The increase in the χT product below 150 K indicates the presence of a ferromagnetic interaction that can be assigned to the laterally interacting DTDA radical-cations.

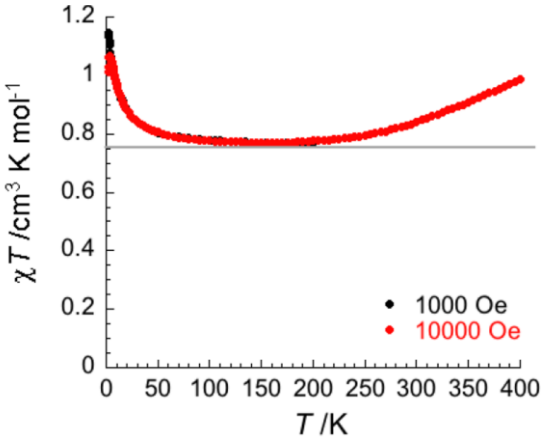

Figure 24. Temperature dependence of the χT product of a neat sample of **89**. The gray line indicates the expected χT value for a system of two S = ½ and g = 2 spins.

5 CONCLUSIONS

The primary aim of this study was to synthetize new 1,2,3,5-dithia- and 1,2,3,5-diselenadiazolyl radical-cations and combine them with the radical-anion of tetracyanoquinodimethane to generate novel radical-ion salts with potentially interesting magnetic and/or conductive properties. As the results presented in this thesis and Papers **I–IV** show, the set goal was met with the synthesis and characterization of the salt [3-Mepy-DTDA][TCNQ] that displayed hysteretic magnetic bistability in the solid state at room temperature. Detailed crystallographic studies showed that the observed behavior originates from temperature-induced reversible breakup and the formation of the σ-dimer of TCNQ radical-anions. This was facilitated by the structurally flexible π-dimer of 3-MepyDTDA *via* intermolecular $S^{\delta+}\cdots N^{\delta-}$ interactions, allowing the key C–C bond to break and form without other major structural changes.

The salt [3-Mepy-DTDA][TCNQ] was an unprecedented example of a two-component magnetically bistable system of molecular organic radicals. Consequently, exhaustive investigations of the different factors affecting its structure and properties were conducted to obtain insight into a new type of multicomponent functional molecular material. These involved probing the effect of the *N*-alkyl chain, the used solvent, and the identity of the radical-cation (DTDA or DSDA) and the radical-anion ("simple" or "complex" TCNQ). The results showed that the crystallization of the desired non-solvates becomes preferred over solvates when using the DSDA radical-cation, longer *N*-alkyl substituents, or higher molecular weight nitrile solvents, although unexpected redox activity was observed with butyronitriles. However, the length of the *N*-alkyl substituent was crucial in determining the structure and properties of the salt. Thus, the methyl derivative gets everything "just right", thereby fulfilling the "Goldilocks' principle".

Although not explicitly discussed in this thesis, subsequent investigations focusing on the effect of the ancillary anion in the double displacement reaction have shown that replacing [3-Mepy-DTDA][OTf] with [3-Mepy-DTDA][SbF_6] allows the isolation and characterization of butyronitrile solvates of the general type [3-Mepy-DTDA][TCNQ] · n PrCN that are not isostructural with the MeCN

and EtCN solvates described in this work but nevertheless yield the same bistable system [3-Mepy-DTDA][TCNQ] upon thermal desolvation. These results strengthen the notion of the key role played by the appropriately sized *N*-methyl substituent in achieving a structure with the different components ideally located relative to each other for the bistability behavior to emerge. Consequently, future work on this research will focus on the *N*-methylated selenium analogue [3-Mepy-DSDA][TCNQ] that is yet to be made. Initially, the strongly bound DSDA π-dimers were thought to prevent significant structural changes from occurring upon desolvation, but in the light of the new results, this conclusion needs to be reassessed.

Overall, the results presented herein are a first step in a long journey to explore the possibilities that combining DTDA/DSDA radical-cations with the TCNQ radical-anion offer. There are undoubtedly many more fascinating discoveries in the field of molecular materials to be made with these species. A great deal of fundamental research is required in each case to obtain sufficient insight to understand the origins of the observed molecular phenomena and identify the factors essential to its modulation, as exemplified by the [3-Mepy-DTDA][TCNQ] system described in this thesis. With the combined efforts of researchers working in the field of molecular materials, discoveries such as magnetically bistable systems will not only continue to thrive fundamental research in chemistry and physics but can also evolve into functional devices with practical applications.

SUMMARY IN FINNISH

Metallit ovat olleet osa ihmiskunnan arkea ja kehitystä varhaishistoriasta lähtien. Esimerkiksi perusmetalleja, kuten rautaa ja kuparia, on osattu erottaa malmeistaan jo tuhansien vuosien ajan. Viimeisten vuosikymmenten teknologinen kehitys ja uudet innovaatiot ovat lisänneet merkittävästi myös muiden kuin perusmetallien käyttöä ja harvinaisten maametallien tarve on kasvanut merkittävästi voimakkaiden kestomagneettien käytön lisääntyessä niin informaatio- kuin energiateknologian sovelluksissa. Nimestään huolimatta harvinaisia maametalleja on lähes kaikkialla maankuoressa, mutta esiintymien pitoisuudet ovat tyypillisesti hyvin pieniä, mikä tekee niiden hyödyntämisestä vaikeaa ja taloudellisesti kannattamatonta. Harvinaisten maametallien saatavuus globaaleilla markkinoilla onkin vahvasti sidottu geopoliittisiin tekijöihin, mistä syystä ne on määritelty EU:n alueella kriittisiksi alkuaineiksi.

Harvinaisia maametalleja tullaan tulevaisuudessa tarvitsemaan yhä enemmän, sillä niitä käytetään useissa vihreän siirtymän kannalta tärkeissä sovelluskohteissa, kuten tuulivoimaloiden turbiineissa sekä sähköautojen moottoreissa. Lisääntynyt riippuvuus harvinaisten maametallien primärituotannosta onkin viimeisen vuosikymmenen aikana muodostanut huoltovarmuusriskin vihreää siirtymää edistäville aloille. Riskiä voidaan pienentää esimerkiksi optimoimalla metallien käyttöä eri sovelluksissa, tehostamalla niiden kierrätystä tai kehittämällä kokonaan uusia molekyyleihin pohjautuvia magneettisia materiaaleja. Näistä etenkin metallien kierrätys ja siihen nivoutuva kiertotalous ovat nousseet keskiöön, sillä vain murto-osa erilaisista kestomagneeteista päätyy nykyään uusiokäyttöön kierrätyksen kautta.

Vaikka molekyyleihin pohjautuvilla magneettisilla materiaaleilla ei välttämättä pystytä korvaamaan harvinaisiin maametalleihin perustuvia magneetteja kaikilla sovellusaloilla, on niihin liittyvä tutkimus tärkeää myös muista syistä. Molekyyleihin perustuvilla magneettisilla materiaaleilla on nimittäin useita ominaisuuksia, jotka metalleilta tai niiden oksideilta eli tyypillisiltä magneettisilta materiaaleilta puuttuvat. Näistä tärkeimmät ovat keveys, liukoisuus, synteettinen muokattavuus ja monitoimisuus. Molekyyleihin perustuvia magneetteja voidaankin hyödyntää aloilla, joihin perinteiset magneetit eivät ominaisuuksiensa puolesta sovellu, kuten molekyylielektroniikassa eli seuraavan sukupolven nanokokoisten elektroniikan komponenttien valmistuksessa.

Monet molekyyleihin perustuvat magneettiset materiaalit sisältävät rakenneosina orgaanisia radikaaleja eli molekyylejä, joissa on yksi tai useampi pariton elektroni. Tällaiset yhdisteet ovat tyypillisesti erittäin reaktiivisia, mutta niitä pystytään stabiloimaan monilla eri tavoilla. Nykyään tunnetaankin useita yhdisteryhmiä eli molekyyliperheitä, joista voidaan valmistaa normaaliolosuhteissa pysyviä radikaaleja, jotka eivät reagoi esimerkiksi toisten radikaalien tai ilmassa olevien happi- ja vesimolekyylien kanssa. Yhden tällaisen perheen muodostavat orgaaniset tiatsyyliradikaalit, jotka sisältävät perusrakenteessaan hiiltä sekä yhden tai useamman typpi–rikki-yksikön (NS). Tähän laajaan ryhmään kuuluu suuri joukko erilaisia radikaaleja, joista osalla on havaittu hyvin mielenkiintoisia

magneettisia ominaisuuksia, kuten ferromagneettisuus ja magneettinen bistabiilisuus.

Ferromagneettisuus on arkielämässä tunnetuin magnetismin muoto, jossa aineen pysyvät magneettiset momentit kytkeytyvät toisiinsa ja järjestäytyvät samansuuntaisesti läpi sen rakenteen. Ferromagneettisuus on siis koko kappaleen, ei kappaleen muodostavien yksittäisten osien ominaisuus. Ferromagneettisten orgaanisista radikaaleista koostuvien materiaalien valmistaminen on valtava kemiallisen insinööritaidon haaste, sillä yleensä parittomien elektronien magneettiset momentit joko järjestäytyvät toisiinsa nähden vastakkaisesti tai eivät järjestäydy ollenkaan. Ferromagneettinen järjestäytyminen saavutetaan tyypillisesti vain erittäin alhaisissa lämpötiloissa ja juuri oikeanlaisen kiinteän tilan rakenteen kautta.

Magneettiset materiaalit voivat usein esiintyä kahdella erilaisella magneettisella tilalla. Kun materiaalin magneettista tilaa voidaan kontrolloida esimerkiksi lämpötilan tai paineen avulla, puhutaan funktionaalisesta magneettisesti bistabiilisesta materiaalista. Toisinaan magneettisen bistabiilisuuden yhteydessä havaitaan hystereesi-ilmiö, jossa yhdisteen magneettinen tila ei muutu välittömästi ulkoista tekijää, kuten lämpötilaa tai painetta, muutettaessa. Tämä mahdollistaa kahden eri tilan esiintymisen samoissa olosuhteissa. Koska materiaalin magneettinen tila riippuu olosuhteissa tehdyistä muutoksista ja muuttuu niiden mukaisesti, voidaan systeemin ajatella ”muistavan” sen, miten se on valmistettu. Tällaiset materiaalit ovat erittäin mielenkiintoisia, sillä niitä voitaisiin käyttää esimerkiksi nanomittakaavan kytkiminä tai informaation tallennuksen perusyksikköinä.

Tämän väitöskirjatutkimuksen ensimmäisessä osassa valmistettiin uusia pyridyylisubstituoituja 1,2,3,5-ditia- (DTDA) ja 1,2,3,5-diselenadiatsolyyliradikaaleja (DSDA) sekä niiden N-metyloituja kationianalogeja. Valmistetut radikaalikationit yhdistettiin tämän jälkeen 7,7´,8,8´-tetrasyanokinodimetaanista (TCNQ) muodostetun anioniradikaalin kanssa, jolloin saatiin kahden radikaalionin muodostamaa suolaa. Valmistetun suolan kiinteän tilan rakenne sisälsi haluttujen ionien lisäksi myös prosessissa käytettyä liuotinta, joka onnistuttiin poistamaan staattisen vakuumin ja lämmityksen avulla. Näin aikaansaatu liuottimeton suola osoittautui kiinteän tilan rakenteeltaan ja ominaisuuksiltaan erittäin mielenkiintoiseksi, sillä sille havaittiin magneettinen bistabiilisuus ja siihen liittyvä hystereesi-ilmiö, jossa korkean lämpötilan rakenteessa olevat monomeeriset TCNQ-radikaalit muodostavat lämpötilan laskiessa C–C-sidoksellisia σ-dimeerejä systeemin magneettisen tilan muuttuessa samanaikaisesti.

Tutkimuksen jälkimmäinen osa keskittyi kartoittamaan havaittuun reversiibeliin magneettiseen bistabiilisuuteen ja hystereesiin vaikuttavia tekijöitä. Täydellisen kokonaiskuvan saamiseksi työssä tutkittiin radikaalikationin *N*-alkyyliketjun, radikaalikationin (DTDA *vs.* DSDA), liuottimen sekä vasta-anionin vaikutusta valmistettujen suolojen kiinteän tilan rakenteisiin ja magneettisiin ominaisuuksiin. Tuloksista nähtiin, että valmistetut suolat kiteytyvät ilman liuotinta *N*-alkyyliketjun pidentyessä, liuottimen molekyylipainon kasvaessa tai käytet-

täessä DSDA-radikaalia vastaavan DTDA-radikaalin sijasta. Tutkimuksen jälkimmäisen osan aikana valmistetuilla suoloilla ei kuitenkaan havaittu magneettista bistabiilisuutta ja siihen liittyvää hystereesi-ilmiötä, mikä osoittaa, että kationiradikaalin *N*-alkyyliketjun pituus on tärkein yksittäinen tekijä haluttujen ominaisuuksien vaatiman kiinteän tilan rakenteen aikaansaamiseksi.

Yhteenvetona voidaan todeta, että väitöskirjatyössä valmistettiin ensimmäinen orgaanisista radikaaleista koostuva kaksikomponenttisysteemi, jolla havaittiin magneettinen bistabiilisuus ja hystereesi-ilmiö lähellä huoneenlämpötilaa. Tehty monitieteellinen perustutkimus antoi lisäksi paljon arvokasta tietoa, jota voidaan käyttää uudenlaisten funktionaalisten molekulaaristen materiaalien suunnittelussa ja valmistamisessa. Tämä voi tulevaisuudessa mahdollistaa myös kyseisiä ilmiöitä hyödyntävät käytännön sovellukset.

REFERENCES

[1] *The Rare Earth Elements: Fundamentals and Applications*, Atwood, D. A. (Ed.), Wiley, 2012.

[2] Dent, P. C. Rare earth elements and permanent magnets. *J. Appl. Phys.* **2012**, *111*, 07A721. DOI:10.1063/1.3676616

[3] Leal Filho, W.; Kotter, R.; Özuyar, P.G.; Abubakar, I.R.; Eustachio, J.H.P.P.; Matandirotya, N.R. Understanding Rare Earth Elements as Critical Raw Materials. *Sustainability* **2023**, *15*, 1919. DOI:10.3390/su15031919

[4] Shao, Z.; Ren, S. Rare-earth-free magnetically hard ferrous materials. *Nanoscale Adv.* **2020**, *2*, 4341–4349. DOI:10.1039/D0NA00519C

[5] *Critical and Rare Earth Elements: Recovery from Secondary Resources*, Abhilash; Akcil, A. (Eds.), CRC Press, 2020.

[6] Miller, J. S. Magnetically ordered molecule-based materials. *Chem. Soc. Rev.* **2011**, *40*, 3266–3296. DOI:10.1039/C0CS00166J

[7] Tamura, M.; Nakazawa, Y.; Shiomi, D.; Nozawa, K.; Hosokoshi, Y.; Ishikawa, M.; Takahashi, M.; Kinoshita, M. Bulk ferromagnetism in the β-phase crystal of the *p*-nitrophenyl nitronyl nitroxide radical. *Chem. Phys. Lett.* **1991**, *186*, 401–404. DOI:10.1016/0009-2614(91)90198-I

[8] Phan, H.; Herng, T. S.; Wang, D.; Li, X.; Zeng, W.; Ding, J.; Loh, K. P.; Wee, A. T. S.; Wu, J. Room-Temperature Magnets Based on 1,3,5-Triazine-Linked Porous Organic Radical Frameworks. *Chem.* **2019**, *5*, 1223–1234. DOI:10.1016/j.chempr.2019.02.024

[9] Hicks, R. The Synthesis and Characterization of Stable Radicals Containing the Thiazyl (SN) Fragment and Their Use as Building Blocks for Advanced Functional Materials. *Stable Radicals: Fundamentals and Applied Aspects of Odd-Electron Compounds*, Hicks, R. (Ed.), Wiley, 2010, pp. 317–380. DOI:10.1002/9780470666975.ch9

[10] *Stable Radicals: Fundamentals and Applied Aspects of Odd-Electron Compounds*, Hicks, R. (Ed.), Wiley, 2010.

[11] Gomberg, M. On tetraphenylmethane. *J. Am. Chem. Soc.* **1898**, *20*, 773–780. DOI:10.1021/ja02072a009

[12] Gomberg, M. An instance of trivalent carbon: triphenylmethyl. *J. Am. Chem. Soc.* **1900**, *22*, 757–771. DOI:10.1021/ja02049a006

[13] Schlenk, W.; Weickel, T.; Herzenstein, A. Ueber Triphenylmethyl und Analoga des Triphenylmethyls in der Biphenylreihe. *Justus Liebigs Ann. Chem.* **1910**, *372*, 1–20. DOI:10.1002/jlac.19103720102

[14] Lankamp, H.; Nauta, W. Th.; MacLean, C. A new interpretation of the monomer-dimer equilibrium of triphenylmethyl- and alkylsubstituted-diphenyl methyl-radicals in solution. *Tetrahedron Lett.* **1968**, *9*, 249–254. DOI:10.1016/S0040-4039(00)75598-5

[15] Armet, O.; Veciana, J.; Rovira, C.; Riera, J.; Castaner, J.; Molins, E.; Rius, J.; Miravitlles, C.; Olivella, S.; Brichfeus, J. Inert Carbon Free Radicals. 8. Polychlorotriphenylmethyl Radicals: Synthesis, Structure, and Spin-Density Distribution. *J. Phys. Chem.* **1987**, *91*, 5608–5616. DOI:10.1021/j100306a023

[16] Ahmed, J.; Mandal, K. Phenalenyl Radical: Smallest Polycyclic Odd Alternant Hydrocarbon Present in the Graphene Sheet. *Chem. Rev.* **2022**, *122*, 11369–11431. DOI:10.1021/acs.chemrev.1c00963

[17] Goto, K.; Kubo, T.; Yamamoto, K.; Nakasuji, K.; Sato, K.; Shiomi, D.; Takui, T.; Kubota, M.; Kobayashi, T.; Yakusi, K.; Ouyang, J. A Stable Neutral Hydrocarbon Radical: Synthesis, Crystal Structure, and Physical Properties of 2,5,8-Tri-*Tert*-Butyl-Phenalenyl. *J. Am. Chem. Soc.* **1999**, *121*, 1619–1620. DOI:10.1021/ja9836242

[18] Kertesz, M. Pancake Bonding: An Unusual Pi-Stacking Interaction. *Chem. Eur. J.* **2019**, *25*, 400–416. DOI:10.1002/chem.201802385

[19] Viehe, H. G.; Janousek, Z.; Merenyi, R. The Captodative Effect. *Acc. Chem. Res.* **1985**, *18*, 148–154. DOI:10.1021/ar00113a004

[20] Coppinger, G. M. A Stable Phenoxy Radical Inert to Oxygen. *J. Am. Chem. Soc.* **1957**, *79*, 501–502. DOI:10.1021/ja01559a073

[21] Lampp, L.; Azarkh, M.; Drescher, M.; Imming, P. Galvinoxyl radicals: Synthesis of new derivatives, determination of low oxygen contents, and stability studies. *Tetrahedron* **2019**, *75*, 2737–2747. DOI:10.1016/j.tet.2019.03.051

[22] Goldschmidt, S.; Renn, K. Zweiwertiger Sticlstoff: Über das α,α-Diphenyl-β-trinitrophenyl hydrazyl. IV. Mitteilung über Amin-Oxydation. *Ber. Dtsch. Chem. Ges. B* **1922**, *55*, 628–643. DOI:10.1002/cber.19220550308

[23] Foti, M. C. Use and Abuse of the DPPH$^{\bullet}$ Radical. *J. Agric. Food. Chem.* **2015**, *63*, 8765–8776. DOI:10.1021/acs.jafc.5b03839

[24] Kuhn, R.; Trischmann, H. Surprisingly Stable Nitrogenous Free Radicals. *Angew. Chem. Int. Ed. Eng.* **1963**, *6*, 294–295. DOI:10.1002/anie.196301552

[25] Neugebauer, F.A.; Fischer, H. 6-Oxoverdazyls. *Angew. Chem. Int. Ed. Eng.* **1980**, *19*, 724–725. DOI:10.1002/anie.198007241

[26] Brook. D. J. R. Coordination Chemistry of Verdazyl Radicals. *Comm. Inorg. Chem.* **2015**, 35, 1–17. DOI:10.1080/02603594.2014.974805

[27] Lebedev, O. L.; Kazarnovskii, S. N. [Catalytic oxidation of aliphatic amines with hydrogen peroxide.] *Zhur. Obshch. Khim.* **1960**, *30*, 1631–1635.

[28] Zhou, Z.; Liu, L. TEMPO and its Derivatives: Synthesis and Applications. *Curr. Org. Chem.* **2014**, *18*, 459–474. DOI:10.2174/13852728113176660151

[29] Danen, W. C.; Newkirk, D. D. Nitrogen-Centered Free Radicals. IX. The Ease of Formation of Thionitroxide Radicals. *J. Am. Chem. Soc.* **1976**, *98*, 516–520. DOI:10.1021/ja00418a03

[30] Demarçay, E. Recherches sur le sulfure d'azote. *C. R. Hebd. Seances Acad. Sci*. **1880**, *91*, 854–822.

[31] Banister, A. J.; Clarke, H. G.; Rayment, I.; Shearer, H. M. M. The Structure of Thiodithiazyl Chlorodisulphate, $S_3N_2S_2O_6Cl$ and Its Preparation from Thiodithiazyl Monochloride, S_3N_2Cl. *Inorg. Nucl. Chem. Lett.* **1974**, *10*, 647–654. DOI:10.1016/0020-1650(74)80008-5

[32] Walatka, V. V.; Labes, M. M.; Perlstein, J. H. Polysulfur Nitride—a One-Dimensional Chain with a Metallic Ground State. *Phys. Rev. Lett.* **1973**, *31*, 1139–1142. DOI:10.1103/PhysRevLett.31.1139

[33] Banister, A. J.; Bricklebank, N.; Lavender, I.; Rawson, J. M.; Gregory, C. I.; Tanner, B. K.; Clegg, W.; Elsegood, M. R. J.; Palacio, F. Spontaneous Magnetization in a Sulfur–Nitrogen Radical at 36 K. *Angew. Chem. Int. Ed. Engl.* **1996**, *35*, 2533–2535. DOI:10.1002/anie.199625331

[34] Alange, G. G.; Banister, A. J.; Bell, B.; Millen, P. W. 1,2,3,5-dithiadiazolium chlorides, $[RCN_2S_2]Cl$. *Inorg. Nucl. Chem. Lett.* **1977**, *13*, 143–144. DOI:10.1016/0020-1650(77)80082-2

[35] Markovski, L. N.; Polumbrik, O. M.; Talanov, V. s.; Shermolovich, Yu. G. 1,2,3,5-Dithiadiazolyles, a new type of persistent sulfurnitrogencontaining radicals. *Tetrahedron Lett.* **1982**, *23*, 761–762. DOI:10.1016/S0040-4039(00)86941-5

[36] Alange, G. G.; Banister, A. J.; Bell, B.; Millen, P. W. Preparation of some 1,2,3,5-dithiadiazolium chlorides from trichlorocyclotrithiazene and nitriles or olefins, and from amidinium salts and sulphur dichloride. *J. Chem. Soc. Perkin Trans. 1* **1979**, 1192–1194. DOI:10.1039/P19790001192

[37] Boeré, R. T.; Oakley, R. T.; Reed, R. W. Preparation of *N,N,N'*-tris(trimethylsilyl)amidines; a convenient route to unsubstituted amidines. *J. Organomet. Chem.* **1987**, *331*, 161–167. DOI:10.1016/0022-328X(87)80017-7

[38] Haynes, D. Crystal engineering with dithiadiazolyl radicals. *CrystEngComm* **2011**, *13*, 4793–4805. DOI:10.1039/C1CE05217A

[39] Knapp, C.; Lork, E.; Gupta, K.; Mews, R. Structure Investigations on 4-Halo-1,2,3,5-Dithiadiazolyl Radicals XCNSSN$^{\bullet}$ (X = F, Cl, Br): The Shortest Intradimer S···S Distance in Dithiadiazolyl Dimers. *Z. Anorg. Allg. Chem.* **2005**, *631*, 1640–1644. DOI:10.1002/zaac.200500052

[40] Vegas, A.; Pérez-Salazar, A.; Banister, A. J.; Hey, R. G. Crystal structure of 4-phenyl-1,2-dithia-3,5-diazole dimer. *J. Chem. Soc. Dalton Trans.* **1980**, 1812–1815. DOI:10.1039/DT9800001812

[41] Shuvaev, K. V.; Decken, A.; Grein, F.; Abedin, T. S. M.; Thompson, L. K.; Passmore, J. NC–$(CF_2)_4$–CNSSN$^{\bullet}$ containing 1,2,3,5-dithiadiazolyl radical dimer exhibiting triplet excited states at low temperature and thermal hysteresis on melting–solidification: structural, spectroscopic, and magnetic characterization. *J. Chem. Soc. Dalton Trans.* **2008**, 4029–4037. DOI:10.1039/b804699a

[42] Bricklebank, N.; Hargreaves, S.; Spey, S. E. Modification of the solid state structures of dithiadiazolyl radicals: crystal structure of *p*-iodophenyl-1,2,3,5-dithiadiazolyl. *Polyhedron* **2000**, *19*, 1163–1166. DOI:10.1016/S0277-5387(00)00384-3

[43] Cordes, A. W.; Haddon, R. C.; Hicks, R. G.; Oakley, R. T.; Palstra, T. T. M. Preparation and Solid-State Structures of (Cyanophenyl)Dithia- and (Cyanophenyl)diselenadiazolyl Radicals. *Inorg. Chem.* **1992**, *31*, 1802–1808. DOI:10.1021/ic00036a016

[44] Clegg, W.; Elsegood, M. R. J. CSD Communication, CCDC 1500540, 2016.

[45] Banister, A. J.; Hansford, M. I.; Hauptman, Z. V.; Wait, S. T.; Clegg, W. Direct insertion of a nitrogen atom into the S–S bond of a 1,2,3,5-dithiadiazole ring in a direct current nitrogen glow discharge, and X-ray crystal structure of 4-methyl-1,2,3,5-dithiadiazole. *J. Chem. Soc. Dalton Trans.* **1989**, 1705–1713. DOI:10.1039/DT9890001705

[46] Höfs, H.-U.; Bats, J. W.; Gleiter, R.; Hartmann, G.; Mews, R.; Eckert-Maksić, M.; Oberhammer, H.; Sheldrick, G. M. Perhalogenierte 1,2,3,5-Dithiadiazolium-Salze und 1,2,3,5-Dithiadiazole. *Chem. Ber.* **1985**, *118*, 3781–3804. DOI:10.1002/cber.19851180930

[47] Alberola, A.; Carter, E.; Constantinides, C. P.; Eisler, D. J.; Murphy, D. M.; Rawson, J. M. Crystal structures, EPR and magnetic properties of 2-$ClC_6H_4CNSSN^{\bullet}$ and 2,5-$Cl_2C_6H_3CNSSN^{\bullet}$. *Chem. Commun.* **2011**, *47* (9), 2532–2534. DOI:10.1039/c0cc04296j

[48] Fairhurst, S. A.; Johnson, K. M.; Sutcliffe, L. H.; Preston, K. F.; Banister, A. J.; Hauptman, Z. V.; Passmore, J. Electron spin resonance study of $CH_3CNSSN^{\bullet}$, $C_6H_5CNSSN^{\bullet}$, and $SNSSN^{\bullet+}$ free radicals. *J. Chem. Soc. Dalton Trans.* **1986**, 1465–1472. DOI:10.1039/DT9860001465

[49] Awere, E. G.; Burford, N.; Mailer, C.; Passmore, J.; Schriver, M. J.; White, P. S.; Banister, A. J.; Oberhammer, H.; Sutcliffe, L. H. The high yield preparation, characterisation, and gas phase structure of the thermally stable $CF_3CSNSCCF_3^{\bullet}$, 4,5-bis(trifluoromethyl)-1,3,2-dithiazolyl and the X-ray crystal structure of benzo-1,3,2-dithiazolyl. *J. Chem. Soc. Chem. Commun.* **1987**, 66–69. DOI:10.1039/C39870000066

[50] Britten, J.; Hearns, N. G. R.; Preuss, K. E.; Richardson, J. F.; Bin-Salamon, S. Mn(II) and Cu(II) Complexes of a Dithiadiazolyl Radical Ligand: Monomer/Dimer Equilibria in Solution. *Inorg. Chem.* **2007**, *46*, 3934–3945. DOI:10.1021/ic0619456

[51] Bond, A. D.; Haynes, D. A.; Pask, C. M.; Rawson, J. M. Concomitant polymorphs: structural studies on the trimorphic dithiadiazolyl radical, ClCNSSN. *J. Chem. Soc. Dalton Trans.* **2002**, 2522–2531. DOI:10.1039/B110922G

[52] Clarke, C. S.; Pascu, S. I.; Rawson, J. M. Further studies on the polymorphic dithiadiazolyl radical, ClNSSN. *CrystEngComm* **2004**, *6*, 79–82. DOI:10.1039/B403430A

[53] Alberola, A.; Clarke, C. S.; Haynes, D. A.; Pascu, S. I.; Rawson, J. M. Crystal structures and magnetic properties of a sterically encumbered dithiadiazolyl radical, 2,4,6-$(F_3C)_3C_6H_2CNSSN^{\bullet}$. *Chem. Commun.* **2005**, 4726–4728. DOI:10.1039/B508371K

[54] Nascimento, M. A.; Heyer, E.; Less, R. J.; Pask, C. M.; Arauzo, A.; Campo, J.; Rawson, J. M. An Investigation of Halogen Bonding as a Structure-Directing Interaction in Dithiadiazolyl Radicals. *Cryst. Growth Des.* **2020**, *20*, 4313–4324. DOI:10.1021/acs.cgd.9b01698

[55] Belluz, P. D. B.; Cordes, A. W.; Kristof, E. M.; Kristof, P. V.; Liblong, S. W.; Oakley, R. T. 1,2,3,5-Diselenadiazolyls as Building Blocks for Molecular Metals. Preparation and Structures of $[PhCN_2Se_2]^+PF6^-$ and $[PhCN_2Se_2]_2$. *J. Am. Chem. Soc.* **1989**, *111*, 9276–9278. DOI:10.1021/ja00208a047

[56] Melen, R. L.; Less, R. J.; Pask, C. M.; Rawson, J. M. Structural Studies of Perfluoroaryldiselenadiazolyl Radicals: Insights into Dithiadiazolyl Chemistry. *Inorg. Chem.* **2016**, *55*, 11747–11759. DOI:10.1021/acs.inorgchem.6b01771

[57] Boeré, R. T.; Hill, N. D. D. High Z′ structures of 1,2,3,5-dithiadiazolyls and of 1,2,3,5-diselenadiazolyls containing the first structurally characterized monomeric diselenadiazolyls. *CrystEngComm* **2017**, 19, 3698–3707. DOI:10.1039/C7CE00863E

[58] Feeder, N.; Less, R. J.; Rawson, J. M.; Oliete, P.; Palacio, F. An unprecedented mode of association in diselenadiazolyl radicals: crystal structures and magnetic properties of $[p\text{-}XC_6F_4CNSeSeN]_2$ (X=Cl, Br). *Chem. Commun.* **2000**, 2449–2450. DOI:10.1039/B004705H

[59] Acker, D. S.; Hertler, W. R. Substituted Quinodimethans. I. Preparation and Chemistry of 7,7,8,8-Tetracyanoquinodimethan. *J. Am. Chem. Soc.* **1962**, *84*, 3370–3374. DOI:10.1021/ja00876a028

[60] Suchanski, M. R.; Van Duyne, R. P. Resonance Raman Spectroelectrochemistry. IV. The Oxygen Decay Chemistry of the Tetracyanoquinodimethane Dianion. *J. Am. Chem. Soc.* **1976**, 98, 250–252. DOI:10.1021/ja00417a049

[61] Kryszewski, M.; Ciesielski, W.; Pęlcherz, J. Decomposition of complexes of TCNQ anion radical salts as a function of time. *Acta Polym.* **1981**, *32*, 524–531. DOI:10.1002/actp.1981.010320903

[62] Kaim, W.; Moscherosch, M. The coordination chemistry of TCNE, TCNQ and related polynitrile π acceptors. *Coord. Chem. Rev.* **1994**, *129*, 157–193. DOI:10.1016/0010-8545(94)85020-8

[63] Goetz, K. P.; Vermulen, D.; Payne, M. E.; Kloc, C.; McNeil, L. E.; Jurchescu, O. D. Charge-transfer complexes: new perspectives on an old class of compounds. *J. Mater. Chem. C* **2014**, *2*, 3065–3076. DOI:10.1039/C3TC32062F

[64] Ferraris, John.; Cowan, D. O.; Walatka, V.; Perlstein, J. H. Electron Transfer in a New Highly Conducting Donor-Acceptor Complex. *J. Am. Chem. Soc.* **1973**, *95*, 948–949. DOI:10.1021/ja00784a066

[65] Kistenmacher, T. J.; Phillips, T. E.; Cowan, D. O. The Crystal Structure of the 1:1 Radical Cation-Radical Anion Salt of 2,2'-Bis-l,3-dithiole (TTF) and 7,7,8,8-Tetracyanoquinodimethane (TCNQ). *Acta Cryst. B* **1974**, *30*, 763–767. DOI:10.1107/S0567740874003669

[66] Tomkiewicz, Y.; Taranko, A. R.; Torrance, J. B. Roles of the Donor and Acceptor Chains in the Metal-Insulator Transition in TTF-TCNQ (Tetrathiafulvalene Tetracyanoquinodimethane). *Phys. Rev. Lett.* **1976**, *36*, 751–754. DOI:10.1103/PhysRevLett.36.751

[67] Wolmershäuser, G.; Schnauber, M.; Wilhelm, T. Highly conducting charge transfer complexes of benzo-1,3,2-dithiazol-2yl and its derivatives with teracyanoquinodimethane. *J. Chem. Soc., Chem. Commun*. **1984**, 573–574. DOI:10.1039/C39840000573

[68] Awaga, K.; Umezono, Y.; Fujita, W.; Yoshikawa, H.; Cui, H.; Kobayashi, H:; Staniland, S. S.; Robertson, N. Diverse magnetic and electrical properties of molecular solids containing the thiazyl radical BDTA, *Inorg. Chim. Acta.* **2008**, *361*, 3761–3770. DOI:10.1016/j.ica.2008.03.065

[69] Bryan, C. D.; Cordes, A. W.; Fleming, R. M.; George, N. A.; Glarum, S. H.; Haddon, R. C.; Oakley, R. T.; Palstra, T. T. M.; Perel, A. S.; Schneemeyer, L. F.; Waszczak, J. V. Conducting charge-transfer salts based on neutral π-radicals, *Nature* **1993**, *365*, 821–823. DOI:10.1038/365821a0

[70] Bryan, C. D.; Cordes, A. W.; Haddon, R. C.; Hicks, R. G.; Kennepohl, D. K.; MacKinnon, C. D.; Oakley, R. T.; Palstra, T. T. M.; Perel, A. S.; Scott, S. R.; Schneemeyer, L. F.; Waszczak, J. V. Molecular conductors from neutral-radical charge-transfer salts: preparation and characterization of an I doped hexagonal phase of 1,2,3,5-dithiadiazolyl ($[HCN_2S_2]^{\bullet}$) *J. Am. Chem. Soc.* 1994, 116, 1205–1210. DOI:10.1021/ja00083a005

[71] Huang, J.; Kingsbury, S.; Kertesz, M. Crystal packing of TCNQ anion π-radicals governed by intermolecular covalent π–π bonding: DFT calculations and statistical analysis of crystal structures. *Phys. Chem. Chem. Phys.* **2008**, *10*, 2625–2635. DOI:10.1039/b717752f

[72] Morosin, B.; Plastas, H. J.; Coleman, L. B.; Stewart, J. M. The crystal structure of the charge-transfer complex between *N*-ethylphenazinium (EtP) and dimerized 7,7,8,8-tetracyanoquinodimethanide (TCNQ) ions, $(C_{14}H_{13}N_2)_2{}^{\bullet}C_{24}H_8N_8$. *Acta Cryst. B* **1978**, *34*, 540–543. DOI:10.1107/S0567740878003507

[73] Radhakrishnan, T. P.; Van Engen, D.; Soos, Z. G. Diamagnetic to Paramagnetic Transition in Trisdimethylaminocyclopropenium Tetracyano-quinodimethanide (TDAC-TCNQ). *Mol. Cryst. Liq. Cryst. Inc. Nonlinear Opt.* **1987**, *150*, 473–492. DOI:10.1080/00268948708074815

[74] Herbstein, F. H.; Kapon, M. Classification of closed shell TCNQ salts into structural families and comparison of diffraction and spectroscopic methods of assigning charge states to TCNQ moieties. *Crystallogr. Rev.* **2008**, *14*, 3–74. DOI:10.1080/08893110801980780

[75] Fritchie, C. J. Jr. The Crystal Structure of *N*-Methylphenazinium Tetracyanoquinodimethanide. *Acta Cryst.* 1966, 20, 892–898. DOI:10.1107/S0365110X66002019

[76] Sanz, F.; Daly, J. J. Crystal and molecular structure of the 2 : 3 complex of *N*-methylphenazinium with αα′α′-tetracyanoquinodimethane, $[(nmp)_2]^{2+}[(tcnq)_3]^{2-}$. *J. Chem. Soc. Perkin Trans.* 2 **1975**, 1146–1150. DOI:10.1039/P29750001146

[77] Harms, R.; Keller, H. J.; Nöthe, D.; Wehe, D. Structure of bis(5-propylphenazinium)-tris[2,2′-(2,5-cyclohexadiene-1,4-diylidene)bis(propanedinitrile)], $(NPP)_2(TCNQ)_3$. *Acta Cryst. B* **1982**, *38*, 2838–2841. DOI:10.1107/S0567740882010073

[78] Gundel, D.; Sixl, H.; Metzger, R. M.; Heimer, N. E.; Harms, R. H.; Keller, H. J.; Nöthe, D.; Wehe, D. Crystal and molecular structure and EPR triplet spin excitons of NBP TCNQ, the 1:1 salt of 5-(1-butyl) phenazinium (NBP) with 2,2′-(2,5-cyclohexadiene-1,4-diylidene)-bispropanedinitrile (TCNQ). *J. Chem. Phys*. **1983**, 79, 3678–3688. DOI:10.1063/1.446287

[79] Heisenberg, W. Zur Theorie des Ferromagnetismus. *Zeit. Phys.* **1928**, *49*, 619–636. DOI:10.1007/BF01328601

[80] Edelstein, A. S.; Mandel, M. Antiferromagnetic to Ferromagnetic Transitions in Organic Free Radicals. *J. Chem. Phys.* **1961**, *35*, 1130–1131. DOI:10.1063/1.1701192

[81] McConnell, H. M. Ferromagnetism in Solid Free Radicals. *J. Chem. Phys.* **1963**, *39*, 1910. DOI:10.1063/1.1734562

[82] Mukai, K.; Nishiguchi, H.; Deguchi, Y. Anomaly in the χ-*T* Curve of Galvinoxyl Radical. *J. Phys. Soc. Jpn.* **1967**, *23*, 125–125. DOI:10.1143/JPSJ.23.125

[83] Allemand, P.-M.; Khemani, K. C.; Koch, A.; Wudl, F.; Holczer, K.; Donovan, S.; Grüner, G.; Thompson, J. D. Organic Molecular Soft Ferromagnetism in a Fullerene C_{60}. *Science* **1991**, *253*, 301–302. DOI:10.1126/science.253.5017.301

[84] Hosokoshi, Y.; Katoh, K.; Nakazawa, Y.; Nakano, H.; Inoue, K. Approach to a Single-Component Ferrimagnetism by Organic Radical Crystals. *J. Am. Chem. Soc.* **2001**, *123*, 7921–7922. DOI:10.1021/ja015711r

[85] Thomson, R. I.; Pask, C. M.; Lloyd, G. O.; Mito, M.; Rawson, J. M. Pressure-Induced Enhancement of Magnetic-Ordering Temperature in an Organic Radical to 70 K: A Magnetostructural Correlation. *Chem. – Eur. J.* **2012**, *18*, 8629–8633. DOI:10.1002/chem.201200760

[86] Alberola, A.; Less, R. J.; Pask, C. M.; Rawson, J. M.; Palacio, F.; Oliete, P.; Paulsen, C.; Yamaguchi, A.; Farley, R. D.; Murphy, D. M. A Thiazyl-Based Organic Ferromagnet. *Angew. Chem. Int. Ed.* **2003**, *42*, 4782–4785. DOI:10.1002/anie.200352194

[87] Chiarelli, R.; Novak, M. A.; Rassat, A.; Tholence, J. L. A ferromagnetic transition at 1.48 K in an organic nitroxide. *Nature* **1993**, *363*, 147–149. DOI:10.1038/363147a0

[88] Fujita, W.; Awaga, K. Organic ferromagnetism of T_c=6.7 K driven by evaporation of crystal Solvent. *Chem. Phys. Lett.* **2002**, *357*, 385–388. DOI:10.1016/S0009-2614(02)00535-3

[89] Fujita, W.; Awaga, K.; Takahashi, M.; Takeda, M.; Yamazaki, T. Spontaneous magnetization below 44 K in (benzo[1,2-d:4,5-d']bis[1,3,2]dithiazole)·$FeCl_4$ driven by evaporation of crystal solvent. *Chem. Phys. Lett.* **2002**, *362*, 97–102. DOI:10.1016/S0009-2614(02)01056-4

[90] Yu, X.; Mailman, A.; Dube, P. A.; Assoud, A.; T. Oakley, R. The first semiquinone-bridged bisdithiazolyl radical conductor: a canted antiferromagnet displaying a spin-flop transition. *Chem. Commun.* **2011**, *47*, 4655–4657. DOI:10.1039/C1CC10598A

[91] Winter, S. M.; Mailman, A.; Oakley, R. T.; Thirunavukkuarasu, K.; Hill, S.; Graf, D. E.; Tozer, S. W.; Tse, J. S.; Mito, M.; Yamaguchi, H. Electronic and magnetic structure of neutral radical FBBO. *Phys. Rev. B* **2014**, *89*, 214403. DOI:10.1103/PhysRevB.89.214403

[92] Yu, X.; Mailman, A.; Lekin, K.; Assoud, A.; Robertson, C. M.; Noll, B. C.; Campana, C. F.; Howard, J. A. K.; Dube, P. A.; Oakley, R. T. Semiquinone-Bridged Bisdithiazolyl Radicals as Neutral Radical Conductors. *J. Am. Chem. Soc.* **2012**, *134*, 2264–2275. DOI:10.1021/ja209841z

[93] Mailman, A.; Winter, S. M.; Wong, J. W. L.; Robertson, C. M.; Assoud, A.; Dube, P. A.; Oakley, R. T. Multiple Orbital Effects and Magnetic Ordering in a Neutral Radical. *J. Am. Chem. Soc.* **2015**, *137*, 1044–1047. DOI:10.1021/ja512235h

[94] Leitch, A. A.; Brusso, J. L.; Cvrkalj, K.; Reed, R. W.; Robertson, C. M.; Dube, P. A.; Oakley, R. T. Spin-canting in heavy atom heterocyclic radicals. *Chem. Commun.* **2007**, 3368–3370. DOI:10.1039/b708756j

[95] Robertson, C. M.; Leitch, A. A.; Cvrkalj, K.; Reed, R. W.; Myles, D. J. T.; Dube, P. A.; Oakley, R. T. Enhanced Conductivity and Magnetic Ordering in Isostructural Heavy Atom Radicals. *J. Am. Chem. Soc.* **2008**, *130*, 8414–8425. DOI:10.1021/ja801070d

[96] Robertson, C. M.; Myles, D. J. T.; Leitch, A. A.; Reed, R. W.; Dooley, B. M.; Frank, N. L.; Dube, P. A.; Thompson, L. K.; Oakley, R. T. Ferromagnetism in a Heavy Atom Heterocyclic Radical Conductor. *J. Am. Chem. Soc.* **2007**, *129*, 12688–12689. DOI:10.1021/ja076841o

[97] Robertson, C. M.; Leitch, A. A.; Cvrkalj, K.; Myles, D. J. T.; Reed, R. W.; Dube, P. A.; Oakley, R. T. Ferromagnetic Ordering in Bisthiaselenazolyl Radicals: Variations on a Tetragonal Theme. *J. Am. Chem. Soc.* **2008**, *130*, 14791–14801. DOI:10.1021/ja8054436

[98] Miller, J. S.; Calabrese, J. C.; Rommelmann, H.; Chittipeddi, S. R.; Zhang, J. H.; Reiff, W. M.; Epstein, A. J. Ferromagnetic Behavior of $[Fe(C_5Me_5)_2]^{\bullet+}[TCNE]^{\bullet-}$. Structural and Magnetic Characterization of Decamethylferrocenium Tetracyanoethenide, $[Fe(C_5Me_5)_2]^{\bullet+}[TCNE]^{\bullet+}\cdot MeCN$ and Decamethylferrocenium Pentacyanopropenide, $[Fe(C_5Me_5)_2]^{\bullet+}[C_3(CN)_5]^-$. *J. Am. Chem. Soc.* **1987**, *109*, 769–781. DOI:10.1021/ja00237a023

[99] Manriquez, J. M.; Yee, G. T.; McLean, R. S.; Epstein, A. J.; Miller, J. S. A Room-Temperature Molecular/Organic-Based Magnet. *Science* **1991**, *252*, 1415–1417. DOI:10.1126/science.252.5011.1415

[100] Yoshizawa, K.; Hoffmann, R. The Role of Orbital Interactions in Determining Ferromagnetic Coupling in Organic Molecular Assemblies *J. Am. Chem. Soc.* **1995**, *117*, 6921–6926. DOI:10.1021/ja00131a014

[101] Kahn, O. *Molecular Magnetism*, Wiley-VHC, 1993.

[102] Kinoshita, M. Ferromagnetism of Organic Radical Crystals. *Jpn. J. Appl. Phys.* **1994**, *33*, 5718–5733. DOI:10.1143/JJAP.33.5718

[103] Beldjoudi, Y.; Arauzo, A.; Palacio, F.; Pilkington, M.; Rawson, J. M. Studies on a "Disappearing Polymorph": Thermal and Magnetic Characterization of α-*p*-$NCC_6F_4CNSSN^{\bullet}$. *J. Am. Chem. Soc.* **2016**, *138*, 16779–16786. DOI:10.1021/jacs.6b10707

[104] Bond, A. D.; Haynes, D. A.; Pask, C. M.; Rawson, J. M. Concomitant polymorphs: structural studies on the trimorphic dithiadiazolyl radical, ClCNSSN. *J. Chem. Soc. Dalton Trans.* **2002**, 2522–2531. DOI:10.1039/B110922G

[105] Winter, S. M.; Oakley, R. T.; Kovalev, A. E.; Hill, S. Spin-orbit effects in heavy-atom organic radical ferromagnets. *Phys. Rev. B* **2012**, *85*, 094430. DOI:10.1103/PhysRevB.85.094430

[106] Mansikkamäki, A., Tuononen, H. M. The Role of Orbital Symmetries in Enforcing Ferromagnetic Ground State in Mixed Radical Dimers. *J. Phys. Chem. Lett.* **2018**, *9*, 3624–3630. DOI:10.1021/acs.jpclett.8b01507

[107] Karimi-Jafari, M.; Padrela, L.; Walker, G. M.; Croker, D. M. Creating Cocrystals: A Review of Pharmaceutical Cocrystal Preparation Routes and Applications. *Cryst. Growth Des.* **2018**, *18*, 6370–6387. DOI:10.1021/acs.cgd.8b00933

[108] Izuoka, A.; Fukada, M,; Sugawara, T.; Sakai, M.; Bandow, S. Magnetic Property of 1,3,5-Tris(4′,4′,5′,5′-tetramethylimidazolin-2-yl)benzene 3′,3′′,3′′′-Trioxide 1′,1′′,1′′′-Trioxyl in 1 : 1 Mixed Crystals with 1,3,5-Trinitrobenzene. *Chem. Lett.* **1992**, 1627–1630. DOI:10.1246/cl.1992.1627

[109] Izuoka, A.; Fukada, M.; Kumai, R.; Itakura, M.; Hikami, S.; Sugawara, T. Magnetically Coupled Molecular System Composed of Organic Radicals with Different Spin Multiplicities. *J. Am. Chem. Soc.* **1994**, *116*, 2609–2610. DOI:10.1021/ja00085a047

[110] Allen, C.; Haynes, D. A.; Pask, C. M.; Rawson, J. M. Co-crystallisation of thiazyl radicals: preparation and crystal structure of [PhCNSSN][C_6F_5CNSSN]. *CrystEngComm* **2009**, *11*, 2048–2050. DOI:10.1039/B906225D

[111] Robinson, W. S.; Haynes, D. A.; Rawson, J. M. Co-crystal formation with 1,2,3,5-dithiadiazolyl radicals. *CrystEngComm* **2013**, *15*, 10205–10211. DOI:10.1039/C3CE41519H

[112] Nascimento, M. A.; Heyer, E.; Clarke, J. J.; Cowley, H. J.; Alberola, A.; Stephaniuk, N.; Rawson, J. M. On the Design of Radical–Radical Cocrystals. *Angew. Chem.* **2019**, *131*, 1385–1389. DOI:10.1002/ange.201812132

[113] Stephaniuk, N. T.; Nascimento, M. A.; Nikoo, S., Heyer, E.; Watanabe, L. K.; Rawson, J. M. Robust S_4···O Supramolecular Synthons: Structures of Radical-Radical Cocrystals [*p*-XC6F_4CNSSN]$_2$[TEMPO] (X=F, Cl, Br, I, CN). *Chem. Eur. J.* 2022, 28, e202103846. DOI:10.1002/chem.202103846

[114] Kahn, O.; Launay, J. P. Molecular bistability, An overview. *Chemtronics* **1988**, *3*, 140–151.

[115] Brooker, S. Spin crossover with thermal hysteresis: practicalities and lessons learnt. *Chem. Soc. Rev.* **2015**, *44*, 2880–2892. DOI:10.1039/C4CS00376D

[116] *Spin-Crossover Materials: Properties and Applications*, Halcrow, M. A. (Ed.), Wiley, 2013.

[117] Paul, A.; Gupta, A.; Konar, S. Magnetic Transition in Organic Radicals: The Crystal Engineering Aspects. *Cryst. Growth Des.* **2021**, *21*, 5473–5489. DOI:10.1021/acs.cgd.1c00731

[118] Li, T.; Tan, G.; Shao, D.; Li, J.; Zhang, Z.; Song, Y.; Sui, Y.; Chen, S.; Fang, Y.; Wang, X. Magnetic Bistability in a Discrete Organic Radical. *J. Am. Chem. Soc.* **2016**, *138*, 10092–10095. DOI:10.1021/jacs.6b05863

[119] Itkis, M. E.; Chi, X.; Cordes, A. W.; Haddon, R. C. Magneto-Opto-Electronic Bistability in a Phenalenyl-Based Neutral Radical. *Science* **2002**, *296*, 1443–144. DOI:10.1126/science.1071372

[120] Shultz, D. A.; Fico, R. M., Jr.; Boyle, P. D.; Kampf, J. W. Observation of a Hysteretic Phase Transition in a Crystalline Dinitroxide Biradical That Leads to Magnetic Bistability. *J. Am. Chem. Soc.* **2001**, *123*, 10403–10404. DOI:10.1021/ja011341v

[121] Fujita, W.; Awaga, K. Room-Temperature Magnetic Bistability in Organic Radical Crystals. *Science* **1999**, *286*, 261–262. DOI:10.1126/science.286.5438.261

[122] Brusso, J. L.; Clements, O. P.; Haddon, R. C.; Itkis, M. E.; Leitch, A. A.; Oak-ley, R. T.; Reed, R. W.; Richardson, J. F. Bistabilities in 1,3,2-Dithiazolyl Radicals. *J. Am. Chem. Soc.* **2004**, *126*, 8256–8265. DOI:10.1021/ja048618m

[123] Barclay, T. M.; Cordes, A. W.; George, N. A.; Haddon, R. C.; Itkis, M. E.; Mashuta, M. S.; Oakley, R. T.; Patenaude, G. W.; Reed, R. W.; Richardson, J. F.; Zhang, H. Redox, Magnetic, and Structural Properties of 1,3,2-Dithiazolyl Radicals. A Case Study on the Ternary Heterocycle $S_3N_5C_4$. *J. Am. Chem. Soc.* **1998**, *120*, 352–360. DOI:10.1021/ja973338a

[124] Bates, D.; Robertson, C. M.; Leitch, A. A.; Dube, P. A.; Oakley, R. T. Magnetic Bistability in Naphtho-1,3,2-Dithiazolyl: Solid State Interconversion of a Thiazyl π-Radical and Its N–N σ-Bonded Dimer. *J. Am. Chem. Soc.* **2018**, *140*, 3846–3849. DOI:10.1021/jacs.7b13699

[125] Lekin, K.; Winter, S. M.; Downie, L. E.; Bao, X.; Tse, J. S.; Desgreniers, S.; Secco, R. A.; Dube, P. A.; Oakley, R. T. Hysteretic Spin Crossover between a Bisdithiazolyl Radical and Its Hypervalent σ-Dimer. *J. Am. Chem. Soc.* **2010**, *132*, 16212–16224. DOI:10.1021/ja106768z

[126] Matsuzaki, H.; Fujita, W.; Awaga, K.; Okamoto H. Photoinduced Phase Transition in an Organic Radical Crystal with Room-Temperature Optical and Magnetic Bistability. *Phys. Rev. Lett.* **2003**, *91*, 017403. DOI:10.1103/PhysRevLett.91.017403

[127] Tanaka, T.; Fujita, W.; Awaga, K. Pressure effects on magnetic bistability in a heterocyclic thiazyl radical TTTA. *Chem. Phys. Lett.* **2004**, *393*, 150–152. DOI:10.1016/j.cplett.2004.05.108

[128] Mills, M. B.; Wohlhauser, T.; Stein, B.; Verduyn, W. R.; Song, E.; Dechambenoit, P.; Rouzières, M.; Clérac, R.; Preuss, K. E. Magnetic Bistability in Crystalline Organic Radicals: The Interplay of H-Bonding, Pancake Bonding, and Electrostatics in 4-(2′-Benzimidazolyl)-1,2,3,5-Dithiadiazolyl. *J. Am. Chem. Soc.* **2018**, *140*, 16904–16908. DOI:10.1021/jacs.8b10370

[129] Brooks, W. V. F.; Burford, N.; Passmore, J.; Schriver, M. J.; Sutcliffe, L. H. Paramagnetic liquids: the preparation and characterisation of the thermally stable radical Bu^{t}CNSNS$^\bullet$ and its quantitative photochemically symmetry allowed rearrangement to a second stable radical Bu^{t}CNSSN$^\bullet$. *J. Chem. Soc. Chem. Commun.* **1987**, 69–71. DOI:10.1039/C39870000069

[130] Du, H.; Haddon, R. C.; Krossing, I.; Passmore, J.; Rawson, J. M.; Schriver, M. J. Thermal Hysteresis in Dithiadiazolyl and Dithiazolyl Radicals Induced by Supercooling of Paramagnetic Liquids Close to Room Temperature: A Study of $F_3CCNSSN$ and an Interpretation of the Behaviour of $F_3CCSNSCCF_3$. *Chem. Commun.* **2002**, 1836–1837. DOI:10.1039/B202627A

[131] Beldjoudi, Y.; Sun, R.; Arauzo, A.; Campo, J.; Less, R. J.; Rawson, J. M. Structural Variations in the Dithiadiazolyl Radicals *p*-ROC_6F_4CNSSN (R = Me, Et, ^{n}Pr, ^{n}Bu): A Case Study of Reversible and Irreversible Phase Transitions in *p*-$EtOC_6F_4CNSSN$. *Cryst. Growth Des.* **2018**, *18*, 179–188. DOI:10.1021/acs.cgd.7b01065

[132] Yan, B.; Horton, P. N.; Weston, S. C.; Russell, A. E.; Grossel, M. C. Novel TCNQ-stacking motifs in (12-crown-4)-complexes of alkali metal TCNQ Salts. *CrystEngComm* **2021**, *23*, 6755–6760. DOI:10.1039/D1CE01075A

[133] Lunelli, B.; Pecile, C. Polarized Infrared Spectra of TCNQ and TCNQ-d_4 Single Crystals. *J. Chem. Phys.* **1970**, *52*, 2375–2377. DOI:10.1063/1.1673316

ORIGINAL PAPERS

I

NON-INNOCENT BASE PROPERTIES OF 3- AND 4-PYRIDYL-DITHIA- AND DISELENADIAZOLYL RADICALS: THE EFFECT OF *N*-METHYLATION

by

Taponen, A. I.; Wong, J. W. L.; Lekin, K.; Assoud, A.; Robertson, C. M.; Lahtinen, M.; Clérac, R.; Tuononen, H. M.; Mailman, A.; Oakley, R. T. 2018

Inorganic Chemistry, 57 (21), 13901–13911

https://doi.org/10.1021/acs.inorgchem.8b02416

Inorganic Chemistry
Article
Cite This: Inorg. Chem. 2018, 57, 13901−13911
pubs.acs.org/IC

Non-Innocent Base Properties of 3- and 4-Pyridyl-dithia- and Diselenadiazolyl Radicals: The Effect of *N*-Methylation

Anni I. Taponen,[†] Joanne W. L. Wong,[‡] Kristina Lekin,[‡] Abdeljalil Assoud,[‡] Craig M. Robertson,[§] Manu Lahtinen,[†] Rodolphe Clérac,[⊥,∥] Heikki M. Tuononen,[†] Aaron Mailman,*[,†,‡] and Richard T. Oakley*[,‡]

[†]Department of Chemistry, University of Jyväskylä, P.O. Box 35, Jyväskylä, Finland
[‡]Department of Chemistry, University of Waterloo, Waterloo, Ontario N2L 3G1, Canada
[§]Department of Chemistry, University of Liverpool, Liverpool, L69 7ZD, United Kingdom
[⊥]Centre National de la Recherche Scientifique, CNRS, CRPP, UMR 5031, 33600 Pessac, France
[∥]Université de Bordeaux, CRPP, UPR 5031, 33600 Pessac, France

Supporting Information

ABSTRACT: Condensation of persilylated nicotinimideamide and isonicotinimideamide with sulfur monochloride affords double salts of the 3-, 4-pyridyl-substituted 1,2,3,5-dithiadiazolylium DTDA cations of the general formula [3-, 4-pyDTDA][Cl][HCl] in which the pyridyl nitrogen serves as a non-innocent base. Reduction of these salts with triphenylantimony followed by deprotonation of the intermediate-protonated radical affords the free base radicals [3-, 4-pyDTDA], the crystal structures of which, along with those of their diselenadiazolyl analogues [3-, 4-pyDSDA], have been characterized by powder or single-crystal X-ray diffraction. The crystal structures consist of "pancake" π-dimers linked head-to-tail into ribbonlike arrays by η^2-S_2---N(py) intermolecular secondary bonding interactions. Methylation of the persilylated (iso)nicotinimide-amides prior to condensation with sulfur monochloride leads to *N*-methylated double chloride salts Me[3-, 4-pyDTDA][Cl]$_2$, which can be converted by metathesis into the corresponding triflates Me[3-, 4-pyDTDA][OTf]$_2$ and then reduced to the *N*-methylated radical triflates Me[3-, 4-pyDTDA][OTf]. The crystal structures of both the *N*-methylated double triflate and radical triflate salts have been determined by single-crystal X-ray diffraction. The latter consist of *trans*-cofacial π-dimers strongly ion-paired with triflate anions. Variable temperature magnetic susceptibility measurements on both the neutral and radical ion dimers indicate that they are diamagnetic over the temperature range 2−300 K.

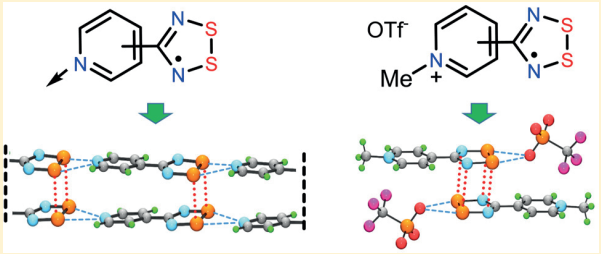

INTRODUCTION

1,2,3,5-Dithiadiazolyl (DTDA) radicals have been widely studied for many years,[1] initially with a view to their utilization as building blocks for molecular magnetic materials,[2] molecular semiconductors, and conductive charge transfer salts $[DTDA]^{\delta+}[X]^{\delta-}$.[3] More recently, they have also been explored as ligands to *d*- and *f*-block metals,[4] fluorophores in solution and polymer composites,[5] external field-driven nonlinear optical switches,[6] and paramagnetic guests in porous[7] and nonporous host frameworks.[8] In the absence of steric protection, DTDA radicals associate in the solid state, forming nominally diamagnetic dimers that display a partial or complete loss of their $S = 1/2$ magnetic signature. Selenium-based (DSDA) analogues have also been investigated, and in these systems the tendency to dimerize is even stronger; however, as with DTDAs,[9] steric effects can impede dimerization.[10] Pairwise association of the radicals by overlap of their singly occupied molecular orbitals (SOMOs) can occur in a variety of ways, some of which are shown in Chart 1. Of these, by far the most common is the *cis*-cofacial mode, which involves the direct superposition of two radicals separated by a pair of 4-center 2-electron[11] S---S (or Se---Se)[12] contacts. The

Chart 1

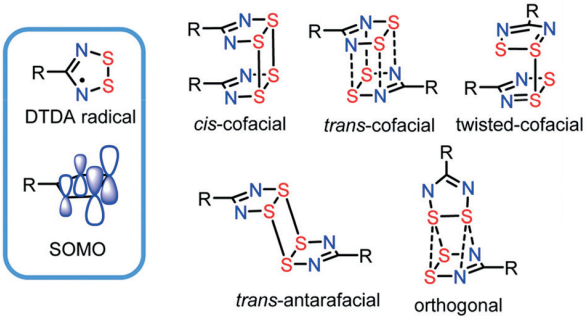

Received: August 27, 2018
Published: October 11, 2018

DOI: 10.1021/acs.inorgchem.8b02416
Inorg. Chem. 2018, 57, 13901−13911

nature of these interactions, now commonly referred to as "pancake" π-bonds,[13] has been the subject of much debate, the focus being on whether the pairing of the SOMOs of two radicals affords an open- or closed-shell singlet state.

Considerable synthetic effort has been directed toward the control of the dimerization mode and packing pattern of the resulting pairs, partly with the intent of encouraging π-stacked dimer arrays, which historically were viewed as the most effective way to introduce a pathway for charge transport.[1c,3a,14] One approach that has served well has been the use of intermolecular secondary bonding interactions (SBIs) between the disulfide (diselenide) unit of the DTDA (DSDA) ring and a lone-pair carrying heteroatom attached to the 4-substituent. The effect was first demonstrated in the 2-, 3-, and 4-cyanophenyl DTDA (DSDA) dimers[15] and later extended to cyanofuryl[16] and cyanothienyl[17] derivatives. In all these materials, the dimers are connected into ribbonlike arrays linked by η^2-S_2---NC SBIs (Figure 1). The resulting ribbons

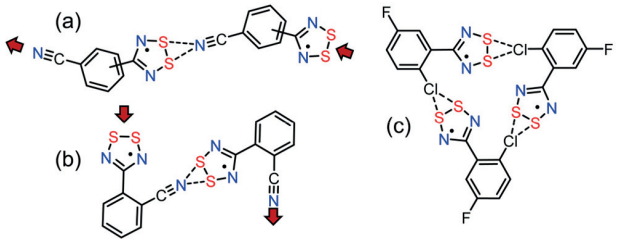

Figure 1. Ribbonlike arrays of radicals (dimers) linked by η^2-S_2···NC SBIs in (a) 3-, 4-cyanophenyl-DTDA and (b) 2-cyanophenyl-DTDA.[15] (c) Triangular motif generated by η^2-S_2···Cl SBIs in 2-chloro-5-fluorophenyl-DTDA.[20]

then pack into layers that, in some cases, afford the desired superimposed π-stack arrays with the DSDA derivatives displaying small bandgap semiconductive properties.[14] From a magnetic perspective, a vital modification of this strategy, developed by Rawson and co-workers in the mid-1900s, involved attachment of a cyano (or nitro) group to an otherwise fully fluorinated phenyl substituent on a DTDA radical.[18] The impact was 2-fold: (i) the η^2-S_2---NC (or η^2-S_2---O_2N) SBIs locked the radicals into ribbons, and (ii) the steric protection afforded by perfluorination of the phenyl group suppressed dimerization. The discovery of these undimerized DTDA radicals and their sometimes startling magnetic properties[19] represents one of the major triumphs in the development of radical-based molecular materials.

Exploration of ligand design and the resulting effect on solid-state architecture continues, and the range of structure-making SBIs has been expanded. The packing of 2-chlorophenyl-substituted DTDA dimers, for example, is dominated by short η^2-S_2---Cl intermolecular contacts that, like η^2-S_2---NC SBIs, are effective in generating layered structures.[20] Likewise, the 2-pyridyl-substituted radicals 2-pyDTDA and 2-pyDSDA and related pyrimidyl derivatives developed by Preuss and co-workers serve as chelating (Chart 2) ligands to paramagnetic metal ions. The resulting coordination complexes display a rich array of magnetic properties, ranging from single molecule magnets to magnetically ordered materials and magneto-thermal switches.[21] In contrast, the related 3-, 4-pyDTDA radicals[22] have received relatively little attention. A number of metal complexes have been reported,[23,24] but information on the radicals themselves is sparse, and the corresponding 3,4-

Chart 2

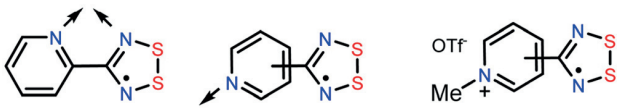

2-pyDTDA 3-, 4-pyDTDA Me[3-, 4-pyDTDA][OTf]

pyDSDA derivatives are, to date, unknown. The relative dearth of information on these particular radicals may stem in part from the presence of a basic nitrogen on the ligand, which has caused some difficulties in their isolation. To address this issue, we provide here full structural characterization of the dimers of the 3-, 4-pyDTDA and 3, 4-pyDSDA derivatives as well as modifications to the synthetic procedures made necessary by the "non-innocent" base properties of the pyridyl ligand. In addition, as a first step in taking advantage of the coordination chemistry of the ligand, we also report the preparation and structural characterization of the *N*-methyl-pyridinium-substituted radical salts Me[3-pyDTDA][OTf] and Me[4-pyDTDA][OTf].

RESULTS AND DISCUSSION

Synthesis. Early synthetic routes to the DTDA framework involving the addition reactions of thiazyl halides[25] or sulfur monochloride/ammonium chloride mixtures[26] to nitriles have been largely replaced by methods based on the condensation of an amidine, more particularly a persilylated amidine,[27] with sulfur monochloride or dichloride to afford an oxidized dithiadiazolylium chloride salt. Reduction of the latter, typically with triphenylantimony, liberates the neutral radical, which may be purified by vacuum sublimation. This methodology, which is easily extended to the preparation of selenium-based analogues,[28] provides the basis for the synthesis of 3-, 4-pyDTDA and 3-, 4-pyDSDA described here.

The necessary persilylated amidines 3- and 4-pyADS were generated by the addition of lithium bis(trimethylsilylamide) to the appropriate nitrile (3-NCpy, 4-NCpy) followed by quenching the intermediate lithiated amidinate with chlorotrimethylsilane (Scheme 1A). Typically, such reactions employ diethyl ether or toluene/ether mixtures as the reaction solvent, but for these pyridyl-substituted nitriles, the use of the more strongly basic solvent tetrahydrofuran is critical to suppress solvation of Li^+ ions with the pyridyl nitrogen and to keep the otherwise insoluble lithiated intermediate in solution. Consistently, the subsequent silylation step can only be effected in tetrahydrofuran at reflux. The resulting persilylated amidines may then be purified by fractional distillation in vacuo.

Most silylated amidines undergo a smooth condensation with excess sulfur mono- or dichloride to afford directly the appropriate dithiadiazolylium chloride salt [DTDA][Cl] as an insoluble yellow-orange solid. However, for both 3- and 4-pyDTDA this general procedure requires modifications arising from the fact that the initial condensation reaction affords *not* the simple salt but its highly moisture-sensitive hydrochloride double salt, that is, [3, 4-pyDTDA][Cl][HCl], in which the pyridyl nitrogen is protonated (Scheme 1B). By contrast, protonated intermediates are not observed in the preparation of the analogous perfluorinated derivative 4-(F_4-py)-DTDA as a result of the weaker base strength of the perfluoropyridyl moiety.[29] Reduction of these double salts with triphenylantimony in MeCN then affords the corresponding hydrochloride

DOI: 10.1021/acs.inorgchem.8b02416
Inorg. Chem. 2018, 57, 13901−13911

Scheme 1

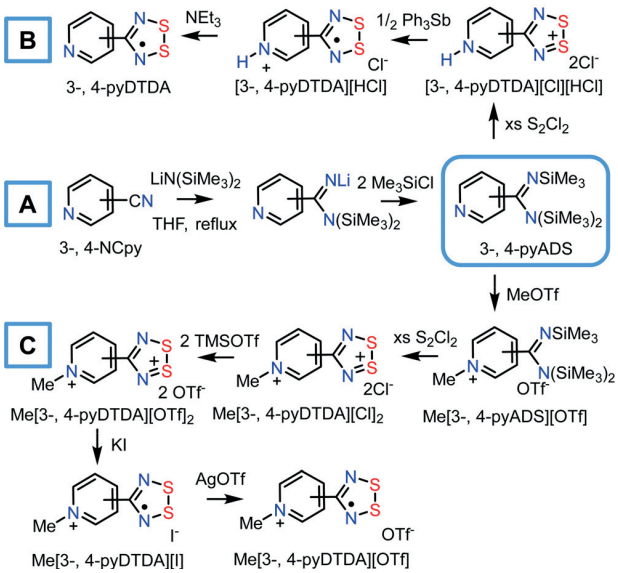

salts of the radical, that is, [3-, 4-pyDTDA][HCl]. Finally, rinsing these insoluble hydrochloride salts with a solution of excess triethylamine in MeCN liberates the free-base radicals 3-, 4-pyDTDA, which may be purified by fractional sublimation in vacuo. The sequence of events may be conveniently tracked by infrared spectroscopy, as illustrated in Figure 2 (see also Figure S1), which shows the spectral changes observed during the preparation of 4-pyDTDA.

To explore more fully the stepwise nature of the synthesis of 3-, 4-DTDA, we pursued the *N*-methylated analogues of the protonated intermediates described above with the goal of obtaining structural information. To this end, we prepared the *N*-methylated amidinium triflate salts Me[3-, 4-pyADS][OTf] by treatment of the respective persilylated amidine with methyl triflate (Scheme 1C). Condensation of these materials with sulfur monochloride afforded the double chloride salts Me[3-, 4-pyDTDA][Cl]$_2$, the methylated analogues of the protonated double salts described above. Metathesis of these chloride salts with trimethylsilyl triflate (TMSOTf) provided access to the corresponding double triflates Me[3-, 4-pyDTDA][OTf]$_2$, crystals of which were suitable for crystallographic work. Finally, reduction of these double salts with potassium iodide yielded the *N*-methyl radical iodides Me[3-, 4-pyDTDA][I], which upon treatment with silver triflate were converted to *N*-methyl radical triflates Me[3-, 4-pyDTDA][OTf], crystals of which were also suitable for crystallographic analysis.

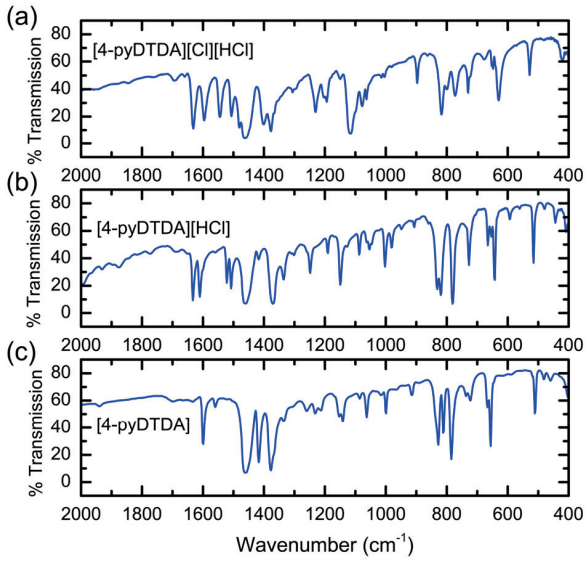

Figure 2. Infrared spectra (as nujol mulls) of intermediates in the synthesis of 4-pyDTDA, as shown in Scheme 1A: (a) [4-pyDTDA][Cl][HCl] double salt, (b) [4-pyDTDA][HCl] protonated radical salt, and (c) neutral [4-pyDTDA].

Preparation of the selenium-based radicals 3-, 4-pyDSDA was more straightforward than that described above for 3-, 4-pyDTDA, possibly because the condensation reaction employed stoichiometric amounts of $SeCl_2$ generated by comproportionation of Se and $SeCl_4$,[28] as a result of which the presence of adventitious HCl (present in S_2Cl_2) was all but eliminated. Accordingly, the simple chlorides [3-, 4-pyDSDA][Cl] were generated directly during the condensation (Scheme 2), and reduction of these salts with triphenylantimony then released the corresponding radical dimers, which could be purified by sublimation in vacuo.

Scheme 2

Crystallography on Radical Dimers. Analytically pure samples of the dimers of the four radicals 3-, 4-pyDTDA and 3-, 4-pyDSDA were generated by fractional sublimation in vacuo. Crystals of 3-pyDTDA and 3-, 4-pyDSDA so obtained were suitable for structural analysis by single-crystal X-ray diffraction methods. Crystal data are summarized in Table S1, and ORTEP drawings of the dimer units are shown in Figure 3.

The almost spherical, powdery nodules of 4-pyDTDA obtained by sublimation did not diffract as single crystals but did generate a reproducible powder X-ray diffraction (PXRD) pattern consisting of a few sharp peaks and some broad "humps" (Figure 4), an appearance characteristic of a disordered nanocrystalline phase.[30] Material obtained by recrystallization from *o*-dichlorobenzene afforded a similar pattern. Changes in sample preparation, such as sample grinding, did not lead to a marked change in line width or resolution of the diffractogram. Attempts to index the PXRD data collected on both laboratory and synchrotron X-ray sources with conventional indexing programs (DICVOL, McMaille, Topas) were unsuccessful, mainly because of the paucity and poor resolution of some of the diffraction peaks, which hindered assignment of a space group and specification of a unit cell. Eventually, however, by comparing the observed diffraction pattern with that predicted for the selenium analogue 4-pyDSDA, we were able to index the data manually to the *C*2/*c* space group and identify a unit cell similar to that observed for both 4-pyDSDA and its perfluorinated variant 4-(F_4-py)DTDA.[29,31]

The PXRD data was subsequently modeled in DASH using synthetic annealing methods based on a molecular unit adapted from the known molecular coordinates of 4-cyanophenyl-DTDA.[15] This procedure afforded a plausible

DOI: 10.1021/acs.inorgchem.8b02416
Inorg. Chem. 2018, 57, 13901−13911

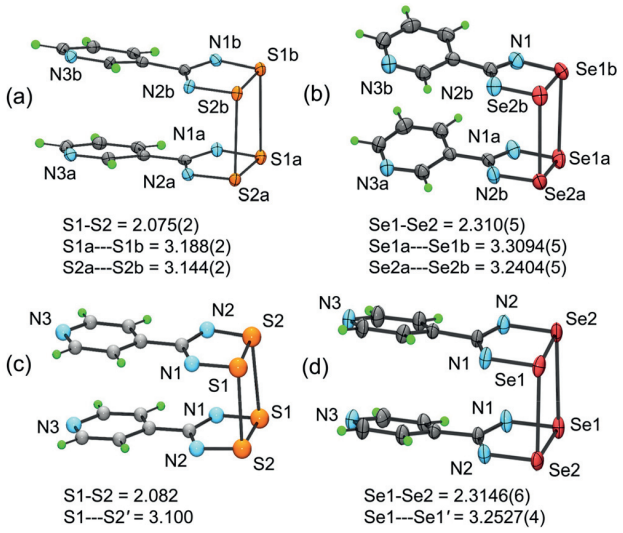

Figure 3. Drawings of dimer units in (a) 3-pyDTDA, (b) 3-pyDSDA, (c) 4-pyDTDA, and (d) 4-pyDSDA with atom numbering and selected metrics in Å; for averaged values, numbers in parentheses are the greater of the difference and the standard deviation. Thermal ellipsoids and standard deviations are not available for 4-pyDTDA.

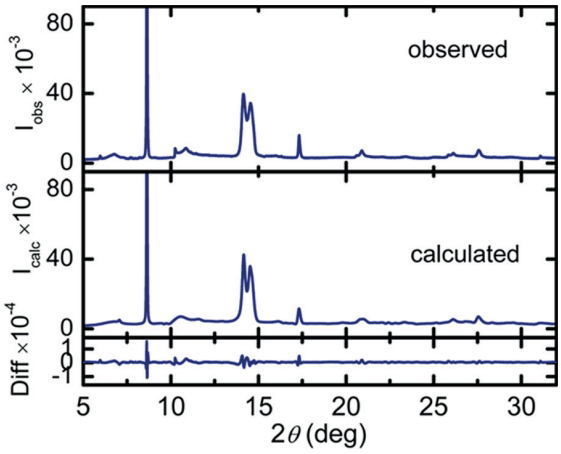

Figure 4. Observed and calculated PXRD pattern for *cis*-cofacial 4-pyDTDA (λ = 0.825925 Å).

solution based on *cis*-cofacial dimers (Figure 3c) linked head-to-tail into antiparallel chains in a fashion very similar to that found for 4-pyDSDA. This solution was refined by Rietveld methods using a rigid-body constraint in which only the unit cell parameters were optimized; the resulting crystal data are provided in Table S2, and the observed/calculated PXRD patterns are presented in Figure 4. Two other solutions with the same cell parameters but based on *trans*-cofacial and *trans*-antarafacial dimers were similarly refined. The resulting (optimized) crystal data are provided in Table S2, and observed and calculated PXRD patterns are presented in Figures S2 and S3. The observation of these additional solutions is symptomatic of a disordered nanocrystalline phase[30] in which there is a large number of faults in the layering of the molecular ribbons.

The molecular metrics for 3-pyDTDA and 3,4-pyDSDA, notably the internal and intradimer S−S (Se−Se) distances, are all nominal for this class of radicals. In the *cis*-cofacial dimer of 4-pyDTDA, positional refinements were not carried out, but the mean intradimer S−S separation (3.10 Å) is consistent with that observed in 4-cyanophenyl-DTDA (3.10(2) Å). The crystal packing of all four dimers follows the pattern observed for the related cyanophenyl derivatives being comprised of ribbonlike arrays of *cis*-cofacial dimers linked head-to-tail by short η^2-S_2---N(py) and η^2-Se_2---N(py) SBIs; summaries of pertinent intermolecular metrics are provided in Figures S4 and S5. In 3-pyDTDA and 3-pyDSDA (Figure 5), which are

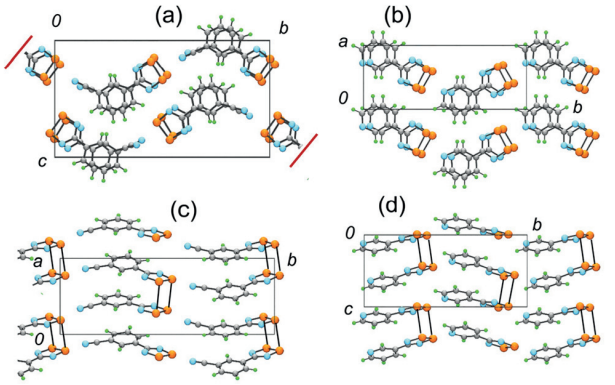

Figure 5. Antiparallel ribbonlike arrays of dimers in (a) α-3-cyanophenyl-DTDA ($P2_1/n$) and (b) 3-pyDTDA ($P2_1$) linked head-to-tail by η^2-S_2---NC and η^2-S_2---N(py) SBIs, respectively. Out-of-register, superimposed π-stacks of dimers for each are shown in (c) and (d). The corresponding DSDA dimers are isostructural.

isostructural, the two radicals in the dimer unit are not related by symmetry, but in 4-pyDTDA and 4-pyDSDA (Figure 6), the two halves of the dimer are related by a 2-fold rotation. In all four cases, the pyridyl group is rotated slightly about the connector C−C linkage, affording C−C−C−N torsion angles ranging from 8.1° in 4-pyDTDA to 16.8° in 4-pyDSDA. Packing patterns for the simulated annealing solutions based on *trans*-cofacial and *trans*-antarafacial 4-pyDTDA dimers are provided in Figures S6 and S7.

Crystallography on *N*-Methylated Salts. Crystals of the *N*-methylated double triflates Me[3-, 4-pyDTDA][OTf]$_2$ and radical ion triflates Me[3-, 4-pyDTDA][OTf] obtained by crystallization from MeCN were all suitable for structural characterization by single-crystal X-ray diffraction. Crystal data for these materials are summarized in Table S3, and ORTEP drawings with intramolecular metrics are provided in Figures 7 and 8. At the molecular level, reduction of the double salts leads to a slight lengthening of the S−S and S−N bonds in accordance with the antibonding nature of the radical SOMO (Chart 1); similar effects are found in neutral DTDA structures. Strong ion pairing between the triflate anion(s) and the DTDA rings is observed in all four salts, and the *trans*-cofacial mode of dimerization found in the radical ion salts is probably driven by the need to facilitate a close electrostatic contact between the triflate anion and *N*-methylpyridinium cation.

The steric bulk of the triflate anions restricts the extent of interdimer interactions in the radical ion salts. In Me[3-pyDTDA][OTf], space group $P\bar{1}$, the ion-paired dimers adopt a 1D head-over-tail slipped π-stack packing pattern running parallel to the *b*-axis with no close interdimer contacts between the inversion-related dimers. In Me[4-pyDTDA][OTf], space

DOI: 10.1021/acs.inorgchem.8b02416
Inorg. Chem. 2018, 57, 13901−13911

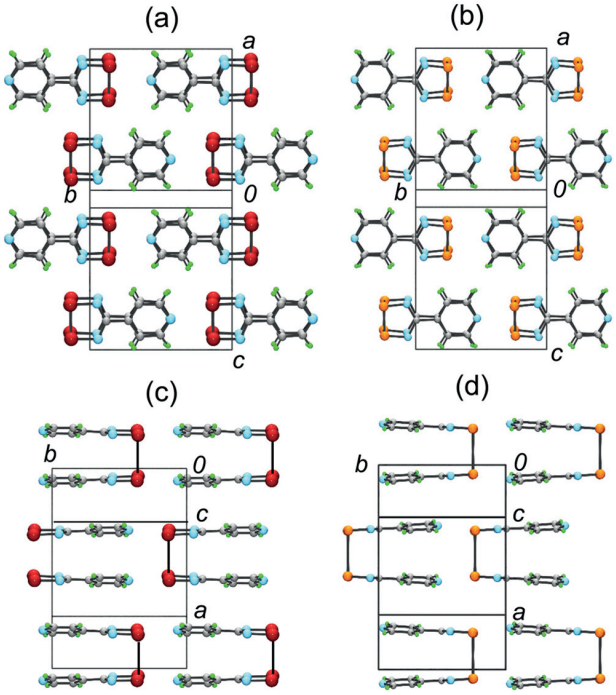

Figure 6. Antiparallel ribbonlike arrays of *cis*-cofacial dimers in (a) 4-pyDSDA and (b) 4-pyDTDA linked head-to-tail by η^2-Se---N(py) and η^2-S_2---N(py) SBIs, respectively, as viewed parallel to *a**. Head-over-tail stacking of π-dimers is shown in (c) and (d).

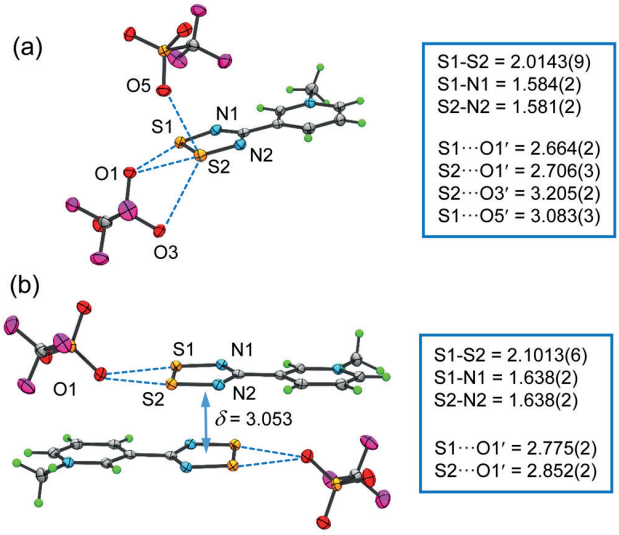

Figure 7. ORTEP drawings (50% ellipsoids) of (a) the asymmetric unit in Me[3-pyDTDA][$OTf]_2$ and (b) the *trans*-cofacial dimer in Me[3-pyDTDA][OTf] with selected bond distances and interionic contacts (dashed lines) in Å (all at 120 K). The $(CN_2S_2)_2$ interplanar separation δ (in Å) is also shown.

group $P2_1/c$, the dimers are aligned into chains in which neighboring dimers are related by *c*-glides, an arrangement that produces a near orthogonal overlap (Figure 9).

EPR Spectroscopy. The X-band EPR spectra (g = 2.0111) of the native radicals 3-, 4-pyDTDA, recorded at ambient temperature on samples dissolved in dichloromethane, display a characteristic quintet pattern (Figure 10) arising from

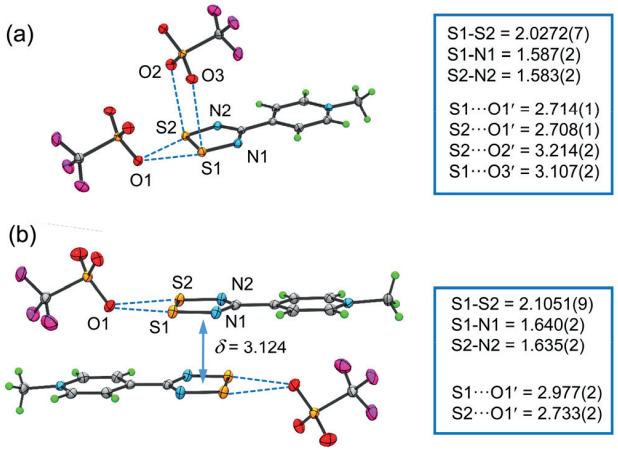

Figure 8. ORTEP drawings (50% ellipsoids) of (a) the asymmetric unit in Me[4-pyDTDA][$OTf]_2$ and (b) the *trans*-cofacial dimer in Me[4-pyDTDA][OTf] with selected bond distances and interionic contacts (dashed lines) in Å (all at 120 K). The $(CN_2S_2)_2$ interplanar separation δ (in Å) is also shown.

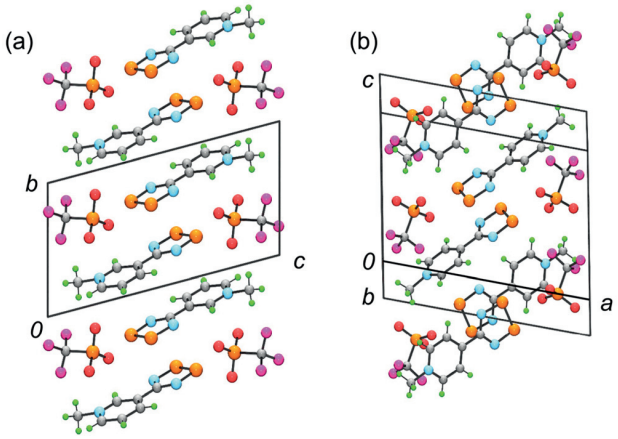

Figure 9. Unit cell drawings for (a) Me[3-pyDTDA][OTf], space group $P\bar{1}$, and (b) Me[4-pyDTDA][OTf], space group $P2_1/c$. In (a), dimers form head-over-tail π-stacks, and in (b), neighboring dimers are related by *c*-glides, which produce a near orthogonal overlap.

hyperfine coupling to two pseudoequivalent ^{14}N nuclei (I = 1); the resulting a_N values (near 0.51 mT) derived by spectral simulation are nominal for this class of radical.[28b,32] As expected, there is no observable hyperfine coupling with the pyridyl nitrogen nuclei, although such interactions may contribute to spectral line broadening. The spectra of the corresponding *N*-methylated cation radicals, obtained from samples of the salts dissolved in MeCN, were almost identical in position and appearance with g = 2.009 and $a_N \approx 0.50$ mT, suggesting that alkylation of the pyridyl ligand induces very little leakage of spin density in the DTDA ring. Isotropic spectral data for the corresponding 3-, 4-pyDSDA radicals could not be measured because the low solubility and high dissociation constants of the respective dimers reduced the signal intensity of the radicals to below the detection limit.

Magnetic Measurements. On the basis of previous experience with other aryl-substituted DSDA dimers, which show little evidence of dissociation in the solid state below 300 K,[14] and the fact that neither of [3-, 4-pyDSDA] displays any EPR signal in the solid state, we have not explored their bulk

DOI: 10.1021/acs.inorgchem.8b02416
Inorg. Chem. 2018, 57, 13901−13911

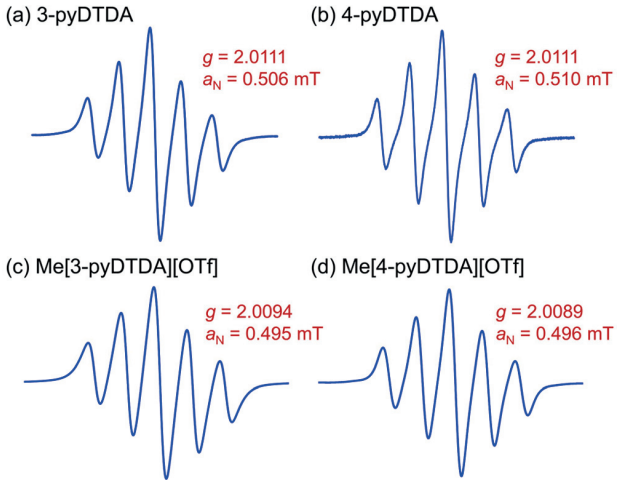

Figure 10. X-band EPR spectra (spectral width = 4 mT) of (a) 3-pyDTDA and (b) 4-pyDTDA in DCM and of (c) Me[3-pyDTDA][OTf] and (d) Me[4-pyDTDA][OTf] in MeCN all at 293 K.

magnetic properties. However, given that DTDA radicals often show complex magnetic behavior with temperature in the solid state, we have performed variable temperature magnetic susceptibility (χ) measurements on both the neutral radicals [3-, 4-pyDTDA] and their *N*-methylated salts Me[3-, 4-pyDTDA][OTf]. Data were collected in cooling mode using a static field H of 0.1 T over the range shown (2−300 K). As may be seen in Figure 11, the resulting plots of χ (corrected for

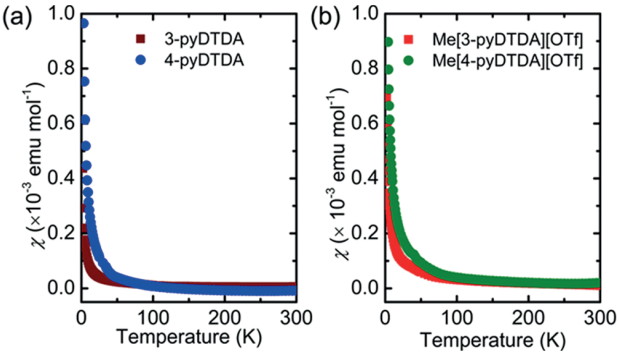

Figure 11. Cooling curve plots of χ versus T for (a) 3-, 4-pyDTDA and (b) Me[3-, 4-pyDTDA][OTf] over the range 2−300 K at a field H = 0.1 T.

diamagnetic contributions) versus T plots are remarkably similar. Both the neutral and charged radicals show essentially diamagnetic behavior with a concentration of free spin defect impurities around the 1% level, which is as expected for DTDA dimers. There is no evidence for thermally induced dissociation up to 300 K, the limit of the experiment.

SUMMARY AND CONCLUSIONS

The chemistry and structural properties of DTDA and DSDA radicals have been extensively studied for many years. A wide range of 4-substituents have been explored with increasing interest in the introduction of ligands that can enhance or complement the coordination chemistry of the radical itself.[21,23,24] In principle, a 3- or 4-pyridyl ligand provides an effective secondary binding site for metal ions, but the basic nature of these ligands also introduces subtleties in the preparation of the radicals to which they are bound. Here, we have provided a detailed account of the preparation of 3-, 4-pyDTDA and their Se-based analogues using procedures that reflect the intermediacy of protonated radicals. Treatment of the protonated intermediates with base allows for isolation and structural characterization of the native radicals. In the solid state, 3-, 4-pyDTDA and 3-, 4-pyDSDA crystallize as diamagnetic dimers linked head-to-tail into ribbonlike arrays by short η^2-S_2---N(py) and η^2-Se_2---N(py) intermolecular secondary bonding interactions. In the case of 4-pyDTDA, disorder in the packing of these molecular ribbons leads to a nanocrystalline morphology.

As a first step in exploiting the basic properties of the 3-, 4-pyridyl ligands, we have prepared the *N*-methylated radical triflates Me[3-, 4-pyDTDA][OTf], the crystal structures of which consist of diamagnetic *trans*-cofacial dimers strongly ion-paired with triflate anions. Development of the charge transfer chemistry of these latter salts and the coordination chemistry of the neutral radicals opens the door to the development of new functional molecular materials with potentially interesting magnetic and/or charge-transport properties.

EXPERIMENTAL SECTION

General Methods and Procedures. The starting materials 3- and 4-cyanopyridine, benzyltriethylammonium chloride, lithium bis(trimethylsilylamide), chlorotrimethylsilane, methyl trifluoromethanesulfonate (methyl triflate), silver trifluoromethanesulfonate (silver triflate), sulfur monochloride, potassium iodide, and triphenylantimony were obtained commercially; all were used as received, save for KI, which was dried in vacuo. Selenium tetrachloride was prepared following the literature procedure.[33] Reagent-grade acetonitrile (MeCN) was dried by distillation from P_2O_5 and CaH_2; anhydrous-grade tetrahydrofuran (THF) was dried by distillation from sodium/benzophenone, and diethyl ether was dried over 4 Å molecular sieves. Unless otherwise specified, all reactions and synthetic procedures were carried out under an atmosphere of nitrogen or argon. Fractional sublimations of all radical dimers were performed in an ATS series 3210 three-zone tube furnace mounted horizontally and linked to a series 1400 temperature control system. Infrared spectra (Nujol mulls, KBr optics) were recorded on a Nicolet Avatar FTIR spectrometer or Bruker Alpha with Platinum ATR module with a diamond IR transmitting crystal at 2 cm^{-1} resolution. NMR spectra were recorded on a Bruker Avance III HD 300 MHz spectrometer using anhydrous deuterated solvents. Elemental analyses were performed in-house on an Elementar Vario EL III elemental analyzer or by MHW Laboratories, Phoenix, AZ 85018.

Preparation of (*E*)-*N*,*N*,*N*′-Tris(trimethylsilyl)-isonicotinimidamide, 4-pyADS. Solid lithium bis(trimethylsilyl)-amide (26.0 g, 0.156 mol) was added to a solution of 4-cyanopyridine (10.4 g, 0.100 mol) in 75 mL of THF. The mixture was heated at reflux for 4 h and then cooled to room temperature, and chlorotrimethylsilane (15.0 mL, 0.118 mol) was then added to afford an off-white precipitate. The mixture was heated for an additional 16 h and then filtered, and the solvent was removed in vacuo to leave an oil that was purified by vacuum distillation at 110 °C/10^{-1} Torr; yield 18.0 g (53.5 mmol, 54%). The distilled oil crystallized upon cooling, and the resulting material could be recrystallized from either MeCN or hexane as colorless needles, mp 45−46 °C. ^{1}H NMR (δ, $CDCl_3$): 8.55 (d, 1H, Ar−H, J = 5.71 Hz), 7.13 (d, 1H, Ar−H, J = 5.61 Hz), 0.05 (s, 9H, -Si(CH_3)$_3$).[34] IR (nujol mull): 1633 (s), 1590 (m), 1548 (w), 1247 (s), 1131 (w), 997 (w), 840 (s), 757 (w) cm^{-1}. Anal. Calcd for $C_{15}H_{31}N_3Si_3$: C, 53.35; H, 9.25; N, 12.44. Found: C, 53.15; H, 9.12; N, 12.63.

Preparation of 4-(Pyridin-4-yl)-1,2,3,5-dithiadiazolyl, 4-pyDTDA. Sulfur monochloride (18.5 g, 0.138 mmol) was added to

DOI: 10.1021/acs.inorgchem.8b02416
Inorg. Chem. 2018, 57, 13901−13911

a solution of 4-pyADS (2.40 g, 8.30 mmol) in 50 mL of anhydrous MeCN. The mixture was heated at reflux for 2 h and then cooled to room temperature, and the light purple precipitate of the double salt [4-pyDTDA][Cl][HCl] was filtered off, washed with 3 × 20 mL of MeCN, and dried in vacuo; yield 2.04 g (8.04 mmol). IR (nujol mull, Figure 2a): 1631 (s), 1597 (s), 1544 (s), 1507 (m), 1483 (w), 1307 (s), 1230 (m), 1193 (w), 1115 (vs), 1076 (w), 894 (w), 817 (m), 772 (m), 629 (s), 529 (m) cm^{-1}. This crude material was added to 50 mL of MeCN along with solid Ph_3Sb (3.81 g, 9.94 mmol) and $[BzEt_3N][Cl]$ (2.14 g, 38 mmol). The resulting slurry was stirred at room temperature for 1 h, and the dark purple precipitate of the crude radical hydrochloride [4-pyDTDA][HCl] was filtered off, washed with 3 × 20 mL of MeCN, and dried in vacuo; yield 1.67 g (7.65 mmol). IR (nujol mull, Figure 2b): 1632 (s), 1609 (s), 1522 (m), 1507 (m), 1370 (s), 1247 (m), 1189 (w), 1150 (s), 1088 (m), 1088 (w), 1001(m), 979 (w), 835 (s), 817 (s), 778 (s), 724 (m), 644 (m), 514 (m) cm^{-1}. Finally, deprotonation of the crude [4-pyDTDA][HCl] was effected by treating a slurry of it (1.42 g, 6.47 mmol) in 40 mL of MeCN with NEt_3 (1.45 g, 14.3 mmol) for 30 min. The purple powder of crude 4-pyDTDA so produced was filtered off, washed with 3 × 20 mL of MeCN, and dried in vacuo; yield 1.10 g (6.03 mmol, 93% from [4-pyDTDA][HCl]). Black microcrystalline nodules of 4-pyDTDA suitable for chemical analysis and magnetic measurements were obtained by vacuum sublimation of the crude material at 10^{-4} Torr in a three-zone tube furnace along a temperature gradient of 50−100 °C; dec >150 °C. IR (nujol mull, Figure 2c and Figure S1): 1597 (m), 1417 (s), 1138 (w), 1061 (w), 998 (w), 826 (s), 808 (m), 785 (s), 655 (m), 511 (m) cm^{-1}. Anal. Calcd for $C_6H_4N_3S_2$: C, 39.54; H, 2.21; N, 23.06. Found: C, 39.56; H, 2.33; N, 23.19.

Preparation of (*E*)-*N*,*N*,*N*′-Tris(trimethylsilyl)-nicotinimidamide, 3-pyADS. Solid lithium bis(trimethylsilyl)-amide (18.0 g, 0.108 mol) was added to a solution of 3-cyanopyridine (10.4 g, 0.100 mol) in 75 mL of anhydrous THF. The reaction was heated at reflux for 4 h and then cooled to room temperature, and chlorotrimethylsilane (15.0 mL, 0.118 mol) was then added to afford an off-white precipitate. The reaction was heated at reflux for an additional 16 h, after which time the precipitate was filtered off and the solvent was removed in vacuo to leave 3-pyADS as an oil that was purified by vacuum distillation at 110 °C/10^{-1} Torr; yield 18.4 g (0.544 mol, 54%). ^{1}H NMR (δ, $CDCl_3$): 8.52 (d, 1H, Ar−H, J = 3.84 Hz), 8.49 (s, 1H, Ar−H), 7.51 (m, 1H, Ar−H), 7.19 (m, 1H, Ar−H), 0.02 (s, 9H, -Si(CH_3)$_3$). Anal. Calcd for $C_{15}H_{31}N_3Si_3$: C, 53.35; H, 9.25; N, 12.44. Found: C, 53.40; H, 9.28; N, 12.22.

Preparation of 4-(Pyridin-3-yl)-1,2,3,5-dithiadiazolyl, 3-pyDTDA. Following the procedure described above for 4-pyDTDA, sulfur monochloride (13.5 g, 0.100 mol) was added to a solution of 3-pyADS (1.70 g, 5.04 mmol) in 50 mL of MeCN. The resulting slurry was heated at reflux for 2 h and then cooled to room temperature, and the orange precipitate of the crude double salt solid [3-pyDTDA][Cl][HCl] was filtered off, washed with 3 × 20 mL of MeCN, and dried in vacuo; yield 1.21 g (4.74 mmol). This crude material was added to 50 mL of MeCN along with solid Ph_3Sb (1.71 g, 4.84 mmol) and $[BzEt_3N][Cl]$ (1.33 g, 5.83 mmol). The resulting slurry was stirred at room temperature for 1 h, and the dark purple precipitate of the crude radical hydrochloride [3-pyDTDA][HCl] was filtered off, washed with 3 × 20 mL of MeCN, and dried in vacuo; yield 0.936 g (4.28 mmol). Deprotonation of the crude [3-pyDTDA][HCl] with NEt_3 (1.09 g, 10.8 mmol) in 25 mL of MeCN for 30 min afforded crude 3-pyDTDA, which was filtered off, washed with 3 × 20 mL of MeCN, and dried in vacuo; yield 0.689 g (3.78 mmol, 88% from [3-pyDTDA][HCl]). Analytically pure crystals of 3-pyDTDA suitable for crystallographic work and magnetic measurements were obtained by vacuum sublimation of the crude product at 10^{-4} Torr in a three-zone tube furnace along a temperature gradient of 50−100 °C to afford a lustrous dark blue crystalline solid; dec >150 °C. IR (nujol mull, Figure S1): 1587 (w), 1187 (w), 1146 (m), 1040 (w), 1024 (m), 832 (m), 807 (s), 781 (s), 699 (s), 667 (m), 627 (w), 512 (m) cm^{-1}. Anal. Calcd for $C_6H_4N_3S_2$: C, 39.54; H, 2.21; N, 23.06. Found: C, 39.36; H, 2.32; N, 23.17.

Preparation of Methyl-(*E*)-*N*,*N*,*N*′-tris(trimethylsilyl)-nicotinimidamide Triflate, Me[3-pyADS][OTf]. A solution of 3-pyADS (4.17 g, 12.3 mmol) in 35 mL of Et_2O was cooled on an ice/water bath while neat methyl triflate (1.60 mL, 13.87 mmol) was added dropwise over 5 min. The reaction was allowed to warm to room temperature and stirred for 16 h to afford a yellow solution. The solvent was flash distilled to leave a white solid, which was washed with 20 mL of toluene, and the fine white solid was collected by filtration and dried in vacuo; yield 5.66 g (11.28 mmol, 91%). ^{1}H NMR (δ, CD_3CN): 9.11 (s, 1H, Ar−H), 8.74 (d, 1H, Ar−H, J = 9 Hz), 8.65 (d, 1H, Ar−H, J = 3 Hz), 8.04 (dd, 1H, Ar−H, J = 3 and 9 Hz), 4.33 (s, 3H, N-Me), 0.02−0.07 (s, br, 27H, -Si(CH_3)$_3$). This material was used for subsequent reactions without further purification.

Preparation of Me[3-pyDTDA][OTf]$_2$. Neat sulfur monochloride (7.93 g, 58.7 mmol) was added dropwise to a solution of Me[3-pyADS][OTf] (7.42 g, 14.8 mmol) in 60 mL of MeCN to afford an orange solution. The mixture was stirred at room temperature for 16 h, and then solid $[BzEt_3N][Cl]$ (6.74 g, 29.6 mmol) was added to afford a heavy orange precipitate of Me[3-pyDTDA][Cl]$_2$. After stirring for 1 h, the crude solid was filtered off, washed with 3 × 40 mL of MeCN, and dried in vacuo. To a slurry of this crude Me[3-pyDTDA][Cl]$_2$ in 50 mL of MeCN was added an excess TMSOTf (12.0 mL, 66.3 mmol) to afford a clear, light blue solution over a white solid. The mixture was stirred at room temperature for 1 h and then filtered, and the volatiles were removed from the filtrate by flash distillation to afford a beige solid that was recrystallized from 20 mL of MeCN at −20 °C as colorless blocks of Me[3-pyDTDA][OTf]$_2$, which were collected by filtration and dried in vacuo; yield 12.0 g (24.3 mmol, 84%). IR (ATR): 3352 (br, m), 3151 (br, m), 3077 (m), 1705 (m), 1645 (m), 1595 (w), 1486 (m), 1412 (m), 1342 (vw), 1257 (s), 1239 (s), 1218 (vs), 1151 (vs), 1017 (vs), 918 (m), 865 (m), 834 (sh, m), 791 (vs), 760 (w), 721 (w), 675 (w), 629 (s), 573 (m), 558 (m), 513 (s), 463 (w), 407 (vw) cm^{-1}. ^{1}H NMR (δ, CD_3CN): 9.23 (s, 1H, Ar−H), 8.47 (d, 1H, Ar−H, J = 7 Hz), 8.71 (d, 1H, Ar−H, J = 6 Hz), 8.14 (dd, 1H, Ar−H, J = 6 and 7 Hz) 4.38 (s, 3H, N-Me). Anal. Calcd for $C_9H_7N_3O_6F_6S_4$: C, 21.82; H, 1.42; N, 8.48. Found: C, 22.81; H, 1.66; N, 8.70.

Preparation of Me[3-pyDTDA][OTf]. A mixture of KI (2.25 g, 13.6 mmol) and Me[3-pyDTDA][OTf]$_2$ (3.03 g, 6.12 mmol) in 70 mL of MeCN was stirred at room temperature for 90 min to afford a lustrous bronze precipitate of Me[3-pyDTDA][I], which was collected by filtration, washed with 5 × 20 mL of MeCN and then 10 mL of DCM, and then dried in vacuo; yield 1.13 g (3.49 mmol, 57%). IR (ATR): 3062 (m), 3012 (m), 2957 (vw), 2936 (w), 1811 (vw), 1775 (w), 1638 (m), 1591 (w), 1504 (m), 1475 (m), 1400 (w), 1378 (m), 1325 (w), 1288 (w), 1256 (m),1210 (s), 1187 (w), 1139 (s), 1123 (s), 1031 (s), 957 (w), 909 (vw), 813 (vs), 774 (vs), 657 (vs), 651 (m), 618 (m), 539 (vw), 511 (s), 486 (s), 446 (m), 408 (m). A small excess of AgOTf (0.666 g, 2.59 mmol) was added to a suspension of Me[3-pyDTDA][I] (0.832 g, 2.57 mmol) in 40 mL of MeCN, and the mixture was stirred for 1 h at room temperature to afford a dark orange solution over a pale yellow precipitate of AgI. The supernatant solution was drawn off with a cannula and concentrated in vacuo to ∼5 mL. Cooling the solution to −20 °C for 24 h afforded lustrous orange blocks of Me[3-pyDTDA][OTf] that were collected by filtration, washed with 2 × 15 mL of DCM, and dried in vacuo; yield 0.344 g (0.993 mmol, 38%). IR (ATR): 3076 (w), 3049 (w), 1703 (w), 1642 (w), 1592 (vw), 1479 (w), 1409 (m), 1257 (vs), 1237 (vs), 1218 (vs), 1201 (vs), 981 (vs), 916 (w), 864 (m), 816 (w), 787 (w), 757 (w), 688 (m), 675 (w), 629 (s), 574 (m), 513 (m), 460 (s), 424 (w). Anal. Calcd for $C_8H_7F_3N_3S_3O_3$: C, 27.74; H, 2.04; N, 12.13. Found: C, 27.52; H, 2.10; N, 12.30.

Preparation of Methyl-(*E*)-*N*,*N*,*N*′-tris(trimethylsilyl)-isonicotinimidamide Triflate, Me[4-pyADS][OTf]. A solution of 4-pyADS (3.45 g, 10.2 mmol) in 30 mL of diethyl ether (Et_2O) was cooled on an ice/water bath while methyl triflate (1.10 mL, 10.0 mmol) in 10 mL of Et_2O was added dropwise over 5 min. The reaction was allowed to warm to room temperature and stirred at 5 °C for 16 h; then, the fine white precipitate of Me[4-pyADS][OTf] was

DOI: 10.1021/acs.inorgchem.8b02416
Inorg. Chem. 2018, 57, 13901−13911

collected by filtration, washed with 2 × 20 mL of Et_2O, and dried in vacuo; yield 4.54 g (9.04 mmol, 88%). ^1H NMR (δ, CD_3CN): 8.64 (d, 1H, Ar−H, J = 6 Hz), 8.281 (s, br, 1H, Ar−H), 8.11 (s, br, 1H, Ar−H), 4.30 (s, 3H, N-Me), 0.30 (s, 9H, -Si$(CH_3)_3$), 0.06 (s, 18H, -Si$(CH_3)_3$). This material was used for subsequent reactions without further purification.

Preparation of Me[4-pyDTDA][OTf]$_2$. Neat sulfur monochloride (9.28 g, 68.8 mmol) was added dropwise to a solution of Me[4-pyADS][OTf] (5.75 g, 11.5 mmol) in 60 mL of MeCN to afford a red-orange solution. The mixture was stirred at room temperature for 16 h; then, solid [$BzEt_3N$][Cl] (5.86 g, 25.7 mmol) was added to afford an orange precipitate. After stirring for 1 h, the bright orange precipitate of Me[4-pyDTDA][Cl]$_2$ was filtered off, washed with 3 × 40 mL of MeCN, and dried in vacuo. To a slurry of this crude Me[4-pyDTDA][Cl]$_2$ in 60 mL of MeCN was added an excess of TMSOTf (8.00 mL, 30.8 mmol) to afford a straw yellow solution, which was stirred at room temperature for 1 h. The solution was filtered, and the volatiles were removed from the filtrate by flash distillation to afford a beige solid that was recrystallized from 25 mL of MeCN at −20 °C to afford pale yellow blocks of Me[4-pyDTDA][OTf]$_2$, which were collected by filtration and dried in vacuo; yield 4.57 g (3.81 mmol, 81%). IR (ATR): 3342 (br, m), 3127 (br, w), 3064 (m), 3026 (w), 1692 (m), 1648 (m), 1584 (w), 1522 (vw), 1485 (m), 1468 (w), 1437 (m), 1398 (w), 1235 (br, vs), 1221 (s), 1165 (s), 1152 (vs), 1105 (s), 1056 (w), 1026 (vs), 997 (m), 905 (w), 871 (w), 856 (m), 844(w), 799 (m), 758 (s), 719 (s), 689 (s), 632 (vs), 573 (m), 554 (w), 516 (s), 495 (w), 442 (m) cm^{-1}. ^1H NMR (δ, CD_3CN): 8.72 (d, 2H, Ar−H, J = 6 Hz), 8.37 (d, 2H, Ar−H, J = 6 Hz), (s, 1H, Ar−H), 4.31 (s, 3H, N-Me). Anal. Calcd for $C_9H_7N_3O_6F_6S_4$: C, 21.82; H, 1.42; N, 8.48. Found: C, 22.13; H, 1.52; N, 8.77.

Preparation of Me[4-pyDTDA][OTf]. A mixture of KI (0.452 g, 2.72 mmol) and Me[4-pyDTDA][OTf]$_2$ (0.632 g, 1.28 mmol) in 20 mL of MeCN was stirred at room temperature for 2 h to afford a lustrous bronze precipitate of Me[4-pyDTDA][I], which was collected by filtration, washed with 5 × 15 mL of MeCN and then 15 mL of DCM, and dried in vacuo; yield 0.296 g (0.913 mmol, 72%). IR (ATR): 3109 (m), 3087 (w), 3035 (m), 3016 (m), 2978 (m), 1693 (vs), 1634 (w), 1585 (w), 1566 (w), 1519 (s), 1469 (vs), 1404 (s), 1367 (w), 1325 (s), 1291 (m), 1257 (s), 1205 (s), 1177 (w), 1144 (vs), 1066 (vs), 1045 (m), 1031 (m), 978 (w), 966 (w), 912 (w), 845 (m), 816 (m), 795 (m), 770 (s), 726 (w), 666 (w), 640 (m), 617 (m), 598 (vw), 511 (m), 485 (m), 440 (m). A small excess of AgOTf (0.479 g, 1.864 mmol) was added to a suspension of Me[4-pyDTDA][I] (0.294 g, 0.907 mmol) in 25 mL of MeCN, and the mixture was stirred for 4 h at room temperature to afford a dark orange solution over a pale yellow precipitate of AgI. The supernatant solution was drawn off using a cannula and concentrated in vacuo to ∼5 mL. Cooling the solution to −20 °C for 24 h afforded lustrous orange plates of Me[4-pyDTDA][OTf] that were collected by filtration, washed with 2 × 15 mL of DCM, and dried in vacuo; yield 0.095 g (0.274 mmol, 30%). IR (ATR): 3132 (w), 3072 (w), 1641 (m), 1583 (w), 1466 (m), 1426 (w), 1396 (m), 1274 (vs), 1253 (vs), 1219 (vs), 1203 (vs), 1147 (vs), 1051 (w), 1020 (vs), 948 (w), 916 (m), 857 (m), 758 (w), 741 (w), 681 (w), 667 (vw), 630 (vs), 573 (s), 553 (m), 516 (vs) 456 (w). Anal. Calcd for $C_8H_7F_3N_3S_3O_3$: C, 27.74; H, 2.04; N, 12.13. Found: C, 27.65; H, 2.15; N, 12.16.

Preparation of 4-(3′-Pyridyl)-1,2,3,5-diselenadiazolyl, 3-pyDSDA. A solution of 3-pyADS (1.00 g, 2.96 mmol) in 10 mL of MeCN was added to a solution of $SeCl_2$ prepared in situ from selenium powder (0.234 g, 2.96 mmol) and $SeCl_4$ (0.654 mg, 2.96 mmol) in 50 mL of MeCN to afford a red-brown precipitate. The mixture was stirred at room temperature for 1 h; then, the crude [3-pyDSDA][Cl] was filtered off, washed with 3 × 15 mL of MeCN, and dried in vacuo; crude yield 0.860 g (2.76 mmol, 93%). IR: 1678 (m), 1585 (w), 1187 (w), 1137 (w), 1039 (w), 1023 (w), 870 (w), 810 (w), 706 (m) cm^{-1}. Powdered triphenylantimony (1.20 g, 3.40 mmol) was then added to a slurry of the crude [3-pyDSDA][Cl] (0.860 g, 2.76 mmol) in 20 mL of MeCN, and the mixture was stirred at room temperature for 16 h. The resulting black precipitate of crude 3-pyDSDA was filtered off, washed with 3 × 15 mL of MeCN, and dried in vacuo; crude yield 0.754 g (2.73 mmol, 99%). Crystals suitable for crystallographic work were obtained by vacuum sublimation at 10^{-4} Torr in a three-zone furnace along a temperature gradient of 60−140 °C; dec >150 °C. IR (nujol mull, Figure S1): 1584 (m), 1420 (s), 1320 (s), 1197 (m), 1129 (m), 1040 (m), 1026 (m), 809 (w), 714 (s), 637 (m) cm^{-1}. Anal. Calcd for $C_6H_4N_3Se_2$: C, 26.11; H, 1.46; N, 15.22. Found: C, 26.18; H, 1.61; N, 15.40.

Preparation of 4-(4′-Pyridyl)-1,2,3,5-diselenadiazolyl, 4-pyDSDA. A solution of 4-pyADS (1.22 g, 3.61 mmol) in 10 mL of MeCN was added to a solution of $SeCl_2$ prepared in situ from selenium powder (0.235 g, 3.60 mmol) and $SeCl_4$ (0.797 g, 3.61 mmol) in 50 mL of MeCN to afford a red-brown precipitate. The mixture was stirred at room temperature for 1 h; then, the crude [4-pyDSDA][Cl] was filtered off, washed with 3 × 15 mL of MeCN, and dried in vacuo; yield 0.976 g (3.13 mmol, 87%). Powdered triphenylantimony (1.51 g, 4.23 mmol) was added to a slurry of crude [4-pyDSDA][Cl] (0.976 g, 3.13 mmol) in 20 mL of degassed MeCN, and the mixture was stirred at room temperature for 16 h. The resulting black precipitate of crude 4-pyDSDA was filtered off, washed with 3 × 15 mL of MeCN, and dried in vacuo; crude yield 0.840 g (3.04 mmol, 97%). Crystals suitable for crystallographic work were obtained by vacuum sublimation at 10^{-4} Torr in a three-zone furnace along a temperature gradient of 60−140 °C; dec >150 °C. IR (nujol mull, Figure S1): 1593 (m), 1412 (m), 1323 (w), 1204 (w), 1064 (w), 998 (m), 830 (m), 727 (m), 707 (w), 660 (m) cm^{-1}. Anal. Calcd for $C_6H_4N_3Se_2$: C, 26.11; H, 1.46; N, 15.22. Found: C, 26.24; H, 1.50; N, 15.20.

EPR Spectroscopy. X-Band EPR spectra for 3- and 4-pyDTDA were recorded at ambient temperature using a Bruker EMX-200 or Magnettech high resolution MS200 spectrometer; sublimed samples of the radicals were dissolved in degassed DCM, and the cation-radicals were dissolved in MeCN and transferred under an argon atmosphere into a quartz flat cell. Hyperfine coupling constants were obtained by spectral simulation using Simfonia and WinSim.[35]

Single-Crystal Crystallography. Crystals of 3-pyDTDA, Me[3-, 4-pyDTDA][OTf]$_2$, and Me[3-, 4-PyDTDA][OTf] were coated with Fomblin oil and mounted on a MiTeGen loop, and those of [3-, 4-PyDSDA] were mounted on glass fibers with epoxy. X-ray data for 3-pyDTDA were collected at 296 K on beamline I19 at the Diamond Light Source (λ = 0.68890 Å) using Rigaku CrystalClear[36] and processed with Bruker APEX2[37] software and SADABS.[38] X-ray data for Me[3-, 4-pyDTDA][OTf]$_2$ and Me[3-, 4-PyDTDA][OTf] were collected at 120 K on an Agilent SupraNova diffractometer equipped with multilayer optics monochromated dual source (Cu and Mo) and Atlas detector using Cu Kα (λ = 1.54184 Å) radiation; data acquisitions, reductions, and analytical face-index-based absorption corrections were made using the program CrysAlisPRO.[39] For 3-, 4-PyDSDA, X-ray data were collected at 296 K using ω scans with a Bruker APEX II CCD detector on a D8 three-circle goniometer and Mo Kα (λ = 0.71073 Å) radiation. In all cases, the structures were solved using the ShelXS[40] program and refined on F^2 by full matrix least-squares techniques with the ShelXL8 program using the interface in the Olex2 (v.1.2) program package.[41]

Powder Crystallography. Powdered samples of sublimed 4-pyDTDA were loaded into borosilicate glass capillaries and sealed. Data were collected at 293 K using synchrotron radiation (λ = 0.825925 Å) available on beamline I11 at the Diamond Light Source. As a result of the paucity and poor resolution of some of the observed reflections attempts to index the data using DICVOL,[42] McMaille,[43] and Topas[44] were unsuccessful. However, starting from the cell settings and space group ($C2/c$) of 4-pyDSDA, manual indexing of the data was eventually achieved. A structure search was then performed in DASH[45] using simulated annealing methods and a molecular unit based on the atomic coordinates of 4-cyanophenyl-DTDA.[15] A rigid body constraint was initially employed followed by release of the ring-to-ring (py-DTDA) torsion angle. A solution was found that closely matched the *cis*-cofacial mode of dimerization and packing observed in 4-pyDSDA (Figures 3 and 6). The occurrence of two other simulated annealing solutions with the same cell parameters and similar profile χ^2 values but comprised of ribbons of *trans*-cofacial

DOI: 10.1021/acs.inorgchem.8b02416
Inorg. Chem. 2018, 57, 13901−13911

and *trans*-antarafacial dimers (Figures S6 and S7) points to a disordered nanocrystalline phase[30] in which there is a large number of faults in the layering of the molecular ribbons. This would explain the poor crystalline growth (powdery nodules) of 4-pyDTDA compared to that of 4-pyDSDA and the low resolution and broad peaks observed in the PXRD diffractogram. Although we prefer the *cis*-cofacial structure, by virtue of its similarity to 4-pyDSDA, all three solutions were individually refined by Rietveld methods[46] using the GSAS program[47] with atomic positions and isotropic thermal parameters taken from the initial DASH refinement. Atomic positions were not further refined and, as a result, standard deviations for atomic coordinates are not available. Final Rietveld indices R_p and R_{wp} for all three models are listed in Table S2. The deposited CIF file for 4-pyDTDA corresponds to the *cis*-cofacial dimer; for completeness, the refined crystal coordinates for the other two models are available in Tables S4 and S5.

Magnetic Susceptibility Measurements. DC magnetic susceptibility measurements were performed at a field of 1000 Oe over the temperature range 2−300 K on a Quantum Design MPMS SQUID magnetometer. Diamagnetic corrections were made using Pascal's constants.[48]

■ ASSOCIATED CONTENT

Supporting Information

The Supporting Information is available free of charge on the ACS Publications website at DOI: 10.1021/acs.inorgchem.8b02416.

Infrared spectra and details of X-ray data collection, CCDC codes, and crystal packing (PDF)

Accession Codes

CCDC 1863391−1863398 contain the supplementary crystallographic data for this paper. These data can be obtained free of charge via www.ccdc.cam.ac.uk/data_request/cif, or by emailing data_request@ccdc.cam.ac.uk, or by contacting The Cambridge Crystallographic Data Centre, 12 Union Road, Cambridge CB2 1EZ, UK; fax: +44 1223 336033.

■ AUTHOR INFORMATION

Corresponding Authors

*E-mail: aaronmailman@gmail.com.
*E-mail: oakley@uwaterloo.ca.

ORCID

Craig M. Robertson: 0000-0002-4789-7607
Manu Lahtinen: 0000-0001-5561-3259
Rodolphe Clérac: 0000-0001-5429-7418
Heikki M. Tuononen: 0000-0002-4820-979X
Aaron Mailman: 0000-0003-2067-8479
Richard T. Oakley: 0000-0002-7185-2580

Notes

The authors declare no competing financial interest.

■ ACKNOWLEDGMENTS

This work was supported by the Natural Sciences and Engineering Research Council of Canada (NSERCC), the University of Jyväskylä, the Academy of Finland (projects 253907 and 289172), the European Union's H2020 research and innovations programme (under the Marie Skłodowska-Curie Grant Agreement 659123), CNRS, the University of Bordeaux, the Région Nouvelle Aquitaine, the GdR MCM-2, and the MOLSPIN COST action CA15128. We thank the Diamond Light Source for access to beamlines I11 and I19.

■ REFERENCES

(1) (a) Oakley, R. T. Cyclic and Heterocyclic Thiazenes. *Prog. Inorg. Chem.* **1988**, *36*, 299. (b) Banister, A. J.; Rawson, J. M. Some Synthetic and Structural Aspects of Dithiadiazoles, RCN_2S_2, and Related Compounds. In *The Chemistry of Inorganic Ring Systems*; Steudel, R., Ed.; Elsevier: Amsterdam, 1992; p 323. (c) Cordes, A. W.; Haddon, R. C.; Oakley, R. T. Heterocyclic Thiazyl and Selenazyl Radicals; Synthesis and Applications in Solid State Architecture. In *The Chemistry of Inorganic Ring Systems*; Steudel, R., Ed.; Elsevier: Amsterdam, 1992; p 295. (d) Rawson, J. M.; Banister, A. J.; Lavender, I. The Chemistry of Dithiadiazolylium and Dithiadiazolyl Rings. *Adv. Heterocycl. Chem.* **1995**, *62*, 137. (e) Haynes, D. A. Crystal engineering with dithiadiazolyl radicals. *CrystEngComm* **2011**, *13*, 4793.

(2) (a) Rawson, J. M.; Luzon, J.; Palacio, F. Magnetic exchange interactions in perfluorophenyl dithiadiazolyl radicals. *Coord. Chem. Rev.* **2005**, *249*, 2631. (b) Rawson, J. M.; Alberola, A.; Whalley, A. Thiazyl radicals: old materials for new molecular devices. *J. Mater. Chem.* **2006**, *16*, 2560.

(3) (a) Oakley, R. T. Chemical Binding within and between Inorganic Rings; the Design and Synthesis of Molecular Conductors. *Can. J. Chem.* **1993**, *71*, 1775. (b) Bryan, C. D.; Cordes, A. W.; Fleming, R. M.; George, N. A.; Glarum, S. H.; Haddon, R. C.; MacKinnon, C. D.; Oakley, R. T.; Palstra, T. T. M.; Perel, A. S. Charge Transfer Salts of Benzene-bridged 1,2,3,5-Dithiadiazolyl Diradicals; Preparation, Structures and Transport Properties of 1,3- and 1,4-$[(S_2N_2C)C_6H_4(CN_2S_2)][X]$ (X = I, Br). *J. Am. Chem. Soc.* **1995**, *117*, 6880. (c) Bryan, C. D.; Cordes, A. W.; Goddard, J. D.; Haddon, R. C.; Hicks, R. G.; MacKinnon, C. D.; Mawhinney, R. C.; Oakley, R. T.; Palstra, T. T. M.; Perel, A. S. Preparation and Characterization of the Disjoint Diradical 4,4′-Bis(1,2,3,5-dithiadiazolyl) $[S_2N_2C\text{-}CN_2S_2]$ and its Iodine Charge Transfer Salt $[S_2N_2C\text{-}CN_2S_2][I]$. *J. Am. Chem. Soc.* **1996**, *118*, 330.

(4) (a) Preuss, K. E. Metal complexes of thiazyl radicals. *Dalton Trans.* **2007**, 2357. (b) Preuss, K. E. Metal-radical coordination complexes of thiazyl and selenazyl ligands. *Coord. Chem. Rev.* **2015**, *289*, 49. (c) Lau, H. F.; Ang, P. C. Y.; Ng, V. W. L.; Kuan, S. L.; Goh, L. Y.; Borisov, A. S.; Hazendonk, P.; Roemmele, T. L.; Boeré, R. T.; Webster, R. D. Coupling of $CpCr(CO)_3$ Heterocyclic Dithiadiazolyl Radicals. Synthetic, X-ray Diffraction, Dynamic NMR, EPR, CV and DFT Studies. *Inorg. Chem.* **2008**, *47*, 632. (d) Lau, H. F.; Ng, V. W. L.; Koh, L. L.; Tan, G. K.; Goh, L. Y.; Roemmele, T. L.; Seagrave, S.; Boeré, R. T. Cyclopentadienylchromium complexes of 1,2,3,5-dithiadiazolyls: η^2 π-complexes of cyclic sulphur-nitrogen compounds. *Angew. Chem., Int. Ed.* **2006**, *45*, 4498.

(5) (a) Beldjoudi, Y.; Osorio-Román, I.; Nascimento, M. A.; Rawson, J. M. A fluorescent dithiadiazolyl radical: structure and optical properties of phenanthrenyl dithiadiazolyl in solution and polymer composites. *J. Mater. Chem. C* **2017**, *5*, 2794. (b) Beldjoudi, Y.; Nascimento, M. A.; Cho, Y. J.; Yu, H.; Aziz, H.; Tonouchi, D.; Eguchi, K.; Matsushita, M. M.; Awaga, K.; Osorio-Roman, I.; Constantinides, C. P.; Rawson, J. M. Multifunctional Dithiadiazolyl Radicals: Fluorescence, Electroluminescence, and Photoconducting Behavior in Pyren-1′-yl-dithiadiazolyl. *J. Am. Chem. Soc.* **2018**, *140*, 6260.

(6) Matsui, H.; Yamane, M.; Tonami, T.; Nagami, T.; Watanabe, K.; Kishi, R.; Kitagawa, Y.; Nakano, M. Theoretical study on the gigantic effect of external static electric field application on the nonlinear optical properties of 1,2,3,5-dithiadiazolyl π-radical dimers. *Mater. Chem. Front.* **2018**, *2*, 785.

(7) Potts, S. V.; Barbour, L. J.; Haynes, D. A.; Rawson, J. M.; Lloyd, G. O. Inclusion of Thiazyl Radicals in Porous Crystalline Materials. *J. Am. Chem. Soc.* **2011**, *133*, 12948.

(8) Nikolayenko, V. I.; Barbour, L. J.; Arauzo, A.; Campo, J.; Rawson, J. M.; Haynes, D. A. Inclusion of a dithiadiazolyl radical in a seemingly non-porous solid. *Chem. Commun.* **2017**, *53*, 11310.

(9) Banister, A. J.; Bricklebank, N.; Clegg, W.; Elsegood, M. R. J.; Gregory, C. I.; Lavender, I.; Rawson, J. M.; Tanner, B. K. The first solid state paramagnetic 1,2,3,5-dithiadiazolyl radical; X-ray crystal

DOI: 10.1021/acs.inorgchem.8b02416
Inorg. Chem. 2018, 57, 13901−13911

structure of [*p*-NCC_6F_4CNSSN]·. *J. Chem. Soc., Chem. Commun.* **1995**, 679.
(10) Boeré, R. T.; Hill, N. D. D. High Z′ structures of 1,2,3,5-dithiadiazolyls and of 1,2,3,5-diselenadiazolyls containing the first structurally characterized monomeric diselenadiazolyls. *CrystEngComm* **2017**, *19*, 3698.
(11) Gleiter, R.; Haberhauer, G. Electron-rich two-, three- and four-center bonds between chalcogens - New prospects for old molecules. *Coord. Chem. Rev.* **2017**, *344*, 263.
(12) (a) Beekman, R. A.; Boeré, R. T.; Moock, K. H.; Parvez, M. Synthesis, electrochemistry, structure and magnetic susceptibility of 5-*tert*-butyl-1,3-bis-(1,2,3,5-dithiadiazolyl)benzene. Structural effects of the bulky substituent. *Can. J. Chem.* **1998**, *76*, 85. (b) Melen, R. L.; Less, R. J.; Pask, C. M.; Rawson, J. M. Structural Studies of Perfluoroaryldiselenadiazolyl Radicals: Insights into Dithiadiazolyl Chemistry. *Inorg. Chem.* **2016**, *55*, 11747.
(13) (a) Beneberu, H. Z.; Tian, Y. H.; Kertesz, M. Bonds or not bonds? Pancake bonding in 1,2,3,5-dithiadiazolyl and 1,2,3,5-diselenadiazolyl radical dimers and their derivatives. *Phys. Chem. Chem. Phys.* **2012**, *14*, 10713. (b) Tian, Y. H.; Kertesz, M. Is There a Lower Limit to the CC Bonding Distances in Neutral Radical π-Dimers? The Case of Phenalenyl Derivatives. *J. Am. Chem. Soc.* **2010**, *132*, 10648. (c) Mou, Z.; Tian, Y.-H.; Kertesz, M. Validation of density functionals for pancake-bonded π-dimers; dispersion is not enough. *Phys. Chem. Chem. Phys.* **2017**, *19*, 24761. (d) Preuss, K. E. Pancake bonds: π-Stacked dimers of organic and light-atom radicals. *Polyhedron* **2014**, *79*, 1. (e) Kertesz, M. Pancake bonding, an unusual pi-stacking interaction. *Chem. - Eur. J.* **2018**, DOI: 10.1002/chem.201802385.
(14) (a) Andrews, M. P.; Cordes, A. W.; Douglass, D. C.; Fleming, R. M.; Glarum, S. H.; Haddon, R. C.; Marsh, P.; Oakley, R. T.; Palstra, T. T. M.; Schneemeyer, L. F.; Trucks, G. W.; Tycko, R. W.; Waszczak, J. V.; Warren, W. W.; Young, K. M.; Zimmerman, N. M. One-Dimensional Stacking of Bifunctional Dithia- and Diselenadiazolyl Radicals; Preparation, Structural and Electronic Properties of 1,3-[$(E_2N_2C)C_6H_4(CN_2E_2)$] (E = S, Se). *J. Am. Chem. Soc.* **1991**, *113*, 3559. (b) Cordes, A. W.; Haddon, R. C.; Hicks, R. G.; Oakley, R. T.; Palstra, T. T. M.; Schneemeyer, L. F.; Waszczak, J. V. Polymorphism of 1,3-Phenylene Bis(diselenadiazolyl); Solid State Structural and Electronic Properties of β-1,3-[(Se_2N_2C)-$C_6H_4(CN_2Se_2)$]. *J. Am. Chem. Soc.* **1992**, *114*, 1729.
(15) Cordes, A. W.; Haddon, R. C.; Hicks, R. G.; Oakley, R. T.; Palstra, T. T. M. Preparation and Solid State Structures of Cyanophenyl Dithia- and Diselenadiazolyl Radicals. *Inorg. Chem.* **1992**, *31*, 1802.
(16) Cordes, A. W.; Chamchoumis, C. M.; Hicks, R. G.; Oakley, R. T.; Young, K. M.; Haddon, R. C. Mono- and Difunctional Furan-based 1,2,3,5-Dithiadiazolyl Radicals; Preparation and Solid State Structures of 2,5-[$(S_2N_2C)OC_4H_2(CN_2S_2)$] and 2,5-[$(S_2N_2C)$-$OC_4H_2(CN)$]. *Can. J. Chem.* **1992**, *70*, 919.
(17) Britten, J. F.; Clements, O. P.; Cordes, A. W.; Haddon, R. C.; Oakley, R. T.; Richardson, J. F. Stacking Efficiency of Diselenadiazolyl π-Dimers. Consequences for Electronic Structure and Transport Properties. *Inorg. Chem.* **2001**, *40*, 6820.
(18) (a) Clarke, C. S.; Haynes, D. A.; Smith, J. N. B.; Batsanov, A. S.; Howard, J. A. K.; Pascu, S. I.; Rawson, J. M. The effect of fluorinated aryl substituents on the crystal structures of 1,2,3,5-dithiadiazolyl radicals. *CrystEngComm* **2010**, *12*, 172. (b) Beldjoudi, Y.; Arauzo, A.; Palacio, F.; Pilkington, M.; Rawson, J. M. Studies on a "Disappearing Polymorph": Thermal and Magnetic Characterization of α-*p*-NCC_6F_4CNSSN. *J. Am. Chem. Soc.* **2016**, *138*, 16779.
(19) (a) Banister, A. J.; Bricklebank, N.; Lavender, I.; Rawson, J. M.; Gregory, C. I.; Tanner, B. K.; Clegg, W.; Elsegood, M. R. J.; Palacio, F. Spontaneous magnetization in a sulfur-nitrogen radical at 36 K. *Angew. Chem., Int. Ed. Engl.* **1996**, *35*, 2533. (b) Thomson, R. I.; Pask, C. M.; Lloyd, G. O.; Mito, M.; Rawson, J. M. Pressure-Induced Enhancement of Magnetic-Ordering Temperature in an Organic Radical to 70 K: A Magnetostructural Correlation. *Chem. - Eur. J.* **2012**, *18*, 8629. (c) Deumal, M.; Rawson, J. M.; Goeta, A. E.; Howard, J. A. K.; Copley, R. C. B.; Robb, M. A.; Novoa, J. J. Studying the Origin of the Antiferromagnetic to Spin-Canting Transition in the beta-*p*-NCC_6F_4CNSSN· Molecular Magnet. *Chem. - Eur. J.* **2010**, *16*, 2741. (d) Alberola, A.; Less, R. J.; Pask, C. M.; Rawson, J. M.; Palacio, F.; Oliete, P.; Paulsen, C.; Yamaguchi, A.; Farley, R. D.; Murphy, D. M. A thiazyl-based organic ferromagnet. *Angew. Chem., Int. Ed.* **2003**, *42*, 4782.
(20) Constantinides, C. P.; Carter, E.; Eisler, D.; Beldjoudi, Y.; Murphy, D. M.; Rawson, J. M. Effects of Halo-Substitution on 2′-Chloro-5′-halo-phenyl-1,2,3,5-dithiadiazolyl Radicals: A Crystallographic, Magnetic, and Electron Paramagnetic Resonance Case Study. *Cryst. Growth Des.* **2017**, *17*, 3017.
(21) (a) Hearns, N. G.; Preuss, K. E.; Richardson, J. F.; Bin-Salamon, S. Design and Synthesis of a 4-(2′-Pyridyl)-1,2,3,5-Dithiadiazolyl Cobalt Complex. *J. Am. Chem. Soc.* **2004**, *126*, 9942. (b) Jennings, M.; Preuss, K. E.; Wu, J. Synthesis and magnetic properties of a 4-(2′-pyrimidyl)-1,2,3,5-dithiadiazolyl dimanganese complex. *Chem. Commun.* **2006**, 341. (c) Britten, J.; Hearns, N. G.; Preuss, K. E.; Richardson, J. F.; Bin-Salamon, S. Mn(II) and Cu(II) Complexes of a Dithiadiazolyl Radical Ligand: Monomer/Dimer Equilibria in Solution. *Inorg. Chem.* **2007**, *46*, 3934. (d) Hearns, N. G.; Fatila, E. M.; Clérac, R.; Jennings, M.; Preuss, K. E. Ni(II) and hs-Fe(II) complexes of a paramagnetic thiazyl ligand, and decomposition products of the iron complex, including an Fe(III) tetramer. *Inorg. Chem.* **2008**, *47*, 10330. (e) Hearns, N. G.; Clérac, R.; Jennings, M.; Preuss, K. E. Manipulating the crystal packing of pyDTDA radical ligand coordination complexes with Mn(II) and Ni(II). *Dalton Trans.* **2009**, 3193. (f) Fatila, E. M.; Goodreid, J.; Clérac, R.; Jennings, M.; Assoud, J.; Preuss, K. E. High-spin supramolecular pair of Mn(II)/thiazyl radical complexes. *Chem. Commun.* **2010**, *46*, 6569. (g) Wu, J.; MacDonald, D. J.; Clérac, R.; Jeon, I.-R.; Jennings, M.; Lough, A. J.; Britten, J.; Robertson, C.; Dube, P. A.; Preuss, K. E. Metal complexes of bridging neutral radical ligands: pymDTDA and pymDSDA. *Inorg. Chem.* **2012**, *51*, 3827. (h) Fatila, E. M.; Mayo, R. A.; Rouzières, M.; Jennings, M. C.; Dechambenoit, P.; Soldatov, D. V.; Mathonière, C.; Clérac, R.; Coulon, C.; Preuss, K. E. Radical-Radical Recognition: Switchable Magnetic Properties and Re-entrant Behavior. *Chem. Mater.* **2015**, *27*, 4023. (i) Fatila, E. M.; Maahs, A. C.; Mills, M. B.; Rouzières, M.; Soldatov, D. V.; Clérac, R.; Preuss, K. E. Ferromagnetic ordering of -[Sm(III)-radical]$_n$- coordination polymers. *Chem. Commun.* **2016**, *52*, 5414.
(22) The proper names for these radicals are 4-(3′-pyridyl)- and 4-(4′-pyridyl)-1,2,3,5-dithiadiazolyl. For convenience, we use the abbreviations 3-pyDTDA and 4-pyDTDA throughout this paper.
(23) Wong, W.-K.; Sun, C.; Wong, W.-Y.; Kwong, D. W. J.; Wong, W.-T. Synthesis and Chemistry of Dithiadiazole Free Radicals [4-(4′-$C_5H_4N)CN_2S_2$] and [4-(3′-$C_5H_4N)CN_2S_2$]; X-ray Crystal Structures of [$Pd_3\{\mu$-SNC(Ar′)NS-*S*,*S*′$\}_2(PPh_3)_4$] (Ar′ = 4′-C_5H_4N, 4′-$C_5H_4NBEt_3$ and 3′-$C_5H_4NBEt_3$). *Eur. J. Inorg. Chem.* **2000**, 1045.
(24) Haynes, D. A.; van Laeren, L. J.; Munro, O. Q. Cobalt Porphyrin-Thiazyl Radical Coordination Polymers: Toward Metal-Organic Electronics. *J. Am. Chem. Soc.* **2017**, *139*, 14620.
(25) (a) Alange, G. G.; Banister, A. J.; Bell, B.; Millen, P. W. 1,2,3,5-Dithiadiazolium Chlorides, [RCN_2S_2]Cl. *Inorg. Nucl. Chem. Lett.* **1977**, *13*, 143. (b) Alange, G. G.; Banister, A. J.; Bell, B.; Millen, P. W. Preparation of some 1,2,3,5-dithiadiazolium chlorides from trichlorocyclotrithiazene and nitriles or olefins, and from amidinium salts and sulfur dichloride. *J. Chem. Soc., Perkin Trans. 1* **1979**, 1192. (c) Höfs, H.-U.; Mews, R.; Clegg, W.; Noltemeyer, M.; Schmidt, M.; Sheldrick, G. M. 4-Chloro-1,2,3,5-dithiadiazolium salts. *Chem. Ber.* **1983**, *116*, 416.
(26) Cordes, A. W.; Haddon, R. C.; Hicks, R. G.; Kennepohl, D. K.; Oakley, R. T.; Schneemeyer, L. F.; Waszczak, J. V. Preparation and Solid State Structure of 1,3,5-Triazine-2,4,6-tris-(1,2,3,5-dithiadiazolyl). *Inorg. Chem.* **1993**, *32*, 1554.
(27) Boeré, R. T.; Oakley, R. T.; Reed, R. W. Preparation of *N,N,N*′-Tris(trimethysilyl)amidines; a Convenient Route to Unsubstituted Amidines. *J. Organomet. Chem.* **1987**, *331*, 161. (b) Boeré, R. T.;

DOI: 10.1021/acs.inorgchem.8b02416
Inorg. Chem. 2018, 57, 13901−13911

Hicks, R. G.; Oakley, R. T. *N,N,N'*-Tris(trimethylsilyl)amidines. *Inorg. Synth.* **1997**, *31*, 94.
(28) (a) Del Bel Belluz, P.; Cordes, A. W.; Kristof, E. M.; Kristof, P.; Liblong, S. W.; Oakley, R. T. 1,2,3,5-Diselenodiazolyls as Building Blocks for Molecular Metals; Preparation and Structures of $[PhCN_2Se_2]^+$ PF_6^- and $[PhCN_2Se_2]_2$. *J. Am. Chem. Soc.* **1989**, *111*, 9276. (b) Cordes, A. W.; Bryan, C. D.; Davis, W. M.; de Laat, R. H.; Glarum, S. H.; Goddard, J. D.; Haddon, R. C.; Hicks, R. G.; Kennepohl, D. K.; Oakley, R. T.; Scott, S. R.; Westwood, N. P. C. Prototypal 1,2,3,5-Dithia- and Diselenadiazolyl $[HCN_2E_2]\cdot$ (E = S, Se); Molecular and Electronic Structures of the Radicals and their Dimers, by Theory and Experiment. *J. Am. Chem. Soc.* **1993**, *115*, 7232.
(29) Robinson, S. W.; Haynes, D. A.; Rawson, J. M. Co-crystal formation with 1,2,3,5-dithiadiazolyl radicals. *CrystEngComm* **2013**, *15*, 10205.
(30) (a) Gorelik, T. E.; Czech, C.; Hammer, S. M.; Schmidt, M. U. Crystal structure of disordered nanocrystalline α^{II}-quinacridone determined by electron diffraction. *CrystEngComm* **2016**, *18*, 529. (b) Lincke, G.; Finzel, H.-U. Studies on the Structure of alpha-Quinacridone. *Cryst. Res. Technol.* **1996**, *31*, 441. Lekin, K.; Leitch, A. A.; Assoud, A.; Yong, W.; Desmarais, J.; Tse, J. S.; Desgreniers, S.; Secco, R. A.; Oakley, R. T. Benzoquinone-Bridged Heterocyclic Zwitterions as Building Blocks for Molecular Semiconductors and Metals. *Inorg. Chem.* **2018**, *57*, 4757.
(31) Domagała, S.; Haynes, D. A. Experimental and theoretical charge density assessments for the 4-perfluoropyridyl- and 4-perflurophenyl-1,2,3,5-dithiadiazolyl radicals. *CrystEngComm* **2016**, *18*, 7116.
(32) Fairhurst, S. A.; Johnson, K. M.; Sutcliffe, L. H.; Preston, K. F.; Banister, A. J.; Hauptman, Z. V.; Passmore, J. Electron spin resonance study of $CH_3CNSSN\cdot$, $C_6H_5CNSSN\cdot$, and $SNSSN\cdot^+$ free radicals. *J. Chem. Soc., Dalton Trans.* **1986**, 1465.
(33) Brauer, G. *Handbook of Preparative Chemistry*; Academic: New York, 1963; Vol. *1*, p 423.
(34) Banerjee, A.; Ngwendson, J. N. US patent 20070179311 A1, 2007.
(35) *WinEPR Simfonia*, version 1.25; Bruker Instruments, Inc.: Billerica, MA, 1996.
(36) *CrystalClear*; Rigaku Corporation: Tokyo, Japan, 2005.
(37) *APEX2*; Bruker AXS Inc.: Madison, WI, 2007.
(38) *SADABS*; Bruker AXS Inc.: Madison, WI, 2001.
(39) *Agilent CrysalisPro*; Agilent Technologies Ltd.: Yarnton, England, 2010.
(40) Sheldrick, G. M. SHELXT - Integrated space-group and crystal-structure determination. *Acta Crystallogr., Sect. A: Found. Crystallogr.* **2008**, *64*, 112.
(41) Dolomanov, O. V.; Bourhis, L. J.; Gildea, R. J.; Howard, J. A. K.; Puschmann, H. J. OLEX2: A Complete Structure Solution, Refinement and Analysis Program. *J. Appl. Crystallogr.* **2009**, *42*, 339.
(42) Boultif, A.; Louer, D. Powder Pattern Indexing with the Dichotomy Method. *J. Appl. Crystallogr.* **2004**, *37*, 724.
(43) Le Bail, A. Monte Carlo indexing with McMaille. *Powder Diffr.* **2004**, *19*, 249.
(44) Coelho, A. A. TOPAS and TOPAS-Academic: an optimization program integrating computer algebra and crystallographic objects written in C++. *J. Appl. Crystallogr.* **2018**, *51*, 210.
(45) David, W. I. F.; Shankland, K.; van de Streek, J.; Pidcock, E.; Motherwell, W. D. S.; Cole, J. C. DASH: a Program for Crystal Structure Determination from Powder Diffraction Data. *J. Appl. Crystallogr.* **2006**, *39*, 910.
(46) Rietveld, H. M. A Profile Refinement Method for Nuclear and Magnetic Structures. *J. Appl. Crystallogr.* **1969**, *2*, 65.
(47) Larson, A. C.; Von Dreele, R. B. General Structure Analysis System (GSAS); Los Alamos National Laboratory Report LAUR 86-748; 2000.
(48) (a) Carlin, R. L. *Magnetochemistry*; Springer-Verlag: New York, 1986. (b) Bain, G. A.; Berry, J. F. Diamagnetic Corrections and Pascal's Constants. *J. Chem. Educ.* **2008**, *85*, 532.

DOI: 10.1021/acs.inorgchem.8b02416
Inorg. Chem. 2018, 57, 13901−13911

II

ROOM-TEMPERATURE MAGNETIC BISTABILITY IN A SALT OF ORGANIC RADICAL IONS

by

Taponen, A. I.; Ayadi, A.; Lahtinen, M. K.; Oyarzabal, I.; Bonhommeau, S.; Rouzières, M.; Mathonière, C.; Tuononen, H. M.; Clérac, R.; Mailman, A. 2021

Journal of the American Chemical Society, *143* (39), 15912–15917.

https://doi.org/10.1021/jacs.1c07468

JACS
JOURNAL OF THE AMERICAN CHEMICAL SOCIETY
pubs.acs.org/JACS
Communication

Room-Temperature Magnetic Bistability in a Salt of Organic Radical Ions

Anni I. Taponen, Awatef Ayadi, Manu K. Lahtinen, Itziar Oyarzabal, Sébastien Bonhommeau, Mathieu Rouzières, Corine Mathonière, Heikki M. Tuononen, Rodolphe Clérac,* and Aaron Mailman*

Cite This: J. Am. Chem. Soc. 2021, 143, 15912−15917
Read Online
ACCESS | Metrics & More | Article Recommendations | Supporting Information

ABSTRACT: Cocrystallization of 7,7′,8,8′-tetracyanoquinodimethane radical anion ($TCNQ^{-\bullet}$) and 3-methylpyridinium-1,2,3,5-dithiadiazolyl radical cation (3-MepyDTDA$^{+\bullet}$) afforded isostructural acetonitrile (MeCN) or propionitrile (EtCN) solvates containing cofacial π dimers of homologous components. Loss of lattice solvent from the diamagnetic solvates above 366 K affords a high-temperature paramagnetic phase containing discrete $TCNQ^{-\bullet}$ and weakly bound π dimers of 3-MepyDTDA$^{+\bullet}$, as evidenced by X-ray diffraction methods and magnetic susceptibility measurements. Below 268 K, a first-order phase transition occurs, leading to a low-temperature diamagnetic phase with $TCNQ^{-\bullet}$ σ dimer and π dimers of 3-MepyDTDA$^{+\bullet}$. This study reveals the first example of cooperative interactions between two different organic radical ions leading to magnetic bistability, and these results are central to the future design of multicomponent functional molecular materials.

Stable organic radicals that exhibit a hysteretic response to an external stimulus (temperature, light, or pressure) display physical properties such as magnetic bistability that are promising for use in nanotechnology devices.[1−6] Neutral organic π radicals have been extensively studied because their electron-exchange interactions can lead to dynamic structures weakly coupled; in which interconversion between radicals ($S = {}^1/_2$) and π or σ dimers ($S = 0$) is possible.[7−20] These cooperative solid-state interactions between different centers allow variation of the crystalline lattice such that hysteretic first-order phase transitions can arise. While this parallels the well-known spin-crossover (SCO) phenomena of transition metal ion complexes,[6] radical-based magnetically bistable systems are comparatively rare. The neutral heterocyclic thiazyl π radicals are among the most successful class of radicals in this regard,[7,9,11,13−18] with only a few examples of nitroxides[8,21−24], triazinyl[25] and spirophenalenyl[26] derivatives known to be bistable. In these examples, magnetic switching typically occurs by breaking/forming antiferromagnetically coupled π dimers, although examples of weakly bonded σ dimers have also been reported.[9,11]

The recently described intramolecular electron exchange in discrete neutral[21,27] and ionic diradicals[10] provides insights into how chemical and electronic structure affects the bistable behavior and the importance of cooperative interactions in the solid state. In this context, we chose to explore the cocrystallization of two different radical ions in a salt to couple the structural and electron-exchange interactions in the solid state.[28] The recently reported 4-(*N*-methylpyridinium-3-yl)-1,2,3,5-dithiadiazolyl radical cation (3-MepyDTDA$^{+\bullet}$)[29] was chosen as the positive radical ion. These DTDA radicals readily form π dimers in the solid state (Chart 1) despite their cationic pyridinium substituent (−R) and are ideal candidates for crystal engineering through intermolecular $S^{\delta+}\cdots N^{\delta-}$ interactions. The quintessential electron acceptor 7,7′,8,8′-tetracyanoquinodimethane (TCNQ) was chosen as a partner for MepyDTDA$^{+\bullet}$ because it forms stable π radical anions ($TCNQ^{-\bullet}$) and its cyanido substituents can act as structure-directing groups. Relatedly, the cation can influence the geometry of $TCNQ^{-\bullet}$ in the solid state, such that discrete π

Chart 1. Common Modes of Dimerization in Substituted 1,2,3,5-Dithiadiazolyl (DTDA) Radicals and 7,7′,8,8′-Tetracyanoquinodimethane (TCNQ) Radical Anion

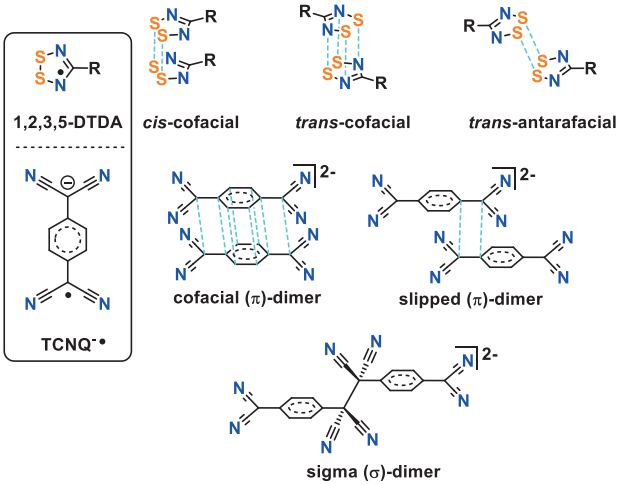

Received: July 18, 2021
Published: September 21, 2021

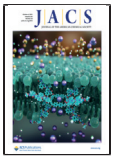

https://doi.org/10.1021/jacs.1c07468
J. Am. Chem. Soc. 2021, 143, 15912−15917

radical anions and/or its π or σ dimers can be observed in the solid state (Chart 1).[30−35] In this work, we demonstrate a surprising twofold single-crystal-to-single-crystal transformation[36−39] involving both the π and σ dimers of $TCNQ^{-\bullet}$ and discrete $TCNQ^{-\bullet}$ radical anion geometries, leading to thermal bistability at room temperature.

A double-displacement reaction between the 18-crown-6 ether (18c6) potassium complex[40] of $TCNQ^{-\bullet}$ and [3-MepyDTDA][OTf] in acetonitrile (MeCN) or propionitrile (EtCN) afforded the 1:1 radical ion salt [3-MepyDTDA][TCNQ] (**1**) as a MeCN or EtCN solvate, respectively (Scheme 1). The two solvates are isostructural, crystallizing in

Scheme 1. Double-Displacement Reaction between [K(18c6)][TCNQ] and [3-MepyDTDA][OTf] to Afford 1·RCN and [K(18c6)][OTf]

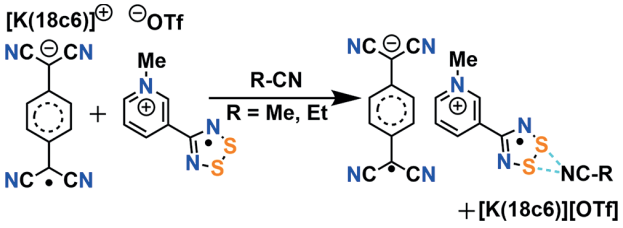

a triclinic unit cell ($P\bar{1}$) containing *trans*-cofacial dimers of 3-$MepyDTDA^{+\bullet}$ and cofacial dimers of $TCNQ^{-\bullet}$ (Chart 1). Each 3-$MepyDTDA^{+\bullet}$ obliquely interacts with one solvent molecule via supramolecular S···N′ contacts (Figure 1a) that are shorter than the sum of the van der Waals radii (ca. 3.26 Å).[41,42] The solvates form alternating $A^+A^+B^-B^-$ π stacks, with hydrogen bonding between the out-of-register neighboring stacks (Figure S13).

Thermogravimetric analysis (TGA) of crystalline samples indicated the onset of desolvation of **1**·EtCN at 365 K, while the loss of lattice solvent from **1**·MeCN occurred with a noticeably higher onset temperature of 396 K. The solvent stoichiometry was verified by the percentage weight loss found from the TGA curve, and the results are consistent with the crystal structures. Both **1**·MeCN and **1**·EtCN displayed high thermal stability after the desolvation alteration, with the onset of decomposition occurring above 480 K (Figures S4−S7 and Table S1).

Variable-temperature magnetic measurements were performed on microcrystalline samples of both **1**·MeCN and **1**·EtCN to determine the effects of the thermal processes on the physical properties. The magnetic susceptibilities of **1**·MeCN and **1**·EtCN were studied over a temperature range of 1.85−400 K in both cooling and heating modes (Figure S9). Both solvates are diamagnetic solids upon cooling from room temperature. Upon heating, however, they displayed a sudden surge in the χT product at temperatures approaching the desolvation onset temperatures recorded by TGA (Figure S4). In the case of **1**·EtCN, the onset of this surge occurs at 350 K, and the χT product rises to 0.38 cm^3 K mol^{-1} at 400 K, which is close to the value of 0.375 cm^3 K mol^{-1} predicted for an $S = {}^1/_2$ Curie paramagnet (g = 2.00). Under identical conditions, the desolvation of **1**·MeCN was less effective, as the χT product reached a value of only 0.24 cm^3 K mol^{-1} at 400 K, the limit of our experiment. Remarkably, the newly formed paramagnetic and desolvated phase did not follow the same track upon cooling, and an abrupt decrease in χT was recorded

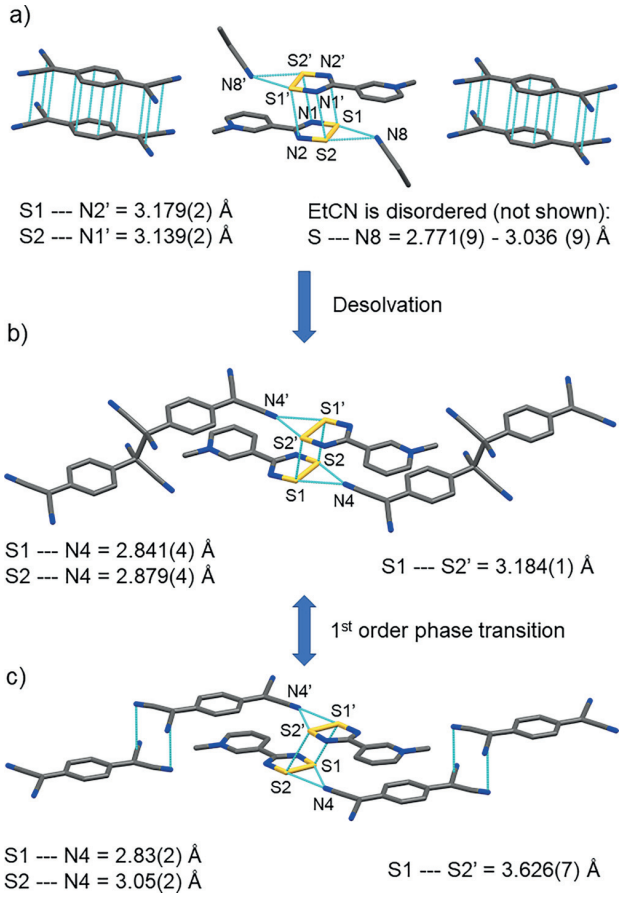

Figure 1. Representative view of the intermolecular interactions in (a) the solvate **1**·EtCN ($P\bar{1}$) at 120 K, (b) the LT phase of **1** ($P2_1/n$) at 120 K, and (c) the HT phase of **1** ($P2_1/n$) at 340 K. Sulfur is shown in yellow, nitrogen in blue, and carbon in gray.

below 290 K. Subsequent heating and cooling cycles indicated a hysteretic response of the magnetic susceptibility near room temperature (263−294 K), consistent with a first-order phase transition for both desolvated **1**·EtCN and **1**·MeCN materials (Figures S10 and S11).

Motivated by the TGA and magnetic susceptibility results, we attempted the desolvation of a crystalline sample of **1**·EtCN. Satisfyingly, after careful heating in vacuo (353−395 K, 10^{-2} bar) over 2 days, crystals suitable for single-crystal X-ray diffraction studies were obtained. Interestingly, the loss of lattice solvent afforded crystals belonging to a higher-symmetry monoclinic ($P2_1/n$) unit cell at 120 K. This low-temperature (LT) phase contains *trans*-antarafacial dimers of 3-$MepyDTDA^{+\bullet}$ with short intermolecular S−S′ contacts (3.184(1) Å), while the TCNQ radicals are now σ-dimerized via a long C−C bond (1.656(8) Å), in contrast to the π dimers found in the solvates (Figure 1b). The newly formed tetrahedral (sp^3) carbon of the σ dimer forces the dicyanomethyl group to project toward the *ab* plane, and this geometry provides a nook where the methyl substituent of the pyridinium ring is nested. The resulting layered structure forms zigzag chains that adopt a chevron motif through short intermolecular CN−S contacts (Figures 1b and S14−S16). The packing optimizes the electrostatic interactions of the terminal dicyanomethanide portion of the σ dimer and the pyridinium ring, affording an array of secondary hydrogen bonding.

https://doi.org/10.1021/jacs.1c07468
J. Am. Chem. Soc. 2021, 143, 15912−15917

The LT phase remains unchanged as it is warmed to 260 K (just below the transition temperature observed by magnetic measurements in Figures S10 and S11), with the σ dimer C−C bond length (1.662(5) Å) not significantly changed. However, a modest change in the β angle from 97.1° to 96.4° and a slight increase in the intermolecular S···S′ interactions occur (Figure 1b and Table S3). At 340 K (above the transition temperature), the monoclinic $P2_1/n$ unit cell is conserved, with a marked change in the β angle from 96.4° to 91.8°. The crystal structure obtained from the high-temperature (HT) data provided clear evidence for discrete TCNQ radicals and significant elongation of the intradimer S−S′ contacts between 3-MepyDTDA$^{+\bullet}$ radicals to 3.626(7) Å (Figure 1c). This value is near the sum of the van der Waals radii of two sulfur atoms (ca. 3.60 Å).[41,42] The layered zigzag chains and the chevron packing of the LT phase are largely maintained in the HT phase along with short intermolecular CN···S contacts between neighboring TCNQ$^{-\bullet}$ and 3-MepyDTDA$^{+\bullet}$ radicals within the same zigzag chain (Figures 1c and S17−S20). Because of the cleavage of the C−C-bonded σ dimer, the two open-shell ($S = {}^1/_2$) TCNQ$^{-\bullet}$ radical anions slip over an inversion center with an interplanar separation of 3.331 Å.

Powder X-ray diffraction (PXRD) data collected for **1**·MeCN (Figure S21) and **1**·EtCN (Figure S22) at room temperature demonstrated that the bulk phases of both solvates are structurally like the corresponding single-crystal structures. Heating of these samples at various intervals up to 417 K led to a shift of diffraction peaks in the powder pattern along with marked changes in the intensities (Figures S23 and S24). This leads to an HT phase of **1** that contains residual traces of **1**·EtCN. However, subsequent cooling clearly indicated a phase transition to the LT phase below 250 K. The HT phase was recovered upon warming to room temperature. Pawley analyses of the collected patterns were consistent with the unit cell parameters obtained from the single-crystal structures (Figure 2 and Tables S4 and S5).

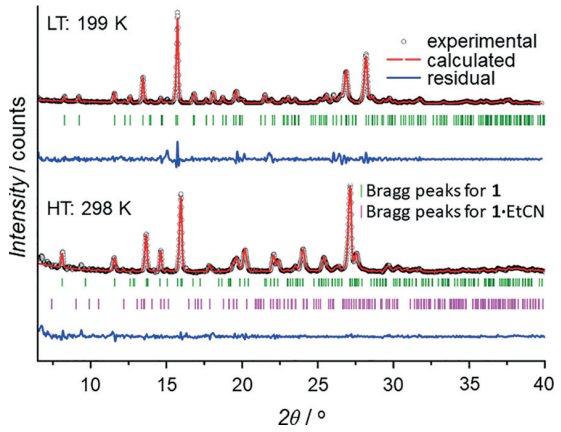

Figure 2. PXRD patterns of the LT phase (top) and HT phase (bottom) obtained by in situ desolvation of **1**·EtCN.

Similar results were obtained for **1**·MeCN (Figure S25), but the TGA results indicated that MeCN is more difficult to remove from the crystal lattice. A solvent-free HT phase of **1** could be most easily obtained by careful heating of crystalline **1**·EtCN in vacuo to achieve desolvation, as evidenced by TGA and Fourier transform infrared (FTIR) spectroscopy (the absence of ν(C≡N) at 2248 cm^{-1} assigned to EtCN; Figure S3) and verified by satisfactory elemental analyses consistent with solvent-free **1**.

The magnetothermal behavior of **1** (Figures 3 and S12) is consistent with the measurements performed on the solvates.

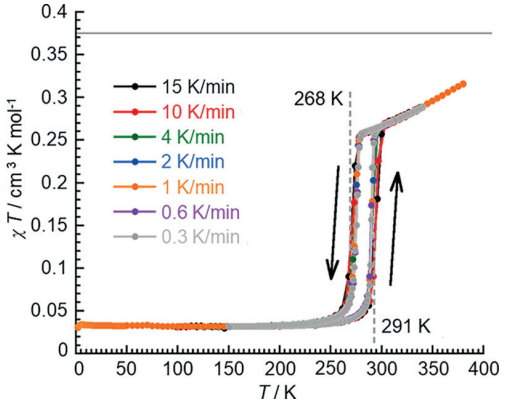

Figure 3. Temperature dependence of the χT product between 1.85 and 380 K measured for **1** at 1 T at different heating−cooling rates. The gray line indicates the expected χT value for an $S = {}^1/_2$ and $g = 2$ Curie paramagnet.

The χT product rises continuously above the transition temperature $T_{1/2}\uparrow$ = 291 K (where $T_{1/2}$ is the temperature at which the LT and HT phases coexist as a 1:1 mixture and ↑ and ↓ arrows indicate that $T_{1/2}$ was measured in heating and cooling mode, respectively) but does not reach the value of 0.375 cm^3 K mol^{-1} expected for an $S = {}^1/_2$ Curie paramagnet (g = 2.00). This suggests that in the HT phase, intramolecular antiferromagnetic (AFM) interactions are present between the TCNQ$^{-\bullet}$ radical anions but the π dimers of 3-MepyDTDA$^{+\bullet}$ remain diamagnetic. Below $T_{1/2}\downarrow$ = 268 K, the χT product decreases and is essentially temperature-independent, consistent with a diamagnetic LT phase. The hysteresis loop between 268 and 291 K appears to be unaltered when cycled between high (15 K min^{-1}) and low (0.3 K min^{-1}) heating−cooling rates, indicating that the dynamics of this first-order phase transition is slower than our experimental time scales.

Differential scanning calorimetry (DSC) data collected on **1** demonstrated a reversible thermal solid−solid transition associated with the structural interconversion between the HT and LT phases of **1** (Figure 4). Nearly identical enthalpies of change (ca. 7 kJ mol^{-1}) were recorded during the heating and cooling phases, highlighting the reproducibility of the thermal process.

Interestingly, in related salts containing the σ dimer of TCNQ$^{-\bullet}$, thermal cleavage to form paramagnetic species has been evidenced only by solid-state electron paramagnetic resonance (EPR) measurements. However, the estimated energies reported for C−C σ-bond cleavage are much greater (24 kJ mol^{-1})[43−45] and occur above 400 K without evidence for a first-order phase transition.

A spectroscopic signature for the phase transition from the HT phase to the LT phase of **1** was measured by Raman and FTIR spectroscopies (Figures 5 and S26−S32). The room-temperature spectra are dominated by stretching modes attributed to TCNQ$^{-\bullet}$. Below 270 K there is a clear difference between the spectra, as multiple ν(C≡N) stretching modes appear in line with σ dimerization.

https://doi.org/10.1021/jacs.1c07468
J. Am. Chem. Soc. 2021, 143, 15912−15917

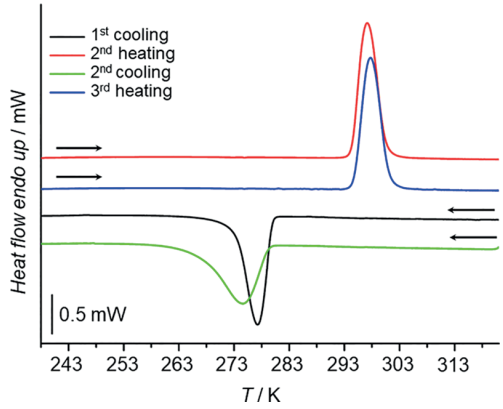

Figure 4. DSC curves of different heating−cooling (10 K min^{-1}) scans for **1**. Scans are shifted on the *y* axis for clarity, and the first heating (not shown) was from 298 to 423 K to verify complete desolvation before the first cooling cycle (see Figure S8).

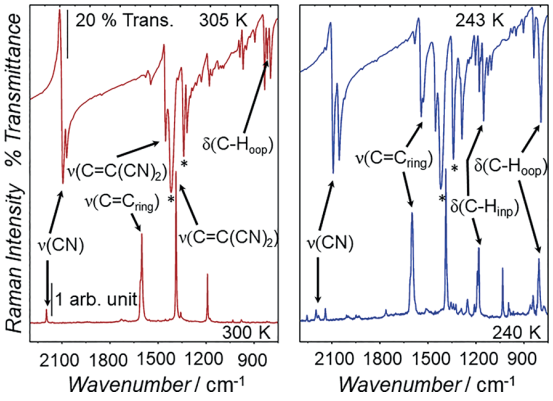

Figure 5. (top) FTIR and (bottom) Raman spectra of the HT phase (red) and LT phase (blue) of **1** with tentative assignments of stretching (ν) and bending (δ) modes (inp = in-plane) of $TCNQ^{-\bullet}$ and its σ dimer. The LT phase displays bending modes, $\delta(C-H_{inp})$, and a strong absorption at 798 cm^{-1} (cf. 806 cm^{-1})[47] assigned to the $\delta(C-H_{oop})$ bending mode (Raman-active only for the σ dimer) attributed to the σ dimer. Asterisks denote Nujol mull peaks.

Complementary information obtained by FTIR spectroscopy indicated a $\delta(C-H)$ bending mode at 822 cm^{-1}, in agreement with the presence of $TCNQ^{-\bullet}$.[46−48] Lastly, the Raman and IR spectra of the LT phase of **1** are consistent with spectra measured for the σ dimer of $TCNQ^{-\bullet}$ found in the ethylphenazenium ($EtPhen^{+}$) salt,[32,43] validating the spectral changes for the phase transition in **1**.

To summarize, we have established that the crystalline solvates **1**·RCN (R = Me, Et) containing $TCNQ^{-\bullet}$ and 3-MepyDTDA$^{+\bullet}$ π dimers tolerate loss of lattice solvent, leading to an HT phase of **1** that undergoes a reversible first-order phase transition associated with the structural interconversion between discrete $TCNQ^{-\bullet}$ radical anions ($S = {}^{1}/_{2}$) and their C−C-bonded σ dimers ($S = 0$). The single-crystal X-ray data illustrate the cooperative role of the structurally flexible π dimer of 3-MepyDTDA$^{+\bullet}$ and the intermolecular $S^{\delta+}-N^{\delta-}$ interactions that bookend the discrete $TCNQ^{-\bullet}$ radical anions. While spin pairing in planar organic radicals typically occurs through overlap of their π orbitals, salt **1** is a relatively rare example of a σ dimer exhibiting magnetic bistability behavior. Furthermore, **1** is an unprecedented example of a two-component magnetically bistable system composed solely of molecular organic radicals and provides impetus for further investigations on related σ dimer systems containing TCNQ and their potential for functional organic materials.

■ ASSOCIATED CONTENT

Supporting Information

The Supporting Information is available free of charge at https://pubs.acs.org/doi/10.1021/jacs.1c07468.

Full description of experimental details, including additional IR, Raman, TGA, DSC, magnetic susceptibility, PXRD, and X-ray diffraction data and illustrations (PDF)

Accession Codes

CCDC 2097021−2097025 contain the supplementary crystallographic data for this paper. These data can be obtained free of charge via www.ccdc.cam.ac.uk/data_request/cif, or by emailing data_request@ccdc.cam.ac.uk, or by contacting The Cambridge Crystallographic Data Centre, 12 Union Road, Cambridge CB2 1EZ, U.K.; fax: +44 1223 336033.

■ AUTHOR INFORMATION

Corresponding Authors

Aaron Mailman − *NanoScience Centre, Department of Chemistry, University of Jyväskylä, FI-40014 Jyväskylä, Finland;* orcid.org/0000-0003-2067-8479; Email: aaron.m.mailman@jyu.fi

Rodolphe Clérac − *Univ. Bordeaux, CNRS, Centre de Recherche Paul Pascal, UMR5031, F-33600 Pessac, France;* orcid.org/0000-0001-5429-7418; Email: clerac@crpp-bordeaux.cnrs.fr

Authors

Anni I. Taponen − *NanoScience Centre, Department of Chemistry, University of Jyväskylä, FI-40014 Jyväskylä, Finland*

Awatef Ayadi − *NanoScience Centre, Department of Chemistry, University of Jyväskylä, FI-40014 Jyväskylä, Finland*

Manu K. Lahtinen − *NanoScience Centre, Department of Chemistry, University of Jyväskylä, FI-40014 Jyväskylä, Finland;* orcid.org/0000-0001-5561-3259

Itziar Oyarzabal − *Univ. Bordeaux, CNRS, Centre de Recherche Paul Pascal, UMR5031, F-33600 Pessac, France; BCMaterials, Basque Center for Materials, Applications and Nanostructures, ES-48940 Leioa, Spain; IKERBASQUE, Basque Foundation for Science, ES-48009 Bilbao, Spain;* orcid.org/0000-0001-9149-2511

Sébastien Bonhommeau − *Univ. Bordeaux, CNRS, Bordeaux INP, ISM, UMR5255, F-33400 Talence, France;* orcid.org/0000-0002-9213-7201

Mathieu Rouzières − *Univ. Bordeaux, CNRS, Centre de Recherche Paul Pascal, UMR5031, F-33600 Pessac, France*

Corine Mathonière − *Univ. Bordeaux, CNRS, Centre de Recherche Paul Pascal, UMR5031, F-33600 Pessac, France*

Heikki M. Tuononen − *NanoScience Centre, Department of Chemistry, University of Jyväskylä, FI-40014 Jyväskylä, Finland;* orcid.org/0000-0002-4820-979X

Complete contact information is available at: https://pubs.acs.org/10.1021/jacs.1c07468

https://doi.org/10.1021/jacs.1c07468
J. Am. Chem. Soc. 2021, 143, 15912−15917

Notes

The authors declare no competing financial interest.

■ ACKNOWLEDGMENTS

The contributions of Noora Svahn to the preparation of starting materials and Elina Hautakangas for assistance with elemental analysis are gratefully acknowledged. A.M. and H.M.T. thank the Academy of Finland for funding (Projects 333565, 336456, and 289172). R.C., C.M., M.R., and I.O. received funding from the University of Bordeaux, the Region Nouvelle Aquitaine, Quantum Matter Bordeaux, and the Centre National de la Recherche Scientifique (CNRS). Raman measurements were performed at the SIV platform funded by the European Union (FEDER) and the Nouvelle Aquitaine Region.

■ REFERENCES

(1) Sato, O. Dynamic Molecular Crystals with Switchable Physical Properties. *Nat. Chem.* **2016**, *8* (7), 644−656.
(2) Ratera, I.; Veciana, J. Playing with Organic Radicals as Building Blocks for Functional Molecular Materials. *Chem. Soc. Rev.* **2012**, *41* (1), 303−349.
(3) Hicks, R. G. A New Spin on Bistability. *Nat. Chem.* **2011**, *3* (3), 189−191.
(4) Hicks, R. *Stable Radicals: Fundamentals and Applied Aspects of Odd-Electron Compounds*; Wiley, 2011.
(5) Rawson, J. M.; Alberola, A.; Whalley, A. Thiazyl Radicals: Old Materials for New Molecular Devices. *J. Mater. Chem.* **2006**, *16* (26), 2560−2575.
(6) Rawson, J. M.; Hayward, J. J. Reversible Spin Pairing in Crystalline Organic Radicals. In *Spin-Crossover Materials*; Wiley, 2013; pp 225−237.
(7) Richardson, J. G.; Mizuno, A.; Shuku, Y.; Awaga, K.; Robertson, N.; Morrison, C. A.; Warren, M. R.; Allan, D. R.; Moggach, S. A. Evaluating the High-Pressure Structural Response and Crystal Lattice Interactions of the Magnetically-Bistable Organic Radical TTTA. *CrystEngComm* **2021**, *23*, 4444−4450.
(8) Dragulescu-Andrasi, A.; Filatov, A. S.; Oakley, R. T.; Li, X.; Lekin, K.; Huq, A.; Pak, C.; Greer, S. M.; McKay, J.; Jo, M.; Lengyel, J.; Hung, I.; Maradzike, E.; DePrince, A. E.; Stoian, S. A.; Hill, S.; Hu, Y.-Y.; Shatruk, M. Radical Dimerization in a Plastic Organic Crystal Leads to Structural and Magnetic Bistability with Wide Thermal Hysteresis. *J. Am. Chem. Soc.* **2019**, *141* (45), 17989−17994.
(9) Bates, D.; Robertson, C. M.; Leitch, A. A.; Dube, P. A.; Oakley, R. T. Magnetic Bistability in Naphtho-1,3,2-Dithiazolyl: Solid State Interconversion of a Thiazyl π-Radical and Its N−N σ-Bonded Dimer. *J. Am. Chem. Soc.* **2018**, *140* (11), 3846−3849.
(10) Li, T.; Tan, G.; Shao, D.; Li, J.; Zhang, Z.; Song, Y.; Sui, Y.; Chen, S.; Fang, Y.; Wang, X. Magnetic Bistability in a Discrete Organic Radical. *J. Am. Chem. Soc.* **2016**, *138* (32), 10092−10095.
(11) Lekin, K.; Winter, S. M.; Downie, L. E.; Bao, X.; Tse, J. S.; Desgreniers, S.; Secco, R. A.; Dube, P. A.; Oakley, R. T. Hysteretic Spin Crossover between a Bisdithiazolyl Radical and Its Hypervalent σ-Dimer. *J. Am. Chem. Soc.* **2010**, *132* (45), 16212−16224.
(12) Clarke, C. S.; Jornet-Somoza, J.; Mota, F.; Novoa, J. J.; Deumal, M. Origin of the Magnetic Bistability in Molecule-Based Magnets: A First-Principles Bottom-Up Study of the TTTA Crystal. *J. Am. Chem. Soc.* **2010**, *132* (50), 17817−17830.
(13) Brusso, J. L.; Clements, O. P.; Haddon, R. C.; Itkis, M. E.; Leitch, A. A.; Oakley, R. T.; Reed, R. W.; Richardson, J. F. Bistabilities in 1,3,2-Dithiazolyl Radicals. *J. Am. Chem. Soc.* **2004**, *126* (26), 8256−8265.
(14) Brusso, J. L.; Clements, O. P.; Haddon, R. C.; Itkis, M. E.; Leitch, A. A.; Oakley, R. T.; Reed, R. W.; Richardson, J. F. Bistability and the Phase Transition in 1,3,2-Dithiazolo[4,5-*b*]pyrazin-2-yl. *J. Am. Chem. Soc.* **2004**, *126* (45), 14692−14693.
(15) Fujita, W.; Awaga, K. Room-Temperature Magnetic Bistability in Organic Radical Crystals. *Science* **1999**, *286* (5438), 261−262.
(16) Fujita, W.; Awaga, K.; Matsuzaki, H.; Okamoto, H. Room-Temperature Magnetic Bistability in Organic Radical Crystals: Paramagnetic-Diamagnetic Phase Transition in 1,3,5-Trithia-2,4,6-Triazapentalenyl. *Phys. Rev. B: Condens. Matter Mater. Phys.* **2002**, *65* (6), 064434.
(17) McManus, G. D.; Rawson, J. M.; Feeder, N.; van Duijn, J.; McInnes, E. J. L.; Novoa, J. J.; Burriel, R.; Palacio, F.; Oliete, P. Synthesis, Crystal Structures, Electronic Structure and Magnetic Behaviour of the Trithiatriazapentalenyl Radical, $C_2S_3N_3$. *J. Mater. Chem.* **2001**, *11* (8), 1992−2003.
(18) Du, H.; Haddon, R. C.; Krossing, I.; Passmore, J.; Rawson, J. M.; Schriver, M. J. Thermal Hysteresis in Dithiadiazolyl and Dithiazolyl Radicals Induced by Supercooling of Paramagnetic Liquids Close to Room Temperature: A Study of $F_3CCNSSN$ and an Interpretation of the Behaviour of $F_3CCSNSCCF_3$. *Chem. Commun.* **2002**, No. 17, 1836−1837.
(19) Alberola, A.; Eisler, D. J.; Harvey, L.; Rawson, J. M. Molecular Tailoring of Spin-Transition Materials: Preparation, Crystal Structure and Magnetism of Trifluoromethyl-Pyridyl-1,3,2-Dithiazolyl. *CrystEngComm* **2011**, *13* (6), 1794−1796.
(20) Matsuzaki, H.; Fujita, W.; Awaga, K.; Okamoto, H. Photo-induced Phase Transition in an Organic Radical Crystal with Room-Temperature Optical and Magnetic Bistability. *Phys. Rev. Lett.* **2003**, *91* (1), 017403.
(21) Shultz, D. A.; Fico, R. M., Jr.; Boyle, P. D.; Kampf, J. W. Observation of a Hysteretic Phase Transition in a Crystalline Dinitroxide Biradical That Leads to Magnetic Bistability. *J. Am. Chem. Soc.* **2001**, *123* (42), 10403−10404.
(22) Matsumoto, S.; Higashiyama, T.; Akutsu, H.; Nakatsuji, S. A Functional Nitroxide Radical Displaying Unique Thermochromism and Magnetic Phase Transition. *Angew. Chem., Int. Ed.* **2011**, *50* (46), 10879−10883.
(23) Nishimaki, H.; Ishida, T. Organic Two-Step Spin-Transition-Like Behavior in a Linear S = 1 Array: 3′-Methylbiphenyl-3,5-diyl Bis(*tert*-butylnitroxide) and Related Compounds. *J. Am. Chem. Soc.* **2010**, *132* (28), 9598−9599.
(24) Nishimaki, H.; Mashiyama, S.; Yasui, M.; Nogami, T.; Ishida, T. Bistable Polymorphs Showing Diamagnetic and Paramagnetic States of an Organic Crystalline Biradical Biphenyl-3,5-diyl Bis(*tert*-butylnitroxide). *Chem. Mater.* **2006**, *18* (16), 3602−3604.
(25) Constantinides, C. P.; Berezin, A. A.; Zissimou, G. A.; Manoli, M.; Leitus, G. M.; Bendikov, M.; Probert, M. R.; Rawson, J. M.; Koutentis, P. A. A Magnetostructural Investigation of an Abrupt Spin Transition for 1-Phenyl-3-trifluoromethyl-1,4-dihydrobenzo[*e*]-[1,2,4]triazin-4-yl. *J. Am. Chem. Soc.* **2014**, *136* (34), 11906−11909.
(26) Itkis, M. E.; Chi, X.; Cordes, A. W.; Haddon, R. C. Magneto-Opto-Electronic Bistability in a Phenalenyl-Based Neutral Radical. *Science* **2002**, *296* (5572), 1443.
(27) Peterson, J. P.; Zhang, R.; Winter, A. H. Effect of Structure on the Spin Switching and Magnetic Bistability of Solid-State Aryl Dicyanomethyl Monoradicals and Diradicals. *ACS Omega* **2019**, *4* (8), 13538−13542.
(28) Nascimento, M. A.; Heyer, E.; Clarke, J. J.; Cowley, H. J.; Alberola, A.; Stephaniuk, N.; Rawson, J. M. On the Design of Radical-Radical Cocrystals. *Angew. Chem., Int. Ed.* **2019**, *58* (5), 1371−1375.
(29) Taponen, A. I.; Wong, J. W. L.; Lekin, K.; Assoud, A.; Robertson, C. M.; Lahtinen, M.; Clérac, R.; Tuononen, H. M.; Mailman, A.; Oakley, R. T. Non-Innocent Base Properties of 3- and 4-Pyridyl-Dithia- and Diselenadiazolyl Radicals: The Effect of N-Methylation. *Inorg. Chem.* **2018**, *57* (21), 13901−13911.
(30) Garcia-Yoldi, I.; Miller, J. S.; Novoa, J. J. Theoretical Study of the Electronic Structure of $[TCNQ]_2^{2-}$ (TCNQ = 7,7,8,8-Tetracyano-*p*-Quinodimethane) Dimers and Their Intradimer, Long, Multicenter Bond in Solution and the Solid State. *J. Phys. Chem. A* **2009**, *113* (25), 7124−7132.

https://doi.org/10.1021/jacs.1c07468
J. Am. Chem. Soc. 2021, 143, 15912−15917

(31) Grossel, M. C.; Evans, F. A.; Hriljac, J. A.; Prout, K.; Weston, S. C. Triplet Excitons in Isolated $TCNQ^{\bullet-}$ Dimers (TCNQ = Tetracyanoquinodimethane). *J. Chem. Soc., Chem. Commun.* **1990**, 1494−1495.
(32) Melby, L. R. Substituted Quinodimethans: VIII. Salts Derived from the 7,7,8,8-Tetracyanoquinodimethan Anion-Radical and Benzologues of Quaternary Pyrazinium Cations. *Can. J. Chem.* **1965**, *43* (5), 1448−1453.
(33) Ballester, L.; Gutiérrez, A.; Perpiñán, M. F.; Azcondo, M. T.; Sánchez, A. E. Interactions of TCNQ in Iron and Nickel Coordination Compounds. *Synth. Met.* **2001**, *120* (1), 965−966.
(34) Dong, V.; Endres, H.; Keller, H. J.; Moroni, W.; Nöthe, D. Dimerization of 7,7,8,8-Tetracyanoquinodimethane (TCNQ) Radical Anions It via σ-Bond Formation: Crystal Structure and EPR Properties of Bis(dipyridyl)platinum(II)-TCNQ, $[Pt(2,2'\text{-Dipy})_2^{2+}(TCNQ)_2^{2-}]$. *Acta Crystallogr., Sect. B: Struct. Crystallogr. Cryst. Chem.* **1977**, *33* (8), 2428−2431.
(35) Radhakrishnan, T. P.; Van Engen, D.; Soos, Z. G. Diamagnetic to Paramagnetic Transition in Trisdimethylaminocyclopropenium Tetracyanoquinodimethanide (TDAC-TCNQ). *Mol. Cryst. Liq. Cryst.* **1987**, *150* (1), 473−492.
(36) Yelgaonkar, S. P.; Campillo-Alvarado, G.; MacGillivray, L. R. Phototriggered Guest Release from a Nonporous Organic Crystal: Remarkable Single-Crystal-to-Single-Crystal Transformation of a Binary Cocrystal Solvate to a Ternary Cocrystal. *J. Am. Chem. Soc.* **2020**, *142* (49), 20772−20777.
(37) Chaudhary, A.; Mohammad, A.; Mobin, S. M. Recent Advances in Single-Crystal-to-Single-Crystal Transformation at the Discrete Molecular Level. *Cryst. Growth Des.* **2017**, *17* (5), 2893−2910.
(38) Liu, J.-L.; Wu, J.-Y.; Huang, G.-Z.; Chen, Y.-C.; Jia, J.-H.; Ungur, L.; Chibotaru, L. F.; Chen, X.-M.; Tong, M.-L. Desolvation-Driven 100-Fold Slow-down of Tunneling Relaxation Rate in Co(II)-Dy(III) Single-Molecule Magnets through a Single-Crystal-to-Single-Crystal Process. *Sci. Rep.* **2015**, *5* (1), 16621.
(39) Hao, Z.-M.; Zhang, X.-M. Solvent Induced Molecular Magnetic Changes Observed in Single-Crystal-to-Single-Crystal Transformation. *Dalton Trans* **2011**, *40* (10), 2092−2098.
(40) Schelter, E. J.; Morris, D. E.; Scott, B. L.; Thompson, J. D.; Kiplinger, J. L. Toward Actinide Molecular Magnetic Materials: Coordination Polymers of U(IV) and the Organic Acceptors TCNQ and TCNE. *Inorg. Chem.* **2007**, *46* (14), 5528−5536.
(41) Bondi, A. Van Der Waals Volumes and Radii. *J. Phys. Chem.* **1964**, *68*, 441−451.
(42) Politzer, P.; Murray, J. S. The Use and Misuse of van Der Waals Radii. *Struct. Chem.* **2021**, *32* (2), 623−629.
(43) Harms, R. H.; Keller, H. J.; Nöthe, D.; Werner, M.; Gundel, D.; Sixl, H.; Soos, Z. G.; Metzger, R. M. Triplet Spin Excitons in a Sigma-Bonded TCNQ Dimer Salt: *N*-Ethylphenazinium TCNQ, $(NEP^{+})_2(TCNQ^{-}-TCNQ^{-})$. *Mol. Cryst. Liq. Cryst.* **1981**, *65* (3−4), 179−196.
(44) Hatfield, W. E.; Hoffmann, S. K.; Corvan, P. J.; Singh, P.; Sethulekshmi, C. N.; Metzger, R. M. Excited Triplet State EPR of Sigma-bonded TCNQ Dimers in $[Cu(DMP)_2]_2[TCNQ]_2$. *J. Phys. Colloq.* **1983**, *44* (C3), C3-1377−C3-1380.
(45) Hoffmann, S. K.; Corvan, P. J.; Singh, P.; Sethulekshmi, C. N.; Metzger, R. M.; Hatfield, W. E. Crystal Structure and Excited Triplet-State Electron Paramagnetic Resonance of the. SIGMA.-Bonded TCNQ Dimer in Bis(2,9-Dimethyl-1,10-Phenanthroline)Copper(I) Tetracyanoquinodimethane Dimer $[Cu(DMP)_2]_2[TCNQ]_2$. *J. Am. Chem. Soc.* **1983**, *105* (14), 4608−4617.
(46) Zhao, H.; Heintz, R. A.; Ouyang, X.; Dunbar, K. R.; Campana, C. F.; Rogers, R. D. Spectroscopic, Thermal, and Magnetic Properties of Metal/TCNQ Network Polymers with Extensive Supramolecular Interactions between Layers. *Chem. Mater.* **1999**, *11* (3), 736−746.
(47) Zhao, H.; Heintz, R. A.; Dunbar, K. R.; Rogers, R. D. Unprecedented Two-Dimensional Polymers of Mn(II) with $TCNQ^{-\bullet}$ (TCNQ = 7,7,8,8-Tetracyanoquinodimethane). *J. Am. Chem. Soc.* **1996**, *118* (50), 12844−12845.
(48) Pukacki, W.; Pawlak, M.; Graja, A.; Lequan, M.; Lequan, R. M. Electronic and Spectral Properties of Organometallic Tetracyano-*p*-Quinodimethane (TCNQ) Salts with Metallocene Stacks. *Inorg. Chem.* **1987**, *26* (8), 1328−1331.

https://doi.org/10.1021/jacs.1c07468
J. Am. Chem. Soc. 2021, 143, 15912−15917

III

ROLE OF ALKYL SUBSTITUENT AND SOLVENT ON THE STRUCTURAL, THERMAL, AND MAGNETIC PROPERTIES OF BINARY RADICAL SALTS OF 1,2,3,5-DITHIA- OR DISELENADIAZOLYL CATIONS AND THE TCNQ ANION

by

Taponen, A. I.; Ayadi, A.; Svahn, N.; Lahtinen, M. K.; Rouzières, M.; Clérac, R.; Tuononen, H. M.; Mailman, A. 2022

Crystal Growth &Design, *22* (12) 7110–7122

https://doi.org/10.1021/acs.cgd.2c00795

CRYSTAL GROWTH & DESIGN

pubs.acs.org/crystal

Article

Role of Alkyl Substituent and Solvent on the Structural, Thermal, and Magnetic Properties of Binary Radical Salts of 1,2,3,5-Dithia- or Diselenadiazolyl Cations and the TCNQ Anion

Anni I. Taponen, Awatef Ayadi, Noora Svahn, Manu K. Lahtinen, Mathieu Rouzières, Rodolphe Clérac,* Heikki M. Tuononen,* and Aaron Mailman*

Cite This: *Cryst. Growth Des.* 2022, 22, 7110−7122

Read Online

ACCESS | Metrics & More | Article Recommendations | Supporting Information

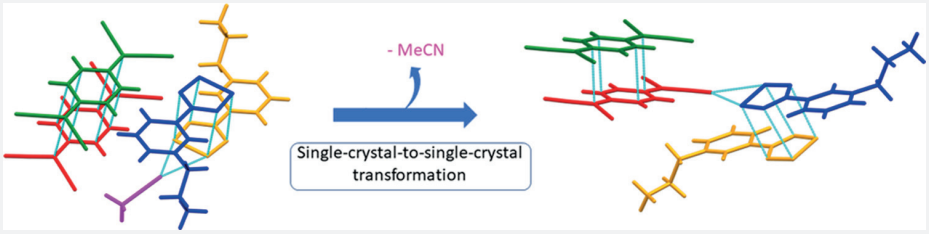

ABSTRACT: The synthesis, structural, thermal, and magnetic properties of a series of simple binary organic salts based on the radical anion of 7,7,8,8-tetracyanoquinodimethane (TCNQ) and 4-(*N*-alkylpyridinium-3-yl)-1,2,3,5-dithiadiazolyl (DTDA), $\mathbf{1}^{R}$ (R = Et, Pr, Bu), radical cations and their heavier selenium analogues (DSDA), $\mathbf{2}^{R}$, are described. Single-crystal X-ray structural analyses reveal that short alkyl substituents on the pyridinium moiety of DTDA/DSDA cations lead to crystallization of isostructural acetonitrile (MeCN) solvates $\mathbf{1}^{Et}$**·MeCN**, $\mathbf{1}^{Pr}$**·MeCN**, $\mathbf{2}^{Et}$**·MeCN**, and $\mathbf{2}^{Pr}$**·MeCN** with *trans*-cofacial DTDA radical cation and eclipsed-cofacial TCNQ radical anion dimers. A slight increase in the substituent chain length to butyl affords the solvate $\mathbf{1}^{Bu}$**·0.5MeCN** or the nonsolvate $\mathbf{1}^{Bu}$. The nonsolvate $\mathbf{1}^{Bu}$ can be exclusively isolated using propionitrile (EtCN), whereas the isostructural selenium analogue $\mathbf{2}^{Bu}$ crystallizes from MeCN. The crystal packing in $\mathbf{1}^{Bu}$**·0.5MeCN** and $\mathbf{1}^{Bu}$**/**$\mathbf{2}^{Bu}$ is distinctively different: rare one-dimensional (1D) columnar π-stacks of evenly spaced TCNQ radical anions with periodic distortions along the vertical stacking direction and *cis*-cofacial DTDA dimers in $\mathbf{1}^{Bu}$**·0.5MeCN** *vs* discrete, non-eclipsed-cofacial TCNQ dimers and *trans*-antarafacial DTDA/DSDA dimers in $\mathbf{1}^{Bu}$**/**$\mathbf{2}^{Bu}$. The nonsolvated structure $\mathbf{1}^{Pr}$ with *trans*-cofacial DTDA and non-eclipsed-cofacial TCNQ dimers can be isolated from EtCN. Single-crystal and powder X-ray diffraction methods confirmed a thermally driven, irreversible, single-crystal-to-single-crystal structural transformation between $\mathbf{1}^{Pr}$**·MeCN** and $\mathbf{1}^{Pr}$. Thermogravimetric analyses of all nonsolvated salts show varied, yet robust, thermal behavior, while the thermal behavior of the solvates is consistent with more facile lattice solvent loss from structures with longer *N*-alkyl chains. Variable-temperature magnetic susceptibility measurements indicate that all structures are diamagnetic at low temperatures. However, thermally populated magnetic states could be observed for $\mathbf{1}^{Et}$**·MeCN**, $\mathbf{1}^{Et}$**·EtCN**, $\mathbf{1}^{Pr}$**·MeCN**, $\mathbf{1}^{Bu}$**·0.5MeCN**, $\mathbf{1}^{Bu}$, and $\mathbf{2}^{Bu}$ at higher temperatures. This can be correlated with desolvation and structural changes that lead to the generation of weakly antiferromagnetically coupled non-eclipsed-cofacial TCNQ dimers, in agreement with results from density functional theory (DFT) calculations.

INTRODUCTION

Ion-paired molecular solids containing the ubiquitous electron acceptor 7,7,8,8-tetracyano-*p*-quinodimethane (TCNQ) have been extensively investigated for constituents of new functional materials exhibiting conductive, optical, and/or magnetic properties. A quintessential example of this class of compounds is the 1:1 charge transfer complex between TCNQ and tetrathiafulvalene (TTF), reported in 1973.[1] It was the first example of an organic solid showing metal-like behavior over a large temperature range and maximum electrical conductivity on par with typical metallic elements, such as copper. This system has been intensively explored even to this day, leading to many groundbreaking results. For example, bringing individual crystals of TTF and TCNQ into direct, mechanical contact, a process dubbed crystal laminating, has been found to create stable and reproducible conducting layers with high carrier density without the need of dopants.[2] Recently, nanostructured TTF−TCNQ was found to exhibit excellent electromagnetic performance and electromagnetic interference

Received: July 15, 2022
Revised: September 29, 2022
Published: October 29, 2022

https://doi.org/10.1021/acs.cgd.2c00795
Cryst. Growth Des. 2022, 22, 7110−7122

shielding effectiveness, opening up the possibility to develop electromagnetic response materials based on charge transfer systems.[3]

The TTF−TCNQ charge transfer complex has a unique and well-defined crystal structure in which the formally ionic constituents form alternating and evenly spaced columnar stacks consisting of noneclipsed subunits. As a result, the stacks behave as decoupled, quasi-one-dimensional (1D) electronic systems that lead to the observed conductivity at high temperatures. However, at very low temperatures, the TTF−TCNQ system becomes an insulator owing to two Peierls transitions that occur independently at 38 and 54 K for TTF and TCNQ, respectively.[4] The evenly spaced, uniform columnar packing of $TCNQ^{\cdot-}$ radical anions is relatively uncommon; however, it is observed, for example, in the *N*-methylphenazinium (NMP) salt that also shows high electrical conductivity for an organic species, though several orders of magnitude less than that of TTF−TCNQ.[5,6]

By far the most common packing type in ion-paired TCNQ salts involves the formation of discrete π-dimers of $TCNQ^{\cdot-}$ radical anions with either an eclipsed or noneclipsed geometry (Chart 1). The former geometry typically involves a transversal

Chart 1. Three Most Common Modes of Dimerization for the 7,7′,8,8′-Tetracyanoquinodimethane Radical Anion ($TCNQ^{\cdot-}$)

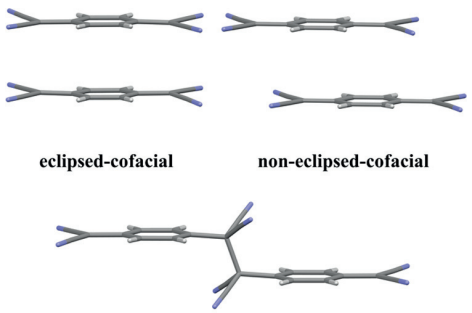

offset of *ca.* 1.0 Å, while the latter is characterized by a longitudinal offset of *ca.* 2.1 Å (Chart 2).[7] In both cases, the unpaired electrons in the dimers are antiferromagnetically coupled *via* strong $\pi-\pi$ interactions, whereas systems with noneclipsed geometry often exhibit thermally accessible triplet states.[8,9] In addition to π-dimerization, $TCNQ^{\cdot-}$ radical anions

Chart 2. Illustration of the Structures of the Binary Salts 1^{R} and 2^{R}, and Their Acetonitrile (MeCN) or Propionitrile (EtCN) Solvates, Consisting of a 1,2,3,5-Dithiadiazolyl (DTDA; E = S) or 1,2,3,5-Diselanadiazolyl (DSDA; E = Se) Radical Cation and a TCNQ Radical Anion

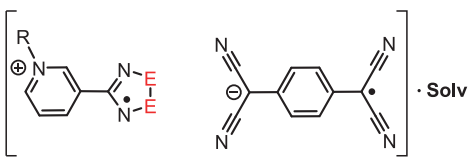

1^{R}, E = S; 2^{R}, E = Se
R = Me, Et, Pr, Bu
Solv = MeCN, EtCN

have been found to form σ-dimers in the solid state with long (1.6−1.7 Å) and thereby weak C−C bonds. There are only a dozen structurally characterized examples of σ-dimers of $TCNQ^{\cdot-}$ reported to date,[9−20] with the first example being the *N*-ethylphenazinium (NEP) salt, [NEP][TCNQ].[21] It is striking that such a simple methyl-to-ethyl substitution in the cationic moiety has such a profound influence on the structure of the anion (evenly spaced π-stacks in [NMP][TCNQ] *vs* σ-dimers in [NEP][TCNQ]) and, therefore, to the physical properties of the compound (highly conducting *vs* insulating).

The majority of simple binary salts of the $TCNQ^{\cdot-}$ radical anion contain diamagnetic counter cations, though there are examples of salts with radical cations.[22,23] Recently, we decided to introduce an additional spin to the system by combining $TCNQ^{\cdot-}$ with the 4-(*N*-methylpyridinium-3-yl)-1,2,3,5-dithiadiazolyl radical cation (3-MePyDTDA$^{+\cdot}$) by solution methods to afford the solvates $\mathbf{1^{Me}}$·MeCN and $\mathbf{1^{Me}}$·EtCN, where $\mathbf{1^{Me}}$ = [3-MePyDTDA$^{+\cdot}$][$TCNQ^{\cdot-}$].[24] Such ion-paired salts of molecular radicals can lead to new functional materials with interesting magnetic and/or conductive properties. We showed that the desolvation of $\mathbf{1^{Me}}$·MeCN and $\mathbf{1^{Me}}$·EtCN containing π-dimers of both 3-MePyDTDA$^{+\cdot}$ and $TCNQ^{\cdot-}$ affords the nonsolvate $\mathbf{1^{Me}}$ that, in turn, undergoes a reversible first-order phase transition associated with structural interconversion between two discrete and noninteracting $TCNQ^{\cdot-}$ radicals ($S = 1/2$) and their C−C-bonded σ-dimers ($S = 0$). The magnetic bistability observed for $\mathbf{1^{Me}}$ results from the structural flexibility of the π-dimer of 3-MePyDTDA$^{+\cdot}$ and the intermolecular $S^{\delta+}\cdots N^{\delta-}$ interactions between 3-MePyDTDA$^{+\cdot}$ and $TCNQ^{\cdot-}$ radicals that allow the formation and breakup of the C−C bond in $TCNQ^{\cdot-}$ dimers (1.656(8) Å) without other structural changes.

In this study, we continue our investigations on the radical-ion salts of DTDA$^{+\cdot}$ and $TCNQ^{\cdot-}$ by probing the effect the alkyl chain length on the pyridinium moiety of the DTDA$^{+\cdot}$ radical cation has on the solid-state architecture. As a first approximation, the replacement of the methyl group by a longer alkyl chain is expected to affect the steric properties of the cation alone because the SOMO of DTDA$^{+\cdot}$ is invariant to such substitution. Combined with the pliability of longer alkyl chains, the increased steric repulsion should favor the formation of nonsolvated crystal structures that, in turn, could be advantageous for the formation of σ-dimers of $TCNQ^{\cdot-}$ and possibly new magnetically bistable systems composed of organic radicals. As a further modification to the molecular structure, we performed an atom-to-atom replacement and investigated the behavior of selenium analogues of DTDA$^{+\cdot}$, that is, 4-(*N*-alkylpyridinium-3-yl)-1,2,3,5-diselenadiazolyl radial-cations (DSDA$^{+\cdot}$). The primary motivation for these investigations comes from the well-studied N-alkylphenazinium salts of $TCNQ^{\cdot-}$ discussed above, in which case the identity of the cationic alkyl chain (methyl, ethyl, or butyl) influences not only the $TCNQ^{\cdot-}$ dimerization mode but also the resultant physical properties. Moreover, despite the known role that the cation plays in the solid-state structure and properties of $TCNQ^{\cdot-}$ salts, only a few systematic studies have been reported on the topic to date.

EXPERIMENTAL SECTION

General Methods and Procedures. Full experimental details for the synthesis and characterization of the precursors **I**−**IV** (see Scheme 1) and the salts $\mathbf{1^{Et}}$·MeCN, $\mathbf{1^{Pr}}$·MeCN, $\mathbf{1^{Bu}}$·0.5MeCN, $\mathbf{1^{Et}}$·EtCN, $\mathbf{1^{Pr}}$,

https://doi.org/10.1021/acs.cgd.2c00795
Cryst. Growth Des. 2022, 22, 7110−7122

1^{Bu}, 2^{Et}·MeCN, 2^{Pr}·MeCN, and 2^{Bu} (Scheme 2), are given in the Supporting Information.

Scheme 1. Synthetic Sequence to the Triflate Salts of 4-(*N*-Alkylpyridinium-3-yl)-1,2,3,5-dithiadiazolyl (E = S) and 4-(*N*-Alkylpyridinium-3-yl)-1,2,3,5-diselenadiazolyl (E = Se) Radical Cations, IV[a]

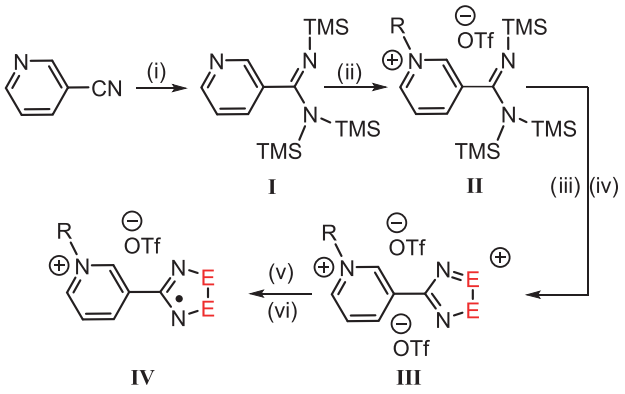

[a]Reagents and general conditions: (i) $LiN(TMS)_2 \cdot Et_2O$, THF, reflux, 16 h, TMSCl; (ii) ROTf, Et_2O, RT, 16 h; (iii) excess S_2Cl_2 or quantitative $SeCl_2$, MeCN, RT, 16 h; (iv) excess TMSOTf, MeCN, RT, 3 h; (v) NBu_4I, MeCN, RT, 3 h; (vi) AgOTf, MeCN, 2 h.

X-ray Crystallography. Variable-temperature single-crystal X-ray diffraction studies were performed on Agilent SuperNova equipped with Atlas CCD detector, dual micro-focus X-ray source (Cu and Mo), and multilayer optics to generate Cu Kα (λ = 1.54184 Å) or Mo Kα (λ = 0.71073 Å) radiation. Crystals were mounted on MiTeGen micro-mounts using Fomblin oil or glass fibers using Wacker silicone paste for low- (<273 K) and high-temperature (>273 K) data collections, respectively. Data acquisitions, reductions, twinning, and analytical face/index-based absorption corrections were made using CrysAlis^{PRO} (v. 39.46).[25] The structures were solved using ShelXT program[26] and refined on F^2 by full-matrix least-squares techniques with the ShelXL program as implemented in Olex (v. 1.2) program package[27] that utilizes the ShelXL-2013 module.[28] C−H hydrogen atoms were calculated to their optimal positions and treated as riding atoms using isotropic displacement parameters 1.2 (aromatic) or 1.5 (aliphatic) times the host atom. Crystallographic data of compounds 1^{Et}·MeCN, 1^{Pr}·MeCN, 1^{Bu}·0.5MeCN, 1^{Et}·EtCN, 1^{Pr}, 1^{Bu}, 2^{Et}·MeCN, 2^{Pr}·MeCN, and 2^{Bu} are compiled in Tables 1 and 2; crystallographic data of derivatives of **IV** are given in the Supporting Information (Tables S1 and S2). In the case of 1^{Bu}·0.5MeCN, poor crystallinity and/or the combination of severe nonmerohedral twinning was persistent across several samples that led to poor data quality. The atom connectivity and crystal packing, however, were clearly established and consistent between two independent data sets. Full crystallographic details are available in the Supporting Information.

Powder X-ray Diffraction. Powder X-ray diffraction measurements were performed on PANalytical X'Pert PRO MPD diffractometer using Cu Kα radiation (λ = 1.5418 Å; 45 kV, 40 mA). In routine experiments, a freshly crystallized and lightly hand-ground powder sample was prepared on zero-background signal generating silicon plate using petrolatum jelly as an adhesive. Diffraction intensities were recorded from spinning samples. In variable-temperature work, a lightly ground sample was placed into an Anton Paar TTK450 temperature-controlled chamber equipped with an automated sample-stage height controller. Diffraction data were acquired by an X'Celerator detector using 2θ ranges of 3−60 and 4−40° in routine and variable-temperature experiments, respectively. A step size of 0.017° and counting times from 60 to 240 s per step were used based on the sample to acquire sufficient diffraction intensities. In variable-temperature measurements, samples were heated/cooled with a heating/cooling rate of 10 K min^{-1} under a nitrogen atmosphere. Each powder pattern was recorded isothermally at the chosen temperature. The diffractometer was aligned using a silicon powder standard material (SRM 640, National Institute of Standards & Technology), and the temperature was calibrated by monitoring the solid-state phase transition of KNO_3 from orthorhombic to trigonal structure (402 K). Data processing and Pawley fits were performed with the program X'Pert HighScore Plus (v. 4.9).[29] The unit cell parameters of the powder samples were refined by Pawley analysis using the corresponding single-crystal structure parameters as the basis of least-squares refinements. Variables used in the fits were zero-offset, polynomial background, sample displacement, and unit cell parameters along with peak profile parameters including peak width, shape, and asymmetry.[30]

Thermogravimetric Analyses (TGA). Thermogravimetric analyses were performed on a PerkinElmer STA 600 simultaneous thermal (TG/DSC) analyzer using open platinum pan under a nitrogen atmosphere (40 mL min^{-1} flow rate) with a heating rate of 10 K min^{-1} over 295−873 K for DTDA and 295−573 K for DSDA variants. Temperature calibration was performed with an indium standard (PerkinElmer, melting point = 429.60 K) and weight calibration by a standard weight of 50.00 mg at room temperature. All samples were freshly prepared and dried *in vacuo* prior to measurements where 3−8 mg of sample was typically used. Recorded TGA data were processed using the Pyris Manager software (v. 13). The desolvation and decomposition temperatures were determined as extrapolated onset values.

Magnetic Susceptibility Measurements. Magnetic measurements were performed on a Quantum Design SQUID MPMS-XL magnetometer housed at the Centre de Recherche Paul Pascal (CRPP) operating at temperatures between 1.8 and 400 K for dc magnetic fields ranging from −7 to 7 T. Measurements were performed on polycrystalline samples 1^{Et}·MeCN, 1^{Et}·EtCN, 1^{Pr}·MeCN, and 1^{Bu}·0.5MeCN, and the nonsolvates 1^{Bu} and 2^{Bu} (21.7, 24.6, 35.1, 24.9, 33.3, and 18.8 mg, respectively) and introduced in a sealed double polyethene/polypropylene bags (3 cm × 0.5 cm × 0.02

Scheme 2. Double-Displacement Reaction between IV and [K(18c6)][TCNQ] Leads to the Radical-Ion Salts $1^{Et,Pr}$·MeCN, 1^{Bu}·0.5MeCN, $2^{Et,Pr}$·MeCN, and 2^{Bu} in MeCN, and 1^{Et}·EtCN and $1^{Pr,Bu}$ in EtCN (1, E = S; 2, E = Se).

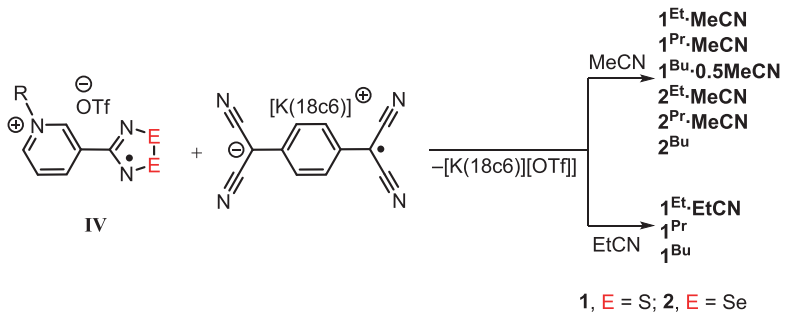

1, E = S; **2**, E = Se

https://doi.org/10.1021/acs.cgd.2c00795
Cryst. Growth Des. 2022, 22, 7110−7122

Table 1. Crystallographic Data for Compounds 1^{Et}·MeCN, 1^{Et}·EtCN, 1^{Pr}·MeCN, 1^{Pr}, 1^{Bu}·0.5MeCN, and 1^{Bu}

	1^{Et}·MeCN	1^{Et}·EtCN	1^{Pr}·MeCN	1^{Pr}	1^{Bu}·0.5MeCN	1^{Bu}
CCDC	2181980	2181982	2181983	2181987	2182780	2181986[b]
formula	$C_{22}H_{16}N_8S_2$	$C_{23}H_{18}N_8S_2$	$C_{23}H_{18}N_8S_2$	$C_{21}H_{15}N_7S_2$	$C_{46}H_{35}N_{15}S_4$	$C_{22}H_{17}N_7S_2$
molecular weight (g mol^{-1})	456.55	470.57	470.59	429.52	926.13	443.54
T (K)	120.00(10)	120.00(10)	120.00(10)	120.00(10)	120.00(10)	120.00(10)
crystal system	triclinic	triclinic	triclinic	triclinic	triclinic	triclinic
space group	$P\bar{1}$	$P\bar{1}$	$P\bar{1}$	$P\bar{1}$	$P\bar{1}$	$P\bar{1}$
a (Å)	8.6768(7)	8.6669(5)	8.8121(5)	8.4212(5)	13.442(3)	6.8439(3)
b (Å)	10.4354(11)	10.4645(6)	10.8960(6)	8.4510(5)	13.464(3)	11.1768(5)
c (Å)	11.9119(10)	13.1169(8)	11.7291(6)	14.1533(8)	13.959(5)	14.2752(7)
α (°)	98.978(8)	74.971(5)	98.130(4)	84.671(5)	92.94(2)	93.617(4)
β (°)	90.426(7)	82.518(5)	92.145(4)	80.088(5)	107.47(3)	90.731(4)
γ (°)	96.364(8)	83.520(4)	97.591(5)	85.166(4)	111.98(2)	106.931(4)
V (Å^3)	1058.46(17)	1135.27(12)	1103.29(11)	985.54(10)	2196.1(11)	1041.99(9)
Z	2	2	2	2	2	2
ρ_{calc} (g cm^{-3})	1.432	1.377	1.416	1.447	1.401	1.414
absorption (μ mm^{-1})	0.280	0.264	0.271	0.295	2.425	0.281
F (000)	472.0	488.0	488.0	444.0	960.0	460.0
2θ range for data collection (deg)	3.978−57.762	4.044−57.77	3.812−57.812	4.852−57.706	6.754−137.994	4.928−57.918
index ranges	$-9 \le h \le 11$	$-10 \le h \le 11$	$-11 \le h \le 9$	$-11 \le h \le 11$	$-16 \le h \le 16$	$-8 \le h \le 9$
	$-14 \le k \le 14$	$-13 \le k \le 13$	$-14 \le k \le 13$	$-11 \le k \le 10$	$-16 \le k \le 16$	$-14 \le k \le 14$
	$-15 \le l \le 14$	$-16 \le l \le 17$	$-14 \le l \le 13$	$-17 \le l \le 19$	$-16 \le l \le 16$	$-19 \le l \le 18$
reflections collected	7601	8934	8432	12,717	11,546	17,696
independent reflections	4739 [R_{int} = 0.0190, R_{sigma} = 0.0383]	5121 [R_{int} = 0.0226, R_{sigma} = 0.0406]	4941 [R_{int} = 0.0184, R_{sigma} = 0.0361]	4573 [R_{int} = 0.0395, R_{sigma} = 0.0456]	11546 [R_{int} = 0.2257[a], R_{sigma} = 0.1951]	4920 [R_{int} = 0.0279, R_{sigma} = 0.0234]
data/restraints/parameters	4739/0/291	5121/0/300	4941/0/300	4573/0/272	11546/236/492	4920/0/281
goodness-of-fit on F^2	1.047	1.067	1.041	1.085	1.114	1.170
final R indices [$I \ge 2\sigma(I)$]	R_1 = 0.0366	R_1 = 0.0406	R_1 = 0.0387	R_1 = 0.0526	R_1 = 0.1617	R_1 = 0.0720
	wR_2 = 0.0861	wR_2 = 0.0938	wR_2 = 0.0946	wR_2 = 0.1602	wR_2 = 0.3912	wR_2 = 0.1941
final R indices [all data]	R_1 = 0.0464	R_1 = 0.0548	R_1 = 0.0460	R_1 = 0.0659	R_1 = 0.2663	R_1 = 0.0746
	wR_2 = 0.0922	wR_2 = 0.1013	wR_2 = 0.1002	wR_2 = 0.1710	wR_2 = 0.4381	wR_2 = 0.1952
$\Delta\rho_{max}/\Delta\rho_{min}$ (e Å^{-3})	0.29/−0.26	0.33/−0.44	0.35/−0.31	0.98/−0.61	2.88/−0.83	0.69/−0.51

[a]Value for R_{int} is determined for the major component of the twin refinement. See the Supporting Information for details. [b]See also CCDC 2181985.

cm; typically 20−40 mg) in a glovebox with a controlled argon atmosphere. Prior to the experiments, the field-dependent magnetization was measured at 100 K on each sample to detect the presence of any bulk ferromagnetic impurity. As expected for paramagnetic or diamagnetic materials, a perfectly linear dependence of the magnetization that extrapolates to zero at zero dc field was systematically observed; the samples appeared to be free of any ferromagnetic impurities. The magnetic susceptibilities were corrected for the sample holder and the intrinsic diamagnetic contributions.

Density Functional Theory. Singlet−triplet gaps were calculated for TCNQ and DTDA dimers using the structural data from low- and high-temperature crystal structures of 1^{Pr} and 1^{Bu}. The calculations were performed with the functionals PBE1PBE-D3BJ[31−36] and LC-ωhPBE[37−40] using def2-TZVP basis sets.[41] The geometries of the dimers were extracted from the solid-state X-ray structures, and the positions of the hydrogen atoms were optimized at the PBE1PBE-D3BJ/def2-TZVP level of theory prior to energy calculations. Broken-symmetry solutions were used for the singlet states while high-spin reference determinants were employed for the triplet states. Two different methods were used as these kinds of calculations are known to be highly sensitive to the choice of density functional. As expected, the singlet−triplet gaps calculated with the two methods differ quantitatively, but the results are in good qualitative agreement with all structural features, notably the separation of the dimers in the solid state, and show that the TCNQ dimers have singlet−triplet gaps that are always smaller than those calculated for the DTDA dimers.

RESULTS AND DISCUSSION

Synthesis. A synthetic route to DTDA radical cation derivatives and the corresponding DSDA congeners,[42] both as their triflate (OTf^-) salts, **IV**, was achieved by modification of our previously reported methodology (Scheme 1).[43] In brief, *N,N,N'*-tris(trimethylsilyl)-3-pyridineimidamide **I** was readily obtained as a viscous yellow oil that could be purified by fractional vacuum distillation and subsequently alkylated with *N*-alkyl triflates to afford the corresponding *N*-alkylpyridinium triflates,[44] **II**, as moisture-sensitive salts. Cyclocondensation of **II** with sulfur monochloride (S_2Cl_2) or freshly prepared selenium dichloride ($SeCl_2$),[45] followed by subsequent metathesis with trimethylsilyl trifluoromethanesulfonate (TMSOTf), provided access to the double triflate salts **III**. The dications in these salts could be readily reduced to the monocation radicals with tetrabutylammonium iodide and converted to their more soluble triflate salts by subsequent treatment with silver triflate (AgOTf). Repeated recrystalliza-

https://doi.org/10.1021/acs.cgd.2c00795
Cryst. Growth Des. 2022, 22, 7110−7122

Table 2. Crystallographic Data for Compounds 2^{Et}·MeCN, 2^{Pr}·MeCN, and 2^{Bu}

	2^{Et}·MeCN	2^{Pr}·MeCN	2^{Bu}
CCDC	2181981	2181984	2182311
formula	$C_{22}H_{16}N_8Se_2$	$C_{23}H_{18}N_8Se_2$	$C_{22}H_{17}N_7Se_2$
molecular weight (g mol^{-1})	550.35	564.37	537.34
T (K)	120.00(10)	120.00(10)	120.00(10)
crystal system	triclinic	triclinic	triclinic
space group	$P\bar{1}$	$P\bar{1}$	$P\bar{1}$
a (Å)	8.7199(5)	8.8519(5)	6.8553(3)
b (Å)	10.4193(5)	10.8610(7)	11.2539(10)
c (Å)	12.0089(6)	11.8794(7)	14.3128(7)
α (°)	98.783(4)	98.194(5)	94.004(6)
β (°)	90.104(4)	91.479(5)	90.361(4)
γ (°)	96.494(4)	97.549(5)	106.859(6)
V (Å^3)	1071.16(10)	1119.48(12)	1053.77(12)
Z	2	2	2
ρ_{calc} (g cm^{-3})	1.706	1.674	1.694
absorption (μ mm^{-1})	3.480	3.332	4.593
F(000)	544.0	560.0	532.0
2θ range for data collection (deg)	3.982−59.322	3.824−57.768	8.232−153.464
index ranges	$-11 \le h \le 12$	$-11 \le h \le 11$	$-8 \le h \le 6$
	$-13 \le k \le 13$	$-13 \le k \le 10$	$-13 \le k \le 14$
	$-16 \le l \le 16$	$-15 \le l \le 15$	$-18 \le l \le 18$
reflections collected	8141	8194	6856
independent reflections	5162 [R_{int} = 0.0178, R_{sigma} = 0.0313]	5006 [R_{int} = 0.0283, R_{sigma} = 0.0661]	6856 [R_{int} = 0.1026[a], R_{sigma} = 0.0173]
data/restraints/parameters	5162/0/291	5006/0/300	6856/0/282
goodness of fit on F^2	1.077	1.020	1.055
final R indices [$I \ge 2\sigma$ (I)]	R_1 = 0.0293	R_1 = 0.0402	R_1 = 0.0516
	wR_2 = 0.0747	wR_2 = 0.0687	wR_2 = 0.1498
final R indices [all data]	R_1 = 0.0351	R_1 = 0.0693	R_1 = 0.0557
	wR_2 = 0.0778	wR_2 = 0.0777	wR_2 = 0.1532
$\Delta\rho_{max}/\Delta\rho_{min}$ (e Å^{-3})	0.85/−0.73	0.61/−0.54	1.33/−1.22

[a]Value for R_{int} is determined for the major component of the twin refinement.

tion from degassed acetonitrile (MeCN) and/or propionitrile (EtCN) afforded **IV** as analytical pure solids in moderate to high yields (Supporting Information).

A double-displacement reaction between **IV** and the highly soluble salt [K(18c6)][TCNQ], prepared according to literature procedures,[24,46] gave 1:1 salts of *N*-alkylated DTDA/DSDA cations and TCNQ anion ($\mathbf{1}^{R}$, E = S; $\mathbf{2}^{R}$, E = Se; R = Et, Pr, Bu) see (Scheme 2). When the syntheses of **1** and **2** were performed in MeCN, crystalline products $\mathbf{1}^{Et}$·**MeCN**, $\mathbf{1}^{Pr}$·**MeCN**, $\mathbf{2}^{Et}$·**MeCN**, and $\mathbf{2}^{Pr}$·**MeCN** with one solvent molecule per asymmetric unit were obtained. In the case of E = S and R = Bu, the crystalline solvate $\mathbf{1}^{Bu}$·**0.5MeCN** was formed, whereas the corresponding selenium derivative $\mathbf{2}^{Bu}$ crystallized without any lattice solvent molecules. Substitution of MeCN with EtCN in the double-displacement reaction gave the solvate $\mathbf{1}^{Et}$·**EtCN** along with two nonsolvated structures $\mathbf{1}^{Pr}$ and $\mathbf{1}^{Bu}$. Unfortunately, similar reactions of the selenium derivatives of **IV** could not be carried out in EtCN due to solubility issues.

Crystal Structures of the Salts IV. Crystals of triflate salts of the *N*-alkylated radical cations **IV** (E = S, Se; R = Et, Pr, Bu) were obtained from MeCN and structurally characterized by single-crystal X-ray diffraction (Tables S1 and S2, Supporting Information). All salts display strong ion-pairing between the triflate anion and the DTDA/DSDA rings. The DTDA/DSDA radicals adopt a *trans*-cofacial dimerization mode in all cases except for E = S and R = Bu (monoclinic, space group I_2/a), where the rare twisted-cofacial mode was found with the butyl chain in an *anti-anti-anti* conformation that protrudes above the plane of the almost coplanar pyridinium and DTDA rings (Figure 1), which are twisted by ϕ = 4.8° (ϕ is defined as the angle between the mean planes through all nonhydrogen atoms of the pyridinium and DTDA/DSDA rings, respectively). In the case of E = Se and R = Bu derivative (triclinic, space group $P\bar{1}$), the pyridinium and DSDA rings are not coplanar (ϕ = 10.4°), and the butyl chain adopts an *anti*-gauche-*anti* conformation that extends laterally from the pyridinium ring (Figure 1). Despite the two different modes of dimerization found for the derivatives of **IV**, the interplanar separation $\delta_{DTDA/DSDA}$, defined as the centroid-to-centroid distance between the two $-CN_2S_2/-CN_2Se_2$ rings of the dimer, falls into very narrow ranges of 3.05−3.12 and 3.17−3.19 Å for the DTDA and DSDA dimers, respectively. In all structures of **IV**, the dimers adopt a one-dimensional (1D) head-over-tail π-stacking pattern like that found in related triflate salts of *N*-methylpyridinium-DTDA derivatives.[43]

Crystal Structures of Ethyl Derivatives $\mathbf{1}^{Et}$·MeCN, $\mathbf{1}^{Et}$·EtCN, and $\mathbf{2}^{Et}$·MeCN. Compounds $\mathbf{1}^{Et}$·**MeCN**, $\mathbf{1}^{Et}$·**EtCN**, and $\mathbf{2}^{Et}$·**MeCN** crystallize in a triclinic unit cell (space group $P\bar{1}$) and are isostructural with the previously reported methyl derivative $\mathbf{1}^{Me}$·**MeCN**. Their asymmetric unit comprises one DTDA/DSDA cation, one TCNQ anion, and one solvent molecule. The DTDA/DSDA radicals are dimerized in *trans*-cofacial manner, while the TCNQ radicals form eclipsed-cofacial dimers. Together the cations and anions generate repeating $A^+-A^+\cdots B^--B^-$ stacking motifs (Figure 2). The

https://doi.org/10.1021/acs.cgd.2c00795
Cryst. Growth Des. 2022, 22, 7110−7122

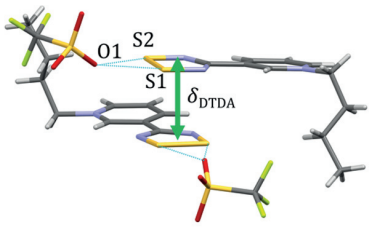

IV (E = S; R = Bu):
δ_{DTDA} = 3.05
S1 ··· O1 = 2.75(1)
S2 ··· O1 = 2.890(8)

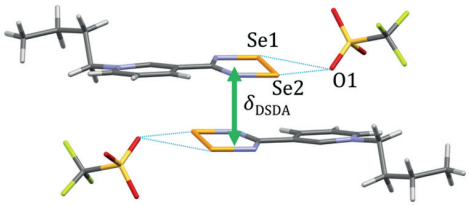

IV (E = Se; R = Bu):
δ_{DSDA} = 3.17
Se1 ··· O1 = 3.014(6)
Se2 ··· O1 = 2.867(7)

Figure 1. Representative view of packing and most important intermolecular interactions in *N*-butyl derivatives of **IV** along with key distances (Å). Minor components of disordered *N*-butyl chains in **IV** (E = S, R = Bu) have been omitted for clarity.

interplanar separation δ_{DTDA} is nearly identical in **1^{Et}·MeCN** and **1^{Et}·EtCN**, 3.15 and 3.16 Å, respectively, and falls within the typical range for *trans*-cofacial DTDA dimers (3.06−3.30 Å) determined from structural data deposited for all DTDA/DSDA radical (or radical cation) derivatives in the Cambridge Structural Database (CSD).[47] The corresponding δ_{DSDA} distance in **2^{Et}·MeCN** is 3.17 Å and, prior to this work, only one structurally characterized example of a DSDA dimer in *trans*-cofacial arrangement had been reported.[48] The centroid-to-centroid distance between two TCNQ radicals, δ_{TCNQ}, is slightly below 3.3 Å in **1^{Et}·MeCN**, **1^{Et}·EtCN**, and **2^{Et}·MeCN**, as is typical for eclipsed-cofacial TCNQ dimers with minor transversal offset (Table S3, Supporting Information). The DTDA/DSDA and pyridinium rings are nearly coplanar (ϕ = 0.9−6.9; Table S3, Supporting Information) in all **1^{Et}·MeCN**, **1^{Et}·EtCN**, and **2^{Et}·MeCN**, which is entirely expected based on existing structural data. Calculations for the phenyl-substituted DTDA radical have shown that ϕ = 0 represents a minimum on the potential energy surface and that even minor perturbations can lead to significant twist angles between the pyridinium and DTDA/DSDA rings.[49] The solvent molecules form supramolecular CN···S/Se interactions with DTDA/DSDA that altogether span a narrow range of 2.888(2)−2.999(2) Å and are significantly shorter than the sum of van der Waals radii for nitrogen and sulfur/selenium atoms (*ca.* 3.35/3.45 Å, respectively). A network of weak C−H···N hydrogen bonds further connects the solvent molecules and DTDA/DSDA cations to TCNQ anions.

Crystal Structures of Propyl Derivatives 1^{Pr}·MeCN, 2^{Pr}·MeCN, and 1^{Pr}. Compounds **1^{Pr}·MeCN** and **2^{Pr}·MeCN** are isostructural with the ethyl derivatives (triclinic unit cell, space group $P\bar{1}$) and contain *trans*-cofacial DTDA/DSDA dimers and eclipsed-cofacial TCNQ dimers forming $A^+-A^+\cdots B^--B^-$ stacking motifs (Figure 2). The key metrical parameters in **1^{Pr}·MeCN** and **2^{Pr}·MeCN**, such as the centroid-to-centroid distances $\delta_{DTDA/DSDA}$ (3.14 and 3.18 Å, respectively) and δ_{TCNQ} (3.25 and 3.27 Å, respectively) as well as CN···S/Se interactions between solvent molecules and DTDA/DSDA cations (2.897(2)−3.007(4) Å), are all similar to those in **1^{Et}·MeCN**, **1^{Et}·EtCN**, and **2^{Et}·MeCN**.

When the double-displacement reaction between **IV** (E = S; R = Pr) and [K(18c6)][TCNQ] was performed in EtCN, **1^{Pr}** could be crystallized without any solvent molecules in the crystal lattice (Table 1). The crystal structure of **1^{Pr}** (triclinic unit cell, space group $P\bar{1}$) shows DTDA radical cations dimerized in *trans*-cofacial manner (Figure 3). In comparison to the solvate **1^{Pr}·MeCN**, the DTDA and pyridinium rings in **1^{Pr}** are not coplanar and the DTDA rings have slipped further on top of each other, though the δ_{DTDA} distance remains essentially unchanged at 3.11 Å (Table S4, Supporting Information). As in **1^{Pr}·MeCN**, the TCNQ anions form cofacial dimers in **1^{Pr}**, but they adopt a noneclipsed geometry with 2.1 Å longitudinal offset (Table S4, Supporting Information), leading to a significantly increased δ_{TCNQ} distance, 3.73 Å, compared to **1^{Pr}·MeCN**. Overall, the DTDA cations form head-over-tail π-stacks $A^+-A^+\cdots A^+-A^+$ and TCNQ dimers form staircase-like $B^-\!-\!B^-\cdots B^-\!-\!B^-$ packing motifs in **1^{Pr}** that are connected by supramolecular CN···S

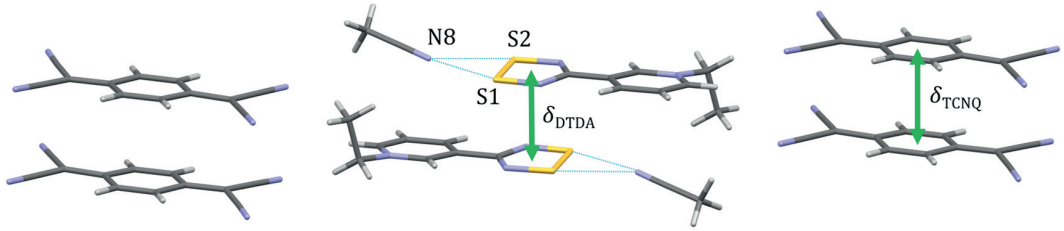

1^{Et}·MeCN:	**1^{Et}·EtCN:**	**2^{Et}·MeCN:**	**1^{Pr}·MeCN:**	**2^{Pr}·MeCN:**
δ_{DTDA} = 3.15	δ_{DTDA} = 3.16	δ_{DSDA} = 3.17	δ_{DTDA} = 3.14	δ_{DSDA} = 3.18
δ_{TCNQ} = 3.26	δ_{TCNQ} = 3.27	δ_{TCNQ} = 3.27	δ_{TCNQ} = 3.25	δ_{TCNQ} = 3.27
S1 ··· N8 = 2.924(2)	S1 ··· N8 = 2.888(2)	Se1 ··· N8 = 2.963(3)	S1 ··· N8 = 2.963(2)	Se1 ··· N8 = 3.007(4)
S2 ··· N8 = 2.914(2)	S2 ··· N8 = 2.906(2)	Se2 ··· N8 = 2.999(2)	S2 ··· N8 = 2.897(2)	Se2 ··· N8 = 2.963(3)

Figure 2. Representative view of packing and most important intermolecular interactions in **1^{Et}·MeCN** and key distances (Å) in the isostructural series **1^{Et}·MeCN**, **1^{Et}·EtCN**, **2^{Et}·MeCN**, **1^{Pr}·MeCN**, and **2^{Pr}·MeCN**.

https://doi.org/10.1021/acs.cgd.2c00795
Cryst. Growth Des. 2022, 22, 7110−7122

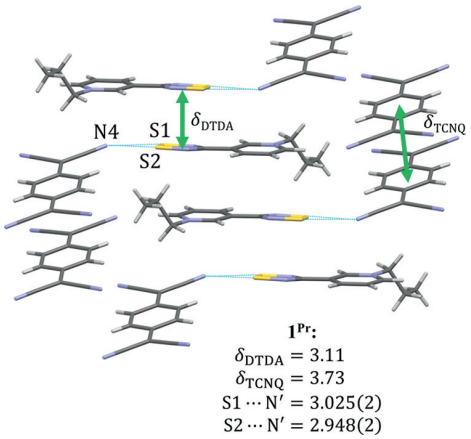

Figure 3. Representative view of packing and most important intermolecular interactions in 1^{Pr} along with key distances (Å).

interactions (2.948(2) and 3.025(2) Å) as well as weak C−H···N hydrogen bonds. The *N*-propyl substituents adopt an *anti-gauche* conformation in 1^{Pr} as opposed to the *anti-anti* conformation found in the solvate 1^{Pr}**·MeCN**.

The structure of 1^{Pr} can also be compared to that of 1^{Me} at low temperatures. Even though the solvates 1^{Me}**·MeCN** and 1^{Pr}**·MeCN** are isostructural, the position adopted by the longer *N*-alkyl chain in the structure of 1^{Pr} and the associated steric effects prevent the formation of C−C-bonded σ-dimers of TCNQ radicals similar to that happens upon desolvation of 1^{Me}**·MeCN** to 1^{Me}. Hence, 1^{Pr} is not expected to show bistability upon increasing the temperature (*vide infra*).

Crystal Structures of Butyl Derivatives 1^{Bu}·0.5MeCN, 1^{Bu}, and 2^{Bu}. The crystal structure of 1^{Bu}**·0.5MeCN** (triclinic unit cell, space group $P\bar{1}$) has two DTDA cations, two TCNQ anions, and only one solvent molecule in the asymmetric unit. The DTDA radicals are arranged in a typical manner to *cis*-cofacial dimers that together form $A^+-A^+\cdots A^+-A^+$ stacks with alternating orientation of the dimeric subunits (Figure 4). The intradimer S···S distances are almost identical, 2.984(7) and

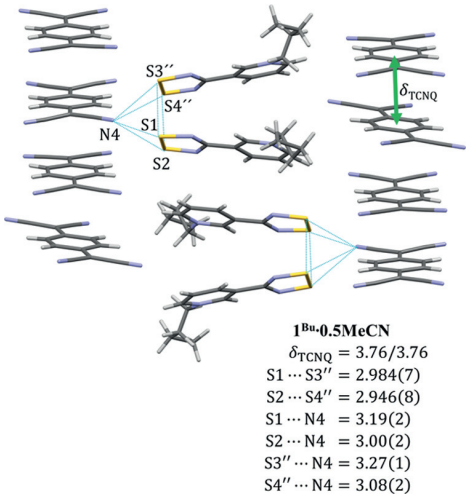

Figure 4. Representative view of packing and most important intermolecular interactions in 1^{Bu}**·0.5MeCN** along with key distances (Å). Solvent molecules and disordered *N*-butyl chains have been omitted for clarity.

2.946(8) Å, and within the typical range for *cis*-cofacial DTDA dimers (2.90−3.20 Å) determined from structural data deposited in the CSD.[47] The DTDA dimers in 1^{Bu}**·0.5MeCN** are significantly wedged with a tilt angle of 12.2° that arises from the steric demand of the butyl substituents in a lateral *anti*-gauche-*anti* conformation like that found in **IV** (E = Se; R = Bu). The wedged arrangement is not uncommon for DTDA radicals but typically observed in the case of halogenated substituents, such as trifluoromethyl- and fluoro- and chlorophenyls.[50,51] The TCNQ anions form evenly spaced staircase-like $B^-\cdots B^-\cdots B^-$ stacks with two virtually identical δ_{TCNQ} distances, 3.756 and 3.76 Å, and a noneclipsed geometry with 2.0 Å longitudinal offset and negligible transversal offset (Table S4, Supporting Information). However, the neighboring TCNQ radicals are not perfectly aligned but are rotated with respect to each other along the π-stacking direction, with the largest rotational angle observed for every fourth anion (Figure S1, Supporting Information). This creates a rare 1D stacking motif with a periodic distortion of every fourth TCNQ radical anion that results in stacking faults similar to those previously encountered in crown complexes of alkali metal salts of TCNQ.[52] The DTDA and TCNQ stacks are connected by supramolecular CN···S interactions (3.00(2)−3.27(1) Å) as well as weak C−H···N hydrogen bonds. The solvent molecules are embedded in the space between neighboring stacks.

Interestingly, the double-displacement reaction between **IV** (E = Se; R = Bu) and [K(18c6)][TCNQ] in MeCN gave the nonsolvated derivative 2^{Bu}. The corresponding sulfur derivative 1^{Bu} could also be synthesized in bulk by performing the analogous double-displacement reaction in EtCN; trace amounts of this product were also formed in MeCN and could be separated from 1^{Bu}**·0.5MeCN** based on crystal morphology and characterized by X-ray crystallography.

Compounds 1^{Bu} and 2^{Bu} are isostructural with one DTDA/DSDA cation and one TCNQ anion in the asymmetric unit (triclinic unit cell, space group $P\bar{1}$). The DTDA/DSDA cations are in a rare *trans*-antarafacial arrangement (*trans*-cofacial in 1^{Pr}) and form head-over-tail $A^+-A^+\cdots A^+-A^+$ π-stacking motifs (Figure 5). The intradimer S···S distance in 1^{Bu} is 3.172(2) Å and falls to the lower end of the typical range for *trans*-antarafacial DTDA dimers (3.13−3.44 Å) determined from structural data deposited in the CSD. The corresponding Se···Se distance in 2^{Bu} is 3.241(1) Å and is comparable to the data reported for the two other structurally characterized examples of such an arrangement of DSDA radicals (3.215(2)−3.334(2) Å).[48,53] However, this comparison is not entirely warranted because the radicals are charge neutral in all published examples and coordinated to two metal centers in one of the two cases. The twist angle between DTDA/DSDA and pyridinium rings is 22.6 and 23.5° in 1^{Bu} and 2^{Bu}, respectively, and thereby significantly greater than in any of the other structures reported. This is presumably due to the weak C−H···N hydrogen-bond network that assembles the TCNQ and pyridinium rings into an almost coplanar arrangement, while simultaneously allowing the DTDA/DSDA cations and TCNQ anions to connect by supramolecular CN···S (2.869(3)Å and 2.962(3) Å) and CN···Se (2.937(5) and 3.017(6) Å) interactions. Like the case of 1^{Pr}, the TCNQ dimers adopt a noneclipsed geometry with *ca.* 2.2 Å longitudinal offset and negligible transversal offset (Table S4, Supporting Information). The dimers form staircase-like $B^-\!-\!B^-\cdots B^-\!-\!B^-$ stacks with two vastly differing δ_{TCNQ} distances, 3.70 and 5.18 Å in

https://doi.org/10.1021/acs.cgd.2c00795
Cryst. Growth Des. 2022, 22, 7110−7122

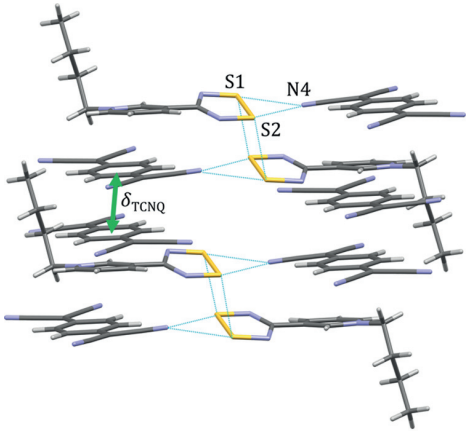

1^{Bu}:	2^{Bu}:
δ_{TCNQ} = 3.70	δ_{TCNQ} = 3.72
S···S = 3.172(2)	Se···Se = 3.241(1)
S1···N4 = 2.962(3)	Se1···N4 = 3.017(6)
S2···N4 = 2.869(3)	Se2···N4 = 2.937(5)

Figure 5. Representative view of packing and most important intermolecular interactions in 1^{Bu} and key distances in isostructural compounds 1^{Bu} and 2^{Bu} (Å).

1^{Bu} and 3.72 and 5.19 Å in 2^{Bu}. The *N*-butyl substituents adopt an *anti-anti-anti* conformation in 1^{Bu} and 2^{Bu}, as opposed to the *anti*-gauche-*anti* conformation found in the solvate **1^{Bu}·0.5MeCN**, preventing the formation of C−C-bonded σ-dimers of TCNQ.

Thermal Behavior of Crystalline Solvates of 1 and 2. The crystallographic data discussed above clearly show the effect of the crystallization solvent and the *N*-alkyl chain length on the dimerization mode of DTDA/DSDA (*cis*-cofacial, *trans*-cofacial, or *trans*-antarafacial) and TCNQ radicals (eclipsed-cofacial or non-eclipsed-cofacial). Interestingly, none of the three nonsolvated structures 1^{Pr}, 1^{Bu}, and 2^{Bu} revealed a σ-dimer of TCNQ akin to the low-temperature (LT) phase of 1^{Me}, indicating that the *N*-methyl substituent plays a role in facilitating the formation of a C−C bond between TCNQ radicals in 1^{Me}. However, it can also be argued that solvent molecules in the crystal lattice of **1^{Me}·MeCN** and **1^{Me}·EtCN** are essential for obtaining the right initial arrangement of cations and anions that then reorganizes upon desolvation to yield the σ-bonded dimer in 1^{Me}. To investigate this further, and to reveal other interesting physical properties for this series of radical-ion salts, the thermal behavior of the solvates **1^{Et}·MeCN**, **1^{Pr}·MeCN**, **1^{Bu}·0.5MeCN**, **1^{Et}·EtCN**, **2^{Et}·MeCN**, and **2^{Pr}·MeCN** was investigated by thermogravimetric analysis (TGA).

The recorded TGA curves allowed the establishment of onset temperatures for the loss of lattice solvent and the %-weight losses calculated from the data were consistent with the stoichiometries established by single-crystal X-ray crystallography (Table S5 and Figures S2−S10, Supporting Information). The variable behavior of the investigated solvates in the release of the solvent, before the onset of decomposition at temperatures >450 K, reflects the varying strength of interactions between solvent molecules and radical ions in the crystal structures of **1^{Et}·MeCN**, **1^{Et}·EtCN**, **1^{Pr}·MeCN**, **1^{Bu}·0.5MeCN**, **2^{Et}·MeCN**, and **2^{Pr}·MeCN** (*vide supra*).

The thermal behavior of the solvates **1^{Et}·MeCN** and **1^{Et}·EtCN** observed in their TGA curves indicated that the solvent is gradually removed from these structures with onset temperatures of 387 and 396 K, respectively. There is only a narrow plateau between the occurrence of desolvation and thermal decomposition at 472 and 452 K for **1^{Et}·MeCN** and **1^{Et}·EtCN**, respectively (Table S5, Figures S2 and S3, Supporting Information). For this reason, we did not attempt a single-crystal-to-single-crystal (SCSC) transformation in these two cases even though the structures contain the shortest *N*-alkyl substituents with the least influence on the packing of TCNQ radicals. The selenium analogue **2^{Et}·MeCN** undergoes a more facile desolvation with an onset temperature of 385 K and decomposition at 452 K. This system was not investigated any further, however, because its *trans*-cofacial DSDA and eclipsed-cofacial TCNQ dimers are strongly

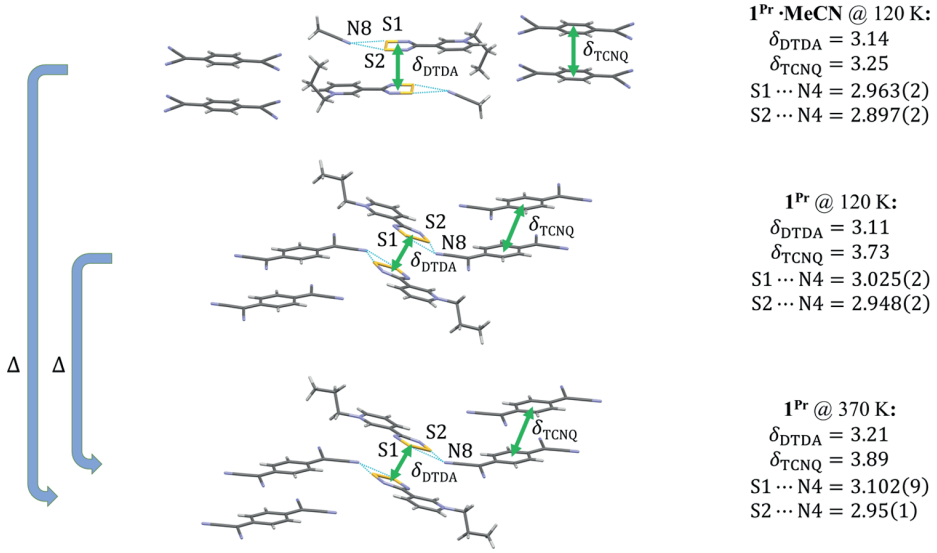

1^{Pr}·MeCN @ 120 K:
δ_{DTDA} = 3.14
δ_{TCNQ} = 3.25
S1···N4 = 2.963(2)
S2···N4 = 2.897(2)

1^{Pr} @ 120 K:
δ_{DTDA} = 3.11
δ_{TCNQ} = 3.73
S1···N4 = 3.025(2)
S2···N4 = 2.948(2)

1^{Pr} @ 370 K:
δ_{DTDA} = 3.21
δ_{TCNQ} = 3.89
S1···N4 = 3.102(9)
S2···N4 = 2.95(1)

Figure 6. Illustration of changes to the solid-state structure of **1^{Pr}·MeCN** upon desolvation to 1^{Pr} and temperature change from 120 to 370 K along with key distances (Å).

https://doi.org/10.1021/acs.cgd.2c00795
Cryst. Growth Des. 2022, 22, 7110−7122

antiferromagnetically coupled, preventing significant changes to both structure and properties upon desolvation.

The two isostructural analogues $\mathbf{1}^{\mathbf{Pr}}$**·MeCN** and $\mathbf{2}^{\mathbf{Pr}}$**·MeCN** displayed a similar behavior in TGA with facile loss of lattice solvent at 354 and 358 K, respectively, and high thermal stability up to >450 K. The robust thermal behavior observed for the salts suggested that an SCSC transformation might be realized in these cases and was attempted for $\mathbf{1}^{\mathbf{Pr}}$**·MeCN**. Again, given the strongly antiferromagnetically coupled *trans*-cofacial DSDA and eclipsed-cofacial TCNQ dimers in $\mathbf{2}^{\mathbf{Pr}}$**·MeCN**, we did not pursue investigations on this system any further.

Careful heating of single crystals of $\mathbf{1}^{\mathbf{Pr}}$**·MeCN** on the goniometer head up to 370 K led to the acquisition of a high-temperature (HT) structure by single-crystal X-ray diffraction that revealed an SCSC transformation to the nonsolvated $\mathbf{1}^{\mathbf{Pr}}$ structure with a triclinic unit cell (space group $P\bar{1}$). The HT crystal structure of $\mathbf{1}^{\mathbf{Pr}}$ is comparable to the LT data discussed above (Table S6, Supporting Information) and shows *trans*-cofacial DTDA dimers and non-eclipsed-cofacial TCNQ dimers with 2.1 Å longitudinal offset and negligible transversal offset (Figure 6). As expected, both δ_{DTDA} and δ_{TCNQ} distances have significantly increased in the HT structure, while the CN···S interactions between cations and anions are much less affected by the change in temperature from 120 to 370 K. The nature of the SCSC transformation observed for $\mathbf{1}^{\mathbf{Pr}}$**·MeCN** effectively confirms that desolvation alone is not sufficient to yield a σ-bonded TCNQ dimer, but the size of the *N*-alkyl substituent plays a key role in the process.

The thermally induced desolvation of $\mathbf{1}^{\mathbf{Pr}}$**·MeCN**, its phase purity, and the associated SCSC transformation to $\mathbf{1}^{\mathbf{Pr}}$ were confirmed in the bulk by variable-temperature powder X-ray diffraction experiments (Tables S7 and S8 and Figures S11–S13, Supporting Information). Subsequent Pawley refinement of the unit cell parameters for each of the powder samples was found to be structurally like the corresponding single-crystal structures. Traces of $\mathbf{1}^{\mathbf{Pr}}$ appear in the bulk of $\mathbf{1}^{\mathbf{Pr}}$**·MeCN** before heating, suggesting that the difference in crystal lattice enthalpy between the solvated and nonsolvated structures is very small. Variable-temperature powder X-ray experiments indicate that the loss of lattice solvent occurs readily above 377 K, with only residual traces of $\mathbf{1}^{\mathbf{Pr}}$**·MeCN** visible in the diffractograms. These results are consistent with the data from TGA (Table S5 and Figure S4, Supporting Information).

In the case of $\mathbf{1}^{\mathbf{Bu}}$**·0.5MeCN**, the solvent molecules in the crystal lattice do not interact strongly with the DTDA radical cation, that is, there are no CN···S interactions in the structure. Instead, the solvent seems to play the role of a space filler in $\mathbf{1}^{\mathbf{Bu}}$**·0.5MeCN**, as indicated by the comparatively low onset temperature for solvent loss at 361 K with decomposition taking place at 457 K (Table S5 and Figure S5, Supporting Information). Unfortunately, the poor quality of single crystals of $\mathbf{1}^{\mathbf{Bu}}$**·0.5MeCN** prevented further investigation of any possible SCSC transformation, but powder X-ray diffraction experiments showed the bulk material to be consistent with the single-crystal structure (Table S7 and Figure S14, Supporting Information).

Both the nonsolvated structures $\mathbf{1}^{\mathbf{Bu}}$ and $\mathbf{2}^{\mathbf{Bu}}$ contain rare *trans*-antarafacial DTDA/DSDA dimers, and Pawley refinement of the unit cell parameters for each of the powder samples was found to be consistent with the corresponding single-crystal structures (Table S8, Figures S15 and S16, Supporting Information). In the case of $\mathbf{1}^{\mathbf{Bu}}$, the nonsolvated material could be obtained from EtCN as sizable single crystals, and an HT single-crystal structure was determined for it at 370 K (Table S6 and Figure S17, Supporting Information). Upon heating, the S···S distance was found to increase significantly from 3.172(2) to 3.312(1) Å, but the value is still within the typical range for DTDA dimers (3.13–3.44 Å). The staircase-like π-stacking of TCNQ dimers along the *a*-axis is maintained in the HT structure of $\mathbf{1}^{\mathbf{Bu}}$, but the δ_{TCNQ} distance has increased from 3.70 to 3.78 Å with very minor changes seen in longitudinal and transversal offsets (Table S4, Supporting Information).

Magnetic Measurements and Computational Investigations. Based on our previous experience with $\mathbf{1}^{\mathbf{Me}}$**·MeCN** and $\mathbf{1}^{\mathbf{Me}}$**·EtCN** that exhibit thermal hysteresis near room temperature due to lattice solvent loss and subsequent first-order phase transition between a paramagnetic HT and a diamagnetic LT phase, the bulk magnetic properties of the solvates $\mathbf{1}^{\mathbf{Et}}$**·MeCN**, $\mathbf{1}^{\mathbf{Et}}$**·EtCN**, $\mathbf{1}^{\mathbf{Pr}}$**·MeCN**, and $\mathbf{1}^{\mathbf{Bu}}$**·0.5MeCN**, and the nonsolvates $\mathbf{1}^{\mathbf{Bu}}$ and $\mathbf{2}^{\mathbf{Bu}}$ were explored. Variable-temperature magnetic susceptibility data using a static field of 1.0 T were collected between 1.85 and 400 K, with different thermal cycling to probe the *in situ* desolvation of the different solvated materials.

All samples are essentially diamagnetic below 300 K, as expected for π-dimers of DTDA and TCNQ radicals with only a very low concentration of spin-defect impurities (Figure 7).

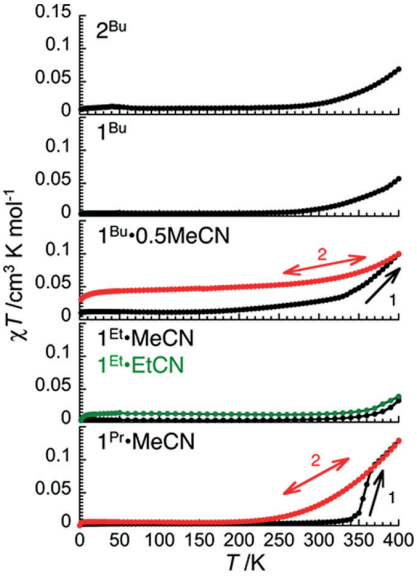

Figure 7. Temperature dependence of the χT product for $\mathbf{1}^{\mathbf{Pr}}$**·MeCN**, $\mathbf{1}^{\mathbf{Et}}$**·MeCN**, $\mathbf{1}^{\mathbf{Et}}$**·EtCN**, $\mathbf{1}^{\mathbf{Bu}}$**·0.5MeCN**, $\mathbf{1}^{\mathbf{Bu}}$, and $\mathbf{2}^{\mathbf{Bu}}$ at 1 T (χ, the *dc* magnetic susceptibility, is defined as M/H per mole of complex).

The solvates $\mathbf{1}^{\mathbf{Et}}$**·MeCN** and $\mathbf{1}^{\mathbf{Et}}$**·EtCN** remained diamagnetic up to 350 K. Above this temperature, only a small increase of the χT product is observed (Figure 7) that is consistent with gradual loss of lattice solvent observed in TGA above 385 K. The magnetic properties upon subsequent cooling from 400 K remain quantitatively unchanged, indicating that solvated and desolvated $\mathbf{1}^{\mathbf{Et}}$ materials possess roughly the same magnetic properties.

In the solvates $\mathbf{1}^{\mathbf{Pr}}$**·MeCN** and $\mathbf{1}^{\mathbf{Bu}}$**·0.5MeCN**, the loss of lattice solvent was evidenced by a steady increase in χT during the first heating cycle with onset temperatures consistent with

https://doi.org/10.1021/acs.cgd.2c00795
Cryst. Growth Des. 2022, 22, 7110–7122

data from TGA (Figures 7, S4 and S5, Supporting Information). A subsequent cooling and heating cycle did not follow the same track of the initial heating. In the case of $\mathbf{1}^{\mathbf{Bu}}$**·0.5MeCN**, the loss of lattice solvent led to a small concentration of spin-defect impurities (∼10%) that presumably arise from isolated TCNQ radicals within the 1D π-stacks or defect sites generated during desolvation. In the nonsolvated material $\mathbf{1}^{\mathbf{Bu}}$, a modest thermal population of the excited magnetic states was observed above 300 K. For $\mathbf{1}^{\mathbf{Pr}}$**·MeCN**, the maximum value of the χT product, *ca.* 0.15 $cm^3K\ mol^{-1}$, was recorded at the highest possible temperature of the experiment (400 K, Figure 7). The value is much lower than expected for an ideal $S = 1/2$ system, 0.375 $cm^3K\ mol^{-1}$. The resulting plot of χT *vs* T plot for $\mathbf{1}^{\mathbf{Pr}}$**·MeCN** after loss of lattice solvent is consistent with thermally populated magnetic states above 250 K that, based on the structural data, arise from the weakly interacting noneclipsed TCNQ dimers in $\mathbf{1}^{\mathbf{Pr}}$. This was probed with DFT using the PBE1PBE and LC-ωhPBE (values reported in parentheses) functionals together with the def2-TZVP basis sets. The calculations revealed a singlet−triplet (S−T) gap of 5 (3) kJ mol^{-1} for the TCNQ dimer in the geometry that it adopts in the HT structure of $\mathbf{1}^{\mathbf{Pr}}$ compared to the S−T gap of 22 (13) kJ mol^{-1} calculated for the DTDA dimer in a similar manner. Corresponding S−T gaps calculated from the LT structure are 12 (8) and 31 (19) kJ mol^{-1} for TCNQ and DTDA, respectively. These values agree with the structural data, that is, the TCNQ radicals are well separated at both temperatures and have small S−T gaps, while the energy gaps calculated for the DTDA radicals are in both cases higher due to δ_{DTDA} being much smaller than δ_{TCNQ} in both structures.

The crystal structures of the isostructural nonsolvates $\mathbf{1}^{\mathbf{Bu}}$ and $\mathbf{2}^{\mathbf{Bu}}$ both showed DTDA/DSDA radicals with a rare *trans*-antarafacial dimerization mode along with non-eclipsed-cofacial TCNQ dimers. The variable-temperature magnetic behavior of $\mathbf{1}^{\mathbf{Bu}}$ and $\mathbf{2}^{\mathbf{Bu}}$ was found to be nearly identical (Figure 7) with thermally populated magnetic states increasing steadily above *ca.* 300 K. The magnetic behavior was found to follow the same track during repeated heating and cooling cycles, as expected based on the available structural data. This magnetic behavior is tentatively attributed to the small S−T gap afforded by the non-eclipsed-cofacial TCNQ dimer geometry at higher temperatures. S−T gaps calculated for TCNQ and DTDA dimers in the geometries they adopt in the HT structure of $\mathbf{1}^{\mathbf{Bu}}$ are 11 (8) and 23 (14) kJ mol^{-1}, respectively. Corresponding values calculated from the LT structure are 19 (13) and 36 (21) kJ mol^{-1} for TCNQ and DTDA, respectively. The calculated values are in accordance with the structural data and show the S−T gaps to be smaller for TCNQ dimers at both temperatures.

CONCLUSIONS

In this work, we have provided a detailed account of the preparation, structural, thermal, and magnetic characterization of a series of simple binary organic radical salts obtained by partnering the ubiquitous 7,7,8,8-tetracyanoquinodimethane radical anion ($TCNQ^{-\cdot}$) with 4-(*N*-alkylpyridinium-3-yl)-1,2,3,5-dithiadiazolyl radical cations ($DTDA^{+\cdot}$) and their selenium analogues ($DSDA^{+\cdot}$).

When using shorter-alkyl-chain substituents ethyl and propyl, the binary salts crystallized as isostructural acetonitrile solvates $\mathbf{1}^{\mathbf{Et}}$**·MeCN**, $\mathbf{1}^{\mathbf{Pr}}$**·MeCN**, $\mathbf{2}^{\mathbf{Et}}$**·MeCN**, and $\mathbf{2}^{\mathbf{Pr}}$**·MeCN**. In these structures, the DTDA and DSDA radicals are dimerized in *trans*-cofacial manner and form supramolecular CN···S/Se interactions with the solvent, whereas the TCNQ radicals form eclipsed-cofacial dimers. A slight increase in the alkyl chain length to butyl, however, led to a distinctly different solvate structure $\mathbf{1}^{\mathbf{Bu}}$**·0.5MeCN** in which the DTDA radicals form *cis*-cofacial dimers with the solvent molecules settled in the space between butyl substituents while the TCNQ radicals are arranged to a rare 1D columnar stacking motif containing periodic distortions along the vertical stacking direction. Changing the solvent from MeCN to EtCN or replacing sulfur for selenium both favored the isolation of nonsolvated structures in the case of $\mathbf{1}^{\mathbf{Pr}}$, $\mathbf{1}^{\mathbf{Bu}}$, and $\mathbf{2}^{\mathbf{Bu}}$; the solvate $\mathbf{1}^{\mathbf{Et}}$**·EtCN** was also obtained. In the nonsolvated structures, the DTDA and DSDA dimers are either in *trans*-cofacial ($\mathbf{1}^{\mathbf{Pr}}$) or *trans*-antarafacial ($\mathbf{1}^{\mathbf{Bu}}$ and $\mathbf{2}^{\mathbf{Bu}}$) arrangement, while the TCNQ radicals adopt noneclipsed dimer geometry with substantial longitudinal offset.

The results from this work confirmed our expectation that the steric repulsion and pliability of longer-alkyl-chain substituents on the cation favor the formation of nonsolvated crystal structures. This was found to be particularly true for crystallizations from EtCN that led exclusively to nonsolvates in the case of $\mathbf{1}^{\mathbf{Pr}}$ and $\mathbf{1}^{\mathbf{Bu}}$; analogous selenium derivatives could not be crystallized from this solvent due to the low solubility of precursor salts **IV** (E = Se, R = Et, Pr, Bu). In all crystal structures containing one solvent molecule per ion, the solvents work as structure-driving agents and arrange the DTDA and DSDA cations to *trans*-cofacial dimers held in place by supramolecular CN···S/Se interactions. Partially solvated and nonsolvated crystal structures show significantly more variation in the arrangement of the ions in the solid state, and there exists no clear structure-driving factor in these cases. Unfortunately, none of the crystal structures obtained in this work revealed the formation of σ-dimers of TCNQ radicals even though $\mathbf{1}^{\mathbf{Pr}}$**·MeCN** was found to be isostructural with $\mathbf{1}^{\mathbf{Me}}$**·MeCN** and could be thermally desolvated to $\mathbf{1}^{\mathbf{Pr}}$. Clearly, the *N*-alkyl group in $\mathbf{1}^{\mathbf{Pr}}$ compared to $\mathbf{1}^{\mathbf{Me}}$ is sufficiently bulky to direct the TCNQ radicals to form their most favorable arrangement, non-eclipsed-cofacial dimers, not only in $\mathbf{1}^{\mathbf{Pr}}$ but also in all nonsolvated crystal structures reported in this work.

All nonsolvated salts displayed varied but robust thermal behavior, while the thermal behavior of the solvates revealed a clear trend for the loss of lattice solvent becoming more facile for systems with longer alkyl chains. The thermally induced desolvation of $\mathbf{1}^{\mathbf{Pr}}$**·MeCN**, its phase purity, and the associated SCSC transformation to $\mathbf{1}^{\mathbf{Pr}}$ were confirmed in the bulk by variable-temperature powder X-ray diffraction experiments. Variable-temperature magnetic susceptibility measurements showed that all investigated structures are diamagnetic at low temperatures. However, thermally populated paramagnetic states could be observed in all investigated cases above 250 K and, in particular, for the nonsolvated systems $\mathbf{1}^{\mathbf{Pr}}$, $\mathbf{1}^{\mathbf{Bu}}$, and $\mathbf{2}^{\mathbf{Bu}}$. This behavior was tentatively assigned to the noneclipsed geometry of TCNQ radical dimers in these structures that leads to a longer separation between the radical ions at higher temperatures and, consequently, to small singlet−triplet gaps. This interpretation was supported by results from DFT calculations.

Considered as a whole, the systematic investigation of structural and solvent effects on the crystal structure, thermal, and magnetic properties of the simple binary salts **1** and **2** and their solvates has provided structural insight that can be applied to related systems in the design of new functional

https://doi.org/10.1021/acs.cgd.2c00795
Cryst. Growth Des. 2022, 22, 7110−7122

molecular materials. In this context, the selenium analogue of 1^{Me}·MeCN, namely, 2^{Me}·MeCN, appears as an interesting target system. Based on the results reported herein, the S-to-Se atom replacement is not expected to lead to desolvation and the crystal structure of 2^{Me}·MeCN is predicted to be isostructural with 1^{Me}·MeCN. Consequently, 2^{Me} might be a suitable platform to observe σ-dimers of TCNQ radicals in the solid state, possibly leading to bistability like that established in the case of 1^{Me}·MeCN. Synthetic work toward this and related systems are currently underway.

■ ASSOCIATED CONTENT

Supporting Information

The Supporting Information is available free of charge at https://pubs.acs.org/doi/10.1021/acs.cgd.2c00795.

Full experimental details for all compounds and computational details, including NMR and IR spectral data, TG curves, PXRD patterns, and variable-temperature single-crystal diffraction data (PDF)

Accession Codes

CCDC 2181974, 2181976−2181977, 2181980−2181989, 2182178, 2182311, 2182459, 2182640, 2182780, and 2207551 contain the supplementary crystallographic data for this paper. These data can be obtained free of charge via www.ccdc.cam.ac.uk/data_request/cif, or by emailing data_request@ccdc.cam.ac.uk, or by contacting The Cambridge Crystallographic Data Centre, 12 Union Road, Cambridge CB2 1EZ, UK; fax: +44 1223 336033.

■ AUTHOR INFORMATION

Corresponding Authors

Aaron Mailman − *Department of Chemistry, NanoScience Centre, University of Jyväskylä, FI-40014 Jyväskylä, Finland;* orcid.org/0000-0003-2067-8479; Email: aaron.m.mailman@jyu.fi

Heikki M. Tuononen − *Department of Chemistry, NanoScience Centre, University of Jyväskylä, FI-40014 Jyväskylä, Finland;* orcid.org/0000-0002-4820-979X; Email: heikki.m.tuononen@jyu.fi

Rodolphe Clérac − *Univ. Bordeaux, CNRS, Centre de Recherche Paul Pascal (CRPP), UMR 5031, 33600 Pessac, France;* orcid.org/0000-0001-5429-7418; Email: rodolphe.clerac@u-bordeaux.fr

Authors

Anni I. Taponen − *Department of Chemistry, NanoScience Centre, University of Jyväskylä, FI-40014 Jyväskylä, Finland*

Awatef Ayadi − *Department of Chemistry, NanoScience Centre, University of Jyväskylä, FI-40014 Jyväskylä, Finland*

Noora Svahn − *Department of Chemistry, NanoScience Centre, University of Jyväskylä, FI-40014 Jyväskylä, Finland*

Manu K. Lahtinen − *Department of Chemistry, NanoScience Centre, University of Jyväskylä, FI-40014 Jyväskylä, Finland;* orcid.org/0000-0001-5561-3259

Mathieu Rouzières − *Univ. Bordeaux, CNRS, Centre de Recherche Paul Pascal (CRPP), UMR 5031, 33600 Pessac, France;* orcid.org/0000-0003-3457-3133

Complete contact information is available at: https://pubs.acs.org/10.1021/acs.cgd.2c00795

Funding

This research was supported by the Academy of Finland under projects 333565, 336456, and 289172.

Notes

The authors declare no competing financial interest.

■ ACKNOWLEDGMENTS

The authors gratefully acknowledge Elina Hautakangas for assistance with elemental analysis, and A.M. and H.M.T. thank the Academy of Finland and the University of Jyväskylä, Department of Chemistry and NanoScience Centre for financial support. R.C. and M.R. received funding from the University of Bordeaux, the Region Nouvelle Aquitaine, Quantum Matter Bordeaux, and the Centre National de la Recherche Scientifique (CNRS).

■ REFERENCES

(1) Ferraris, J.; Cowan, D. O.; Walatka, V.; Perlstein, J. H. Electron Transfer in a New Highly Conducting Donor-Acceptor Complex. *J. Am. Chem. Soc.* **1973**, *95*, 948−949.

(2) Alves, H.; Molinari, A. S.; Xie, H.; Morpurgo, A. F. Metallic Conduction at Organic Charge-Transfer Interfaces. *Nat. Mater.* **2008**, *7*, 574−580.

(3) Wu, L.; Wu, F.; Sun, Q.; Shi, J.; Xie, A.; Zhu, X.; Dong, W. A TTF−TCNQ Complex: An Organic Charge-Transfer System with Extraordinary Electromagnetic Response Behavior. *J. Mater. Chem. C* **2021**, *9*, 3316−3323.

(4) Tomkiewicz, Y.; Taranko, A. R.; Torrance, J. B. Roles of the Donor and Acceptor Chains in the Metal-Insulator Transition in TTF-TCNQ (Tetrathiafulvalene Tetracyanoquinodimethane). *Phys. Rev. Lett.* **1976**, *36*, 751−754.

(5) Melby, L. R. Substituted Quinodimethans: VIII. Salts Derived from the 7,7,8,8-Tetracyanoquinodimethan Anion-Radical and Benzologues of Quaternary Pyrazinium Cations. *Can. J. Chem.* **1965**, *43*, 1448−1453.

(6) Fritchie, C. J. The Crystal Structure of N-Methylphenazinium Tetracyanoquinodimethanide. *Acta Crystallogr.* **1966**, *20*, 892−898.

(7) Huang, J.; Kingsbury, S.; Kertesz, M. Crystal Packing of TCNQ Anion π -Radicals Governed by Intermolecular Covalent $\pi - \pi$ Bonding: DFT Calculations and Statistical Analysis of Crystal Structures. *Phys. Chem. Chem. Phys.* **2008**, *10*, 2625−2635.

(8) Gundel, D.; Sixl, H.; Metzger, R. M.; Heimer, N. E.; Harms, R. H.; Keller, H. J.; Nöthe, D.; Wehe, D. Crystal and Molecular Structure and EPR Triplet Spin Excitons of NBP TCNQ, the 1:1 Salt of 5-(1-butyl) Phenazinium (NBP) with 2,2′- (2,5-cyclohexadiene-1,4-diylidene)-bispropanedinitrile (TCNQ). *J. Chem. Phys.* **1983**, *79*, 3678−3688.

(9) Hoffmann, S. K.; Corvan, P. J.; Singh, P.; Sethulekshmi, C. N.; Metzger, R. M.; Hatfield, W. E. Crystal Structure and Excited Triplet-State Electron Paramagnetic Resonance of the σ-Bonded TCNQ Dimer in Bis(2,9-Dimethyl-1,10-Phenanthroline) Copper(I) Tetracyanoquinodimethane Dimer $[Cu(DMP)_2]_2[TCNQ]_2$. *J. Am. Chem. Soc.* **1983**, *105*, 4608−4617.

(10) Radhakrishnan, T. P.; Van Engen, D.; Soos, Z. G. Diamagnetic to Paramagnetic Transition in Trisdimethylaminocyclopropenium Tetracyanoquinodimethanide (TDAC-TCNQ). *Mol. Cryst. Liq. Cryst. Incorporating Nonlinear Opt.* **1987**, *150*, 473−492.

(11) Dong, V.; Endres, H.; Keller, H. J.; Moroni, W.; Nöthe, D. Dimerization of 7,7,8,8-Tetracyanoquinodimethane (TCNQ) Radical Anions via σ-Bond Formation: Crystal Structure and EPR Properties of Bis(Dipyridyl)Platinum(II)−TCNQ, $[Pt(2,2'\text{-Dipy})_2^{2+}(TCNQ)_2^{2-}]$. *Acta Crystallogr., Sect. B: Struct. Crystallogr. Cryst. Chem.* **1977**, *33*, 2428−2431.

(12) Černák, J.; Kuchár, J.; Hegedüs, M. Disorder of the Dimeric TCNQ−TCNQ Unit in the Crystal Structure of $[Ni(Bpy)_3]_2(TCNQ{-}TCNQ)(TCNQ)_2{\cdot}6H_2O$ (TCNQ is 7,7,8,8-Tetra-

cyanoquinodimethane). *Acta Crystallogr., Sect. E: Crystallogr. Commun.* **2017**, *73*, 8−12.
(13) Shimomura, S.; Horike, S.; Matsuda, R.; Kitagawa, S. Guest-Specific Function of a Flexible Undulating Channel in a 7,7,8,8-Tetracyano-*p*-Quinodimethane Dimer-Based Porous Coordination Polymer. *J. Am. Chem. Soc.* **2007**, *129*, 10990−10991.
(14) Shimomura, S.; Higuchi, M.; Matsuda, R.; Yoneda, K.; Hijikata, Y.; Kubota, Y.; Mita, Y.; Kim, J.; Takata, M.; Kitagawa, S. Selective Sorption of Oxygen and Nitric Oxide by an Electron-Donating Flexible Porous Coordination Polymer. *Nat. Chem.* **2010**, *2*, 633−637.
(15) Zhao, H.; Heintz, R. A.; Ouyang, X.; Dunbar, K. R.; Campana, C. F.; Rogers, R. D. Spectroscopic, Thermal, and Magnetic Properties of Metal/TCNQ Network Polymers with Extensive Supramolecular Interactions between Layers. *Chem. Mater.* **1999**, *11*, 736−746.
(16) Kim, J.; Silakov, A.; Yennawar, H. P.; Lear, B. J. Structural, Electronic, and Magnetic Characterization of a Dinuclear Zinc Complex Containing $TCNQ^{-}$ and a μ-$[TCNQ{-}TCNQ]^{2-}$ Ligand. *Inorg. Chem.* **2015**, *54*, 6072−6074.
(17) Černák, J.; Hegedüs, M.; Váhovská, L.; Kuchár, J.; Šoltésová, D.; Čižmár, E.; Feher, A.; Falvello, L. R. Syntheses, Crystal Structures and Magnetic Properties of Complexes Based on $[Ni(L\text{-}L)_3]^{2+}$ Complex Cations with Dimethylderivatives of 2,2′-Bipyridine and TCNQ. *Solid State Sci.* **2018**, *77*, 27−36.
(18) Mikami, S.; Sugiura, K.; Miller, J. S.; Sakata, Y. Two-Dimensional Honeycomb Network Formed by Porphyrinatomanganese(III) and μ_4-σ-Dimerized 7,7,8,8-Tetracyano-*p*-Quinodimethane Dianion. *Chem. Lett.* **1999**, *28*, 413−414.
(19) Zhao, H.; Heintz, R. A.; Dunbar, K. R.; Rogers, R. D. Unprecedented Two-Dimensional Polymers of Mn(II) with $TCNQ^{\cdot-}$ (TCNQ = 7,7,8,8-Tetracyanoquinodimethane). *J. Am. Chem. Soc.* **1996**, *118*, 12844−12845.
(20) Karadas, F.; Avendano, C.; Hilfiger, M. G.; Prosvirin, A. V.; Dunbar, K. R. Use of a Rhenium Cyanide Nanomagnet as a Building Block for New Clusters and Extended Networks. *Dalton Trans.* **2010**, *39*, 4968−4977.
(21) Morosin, B.; Plastas, H. J.; Coleman, L. B.; Stewart, J. M. The Crystal Structure of the Charge-Transfer Complex between N-Ethylphenazinium (EtP) and Dimerized 7,7,8,8-Tetracyanoquinodimethanide (TCNQ) Ions, $(C_{14}H_{13}N_2)_2{\cdot}C_{24}H_8N_8$. *Acta Crystallogr., Sect. B: Struct. Crystallogr. Cryst. Chem.* **1978**, *34*, 540−543.
(22) Koivisto, B. D.; Hicks, R. G. The Magnetochemistry of Verdazyl Radical-Based Materials. *Coord. Chem. Rev.* **2005**, *249*, 2612−2630.
(23) Mukai, K.; Jinno, S.; Shimobe, Y.; Azuma, N.; Taniguchi, M.; Misaki, Y.; Tanaka, K.; Inoue, K.; Hosokoshi, Y. Genuine Organic Magnetic Semiconductors: Electrical and Magnetic Properties of the TCNQ and Iodide Salts of Methylpyridinium-Substituted Verdazyl Radicals. *J. Mater. Chem.* **2003**, *13*, 1614−1621.
(24) Taponen, A. I.; Ayadi, A.; Lahtinen, M. K.; Oyarzabal, I.; Bonhommeau, S.; Rouzières, M.; Mathonière, C.; Tuononen, H. M.; Clérac, R.; Mailman, A. Room-Temperature Magnetic Bistability in a Salt of Organic Radical Ions. *J. Am. Chem. Soc.* **2021**, *143*, 15912−15917.
(25) CrysAlisPRO, Oxford Diffraction /Agilent Technologies UK Ltd, Yarnton, England.
(26) Sheldrick, G. M. *SHELXT* − Integrated space-group and crystal-structure determination. *Acta Crystallogr., Sect. A: Found. Adv.* **2015**, *71*, 3−8.
(27) Dolomanov, O. V.; Bourhis, L. J.; Gildea, R. J.; Howard, J. A. K.; Puschmann, H. *OLEX2*: a complete structure solution, refinement and analysis Program. *J. Appl. Crystallogr.* **2009**, *42*, 339−341.
(28) Gruene, T.; Hahn, H. W.; Luebben, A. V.; Meilleur, F.; Sheldrick, G. M. Refinement of macromolecular structures against neutron data with *SHELXL2013*. *J. Appl. Crystallogr.* **2014**, *47*, 462−466.
(29) Degen, T.; Sadki, M.; Bron, E.; König, U.; Nénert, G. The HighScore Suite. *Powder Diffr.* **2014**, *29*, S13−S18.
(30) Pawley, G. S. Unit-Cell Refinement from Powder Diffraction Scans. *J. Appl. Crystallogr.* **1981**, *14*, 357−361.
(31) Grimme, S.; Ehrlich, S.; Goerigk, L. Effect of the Damping Function in Dispersion Corrected Density Functional Theory. *J. Comput. Chem.* **2011**, *32*, 1456−1465.
(32) Grimme, S.; Antony, J.; Ehrlich, S.; Krieg, H. A Consistent and Accurate Ab Initio Parametrization of Density Functional Dispersion Correction (DFT-D) for the 94 Elements H-Pu. *J. Chem. Phys.* **2010**, *132*, 154104.
(33) Adamo, C.; Barone, V. Toward Reliable Density Functional Methods without Adjustable Parameters: The PBE0 Model. *J. Chem. Phys.* **1999**, *110*, 6158−6170.
(34) Ernzerhof, M.; Scuseria, G. E. Assessment of the Perdew−Burke−Ernzerhof Exchange-Correlation Functional. *J. Chem. Phys.* **1999**, *110*, 5029−5036.
(35) Perdew, J. P.; Burke, K.; Ernzerhof, M. Generalized Gradient Approximation Made Simple [Phys. Rev. Lett. 77, 3865 (1996)]. *Phys. Rev. Lett.* **1997**, *78*, 1396.
(36) Perdew, J. P.; Burke, K.; Ernzerhof, M. Generalized Gradient Approximation Made Simple. *Phys. Rev. Lett.* **1996**, *77*, 3865−3868.
(37) Vydrov, O. A.; Scuseria, G. E.; Perdew, J. P. Tests of Functionals for Systems with Fractional Electron Number. *J. Chem. Phys.* **2007**, *126*, 154109.
(38) Vydrov, O. A.; Scuseria, G. E. Assessment of a Long-Range Corrected Hybrid Functional. *J. Chem. Phys.* **2006**, *125*, 234109.
(39) Vydrov, O. A.; Heyd, J.; Krukau, A. V.; Scuseria, G. E. Importance of Short-Range versus Long-Range Hartree-Fock Exchange for the Performance of Hybrid Density Functionals. *J. Chem. Phys.* **2006**, *125*, 074106.
(40) Henderson, T. M.; Izmaylov, A. F.; Scalmani, G.; Scuseria, G. E. Can Short-Range Hybrids Describe Long-Range-Dependent Properties? *J. Chem. Phys.* **2009**, *131*, 044108.
(41) Weigend, F.; Ahlrichs, R. Balanced Basis Sets of Split Valence, Triple Zeta Valence and Quadruple Zeta Valence Quality for H to Rn: Design and Assessment of Accuracy. *Phys. Chem. Chem. Phys.* **2005**, *7*, 3297−3305.
(42) Throughout the rest of the text, the abbreviations DTDA/DSDA and TCNQ refer to the radical-cations and -anions, respectively, without explicitly specifying the charge or the unpaired electron.
(43) Taponen, A. I.; Wong, J. W. L.; Lekin, K.; Assoud, A.; Robertson, C. M.; Lahtinen, M.; Clérac, R.; Tuononen, H. M.; Mailman, A.; Oakley, R. T. Non-Innocent Base Properties of 3- and 4-Pyridyl-Dithia- and Diselenadiazolyl Radicals: The Effect of N -Methylation. *Inorg. Chem.* **2018**, *57*, 13901−13911.
(44) Aubert, C.; Bégué, J.-P. A Simple Preparation of Alkyl Trifluoromethanesulfonates (Triflates) from Alkyl Trimethylsilyl Ethers. *Synthesis* **1985**, *1985*, 759−760.
(45) Lamoureux, M.; Milne, J. The Disproportionation of Diselenium Dichloride, Se_2Cl_2, and Diselenium Dibromide, Se_2Br_2. *Can. J. Chem.* **1989**, *67*, 1936−1941.
(46) Schelter, E. J.; Morris, D. E.; Scott, B. L.; Thompson, J. D.; Kiplinger, J. L. Toward Actinide Molecular Magnetic Materials: Coordination Polymers of U(IV) and the Organic Acceptors TCNQ and TCNE. *Inorg. Chem.* **2007**, *46*, 5528−5536.
(47) Groom, C. R.; Bruno, I. J.; Lightfoot, M. P.; Ward, S. C. The Cambridge Structural Database. *Acta Crystallogr., Sect. B: Struct. Sci., Cryst. Eng. Mater.* **2016**, *72*, 171−179.
(48) Wu, J.; MacDonald, D. J.; Clérac, R.; Jeon, I.-R.; Jennings, M.; Lough, A. J.; Britten, J.; Robertson, C.; Dube, P. A.; Preuss, K. E. Metal Complexes of Bridging Neutral Radical Ligands: PymDTDA and PymDSDA. *Inorg. Chem.* **2012**, *51*, 3827−3839.
(49) Constantinides, C. P.; Eisler, D. J.; Alberola, A.; Carter, E.; Murphy, D. M.; Rawson, J. M. Weakening of the π^*−π^* Dimerisation in 1,2,3,5-Dithiadiazolyl Radicals: Structural, EPR, Magnetic and Computational Studies of Dichlorophenyl Dithiadiazolyls, $Cl_2C_6H_3CNSSN$. *CrystEngComm* **2014**, *16*, 7298−7312.
(50) Höfs, H.-U.; Bats, J. W.; Gleiter, R.; Hartmann, G.; Mews, R.; Eckert-Maksić, M.; Oberhammer, H.; Sheldrick, G. M. Perhalogenierte 1,2,3,5-Dithiadiazolium-Salze und 1,2,3,5-Dithiadiazole. *Chem. Ber.* **1985**, *118*, 3781−3804.

https://doi.org/10.1021/acs.cgd.2c00795
Cryst. Growth Des. 2022, 22, 7110−7122

(51) Allen, C.; Haynes, D. A.; Pask, C. M.; Rawson, J. M. Co-Crystallisation of Thiazyl Radicals: Preparation and Crystal Structure of [PhCNSSN][C_6F_5CNSSN]. *CrystEngComm* **2009**, *11*, 2048−2050.
(52) Yan, B.; Horton, P. N.; Weston, S. C.; Russell, A. E.; Grossel, M. C. Novel TCNQ-Stacking Motifs in (12-Crown-4)-Complexes of Alkali Metal TCNQ Salts. *CrystEngComm* **2021**, *23*, 6755−6760.
(53) Melen, R. L.; Less, R. J.; Pask, C. M.; Rawson, J. M. Structural Studies of Perfluoroaryldiselenadiazolyl Radicals: Insights into Dithiadiazolyl Chemistry. *Inorg. Chem.* **2016**, *55*, 11747−11759.

https://doi.org/10.1021/acs.cgd.2c00795
Cryst. Growth Des. 2022, 22, 7110−7122

IV

ROLE OF SOLVENT AND COUNTERION ON THE FORMATION OF SIMPLE, MIXED AND COMPLEX CYANOCARBON SALTS OF 1,2,3,5-DITHIADIAZOLYL RADICAL CATION AND THERMALLY INDUCED STRUCTURAL TRANSFORMATIONS OF THEIR SOLVATES

by

Naik, A.; Taponen, A. I.; Horváth, D.; Ayadi, A.; Svahn, N.; Lahtinen, M. K.; Rouzières, M.; Clérac, R.; Tuononen, H. M.; Mailman, A. 2023

Manuscript in preparation

Request a copy from author.

DEPARTMENT OF CHEMISTRY, UNIVERSITY OF JYVÄSKYLÄ
RESEARCH REPORT SERIES

1. Vuolle, Mikko: Electron paramagnetic resonance and molecular orbital study of radical ions generated from (2.2)metacyclophane, pyrene and its hydrogenated compounds by alkali metal reduction and by thallium(III)trifluoroacetate oxidation. (99 pp.) 1976
2. Pasanen, Kaija: Electron paramagnetic resonance study of cation radical generated from various chlorinated biphenyls. (66 pp.) 1977
3. Carbon-13 Workshop, September 6-8, 1977. (91 pp.) 1977
4. Laihia, Katri: On the structure determination of norbornane polyols by NMR spectroscopy. (111 pp.) 1979
5. Nyrönen, Timo: On the EPR, ENDOR and visible absorption spectra of some nitrogen containing heterocyclic compounds in liquid ammonia. (76 pp.) 1978
6. Talvitie, Antti: Structure determination of some sesquiterpenoids by shift reagent NMR. (54 pp.) 1979
7. Häkli, Harri: Structure analysis and molecular dynamics of cyclic compounds by shift reagent NMR. (48 pp.) 1979
8. Pitkänen, Ilkka: Thermodynamics of complexation of 1,2,4-triazole with divalent manganese, cobalt, nickel, copper, zinc, cadmium and lead ions in aqueous sodium perchlorate solutions. (89 pp.) 1980
9. Asunta, Tuula: Preparation and characterization of new organometallic compounds synthesized by using metal vapours. (91 pp.) 1980
10. Sattar, Mohammad Abdus: Analyses of MCPA and its metabolites in soil. (57 pp.) 1980
11. Bibliography 1980. (31 pp.) 1981
12. Knuuttila, Pekka: X-Ray structural studies on some divalent 3d metal compounds of picolinic and isonicotinic acid N-oxides. (77 pp.) 1981
13. Bibliography 1981. (33 pp.) 1982
14. 6^{th} National NMR Symposium, September 9-10, 1982, Abstracts. (49 pp.) 1982
15. Bibliography 1982. (38 pp.) 1983
16. Knuuttila, Hilkka: X-Ray structural studies on some Cu(II), Co(II) and Ni(II) complexes with nicotinic and isonicotinic acid N-oxides. (54 pp.) 1983
17. Symposium on inorganic and analytical chemistry May 18, 1984, Program and Abstracts. (100 pp.) 1984
18. Knuutinen, Juha: On the synthesis, structure verification and gas chromatographic determination of chlorinated catechols and guaiacols occuring in spent bleach liquors of kraft pulp mill. (30 pp.) 1984
19. Bibliography 1983. (47 pp.) 1984
20. Pitkänen, Maija: Addition of BrCl, B_2 and Cl_2 to methyl esters of propenoic and 2-butenoic acid derivatives and ^{13}C NMR studies on methyl esters of saturated aliphatic mono- and dichlorocarboxylic acids. (56 pp.) 1985
21. Bibliography 1984. (39 pp.) 1985
22. Salo, Esa: EPR, ENDOR and TRIPLE spectroscopy of some nitrogen heteroaromatics in liquid ammonia. (111 pp.) 1985

23. Humppi, Tarmo: Synthesis, identification and analysis of dimeric impurities of chlorophenols. (39 pp.) 1985
24. Aho, Martti: The ion exchange and adsorption properties of sphagnum peat under acid conditions. (90 pp.) 1985
25. Bibliography 1985 (61 pp.) 1986
26. Bibliography 1986. (23 pp.) 1987
27. Bibliography 1987. (26 pp.) 1988
28. Paasivirta, Jaakko (Ed.): Structures of organic environmental chemicals. (67 pp.) 1988
29. Paasivirta, Jaakko (Ed.): Chemistry and ecology of organo-element compounds. (93 pp.) 1989
30. Sinkkonen, Seija: Determination of crude oil alkylated dibenzothiophenes in environment. (35 pp.) 1989
31. Kolehmainen, Erkki (Ed.): XII National NMR Symposium Program and Abstracts. (75 pp.) 1989
32. Kuokkanen, Tauno: Chlorocymenes and Chlorocymenenes: Persistent chlorocompounds in spent bleach liquors of kraft pulp mills. (40 pp.) 1989
33. Mäkelä, Reijo: ESR, ENDOR and TRIPLE resonance study on substituted 9,10-anthraquinone radicals in solution. (35 pp.) 1990
34. Veijanen, Anja: An integrated sensory and analytical method for identification of off-flavour compounds. (70 pp.) 1990
35. Kasa, Seppo: EPR, ENDOR and TRIPLE resonance and molecular orbital studies on a substitution reaction of anthracene induced by thallium(III) in two fluorinated carboxylic acids. (114 pp.) 1990
36. Herve, Sirpa: Mussel incubation method for monitoring organochlorine compounds in freshwater recipients of pulp and paper industry. (145 pp.) 1991
37. Pohjola, Pekka: The electron paramagnetic resonance method for characterization of Finnish peat types and iron (III) complexes in the process of peat decomposition. (77 pp.) 1991
38. Paasivirta, Jaakko (Ed.): Organochlorines from pulp mills and other sources. Research methodology studies 1988-91. (120 pp.) 1992
39. Veijanen, Anja (Ed.): VI National Symposium on Mass Spectrometry, May 13-15, 1992, Abstracts. (55 pp.) 1992
40. Rissanen, Kari (Ed.): The 7. National Symposium on Inorganic and Analytical Chemistry, May 22, 1992, Abstracts and Program. (153 pp.) 1992
41. Paasivirta, Jaakko (Ed.): CEOEC'92, Second Finnish-Russian Seminar: Chemistry and Ecology of Organo-Element Compounds. (93 pp.) 1992
42. Koistinen, Jaana: Persistent polychloroaromatic compounds in the environment: structure-specific analyses. (50 pp.) 1993
43. Virkki, Liisa: Structural characterization of chlorolignins by spectroscopic and liquid chromatographic methods and a comparison with humic substances. (62 pp.) 1993
44. Helenius, Vesa: Electronic and vibrational excitations in some

biologically relevant molecules. (30 pp.) 1993

45. Leppä-aho, Jaakko: Thermal behaviour, infrared spectra and x-ray structures of some new rare earth chromates(VI). (64 pp.) 1994
46. Kotila, Sirpa: Synthesis, structure and thermal behavior of solid copper(II) complexes of 2-amino-2- hydroxymethyl-1,3-propanediol. (111 pp.) 1994
47. Mikkonen, Anneli: Retention of molybdenum(VI), vanadium(V) and tungsten(VI) by kaolin and three Finnish mineral soils. (90 pp.) 1995
48. Suontamo, Reijo: Molecular orbital studies of small molecules containing sulfur and selenium. (42 pp.) 1995
49. Hämäläinen, Jouni: Effect of fuel composition on the conversion of fuel-N to nitrogen oxides in the combustion of small single particles. (50 pp.) 1995
50. Nevalainen, Tapio: Polychlorinated diphenyl ethers: synthesis, NMR spectroscopy, structural properties, and estimated toxicity. (76 pp.) 1995
51. Aittola, Jussi-Pekka: Organochloro compounds in the stack emission. (35 pp.) 1995
52. Harju, Timo: Ultrafast polar molecular photophysics of (dibenzylmethine)borondifluoride and 4-aminophthalimide in solution. (61 pp.) 1995
53. Maatela, Paula: Determination of organically bound chlorine in industrial and environmental samples. (83 pp.) 1995
54. Paasivirta, Jaakko (Ed.): CEOEC'95, Third Finnish-Russian Seminar: Chemistry and Ecology of Organo-Element Compounds. (109 pp.) 1995
55. Huuskonen, Juhani: Synthesis and structural studies of some supramolecular compounds. (54 pp.) 1995
56. Palm, Helena: Fate of chlorophenols and their derivatives in sawmill soil and pulp mill recipient environments. (52 pp.) 1995
57. Rantio, Tiina: Chlorohydrocarbons in pulp mill effluents and their fate in the environment. (89 pp.) 1997
58. Ratilainen, Jari: Covalent and non-covalent interactions in molecular recognition. (37 pp.) 1997
59. Kolehmainen, Erkki (Ed.): XIX National NMR Symposium, June 4-6, 1997, Abstracts. (89 pp.) 1997
60. Matilainen, Rose: Development of methods for fertilizer analysis by inductively coupled plasma atomic emission spectrometry. (41 pp.) 1997
61. Koistinen, Jari (Ed.): Spring Meeting on the Division of Synthetic Chemistry, May 15-16, 1997, Program and Abstracts. (36 pp.) 1997
62. Lappalainen, Kari: Monomeric and cyclic bile acid derivatives: syntheses, NMR spectroscopy and molecular recognition properties. (50 pp.) 1997
63. Laitinen, Eira: Molecular dynamics of cyanine dyes and phthalimides in solution: picosecond laser studies. (62 pp.) 1997
64. Eloranta, Jussi: Experimental and theoretical studies on some

quinone and quinol radicals. (40 pp.) 1997

65. Oksanen, Jari: Spectroscopic characterization of some monomeric and aggregated chlorophylls. (43 pp.) 1998
66. Häkkänen, Heikki: Development of a method based on laser-induced plasma spectrometry for rapid spatial analysis of material distributions in paper coatings. (60 pp.) 1998
67. Virtapohja, Janne: Fate of chelating agents used in the pulp and paper industries. (58 pp.) 1998
68. Airola, Karri: X-ray structural studies of supramolecular and organic compounds. (39 pp.) 1998
69. Hyötyläinen, Juha: Transport of lignin–type compounds in the receiving waters of pulp mills. (40 pp.) 1999
70. Ristolainen, Matti: Analysis of the organic material dissolved during totally chlorine-free bleaching. (40 pp.) 1999
71. Eklin, Tero: Development of analytical procedures with industrial samples for atomic emission and atomic absorption spectrometry. (43 pp.) 1999
72. Välisaari, Jouni: Hygiene properties of resol-type phenolic resin laminates. (129 pp.) 1999
73. Hu, Jiwei: Persistent polyhalogenated diphenyl ethers: model compounds syntheses, characterization and molecular orbital studies. (59 pp.) 1999
74. Malkavaara, Petteri: Chemometric adaptations in wood processing chemistry. (56 pp.) 2000
75. Kujala Elena, Laihia Katri, Nieminen Kari (Eds.): NBC 2000, Symposium on Nuclear, Biological and Chemical Threats in the 21st Century. (299 pp.) 2000
76. Rantalainen, Anna-Lea: Semipermeable membrane devices in monitoring persistent organic pollutants in the environment. (58 pp.) 2000
77. Lahtinen, Manu: *In situ* X-ray powder diffraction studies of Pt/C, CuCl/C and Cu_2O/C catalysts at elevated temperatures in various reaction conditions. (92 pp.) 2000
78. Tamminen, Jari: Syntheses, empirical and theoretical characterization, and metal cation complexation of bile acid-based monomers and open/closed dimers. (54 pp.) 2000
79. Vatanen, Virpi: Experimental studies by EPR and theoretical studies by DFT calculations of α-amino-9,10-anthraquinone radical anions and cations in solution. (37 pp.) 2000
80. Kotilainen, Risto: Chemical changes in wood during heating at 150-260 °C. (57 pp.) 2000
81. Nissinen, Maija: X-ray structural studies on weak, non-covalent interactions in supramolecular compounds. (69 pp.) 2001
82. Wegelius, Elina: X-ray structural studies on self-assembled hydrogen-bonded networks and metallosupramolecular complexes. (84 pp.) 2001
83. Paasivirta, Jaakko (Ed.): CEOEC'2001, Fifth Finnish-Russian Seminar: Chemistry and Ecology of Organo-Element Compounds. (163 pp.) 2001
84. Kiljunen, Toni: Theoretical studies on spectroscopy and

atomic dynamics in rare gas solids. (56 pp.) 2001

85. Du, Jin: Derivatives of dextran: synthesis and applications in oncology. (48 pp.) 2001
86. Koivisto, Jari: Structural analysis of selected polychlorinated persistent organic pollutants (POPs) and related compounds. (88 pp.) 2001
87. Feng, Zhinan: Alkaline pulping of non-wood feedstocks and characterization of black liquors. (54 pp.) 2001
88. Halonen, Markku: Lahon havupuun käyttö sulfaattiprosessin raaka-aineena sekä havupuun lahontorjunta. (90 pp.) 2002
89. Falábu, Dezsö: Synthesis, conformational analysis and complexation studies of resorcarene derivatives. (212 pp.) 2001
90. Lehtovuori, Pekka: EMR spectroscopic studies on radicals of ubiquinones Q-*n*, vitamin K_3 and vitamine E in liquid solution. (40 pp.) 2002
91. Perkkalainen, Paula: Polymorphism of sugar alcohols and effect of grinding on thermal behavior on binary sugar alcohol mixtures. (53 pp.) 2002
92. Ihalainen, Janne: Spectroscopic studies on light-harvesting complexes of green plants and purple bacteria. (42 pp.) 2002
93. Kunttu, Henrik, Kiljunen, Toni (Eds.): 4th International Conference on Low Temperature Chemistry. (159 pp.) 2002
94. Väisänen, Ari: Development of methods for toxic element analysis in samples with environmental concern by ICP-AES and ETAAS. (54 pp.) 2002
95. Luostarinen, Minna: Synthesis and characterisation of novel resorcarene derivatives. (200 pp.) 2002
96. Louhelainen, Jarmo: Changes in the chemical composition and physical properties of wood and nonwood black liquors during heating. (68 pp.) 2003
97. Lahtinen, Tanja: Concave hydrocarbon cyclophane π-prismands. (65 pp.) 2003
98. Laihia, Katri (Ed.): NBC 2003, Symposium on Nuclear, Biological and Chemical Threats – A Crisis Management Challenge. (245 pp.) 2003
99. Oasmaa, Anja: Fuel oil quality properties of wood-based pyrolysis liquids. (32 pp.) 2003
100. Virtanen, Elina: Syntheses, structural characterisation, and cation/anion recognition properties of nano-sized bile acid-based host molecules and their precursors. (123 pp.) 2003
101. Nättinen, Kalle: Synthesis and X-ray structural studies of organic and metallo-organic supramolecular systems. (79 pp.) 2003
102. Lampiselkä, Jarkko: Demonstraatio lukion kemian opetuksessa. (285 pp.) 2003
103. Kallioinen, Jani: Photoinduced dynamics of $Ru(dcbpy)_2(NCS)_2$ – in solution and on nanocrystalline titanium dioxide thin films. (47 pp.) 2004
104. Valkonen, Arto (Ed.): VII Synthetic Chemistry Meeting and XXVI Finnish NMR Symposium. (103 pp.) 2004

105. Vaskonen, Kari: Spectroscopic studies on atoms and small molecules isolated in low temperature rare gas matrices. (65 pp.) 2004
106. Lehtovuori, Viivi: Ultrafast light induced dissociation of $Ru(dcbpy)(CO)_2I_2$ in solution. (49 pp.) 2004
107. Saarenketo, Pauli: Structural studies of metal complexing Schiff bases, Schiff base derived *N*-glycosides and cyclophane π-prismands. (95 pp.) 2004
108. Paasivirta, Jaakko (Ed.): CEOEC'2004, Sixth Finnish-Russian Seminar: Chemistry and Ecology of Organo-Element Compounds. (147 pp.) 2004
109. Suontamo, Tuula: Development of a test method for evaluating the cleaning efficiency of hard-surface cleaning agents. (96 pp.) 2004
110. Güneş, Minna: Studies of thiocyanates of silver for nonlinear optics. (48 pp.) 2004
111. Ropponen, Jarmo: Aliphatic polyester dendrimers and dendrons. (81 pp.) 2004
112. Vu, Mân Thi Hong: Alkaline pulping and the subsequent elemental chlorine-free bleaching of bamboo (*Bambusa procera*). (69 pp.) 2004
113. Mansikkamäki, Heidi: Self-assembly of resorcinarenes. (77 pp.) 2006
114. Tuononen, Heikki M.: EPR spectroscopic and quantum chemical studies of some inorganic main group radicals. (79 pp.) 2005
115. Kaski, Saara: Development of methods and applications of laser-induced plasma spectroscopy in vacuum ultraviolet. (44 pp.) 2005
116. Mäkinen, Riika-Mari: Synthesis, crystal structure and thermal decomposition of certain metal thiocyanates and organic thiocyanates. (119 pp.) 2006
117. Ahokas, Jussi: Spectroscopic studies of atoms and small molecules isolated in rare gas solids: photodissociation and thermal reactions. (53 pp.) 2006
118. Busi, Sara: Synthesis, characterization and thermal properties of new quaternary ammonium compounds: new materials for electrolytes, ionic liquids and complexation studies. (102 pp.) 2006
119. Mäntykoski, Keijo: PCBs in processes, products and environment of paper mills using wastepaper as their raw material. (73 pp.) 2006
120. Laamanen, Pirkko-Leena: Simultaneous determination of industrially and environmentally relevant aminopolycarboxylic and hydroxycarboxylic acids by capillary zone electrophoresis. (54 pp.) 2007
121. Salmela, Maria: Description of oxygen-alkali delignification of kraft pulp using analysis of dissolved material. (71 pp.) 2007
122. Lehtovaara, Lauri: Theoretical studies of atomic scale impurities in superfluid ^{4}He. (87 pp.) 2007
123. Rautiainen, J. Mikko: Quantum chemical calculations of structures, bonding, and spectroscopic properties of some sulphur and selenium iodine cations. (71 pp.) 2007
124. Nummelin, Sami: Synthesis, characterization, structural and

retrostructural analysis of self-assembling pore forming dendrimers. (286 pp.) 2008

125. Sopo, Harri: Uranyl(VI) ion complexes of some organic aminobisphenolate ligands: syntheses, structures and extraction studies. (57 pp.) 2008
126. Valkonen, Arto: Structural characteristics and properties of substituted cholanoates and *N*-substituted cholanamides. (80 pp.) 2008
127. Lähde, Anna: Production and surface modification of pharmaceutical nano- and microparticles with the aerosol flow reactor. (43 pp.) 2008
128. Beyeh, Ngong Kodiah: Resorcinarenes and their derivatives: synthesis, characterization and complexation in gas phase and in solution. (75 pp.) 2008
129. Välisaari, Jouni, Lundell, Jan (Eds.): Kemian opetuksen päivät 2008: uusia oppimisympäristöjä ja ongelmalähtöistä opetusta. (118 pp.) 2008
130. Myllyperkiö, Pasi: Ultrafast electron transfer from potential organic and metal containing solar cell sensitizers. (69 pp.) 2009
131. Käkölä, Jaana: Fast chromatographic methods for determining aliphatic carboxylic acids in black liquors. (82 pp.) 2009
132. Koivukorpi, Juha: Bile acid-arene conjugates: from photoswitchability to cancer cell detection. (67 pp.) 2009
133. Tuuttila, Tero: Functional dendritic polyester compounds: synthesis and characterization of small bifunctional dendrimers and dyes. (74 pp.) 2009
134. Salorinne, Kirsi: Tetramethoxy resorcinarene based cation and anion receptors: synthesis, characterization and binding properties. (79 pp.) 2009
135. Rautiainen, Riikka: The use of first-thinning Scots pine (*Pinus sylvestris*) as fiber raw material for the kraft pulp and paper industry. (73 pp.) 2010
136. Ilander, Laura: Uranyl salophens: synthesis and use as ditopic receptors. (199 pp.) 2010
137. Kiviniemi, Tiina: Vibrational dynamics of iodine molecule and its complexes in solid krypton - Towards coherent control of bimolecular reactions? (73 pp.) 2010
138. Ikonen, Satu: Synthesis, characterization and structural properties of various covalent and non-covalent bile acid derivatives of N/O-heterocycles and their precursors. (105 pp.) 2010
139. Siitonen, Anni: Spectroscopic studies of semiconducting single-walled carbon nanotubes. (56 pp.) 2010
140. Raatikainen, Kari: Synthesis and structural studies of piperazine cyclophanes – Supramolecular systems through Halogen and Hydrogen bonding and metal ion coordination. (69 pp.) 2010
141. Leivo, Kimmo: Gelation and gel properties of two- and three-component Pyrene based low molecular weight organogelators. (116 pp.) 2011
142. Martiskainen, Jari: Electronic energy transfer in light-harvesting complexes isolated from *Spinacia oleracea* and from three

photosynthetic green bacteria *Chloroflexus aurantiacus*, *Chlorobium tepidum*, and *Prosthecochloris aestuarii*. (55 pp.) 2011

143. Wichmann, Oula: Syntheses, characterization and structural properties of [O,N,O,X´] aminobisphenolate metal complexes. (101 pp.) 2011
144. Ilander, Aki: Development of ultrasound-assisted digestion methods for the determination of toxic element concentrations in ash samples by ICP-OES. (58 pp.) 2011
145. The Combined XII Spring Meeting of the Division of Synthetic Chemistry and XXXIII Finnish NMR Symposium. Book of Abstracts. (90 pp.) 2011
146. Valto, Piia: Development of fast analysis methods for extractives in papermaking process waters. (73 pp.) 2011
147. Andersin, Jenni: Catalytic activity of palladium-based nanostructures in the conversion of simple olefinic hydro- and chlorohydrocarbons from first principles. (78 pp.) 2011
148. Aumanen, Jukka: Photophysical properties of dansylated poly(propylene amine) dendrimers. (55 pp.) 2011
149. Kärnä, Minna: Ether-functionalized quaternary ammonium ionic liquids – synthesis, characterization and physicochemical properties. (76 pp.) 2011
150. Jurček, Ondřej: Steroid conjugates for applications in pharmacology and biology. (57 pp.) 2011
151. Nauha, Elisa: Crystalline forms of selected Agrochemical actives: design and synthesis of cocrystals. (77 pp.) 2012
152. Ahkola, Heidi: Passive sampling in monitoring of nonylphenol ethoxylates and nonylphenol in aquatic environments. (92 pp.) 2012
153. Helttunen, Kaisa: Exploring the self-assembly of resorcinarenes: from molecular level interactions to mesoscopic structures. (78 pp.) 2012
154. Linnanto, Juha: Light excitation transfer in photosynthesis revealed by quantum chemical calculations and exiton theory. (179 pp.) 2012
155. Roiko-Jokela, Veikko: Digital imaging and infrared measurements of soil adhesion and cleanability of semihard and hard surfaces. (122 pp.) 2012
156. Noponen, Virpi: Amides of bile acids and biologically important small molecules: properties and applications. (85 pp.) 2012
157. Hulkko, Eero: Spectroscopic signatures as a probe of structure and dynamics in condensed-phase systems – studies of iodine and gold ranging from isolated molecules to nanoclusters. (69 pp.) 2012
158. Lappi, Hanna: Production of Hydrocarbon-rich biofuels from extractives-derived materials. (95 pp.) 2012
159. Nykänen, Lauri: Computational studies of Carbon chemistry on transition metal surfaces. (76 pp.) 2012
160. Ahonen, Kari: Solid state studies of pharmaceutically important molecules and their derivatives. (65 pp.) 2012

161. Pakkanen, Hannu: Characterization of organic material dissolved during alkaline pulping of wood and non-wood feedstocks. (76 pp.) 2012
162. Moilanen, Jani: Theoretical and experimental studies of some main group compounds: from closed shell interactions to singlet diradicals and stable radicals. (80 pp.) 2012
163. Himanen, Jatta: Stereoselective synthesis of Oligosaccharides by *De Novo* Saccharide welding. (133 pp.) 2012
164. Bunzen, Hana: Steroidal derivatives of nitrogen containing compounds as potential gelators. (76 pp.) 2013
165. Seppälä, Petri: Structural diversity of copper(II) amino alcohol complexes. Syntheses, structural and magnetic properties of bidentate amino alcohol copper(II) complexes. (67 pp.) 2013
166. Lindgren, Johan: Computational investigations on rotational and vibrational spectroscopies of some diatomics in solid environment. (77 pp.) 2013
167. Giri, Chandan: Sub-component self-assembly of linear and non-linear diamines and diacylhydrazines, formulpyridine and transition metal cations. (145 pp.) 2013
168. Riisiö, Antti: Synthesis, Characterization and Properties of Cu(II)-, Mo(VI)- and U(VI) Complexes With Diaminotetraphenolate Ligands. (51 pp.) 2013
169. Kiljunen, Toni (Ed.): Chemistry and Physics at Low Temperatures. Book of Abstracts. (103 pp.) 2013
170. Hänninen, Mikko: Experimental and Computational Studies of Transition Metal Complexes with Polydentate Amino- and Aminophenolate Ligands: Synthesis, Structure, Reactivity and Magnetic Properties. (66 pp.) 2013
171. Antila, Liisa: Spectroscopic studies of electron transfer reactions at the photoactive electrode of dye-sensitized solar cells. (53 pp.) 2013
172. Kemppainen, Eeva: Mukaiyama-Michael reactions with α-substituted acroleins – a useful tool for the synthesis of the pectenotoxins and other natural product targets. (190 pp.) 2013
173. Virtanen, Suvi: Structural Studies of Dielectric Polymer Nanocomposites. (49 pp.) 2013
174. Yliniemelä-Sipari, Sanna: Understanding The Structural Requirements for Optimal Hydrogen Bond Catalyzed Enolization – A Biomimetic Approach.(160 pp.) 2013
175. Leskinen, Mikko V: Remote β-functionalization of β'-keto esters. (105 pp.) 2014
176. 12th European Conference on Research in Chemistry Education (ECRICE2014). Book of Abstracts. (166 pp.) 2014
177. Peuronen, Anssi: N-Monoalkylated DABCO-Based N-Donors as Versatile Building Blocks in Crystal Engineering and Supramolecular Chemistry. (54 pp.) 2014
178. Perämäki, Siiri: Method development for determination and recovery of rare earth elements from industrial fly ash. (88 pp.) 2014

179. Chernyshev, Alexander, N.: Nitrogen-containing ligands and their platinum(IV) and gold(III) complexes: investigation and basicity and nucleophilicity, luminescence, and aurophilic interactions. (64 pp.) 2014
180. Lehto, Joni: Advanced Biorefinery Concepts Integrated to Chemical Pulping. (142 pp.) 2015
181. Tero, Tiia-Riikka: Tetramethoxy resorcinarenes as platforms for fluorescent and halogen bonding systems. (61 pp.) 2015
182. Löfman, Miika: Bile acid amides as components of microcrystalline organogels. (62 pp.) 2015
183. Selin, Jukka: Adsorption of softwood-derived organic material onto various fillers during papermaking. (169 pp.) 2015
184. Piisola, Antti: Challenges in the stereoselective synthesis of allylic alcohols. (210 pp.) 2015
185. Bonakdarzadeh, Pia: Supramolecular coordination polyhedra based on achiral and chiral pyridyl ligands: design, preparation, and characterization. (65 pp.) 2015
186. Vasko, Petra: Synthesis, characterization, and reactivity of heavier group 13 and 14 metallylenes and metalloid clusters: small molecule activation and more. (66 pp.) 2015
187. Topić, Filip: Structural Studies of Nano-sized Supramolecular Assemblies. (79 pp.) 2015
188. Mustalahti, Satu: Photodynamics Studies of Ligand-Protected Gold Nanoclusters by using Ultrafast Transient Infrared Spectroscopy. (58 pp.) 2015
189. Koivisto, Jaakko: Electronic and vibrational spectroscopic studies of gold-nanoclusters. (63 pp.) 2015
190. Suhonen, Aku: Solid state conformational behavior and interactions of series of aromatis oligoamide foldamers. (68 pp.) 2016
191. Soikkeli, Ville: Hydrometallurgical recovery and leaching studies for selected valuable metals from fly ash samples by ultrasound-assisted extraction followed by ICP-OES determination. (107 pp.) 2016
192. XXXVIII Finnish NMR Symposium. Book of Abstracts. (51 pp.) 2016
193. Mäkelä, Toni: Ion Pair Recognition by Ditopic Crown Ether Based bis-Urea and Uranyl Salophen Receptors. (75 pp.) 2016
194. Lindholm-Lehto, Petra: Occurrence of pharmaceuticals in municipal wastewater treatment plants and receiving surface waters in Central and Southern Finland. (98 pp.) 2016
195. Härkönen, Ville: Computational and Theoretical studies on Lattice Thermal conductivity and Thermal properties of Silicon Clathrates. (89 pp.) 2016
196. Tuokko, Sakari: Understanding selective reduction reactions with heterogeneous Pd and Pt: climbing out of the black box. (85 pp.) 2016
197. Nuora, Piia: Monitapaustutkimus LUMA-Toimintaan liittyvissä oppimisympäristöissä tapahtuvista kemian oppimiskokemuksista. (171 pp.) 2016

198. Kumar, Hemanathan: Novel Concepts on The Recovery of By-Products from Alkaline Pulping. (61 pp.) 2016
199. Arnedo-Sánchez, Leticia: Lanthanide and Transition Metal Complexes as Building Blocks for Supramolecular Functional Materials. (227 pp.) 2016
200. Gell, Lars: Theoretical Investigations of Ligand Protected Silver Nanoclusters. (134 pp.) 2016
201. Vaskuri, Juhani: Oppiennätyksistä opetussuunnitelman perusteisiin - lukion kemian kansallisen opetussuunnitelman kehittyminen Suomessa vuosina 1918-2016. (314 pp.) 2017
202. Lundell Jan, Kiljunen Toni (Eds.): 22nd Horizons in Hydrogen Bond Research. Book of Abstracts. 2017
203. Turunen, Lotta: Design and construction of halogen-bonded capsules and cages. (61 pp.) 2017
204. Hurmalainen, Juha: Experimental and computational studies of unconventional main group compounds: stable radicals and reactive intermediates. (88 pp.) 2017
205. Koivistoinen Juha: Non-linear interactions of femtosecond laser pulses with graphene: photo-oxidation, imaging and photodynamics. (68 pp.) 2017
206. Chen, Chengcong: Combustion behavior of black liquors: droplet swelling and influence of liquor composition. (39 pp.) 2017
207. Mansikkamäki, Akseli: Theoretical and Computational Studies of Magnetic Anisotropy and Exchange Coupling in Molecular Systems. (190 p. + included articles) 2018.
208. Tatikonda, Rajendhraprasad: Multivalent N-donor ligands for the construction of coordination polymers and coordination polymer gels. (62 pp.) 2018
209. Budhathoki, Roshan: Beneficiation, desilication and selective precipitation techniques for phosphorus refining from biomass derived fly ash. (64 pp.) 2018
210. Siitonen, Juha: Synthetic Studies on 1-azabicyclo[5.3.0]decane Alkaloids. (140 pp.) 2018
211. Ullah, Saleem: Advanced Biorefinery Concepts Related to Non-wood Feedstocks. (57 pp.) 2018
212. Ghalibaf, Maryam: Analytical Pyrolysis of Wood and Non-Wood Materials from Integrated Biorefinery Concepts. (106 pp.) 2018

DEPARTMENT OF CHEMISTRY, UNIVERSITY OF JYVÄSKYLÄ
DISSERTATIONS PUBLISHED IN THE JYU DISSERTATIONS RESEARCH SERIES

1. Bulatov, Evgeny: Synthetic and structural studies of covalent and non-covalent interactions of ligands and metal center in platinum(II) complexes containing 2,2′-dipyridylamine or oxime ligands. (58 pp.) 2019. JYU Dissertations 70.
2. Annala, Riia: Conformational Properties and Anion Complexes of Aromatic Oligoamide Foldamers. (80 pp.) 2019. JYU Dissertations 84.
3. Isoaho, Jukka Pekka: Dithionite Bleaching of Thermomechanical Pulp - Chemistry and Optimal Conditions. (73 pp.) 2019. JYU Dissertations 85.
4. Nygrén, Enni: Recovery of rubidium from power plant fly ash. (98 pp.) 2019. JYU Dissertations 136.
5. Kiesilä, Anniina: Supramolecular chemistry of anion-binding receptors based on concave macromolecules. (68 pp.) 2019. JYU Dissertations 137.
6. Sokolowska, Karolina: Study of water-soluble p-MBA-protected gold nanoclusters and their superstructures. (60 pp.) 2019. JYU Dissertations 167.
7. Lahtinen, Elmeri: Chemically Functional 3D Printing: Selective Laser Sintering of Customizable Metal Scavengers. (71 pp.) 2019. JYU Dissertations 175.
8. Larijani, Amir: Oxidative reactions of cellulose under alkaline conditions. (102 pp.) 2020. JYU Dissertations 217.
9. Kolari, Kalle: Metal-metal contacts in late transition metal polymers. (60 pp.) 2020. JYU Dissertations 220.
10. Kauppinen, Minttu: Multiscale computational investigation of catalytic properties of zirconia supported noble metals. (87 pp.) 2020. JYU Dissertations 231.
11. Ding, Xin: Halogen Bond in Crystal Engineering: Structural Studies on Crystals with Ruthenium Centered Complexes and 1-(4-Pyridyl)-4-thiopyridine Zwitterion as Halogen Bond Acceptors. (59 pp.) 2020. JYU Dissertations 323.
12. Neuvonen, Antti: Toward an Understanding of Hydrogen-Bonding Bifunctional Organocatalyst Conformations and Their Activity in Asymmetric Mannich Reactions. (77 pp.) 2020. JYU Dissertations 336.
13. Kortet, Sami: 2,5-Diarylpyrrolidines and Pyroglutamic-Acid-Derived 2-Diarylmethyl-5-Aryl-Pyrrolidines: Their Synthesis and Use in Asymmetric Synthesis. (221 pp.) 2020. JYU Dissertations 337.
14. Saarnio, Ville: Fluorescent probes, noble metal nanoparticles and their nanocomposites: detection of nucleic acids and other biological targets. (80 pp.) 2021. JYU Dissertations 361.
15. Chernysheva, Maria: σ-hole interactions: the effect of the donors and acceptors nature in selenoureas, thioureas, halogenated species, substituted benzenes, and their adducts. (72 pp.) 2021. JYU Dissertations 370.
16. Bulatova, Margarita: Noncovalent interactions as a tool for supramolecular self-assembly of metallopolymers. (62 pp.) 2021. JYU Dissertations 377.

17. Romppanen, Sari: Laser-spectroscopic studies of rare earth element- and lithium-bearing minerals and rocks. (66 pp.) 2021. JYU Dissertations 393.
18. Kukkonen, Esa: Nonlinear optical materials through weak interactions and their application in 3D printing. (58 pp.) 2021. JYU Dissertations 441.
19. Kuosmanen, Riikka: The Effect of Structure on the Gel Formation Ability and the Properties of Bile Acid Based Supramolecular Organogels. (68 pp.) 2021. JYU Dissertations 465.
20. Reuna, Sini: Development of a Method for Phosphorus Recovery from Wastewaters. (67 pp.) 2022. JYU Dissertations 486.
21. Taipale, Essi: Synthetic and Structural Studies on the Effect of Non-Covalent Interactions on N(*sp2*)-Heterocyclic Molecules. (67 pp.) 2022. JYU Dissertations 496.
22. Järvinen, Teemu: Molecular Dynamics View on Matrix Isolation. (143 pp.) 2022. JYU Dissertations 544.
23. Kumar, Parveen: Synthesis and Structural Studies on Halogen(I) Complexes. (160 pp.) 2022. JYU Dissertations 549.
24. Forsblom, Samu: Design and Construction of Metal-Organic Polyhedra. (212 pp.) 2022. JYU Dissertations 569.
25. Korpelin, Ville: Computational Studies of Catalytic Active Site Properties and Reactions at the Metal–Oxide Interface. (78 pp.) 2022. JYU Dissertations 578.
26. Vuori, Hannu: Extending Benson Group Increment Theory to Compounds of Phosphorus, Silicon, and Boron with Computational Chemistry. (59 pp.) 2022. JYU Dissertations 581.
27. Pallerla, Rajanish: Studies Towards Synthesis of Favipiravir & Humilisin E. (139 pp.) 2023. JYU Dissertations 611.